The zebrafish as a model for *pink1/gba1* deficiency

Marcus Edmund Frank Keatinge

Thesis submitted for the degree of Doctor of Philosophy

University of Sheffield

Department of Neuroscience

September 2014

Acknowledgements

I would firstly like to thank my supervisor, Professor Oliver Bandmann, who has supported and motivated me throughout my PhD experience. His enthusiasm and passion for science has encouraged my own, giving me freedom, and helping me develop my ideas. But also remaining patient and always pushing me further, mentoring me as a scientist.

Many thanks also to the BBSRC, MRC, Parkinson's UK, and patient donations for providing the funding and equipment that has allowed me to discover, explore and build my research skills.

Special thanks go to Eli Lilly my industrial sponsors, and to Dr Michael J. O'Neill my industrial supervisor. They have not only provided financial support, but also excellent advice and scientific expertise.

I would like to thank everyone in the Bateson Centre and SITRAN, specifically those of D38, who have aided and inspired me over the last four years. Especially fellow students, who I owe many thanks, Alex McGowan, Rebecca Bright, Guy Yealland, Lisa Trollope and Aimee McTighe, who have helped focus me and have always been there in times of need.

I owe many thanks to Dr Phillipa Carling and Dr Marc DaCosta for proofreading my thesis and correcting my grasp of written English, which I imagine required much time and effort.

For keeping me sane and my spirits high, since embarking on this academic journey, I would like to thank everyone who lived in and was affiliated with, ROSLIN ROAD for so many years. Including Ashley Regan, William Clark, Leanne Winn, Sinead Balgobin, Catherine Dickinson, Rebecca Bell, Rebecca Grevitt, Stephanie Sardinha, Rob Raine, Chris Wright, Anthony Hestlehurst, Andrew Timmis, Oliver Farrell, John Londesborough, Rachel Lockhart and Louise Harrington.

A Special mention goes to my PhD friends, outside of Sheffield, but who have remained in constant contact, even when on the other side of the planet, always giving advice and great company, Liam Lawlor and Reiss Reid.

I would like to thank my family for putting up with me for all this time and always providing support and encouragement, helping me through this process.

Finally, I thank my partner Alex for his continuous support, love and understanding, over the past four years, no matter how far apart we have been.

Abstract

Introduction

Parkinson's disease is the second most common neurodegenerative disorder. There is currently no cure, and only symptomatic treatment is available. Homozygous mutations in *PINK1* result in early onset Parkinson's disease. Homozygous mutations in *GBA1* lead to Gaucher's disease, whilst heterozygous mutations in *GBA1* are the most common risk factor for Parkinson's disease. Research in both areas is hindered by a lack of suitable loss of function vertebrate models. The zebrafish has recently emerged as an effective model for disease.

Hypothesis

Loss of function zebrafish models in *pink1/gba1* will suitably model the human disease, allowing the study of gene-gene interactions and identifying potential new drug targets.

Results

The glycolytic inhibitor *tigarb*, was found to be upregulated in *pink1* -/- embryos; its inhibition completely preventing Th neuron reduction and mitochondrial dysfunction. Inhibition of the tumour suppressor *vhl* was also found to rescue Th neuron reduction in the *pink1* -/- embryos, but this requires further validation.

A *gba1* orthologue in zebrafish was identified. Its expression was shown to be constant and not spatially restricted. Inhibition of *gba1* at embryological stages showed no signs of Th neuron reduction. Stable mutants were successfully constructed and found to have marked phenotypes reminiscent of type II Gaucher's disease, ultimately leading to death at 12 weeks of age. Some mild phenotypes were also identified in heterozygous *gba1* mutant zebrafish

Conclusions

Zebrafish are an effective model for both *pink1* and *gba1* deficiency. Gene-gene interaction studies identified *tigarb* and *vhl* as a potential target for disease modifying therapy in Parkinson's disease. Zebrafish are also an effective model for Gaucher's disease, whilst heterozygous phenotypes may reveal mechanisms of *gba1* linked Parkinson's disease.

Contents

FIGURES AND TABLES

Abbreviations

-/- : Homozygous
-/+: Heterozygous
23BPG: 2,3 bi-phosphoglycerate
BMP: Bone morphogenetic protein
Cas9: CRISPR associated protein 9
CBE: Conduritol b epoxide
CNS: Central nervous system
CRISPR: Clustered regularly interspaced short palindromic repeats
DA: Dopaminergic
DAT: Dopamine Transporter
Del: Deletion
Dj1: Parkinson disease (autosomal recessive, early onset) 7
DNJ:N-Butyldeoxynojirimycin
DPF: Days post fertilisation
ENU:N-ethyl-N-nitrosourea
PFK-2/FBPase-2:6-phosphofructo-2-kinase/fructose-2,6-bisphosphatase
GD: Gaucher's disease
gDNA: Genomic DNA
GBA1: Glucocerebrosidase 1
GWAS: Genome wide association study
HIF1□: Hypoxia-inducible factor 1-alpha
HK2: Hexokinase 2
Hpf: Hours post fertilisation
KD: Knockdown
KO: Knockout
L-Dopa: L-3,4-Dihydroxyphenylalanine
LRRK2: leucine rich repeat kinase 2
MPTP: 1-methyl-4-phenyl-1, 2, 3, 6-tetrahydropyridine
NaT: Sodium taurocholate
NMD: Nonsense mediated decay
NMS: Non motor symptoms
OMM: Outer mitochondrial membrane
OR: Odds ratio
PCR: Polymerase chain reaction
PHD: Prolyl hydroxylase
ROS: Reactive oxygen species
PAM: Proto-spacer adjacent motif
PARKIN: PARKINSON DISEASE 2, AUTOSOMAL RECESSIVE JUVENILE
PARL: Presenelin associated rhomboid like protein
PAS: Periodic acid–Schiff
PD: Parkinson's disease
PINK1: PTEN-induced putative kinase 1
PFA: Paraformaldehyde
SNCA: Alpha synuclein
SNP: Single nucleotide polymorphism
SSDNA: Single stranded DNA molecules

TALEN: Transcription activator-like effector nuclease
TH: Tyrosine hydroxylase
TIGAR: p53-Inducible Regulator of Glycolysis and Apoptosis
UPR: Unfolded protein response
VHL: Von Hippel-Lindau
WISH: Whole mount in situ hybridisation
WPF: Weeks post fertilisation
ZFN: Zinc-finger nucleases

1 Introduction

1.1 Parkinson's disease; incidence, symptoms and treatments

1.1.1 General introduction

Parkinson's disease (PD) is a common neurodegenerative movement disorder, affecting approximately 13.4 persons per 100,000 of the population.[1] The pathological hallmark of the disease is the cell death of the dopaminergic (DA) neurons in the substantia nigra.[2] Within the surviving neurons, protein inlusions, known as Lewy bodies are usually found, that are composed of alpha synuclein and ubiquitin, and are believed to be driving pathology.[3] The DA neuron loss leads to a decrease of dopamine in the striatum and causes the classical parkinsonian symptoms of bradykinesia, freezing, abnormal gait, and tremor.[4] Non-motor symptoms (NMS) are often overlooked, and include, among others depression; dementia and apathy.[5] These can be as disabling to the patient as the motor symptoms. No cure for PD currently exists, and only symptomatic treatment is available. Although initially effective, the benefit of the currently available medications, such as Levodopa, reduces over time. Patients can then exhibit side effects such as dyskinesias.[6]

The cause of PD is mostly unknown, with the majority of cases being sporadic in nature.[7] However, a small group of patients develop the disease due to monogenically inherited genetic defects.[8] By studying these genetic subtypes, it is hoped that insight will be gained into the disease pathogenesis of the whole patient population. By using genetics or chemicals to model the disease, the disease process can be further elucidated, in turn hopefully leading to the development of disease-modifying treatments.

1.1.1 Incidence of Parkinson's disease

Affecting 1% of the total population by the age of 65, rising to 6% of the total population by the age of 85, PD is the second most common form of neurodegeneration facing the western world after Alzheimer's disease.[1, 9, 10] It is mostly a disease of the elderly, with classical PD presenting by those in their 60's and older (See Figure 1).

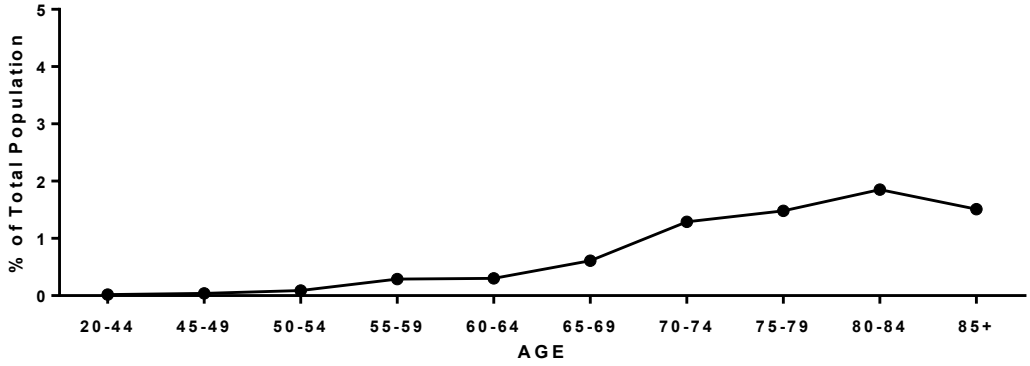

Figure 1 Incidence of PD by age. The Incidence of PD as a percentage of the total population, per age range. Incidence is approximately 0.1% of the general population, at the 50-54 age group, rising to 2% at the 80-84 age group. PD clearly rises with age, making age the biggest risk factor in disease development. Adapted from Kowal *et al*, with permission.[10]

Patients developing the disease before the age of 50 have been arbitrarily defined as early onset cases, although this can also be defined as an age of onset <40 years of age. [11, 12] These make up a minority of patients, for example, in UK studies focusing on idiopathic PD, out of a total of 156 patients, 20 were below 50 years of age, making up 12% of the patient population.[13] Similar findings have also been shown in other countries such as Japan, with an early onset PD (EOPD) population comprising 10% of the total disease group.[11] Early onset cases are more likely to have an underlying genetic cause to their illness, such as mutations in *PINK1* or *PARK2/PARKIN*.[8, 9, 14, 15] This has become a feature of other common diseases with, as yet, mostly unknown cause, where some early onset cases can be explained by single gene mutations, such as *BRCA1* in early onset breast cancer, and *APP* in familial Alzheimer's disease.[16, 17] This is exemplified in studies where *PARK2* mutations were analysed in early and late onset patients. In a study focusing purely on early onset cases, of 253 patients, 18 (7.1%) were homozygous/compound heterozygous for *PARK2* mutations, with the mutation frequency decreasing with age of onset. Two studies focusing on late onset PD with a combined total of 250 patients, did not detect homozygous *PARK2* mutations in any of the individuals.[18-20]

Familial PD, defined as having a patient with a first degree relative also positive for PD, makes up a significant component of the patient population, however the majority of patients (approximately 90%) have no identifiable cause of the disease, and are hence "sporadic" in nature.[9, 21] Both sexes are affected by the disease, although for reasons unknown, incidence is twice as high for men compared to women.[1, 22]

Incidence by race has been analysed in many studies, but typically the data is either conflicting or not significant. [1] With the majority of PD cases defined as sporadic, the only major factor predicative of disease risk is age.[1, 9, 23] As we live in an aging society, the cases of PD, like other diseases of the elderly, will continue to rise relative to the rest of the population. Estimates have been made which projects patient numbers doubling by 2030.[24] This puts increasing strain on primary care givers. This burden is not only physical and emotional for patients and carers, but also causes considerable financial cost to the patient and to their healthcare systems (see Figure 2 for projected PD related healthcare costs for the USA). Studies have shown that patients cost about $14,000 per annum, but this cost is tripled when taking into account patients suffering from additional dementia.[10, 25]

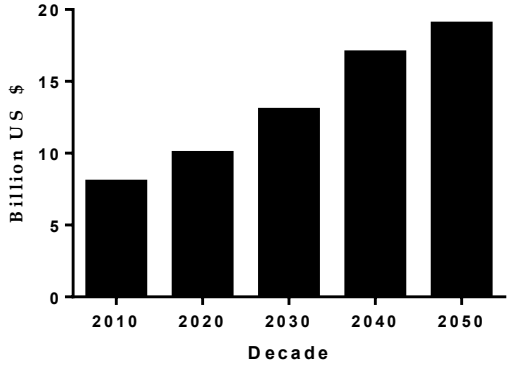

Figure 2. The projected cost of PD treatment and care in the USA. From 2010-2050, due to higher incidence rates, PD care costs rises substantially, from $7 billion, to $20 by 2050. Figure adapted from Kowal *et al*., with permission.[10]

1.1.2 Diagnosis

PD can be difficult to diagnose clinically. Not only can other diseases present with "parkinsonian" symptoms, but diagnosis of *bona fide* PD is complicated by heterogeneous symptoms at clinical presentation.[26, 27] Traditionally, diagnosis was made upon the exhibition of two of the cardinal motor symptoms, such as bradykinesia, resting tremor and rigidity; however, this can cause misdiagnosis of other parkinsonian diseases such as multiple system atrophy, and progressive supranuclear palsy.[28] The addition of other criteria, such as response to Levodopa (L-Dopa), has helped to improve diagnosis. These additions have provided the framework for unified criteria such as the UK Parkinson's Disease Society Brain Bank clinical diagnostic criteria. [26]

1.1.3 Motor symptoms

Among the clinical features of PD, motor symptoms are the most striking at clinical presentation. The cardinal signs are considered to be tremor, bradykinesia, rigidity and postural instability.[4] Bradykinesia describes a slowness of movement, which can cause difficulty in daily life, especially when undertaking tasks in which precise motor control is required. Spontaneous movement such as blinking and swallowing is also effected.[29-31] Tremor, more specifically resting tremor, is the most recognisable symptom of PD. It presents typically in an asymmetrical fashion at onset. However, it is noted that the tremor typically disappears during action, or with sleep.[32, 33] Postural instability, generally occurring in late stage PD, is due to an impairment of postural reflexes. This is an important cause of the typical falls by patients (often leading to hip fractures) in PD.[4, 34] Approximately 50% of PD patients develop freezing, which typically occurs during walking; the freezing episode manifests as a sudden inability to move.[35, 36]

1.1.4 Non-Motor Symptoms (NMS)

Although considered a movement disorder, PD also manifests with a large set of NMS. These lead not only to disability, but also to a decrease in the quality of life and a shortened lifespan. These symptoms classically manifest as difficulties with sleep, autonomic dysfunction, pain, neuropsychiatric issues and dementia.[4, 37] Of note, many of these symptoms manifest early in the course of the disease, and can precede motor symptoms by decades. [38-40]

Issues affecting sleep are extremely common in patients and present in several different forms. Nearly all patients exhibit disturbed sleep, the cause being multifactorial in nature.[41] These include REM sleep behaviour disorder, which causes patients to physically act out their own dreams, sometimes resulting in kicking and screaming whilst still asleep.[42] Patients can also develop excessive daytime sleepiness, characterised by a lack of energy, regardless of the quality or the length of the previous night time sleep. Studies have demonstrated that patients can go from a wakeful state to one of sleep extremely quickly (approximately 2 seconds), in a similar way to narcoleptic patients.[43] Neuropsychiatric symptoms can manifest with depression, anxiety, apathy, psychosis and hallucinations. All of these are clearly disabling to the patients, negatively affecting them, not only through their own quality of life, but also

that of their caregiver. Psychosis, in particular, is the most common cause of nursing home administration for patients, and therefore one of the most costly.[44-46]

Approximately 40% of PD patients develop dementia, which worsens with age.[47] Attention and memory are mostly affected, and in addition, a change of personality can occur.[48] Dementia also has substantial economic impact on carers and the health care system. Demented PD patients cost 3.3 times more ($42,000) than PD patients without dementia. The majority of costs (67%) are due to institutional cases.[25]

Autonomic dysfunction, another key NMS, is an umbrella term for many difficulties experienced by patients, including drooling, sweating, swallowing and constipation.[49] Of these, constipation is one of the most common, but also the most frequently reported NMS. Occurring in approximately 70% of patients (depending on the study), this causes a decrease in bowel movement frequency, which may then worsen with the severity of disease.[50, 51]

Pain is another unexpectedly common, yet often overlooked, PD NMS, with substantial pain being present in over 40% of patients. Partly exacerbated by motor symptoms; the pain sensation felt by patients is varied and can be experienced as musculoskeletal pain, neuropathic pain, dystonia-related pain, primary pain and akathitic dysfunction. The most severe pain sensations are due to the sustained muscle contractions caused by dystonia. Some forms of pain in PD can be alleviated with PD medication, others treated by physical therapy.[52, 53]

Olfactory dysfunction, a loss of sense of smell, is also very common in PD patients (90%) but often not appreciated by the patient until tested. This particular symptom is so prevalent in patients, it has been suggested olfactory tests could be more robust at identifying PD than motor tests.[54, 55] Olfaction presents as defects in odour detection and identification, but can also result in a decrease in effective odor discrimination. Defects in olfaction may additionally correlate with disease severity, but this requires further investigation. [56]

1.1.5 Parkinson's disease treatments

There is no current cure for PD, but there are effective symptomatic treatments, not only for motor symptoms, but also for at least some of the non-motor symptoms. L-3,4-Dihydroxyphenylalanine (L-Dopa) is the precursor to a group of neurotransmitters, the catecholamines, that includes epinephrine and more importantly in PD, dopamine. L-

Dopa (also known as Levodopa) has been the main treatment option for dopamine replacement therapy for the last 40 years. It is so effective at reversing the motor symptoms, and the patient response is so robust, that it can aid the diagnosis.[57-59] Unfortunately, over time, patients can develop a new set of motor complications as a direct result of the L-Dopa therapy, particularly at higher doses. Known as dyskinesias, these are involuntary movements made by the patient, and can become equally as disabling as the original motor symptoms.[58, 60] After 5 years of L-Dopa treatment, it has been estimated that approximately 50% of patients experience these motor complications. [61]

Alternatives to L-Dopa are dopamine agonists, such as apomorphine and Pramipexole, which activate dopamine receptors directly. Although effective in treating motor symptoms, they are less efficacious than L-Dopa. They also eventually result in dyskinesias and other side effects seen in L-Dopa therapy.[62]

To enhance L-Dopa therapy efficacy, it can be utilised in conjunction with catechol-O-methyl transferase inhibitors, such as Entacapone. These act by delaying L-Dopa metabolism, increasing its half-life within the brain. Double blind placebo controlled trials have shown it to effectively enhance motor function in conjunction with L-Dopa. [63]

For patients that don't respond to pharmacological agents, or experience too many side effects, surgical techniques can be utilised in the form of deep brain stimulation. These are now seen as an effective method of treating motor symptoms in advanced PD patients. Classically, an electrical lead is utilised to target the sub-thalamic nucleus or globus pallidus pars interna, emitting high frequency electrical impulses to the brain. [64-66]

Although the described treatments are very efficient at relieving symptoms, they are not neuroprotective. Consequently, future therapies must prevent, or at least slow DA cell death, in order to normalise life expectancy and improve motor control and cognition.[67]

1.2 Causes of Parkinson's disease

1.2.1 Monogenically-inherited, Mendelian forms of Parkinson's disease

Previously, in order to determine the genetic component of disease, twin studies were utilised, measuring concordance between monozygotic and dizygotic twins. Monozygotic twins have virtually identical genetic material. Genetic causes are inferred if concordances are higher in monozygotic twins than in dizygotic twins, as the latter only share 50% of their genetic material. [68] A large 2011 study in the Swedish population, found concordance of monozygotic twins for sporadic PD was 11%, whilst only 4% for dizygotic twins, implying a genetic contribution to PD development. In a separate study, early onset PD was analysed for concordance in twin pairs, concordance was 100% in monozygotic and 17% in dizygotic twins, demonstrating a very strong genetic factor, but only in PD patients with age of onset <50. [69, 70]

Studies such as these have difficulty in identifying the causes of complex traits, due to incomplete penetrance and genetic heterogeneity, especially for late onset PD. In terms of sporadic PD, studies suggest that up to 30% of patients have a family history of the disease, with first degree relatives having a 2-7 increase relative risk.[71] Studies such as these have been varied due to methodological issues, but strong correlations have been reported for early onset PD compared to late, in a similar manner to twin studies. A meta-analysis of 29 familial studies of patients having a first degree relative also having PD had a relative risk of 2.9, whilst relative risk was 4.4 for pairs of siblings. When relative risk was split between late onset and early onset, the risk was 2.7 and 4.7 respectively. [21, 23]

As the human genome became more annotated and understood, linkage analysis was utilised to locate highly penetrant, rare disease causing mutations. Requiring very large family pedigrees, the disease causing mutation is tracked in the genome by co-segregation with genetic markers, such as restriction fragment length polymorphisms and microsatellites. Once a small enough region has been identified which co-segregates with the disease, all genes within that region can be sequenced in patients to identify potential pathogenic mutations. Missense mutations that effect conserved residues, or nonsense mutations, insertions and deletions, would aid in the identification of the disease gene. These are further screened in healthy controls (such as unaffected family members) to identify which mutations lead to the specific disease. This allows for the identification of mutations that are inherited in an autosomal

recessive manner, or autosomal dominant manner, and are generally highly penetrant with an early age of onset. For example, Huntington's disease (autosomal dominant) and cystic fibrosis (autosomal recessive) were both discovered in this manner by linkage analysis.[72-74]

The first PD gene to be discovered was a point mutation in alpha synuclein *(SNCA)*, in 3 large Greek/Italian pedigrees, leading to amino acid change of Ala53Thr. The point mutation caused early onset PD in an autosomal dominant manner, suggesting a toxic gain of function of the mutation, with onset being between 30-50 years of age in all cases.[75] Duplications and triplications of the *SNCA* locus have also been reported in large PD families which are also inherited in an autosomal dominant fashion. The age of onset being either late or early respectively. With the existence of WT *SNCA* duplication causing late onset PD and triplication leading to early onset, these data show the effect gene dosage has on the disease course and progression in familial PD.[76, 77] But, highly penetrant disease causing *SNCA* mutations are rare.[78] The function of the alpha synuclein protein is still unknown but is believed to be involved in snare complex formation at synaptic terminals, required for long term neuronal health.[79] The pathogenic mechanism leading to PD is still uncertain, however; due to the apparent dosage effects, and furthermore, due to its presence in Lewy bodies, it is believed to be caused by alpha synuclein protein aggregation, which overwhelms the proteosomal and autophagy pathways, ultimately leading to DA neuronal death.

Linkage analysis has also been utilised to discover mutations in the genes for *PINK1*, *PARK2* and *DJ-1*. All lead to early onset forms of PD that are inherited in an autosomal recessive fashion. Large deletions, insertions and exonic rearrangements have all been recorded for each of these genes, as well as missense and nonsense point mutations, all leading to loss of function.[8, 15, 80, 81]

Homozygous/compound heterozygous mutations in the *PARK2* gene that codes for the E3 ubiquitin ligase PARKIN are some of the most common genetic causes of early onset PD.[14] Patients present with typical PD but generally at a very early age (<45 years); however not all patients show signs of Lewy body pathology at autopsy. Symptoms progress very slowly, and respond very well to standard L-Dopa treatments, but these patients can then also develop dyskinesias. [80, 82] [80, 83] Although homozygous mutations are clearly a cause of EOPD, some studies have suggested a

link between *PARK2* heterozygous mutations or single nucleotide polymorphisms (SNPs) and sporadic PD, although this remains controversial.[84]

Homozygous mutations in *PARK7* coding for DJ1, also cause EOPD, but are very rare; estimates of *PARK7* mutation frequency from several studies have suggested they are responsible for only 1% of EOPD.[81, 85] The function of DJ1 is still unknown, but it is believed to be an onco-protein that is involved in the response to oxidative stress, and may have a role in mitochondrial health.[86, 87]

The *PINK1* gene is another early onset PD gene, and as the focus of this study, will be addressed later in this thesis in greater detail.

Mutations in *LRRK2* (leucine rich repeat kinase 2) are one of the more frequent causes of familial PD. They were also discovered through linkage studies and sequencing. To date, only missense mutations have been reported, the disease manifesting in an autosomal dominant fashion with incomplete penetrance. Unlike the disease genes previously discussed, *LRRK2*-linked PD is a cause of late onset PD, likely to be caused from toxic gain of function mutations. Clinical presentation resembles that of sporadic PD, with at least some patients developing Lewy bodies. *LRRK2* mutations, especially the G2019S mutation, are very common. Its occurrence varies greatly between populations, with a frequency 1-3% in sporadic PD, and can be as high as 40% in familial PD.[88-90] The *LRRK2* gene, possessing 51 exons, encodes a very large protein, 2527 amino acids in length. Its function is still not completely understood, but is known to be part of the ROCO protein family. This possesses ROC and COR domains, as well as GTPase and kinase functions.[91]

Another important gene in PD genetics is glucocerebrosidase 1 (*GBA1*). Homozygous mutations in this gene present as Gaucher's disease (GD), whilst heterozygosity for *GBA1* mutations remains the most common risk factor for PD. Clinically almost identical to idiopathic PD, several multicentre analyses have compiled the odds ratio (OR) of *GBA1* mutations for PD risk as being 5.0-7.0.[92-94] This gene is also one of the focuses of this study, so shall be addressed later in the thesis in greater detail.

As sequencing technologies have become more advanced in the post genomics era, whole exome sequencing has been utilised to find highly penetrant rare PD genes. Recently, this has allowed the identification of the pAsp620Asn mutation in the *VPS35* gene in a large Austrian pedigree. The mutation segregates with the disease in an

autosomal dominant form, but with incomplete penetrance.[95] Subsequent screening studies have identified these mutations as a rare cause of LOPD.[96] The VPS35 protein, part of the retromer complex, is involved in vesicle transport, shuttling vesicles between organelles such as the mitochondria and peroximsomes.[97] Proteomic studies have also demonstrated its presence in cortical Lewy bodies.[98]

1.2.2 Common genetic variants identified by GWAS

Although linkage analysis and whole genome sequencing are powerful tools in finding rare genetic causes of PD with large effects, genome wide association studies (GWAS) must be employed to identify common genetic defects that have a small and potentially additive effect in disease development. GWAS, using single nucleotide polymorphism (SNP) genotyping arrays, that sequences a specific set of SNPs that can be considered representative for large genomic blocks, due to linkage disequilibrium. These are compared between cases and controls, to identify SNPs that occur in cases at a different frequency from the controls. These specific SNPs are markers for genomic regions associated with disease, as opposed to identifying specific genes that are causal or protective.[99]

The genomic regions co segregating with the SNP implicated in disease will only ever have a small effect toward disease risk, with an average OR of 1.33, and will only explain a small proportion of genetic variability within a population. The SNPs only mark a genomic region as associated with disease, and may not be identifying the pathogenic variant. Extensive sequencing for the region would then be required to fully identify the actual pathogenic mutations, as well as identifying the rarer variants that may affect disease at that specific locus. [99]

The arrays are limited as they will only detect common SNPs that are present in the population with a frequency of >5%. Consequently, although they can identify common variants with low genetic contribution to disease, and linkage analysis can identify rare variants that have high penetrance, both techniques cannot identify variants that are of intermediate frequency <5% and are of intermediate penetrance. For example, *GBA1* variants which are causal for PD, and *TREM2* variants that are causal for Alzheimer's disease.[93, 99, 100]

Initial GWAS were hampered by underpowered studies, but now many have been collated into meta-analyses which hold considerably more power.[101, 102] In the most

comprehensive meta-analysis of PD GWAS and candidate gene analysis, Lill *et al.*, combined data from several different studies to analyse SNPs from 16,432 PD cases and 48,810 controls. This work identified variants at 12 different genomic loci, including *ITGA8*, a gene that had previously not been identified in preceding PD GWAS studies due to low power. Loci of particular interest included *MAPT*, a gene encoding tau, a key protein in Alzheimer's disease pathology, but also in PD, due to its presence in Lewy bodies.[102-104]

Other loci of interest included those for *SNCA, LRRK2* and *GBA1*, as not being rare genes with high penetrance, but have been identified as causal for PD. Yet, those variants identified by the meta GWAS are common variants with high odds ratios. The *GBA1* SNP for allele N370S had an OR of 3.51, unusually high for common variants; the OR for the majority of variants from the meta-analysis was 1.10-1.35. It must be noted though that this SNP was identified from meta-analysis of candidate gene studies, as standard SNP arrays do not detect N370S SNP as its frequency at 1% is too low in the general population. For a table summarising the main PD genes identified see Table 1 (highly penetrant genes) and Table 2 (GWAS identified genes).

Although their overall contribution to the disease is small, the variants are likely to have an additive, synergistic or complex effect with each other and the environment. These also exclude structural variants that will be elucidated by whole genome sequencing once the technology has become cost effective. Extensive deep sequencing of each variant must be undertaken, as well as confirmatory *in vivo* studies to elucidate the disease causing mechanism of the variant.[102]

GENE	INHERITENCE	TYPE	MUTATIONS	FUNCTION
SNCA	Autosomal Dominant	Early Onset PD	Missense, Duplications and Triplications	Synaptic Vesicle Formation
PARKIN	Autosomal Recessive	Early Onset PD	Missense, Nonsense, Deletions	E3 Ubiquitin ligase
PINK1	Autosomal Recessive	Early Onset PD	Missense, Nonsense, Deletions	Mitophagy Inducer
DJ-1	Autosomal Recessive	Early Onset PD	Missense, Deletions	Oxidative Stress Sensor
LRRK2	Autosomal Dominant	Classical PD	7 Pathogenic Missense Mutations	Autophagy
VPS35	Autosomal Dominant	Classical PD	Missense Variants	Retromer Complex Formation
EIF4G1	Autosomal Dominant	Classical PD	Missense Variants	Translation Initiation
GBA	RISK FACTOR	Classical PD	Missense, Small InDels	Ceramide Metabolism

Table 1. A summary of PD linked genes. A list of all recorded PD linked genes with high penetrance listing their mode of inheritance, type of PD and types of mutations. Table adapted with permission from Lubbe *et al*.[105]

LOCUS	ODDS RATIO	N samples
GBA	3.51	44,851
SYT11/RAB25	1.73	17,300
PARK16	0.91	69,262
STK39	1.19	35,159
MCCC1/LAMP3	0.86	46,502
DGKQ	1.21	57,716
BST1	0.88	47,586
SNCA	1.29	79,494
ITGA8	0.88	61,036
LRRK2	1.17	34,123
CCDC62/HIP1R	1.15	38,367
MAPT/STH	0.78	50,389

Table 2. A Summary of GWAS identified genes implicated in PD. A list gene loci identified as causal for PD from the PD GWAS Meta-analysis with accompanying odds ratios and samples sizes. Table adapted with permission from Lill *et el*.[102]

1.2.3 Environmental causes of Parkinson's disease and protective factors

Environmental factors have additionally been implicated in the causality of PD, and exposure is likely to increase risk development, especially in conjunction with genetic risk factors. Thus far, exposure to pesticides, insecticides and herbicides have been implicated with disease development, with coffee drinking, and smoking having the opposite effect.[23] Many studies have investigated generalised exposure to pesticides, including meta-analyses, producing conflicting data, some studies suggest a high odds ratios of 1.3-3.7. However this is controversial as some studies have not identified any correlation, or any correlation that is statistically significant.[106-110] The most studied chemicals are rotenone and paraquat, both commonly utilised in agriculture. The former is a pesticide capable of acting as a mitochondrial Complex I inhibitor, and the latter, a herbicide that produces reactive oxygen species (ROS). Both have been shown to cause selective degeneration of DA neurons in numerous studies in rats and mice.[111, 112] Drinking well water and rural living have also been implicated in increased prevalence of PD, but these are perhaps compounded by additional exposure to pesticides.[23, 113, 114]

In contrast, smoking and coffee drinking have been found to be neuroprotective against PD. Coffee intake and PD prevalence has been studied extensively. A meta-analysis pooling data from 5 cohort and 8 case control studies identified a relative risk

of developing PD of 0.69 compared to non-coffee drinkers. Several meta- analyses have been conducted investigating the neuroprotective capacity of smoking. A study from Hernan *et al.,* pooling data from 44, studies found the relative risk of PD development to be 0.8 for past smokers, and 0.39 for current smokers. [115]

1.3 Models of Parkinson's disease

1.3.1 Toxin induced Models of Parkinson's disease

Initially in PD research, toxin induced models were utilised to study the disease process and assay new pharmacological therapies. The classical PD toxin is MPTP (1-methyl-4-phenyl-1, 2, 3, 6-tetrahydropyridine) which causes the selective loss of DA neurons. It was discovered as a result of drug addicts attempting to manufacture synthetic heroin. MPTP was created as a by-product, and once injected, the users developed symptoms identical to idiopathic PD.[116]

Biochemically, MPTP is rapidly metabolised to MPP+, where it selectively enters the DA cells through the action of DAT (Dopamine Transporter).[117] Once intracellular, MPP+ can accumulate in mitochondria and inhibit mitochondrial Complex I of the electron transport chain, impairing respiration.[118, 119] It has become the toxin of choice to induce PD symptoms and DA neuronal cell loss in a variety of model organisms including fish, mice and primates.[120-122]

The second classical chemical utilised for toxin-induced models of PD is 6-hydroxydopamine, an analogue of dopamine in its hydroxylated form. This can lead to neuronal cell death by oxidative stress and Complex I inhibition.[123, 124] It is fairly specific for DA neurons due to preferential uptake by DAT. However, unlike MPTP, it cannot cross the blood brain barrier and must be directly injected into the brain, requiring surgery.[123] It effectively destroys 60% of the Tyrosine Hydroxylase (TH) neurons in the brains of mice and rats, leading to motor defects. An advantage of its use is that unilateral injections allow for the uninjected half of the brain to be utilised as an internal control.[125]

Although chemical and toxin induced models are effective in producing symptoms such as DA cell death and some motor symptoms, they fail to fully recapitulate the disease features, such as Lewy body formation. DA neuronal death in these models is generally acute in nature, whilst in idiopathic PD this loss is progressive. Although

toxin models are useful at modelling the end stage PD, they fail to accurately model the pre-symptomatic and early stages of the disease.[126]

1.3.2 Genetic models of Parkinson's disease

Using reverse genetic and transgenic strategies, molecular tools such as the Cre LOX system have been utilised to generate knockout (KO), conditional KO and knockin animals for many of the PD related genes thus far discovered. [127-129]

1.3.2.1 Models of Parkin Deficiency

parkin KO drosophila (whose entire *parkin* coding sequence had been deleted), were generated using a transposon mutagenesis screen. Homozygous mutants, although develop normally, accumulate marked phenotypes with age, ultimately leading to decreased lifespan. This is coupled with male sterility due to a defective mitochondrial compartment in the maturing spermatids. Mutants developed abnormal wing posture, accompanied by a decrease in flight ability, due to apoptotic flight muscles. The flight muscles were revealed to have large, swollen, disintegrating mitochondria. Structural alterations were recorded in the TH neurons, although no specific Th neuron reduction itself was detected. This study demonstrated the importance of *parkin* for mitochondrial homeostasis, due to the cell death of mitochondrial rich tissues such as muscle and sperm. [130]

Several different *Parkin* KO mice have been generated through homologous recombination with embryonic stem cells. All demonstrate a distinct lack of neurodegeneration of TH neurons. The first KO described by Itier *et al*., did not present any cell loss in TH or DAT neurons up to 24 months, although a decrease in DAT protein was observed. Defects in cognition and neurotransmission were also recorded. At the biochemical level, homozygous mutants additionally showed mitochondrial dysfunction, yet in the absence of any gross mitochondrial morphological abnormalities.[131, 132] Separate studies using different *Parkin* KO alleles confirmed the lack of TH cell loss, but could not replicate the defects in cognition and neurotransmission.[133]

1.3.2.2 Models of DJ1 deficiency

Dj1 loss of function studies have also been conducted in *Drosophila* and mice. *Drosophila* possess 2 orthologues of the human *DJ1* with high homology (50-70%). In contrast to the *parkin* KO flies, single or double KO *dj1* flies develop normally, with

similar viability and morphology to WT. This is accompanied by an absence of neurodegeneration; implying *dj1* status does not affect neuronal homeostasis. However, *dj1* mutants were found to have a marked increase in sensitivity to oxidative stress, such as H_2O_2 (10 fold greater sensitivity), confirming *dj1's* function as a oxidative stress responsive protein.[134] *Dj1* KO mice have similar phenotypes to KO flies. Homozygous mutants develop normally without an effect on viability. There is a complete absence of neurodegeneration, but an increased sensitivity to oxidative stress.[135, 136]

1.3.2.3 Knock –In and Knock – Out LRRK2 models

As *LRRK2* mutations are thought to be pathogenic, either predominantly or exclusively due to a toxic gain of function, transgenic knockin methods have been employed to investigate these *LRRK2* mutations in flies and mice. In addition, KO strategies have also been employed to investigate the biological function of LRRK2 *in vivo*. In *Drosophila*, KO study reports have been conflicting. Some studies report no overt phenotype or TH neuron loss, while others report extreme phenotypes reminiscent of *parkin* KO flies.[137, 138] KO mice also develop normally with a lack of neurodegeneration and a sensitivity to MPTP, suggesting Lrrk2 is dispensable for normal neuronal homeostasis, at least in vertebrates. SNCA pathology was reported, not in the brain, but in the kidney, of one *Lrrk2* KO line.[139]

Transgenic approaches have been equally inconsistent, transgenic flies overexpressing mutant *lrrk2* have been described as either asymptomatic, or as developing parkinsonian like phenotypes with TH neuron loss.[137, 140] Similar findings have been reported in *Lrrk2* transgenic mice as either asymptomatic or developing late onset TH neuron loss. But this may be dependent on the type of *Lrrk2* mutation being over expressed, and the level of expression achieved.[141, 142]

1.4 The zebrafish as a model for disease

1.4.1 The zebrafish as a model organism

Over the past 15 years the zebrafish (*Danio rerio*) has been firmly established as a model for biomedical research. Zebrafish are vertebrates, and have greater genetic homology to humans than flies. Maintenance costs are a fraction of those for keeping mice. Their genome has been sequenced, and is currently in its 9th version. Unlike other model

organisms, such as *Xenopus*, they possess a diploid genome and a similar complement of genes to humans. At least 70% of human genes have an obvious zebrafish orthologue.[143]

Zebrafish were initially utilised as a model species for development, due to rapid embryogenesis and transparency. Zebrafish embryos develop from a single cell to a whole organism, with its entire body plan and major organs established, within 24 hours. The majority of development is completed by 5 days post fertilisation and sexual maturity is reached by 2.5 months of age. Consequently, generation time is comparatively small. As they develop *ex vivo* and in great numbers, this allows the study of mutations that may be embryonic lethal. Their small size makes them cost effective, with a single female being capable of producing hundreds of eggs per week. Breeding is controlled by a simple light cycle (14 hours light, 10 hours dark) allowing manipulation of embryo production, as breeding takes place when the lights are turned on. [144] Their transparency allows *in vivo* imaging in real time, especially when using transgenic reporter lines.[145]

Zebrafish are also a suitable model for phenotypic drug screening. Embryos can fit into 96-well plates and be utilised to screen compound libraries for their biological effect. Drugs can be dispensed and absorbed directly into the raising media.[146] Since whole animals are utilised in these screens, the assay simultaneously evaluates bioavailability, toxicity and teratogenicity. This allows the identification of small molecules that suppress disease, or induce phenotypes.[146, 147] Focusing on ameliorating a specific phenotype, zebrafish chemical screens make no assumption on the molecular target, allowing identification of unknown rescue mechanisms. For example, a chemical screen undertaken in a classic study by Yu *et al,*. resulted in the discovery of the first bone morphogenetic protein (BMP) antagonists.[148] BMP is required for correct dorso-ventral patterning, and by using a simple developmental readout, it was possible to screen a library of compounds for chemicals that effect developmental patterning. A lead compound was discovered, known as dysomorphin, and was found to inhibit the BMP type 1 receptor, but not the highly homologous TGF-β-receptor. Since its discovery, dysomorphin has been successfully tested in mouse models of BMP dysregulation, such as fibrodysplasia ossificans progressive.[148, 149] See Figure 3 for a flow chart illustrating the sequential steps of phenotypic drug discovery in zebrafish compared to traditional high throughput *in vitro* drug screening.

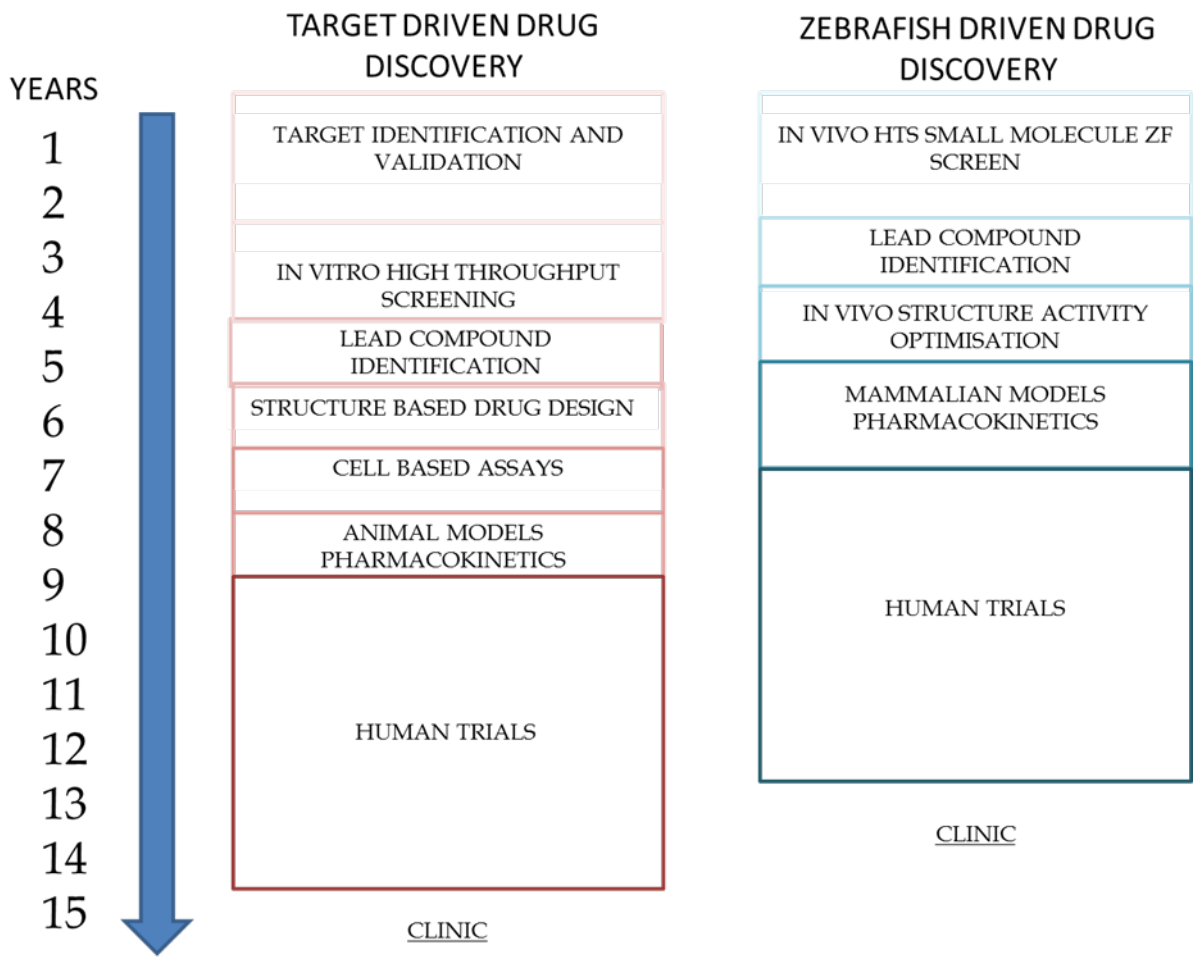

Figure 3. Phenotypic drug discovery using zebrafish. A flow diagram illustrating the sequential steps of phenotypic drug discovery using zebrafish, compared to traditional high throughput drug discovery hit to lead process. As zebrafish screening simultaneously assays for bioavailability, toxicity and efficacy, the time to reach the clinic is considerably reduced. Adapted with permission from Bowman *et al*.[150]

1.4.2 Zebrafish genetic tools

Different genomic tools for targeted genome modification and RNA interference strategies are in use to study the consequences of loss of function mutations in zebrafish. RNA interference strategies include the use of Morpholinos, a knockdown (KD) technology ideal for fast genetic inhibition studies. Stable mutants can be generated by large-scale N-ethyl-N-nitrosourea (ENU) mutagenesis screens, which create point mutations at random. For precise genome editing, technologies such as zinc-finger nucleases (ZFNs), transcription activator-like effector nuclease (TALEN) systems and the clustered-regularly-interspaced-short-palindromic-repeats (CRISPR)/CRISPR associated protein 9 (Cas9) systems can be utilised.[127, 151, 152] Due to their small size and low cost, large genetic screens can be carried out, such as the

zebrafish mutation project (ZMP), which aims to create a loss of function mutation for every zebrafish gene.[153]

Morpholinos have emerged as a powerful efficient RNA inference technology for KD studies in zebrafish. Morpholinos are 25-mer modified oligonucleotides, containing a morpholine instead of deoxyribose rings that effectively bind to RNA nucleotides through RNase H independent mechanisms. They can either be targeted to bind to the 5' untranslated region of the mature RNA species, blocking translation, or can be targeted to the exon junctions of the pre-mRNA complex, interfering with splicing and leading to exon skip or intron inclusion in the mature mRNA species. Morpholinos are micro-injected into the zebrafish embryos at the single cell stage. Effective KD is assessed by either western blot (translation blocking) or RT-PCR (splice blocker), and typically lasts for 3-5 days. They are cost effective, 300nmols costing $400, and can be kept at room temperature for up to 5 years. They allow for fast and effective loss of function studies in zebrafish embryos.[152, 154, 155]

However, Morpholino KD has its draw backs, as a significant proportion of Morpholinos produce off target effects. These classically cause a delay in development, heart oedema, neural apoptosis and craniofacial defects. These non-specific off-target effects are often p53-mediated. Consequently, co-knockdown of p53 with the Morpholino targeting the gene of interest has been utilised to ameliorate at least some of the off target effects. It has been estimated that 15-20% of Morpholinos produce off target effects in zebrafish embryos. However, in the author's experience, this figure is likely to be closer to 40% in practice, and is dependent on the target gene. Consequently, unless a stable loss of function mutant can validate the Morpholino phenotypes, Morpholino data should be interpreted with caution, especially when investigating cell death. Morpholino KD, although fast at inhibiting gene function at the embryonic stages, their effects are only transient and wear off 3-5dpf. Consequently they cannot be used for loss of function genetic studies in adult Zebrafish.[156]

Morpholino KD is fast and cost effective but is transient in nature and may produce off target effects; consequently it is preferable to work with stable mutant lines to investigate loss of function genetic studies. Generating stable mutants through ENU screens are not targeted and induce point mutations at random. Consequently directed genome editing is now the preferred method to generate loss of function mutants. Originally, this was achieved using ZFN technology, where pairs of zinc fingers that

bind specific sequences of DNA (9bp each) are constructed and fused to a *FOK1* endonuclease. Once bound to the specific DNA sequences, the FOK1 subunits dimerise, creating the stranded DNA breaks which can induce small insertions and deletions into the DNA sequence due to error-prone non homologous end joining.[157] The main drawbacks of this technique were difficulty in construction for in-house methods and the rarity of potential binding sites. Commercially available ZFNs were not cost effective at $20,000 each.[158]

Targeted genome editing became much more technically simple with the invention of the TALEN system. Similar to ZFNs, TALENs function in pairs, to create small indels and are composed of a specific DNA binding element fused to a FOK1 endonuclease. The DNA binding element is a transcription activator-like effector from the plant pathogen *Xanthomonas*. Target specificity is determined by approximately 15 'repeat di variable' residues (RVDs), each binding to a specific DNA nucleotide. By engineering the composition of the RVDs, they can be designed to bind to specific DNA sequences. Although still context dependent, TALENs are much more versatile, with binding sites appearing on average every 35bp. Due to the availability of TALEN construction in kit form and their fast assembly (approximately 1 week), TALEN mutagenesis is rapid, cost effective and user friendly.[159]

The CRISPR cas9 technology has recently been introduced as a further genome editing technology. It exploits the CAS systems within prokaryotic organisms that provide them with adaptive antiviral activity. The cas9 protein complexes with the CrRNA (CRISPR RNA), and the trans-activating crRNA (tracrRNA). It then becomes an endonuclease, binding to specific foreign DNA and cleaving it in two. The RNA molecules can be fused together to form a single RNA species, the guide RNA (gRNA). By altering the binding sequence it can be engineered to bind to specific DNA sequences, without the need for changing the cas9 protein complement, allowing targeted binding and cleaving of specific genomic sequences. Its only requirement is a 20bp DNA sequence with a proto-spacer adjacent motif (PAM) site, consisting of 5'-NGG-3'.[160, 161] CRISPRs have the advantage over TALENs that the protocol is even faster and user friendly, the requirement after site selection is to generate an ultramer for the gRNA template and transcribe the appropriate RNA species. It has a generation time of a single day. Although still context-dependent, PAM sites are a frequent feature of all genomes. So where a site is not suitable for TALEN mutagenesis, it will likely contain a PAM site, and vice versa. The drawback of CRISPRs compared to TALENs is

that, as they bind a shorter sequence of DNA, they produce far more off target effects than TALENs. In the context of zebrafish mutations, this is not necessarily a major problem, but any identified allele would need to be outcrossed several times to a WT background.[162] See Figure 4, for an illustration demonstrating TALEN and CRISPR function.

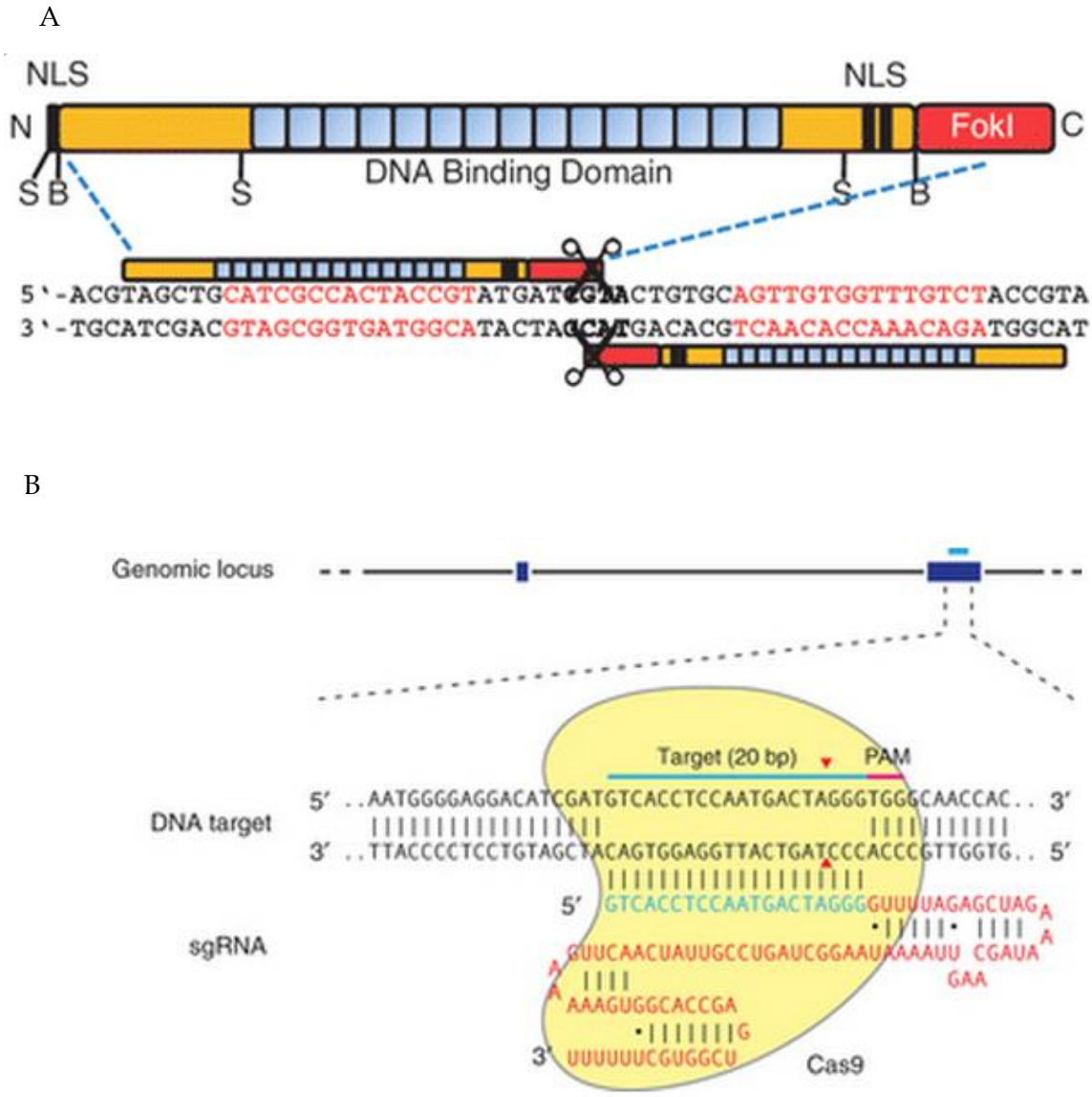

Figure 4. TALEN and CRISPR/CAS9 activity. TALEN cutting (Figure 4A) occurs between the pairs of TALENs in the spacer region. CAS9 (Figure 4B) cuts the DNA helix directly upstream from the PAM site. As TALENs require a larger binding region of 30 bases, they produce less off target background mutations compared to the CAS9 system that only binds to 20 bases. Figures reproduced with permission from Cermak *et al.* and Ran *et al*.[159, 163]

TALENs and CRISPRs have the additional advantage (over ENU screens) of not just causing insertions and deletions, but can also generate targeted point mutations to the genome. By using the genome editor in conjunction with single-stranded DNA

molecules (ssDNA), once the target has been cleaved, the ssDNA can act as a template for homology directed repair. This has been utilised in zebrafish to change single bases, effectively inserting loxP sites and restriction sites into genomic DNA. In the context of modelling PD, this could in theory be utilised to generate toxic gain of function mutations, as seen in human patients, such as the *LRRK2* G2019S mutations, without the need for the generation of transgenic lines.[161]

1.4.3 Zebrafish as a vertebrate model of human neurodegenerative diseases

Zebrafish have been utilised as a model organism for many neurodegenerative diseases, including PD. There are some notable differences between the brains of humans and zebrafish, but the functional organisation remains very similar. The DA neurons that project to the ventral telencephalon in zebrafish are found in the posterior tuberculum of the ventral diencephalon, making these neurons analogous to those seen in the mammalian nigrostriatal system.[164] In zebrafish embryos, the DA neuronal system is established very early, with the first TH-positive neurons emerging 18 hours post fertilisation (hpf). By 3 days post fertilisation (dpf), the DA system is extremely well established and has been well characterised, with comprehensive maps of all TH neuron clusters within the central nervous system (CNS) of both embryos and adults. The small number of neurons and transparency of the embryos allows for simple quantification of the DA system, using markers for TH or DAT. [165] MPP+ studies on embryos and adult zebrafish have induced parkinsonian like phenotypes, including TH neuron loss and movement deficits, further implicating these neuronal clusters as the zebrafish equivalent of the substantia nigra in rodents and humans.[120, 166] Toxin exposure, such as those just described in zebrafish, have the additional advantage that drugs can be simply administered to embryo E3 media, not requiring invasive procedures for administration. The generation of transgenic GFP reporter lines for DA neuronal system, such as DAT, allow for the analysis of DA neuronal death in real time.[167]

Specifically in terms of modelling PD, loss of function studies have been performed using Morpholino KD. Several have been conducted on monogenically inherited PD genes, such as the autosomal recessive inherited genes *parkin, pink1 and dj1,* but also to study the functional consequences of *lrrk2* deficiency. Zebrafish do not possess an orthologue of *SNCA*.

parkin loss of function has been investigated in a study by Flinn *et al.,* who demonstrated that Morpholino KD of *parkin* led to a 25% reduction in TH neurons, and a decrease in mitochondrial Complex I activity at 3dpf, as well as an increased susceptibility to MPP+. Analysis of *HuC* expression (a pan neuronal marker of post-mitotic neurons) and *islet1* (a motor neuron marker) showed no change between morphants and uninjected controls, demonstrating that the effects of *parkin* KD were specific for DA neurons. Swimming behaviour was also unaltered, but this was likely to be due to the comparatively mild TH neuron loss. PD patients only develop motor symptoms after a reduction of at least 50% of their DA neurons. As *Parkin* KO mice do not exhibit neurodegeneration, the *parkin* KD zebrafish represented the first *parkin* deficient vertebrate model of Th neuron reduction.[168]

However, a similar study by Fett *et al.,* found no reduction in TH neurons at the same time point. This discrepancy could be due to different KD efficiencies. [169] *PARK2*-mediated PD is due to loss of function of the protein. Flinn *et al's* Morpholinos achieved a KD of approximately 90%, whilst those utilised by Fett *et al.*, only reduced expression by 50%. Consequently, Fett *et al.,* only induced a representative heterozygous state, which may not be enough loss of *parkin* to induce Th neuron reduction.[168, 169]

dj1 KD in zebrafish resulted in phenotypes similar to KO mice and *Drosophila*. *dj1* KD did not result in loss of TH neurons, but led to an increased sensitivity to oxidative stress after H_2O_2 exposure and proteosome inhibition after treatment with MG132. *Dj1* KD also resulted in a large upregulation of p53. Inhibition of the protein (p53) with phifithrin alpha completely rescued the Th neuron reduction caused in *dj1* morphants by MG132.[134, 135, 170]

Several studies have focused on KD of *lrrk2*, but have presented conflicting data, even when using identical reagents. Sheng *et al.,* originally utilised a start site Morpholino to completely block translation of *lrrk2,* and found morphants to be lethal by 3dpf. The embryos showed signs of developmental delay, small head size and heart oedema, compared to uninjected controls. Sheng *et al.,* also utilised a splice site Morpholino to KD the WD40 domain, in order to produce a weaker phenotype. Morphants developed normally, but showed a decrease in DA neurons and an increase in apoptosis. Morphants additionally had a movement defect that could be rescued by L-Dopa. In contrast to these findings, and using identical reagents, Ren *et al.,* could not record any

change in DAT neuron count or TH neuron count between morphants and uninjected controls. [171, 172]

pink1 loss of function studies have been investigated by three independent groups with a Morpholino strategy, all reporting different phenotypes. KD with start site Morpholinos by Anichtchik *et al.,* exhibited phenotypes of developmental delay, small heads, and gross deformity accompanied by apoptosis. The majority of morphants did not survive past 3dpf. The TH neurons were reduced in number by 30%, compared to uninjected controls, but this may have been due to developmental retardation as opposed to cell death per se.[173]

A KD study by Xi *et al.*, also using start sites Morpholinos, only reported minor deformities in morphants, and a Th neuron reduction of 8% as opposed to 30%. However, the TH neurons showed disorganisation and mispatterning. The KD was also embryonic lethal, with most morphants not surviving to 10 dpf. [174]

Sallinen *et al.*, have also reported *pink1* phenotypes, but using splice site Morpholinos. In sharp contrast to previous findings, the morphants displayed no overt deformity or decrease in TH neuron count. Although morphants did display an increased sensitivity to sub effective doses of MPTP.[175]

The discrepancies between phenotypes in each study are most likely explained by classical p53 mediated off target effects, especially in the study by Anichtchik *et al.,* whose KD features all the main deformities described as off target by Robu *et al*. When one considers the phenotypes of loss of function D*rosophila* and mice, one would expect possibly an intermediate phenotype when using a zebrafish model. Even though *Drosophila pink1* KO have an marked phenotype with reduced lifespan, they still successfully complete development and maturation, unlike the morphants described by Anichtchik and Xi, that are both deformed and are embryonic lethal.[176] Other likely explanations are the use of different Morpholinos, and KD efficacies, each group using different Morpholino sequences. The lack of a significant phenotype in Sallinens *et al.,* study was possibly due to lack of efficacy, many of their TH neuron counts were recorded at 5dpf as the Morpholino was losing effect. Although their study was very thorough in demonstrating that their Morpholinos were non-toxic. The lack of agreement in Th neuron reduction by all groups, may also be due to method of TH neuron counting, Anichtchik counting all TH positive neurons within the brain, Xi *et al.,* counting only those in the ventral diencephalon (using counting clusters for

mispatterning studies) and Sallinen *et al.*, counting only individual TH groups described by Rink *et al*.[165 173-175] See Figure 5 for an illustration of the location of the TH positive groups in Zebrafish larvae counted by Sallinen *et al*., which are the same as those counted as part of this thesis.

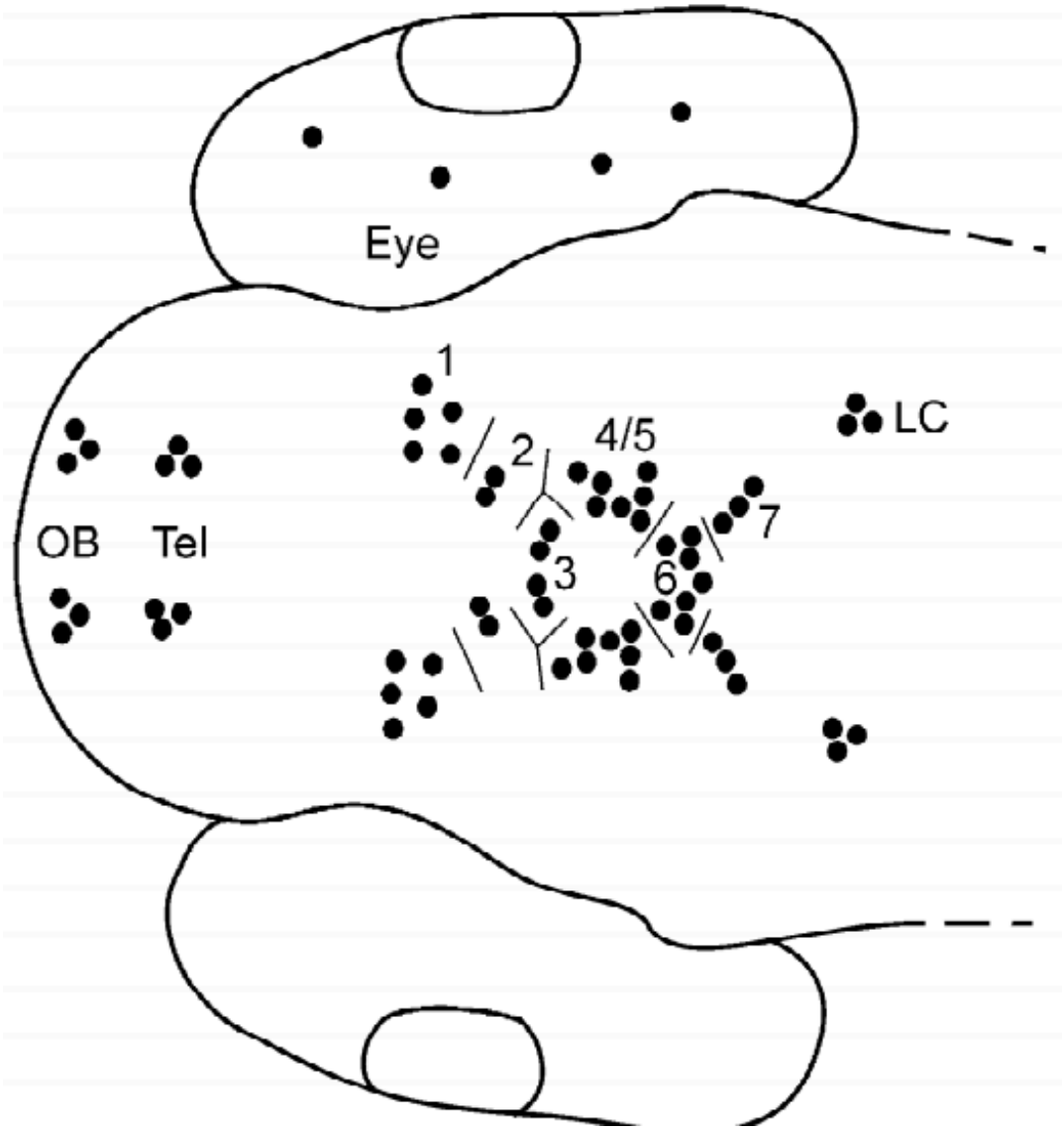

Figure 5. TH positive neuronal groups in 5dpf Zebrafish. TH neuronal groups counted in this thesis as defined by Rink and Wulliman are located in the diencephalon of the zebrafish larva. Only groups I, II, IV and V believed to be analogous to the substantia nigra in humans and thus are only counted during TH experiments in this thesis. Figure reproduced from Rink and Wulliman 2002.

Apart from PD, zebrafish have also been utilised to model Huntington's disease and motor neuron disease. The zebrafish Huntington's model offers many insights, as mouse KO are embryonic lethal, death occurring at embryonic days 7-8. From a reverse

genetics stance, although demonstrating the importance of *Htt* in vertebrate gastrulation, mouse *Htt* loss of function mutants are impractical to study due to the nature of their *in vivo* development. This is not an issue for zebrafish that are transparent and develop *ex vivo*.[177] KD of *htt* in zebrafish resulted in defects in iron homeostasis and iron deficiency.[178, 179]Additional KD studies have shown an aggressive phenotype of a small head, CNS apoptosis, enlarged brain ventricles and a sharp decrease in Bdnf levels (60% decrease). Application of Bdnf protein to morphants ameliorated many of the phenotypes caused by KD of *htt,* demonstrating Bdnf levels strongly influence the *htt* KO phenotype.[180]

As HD mutations are toxic gain of function in nature, Morpholino studies, although useful for understanding protein function, do not model the natural history of the disease seen in human patients. Consequently, over expression studies in zebrafish embryos expressing the poly-glutamine expansions (seen in human patients) are more appropriate. One such study over expressed the N-terminal of Htt containing 102 Q repeats, modelling the Htt expansion seen in HD with the GFP construct, allowing for imaging of polyQ aggregates by fluorescent microscopy in real time. Large cytoplasmic inclusions were detected just after 24hpf which grew larger over time by absorbing soluble Q102-GFP. The model was utilised to test known inhibitors of PolyQ aggregation as a proof of principle, then successfully tested experimental compounds for efficacy.[181]

Zebrafish have also been utilised to model familial forms of *SOD1* linked motor neuron disease, in both loss of function and overexpression models. In the former, a stable T70I mutant was generated from an ENU mutagenesis screen. Homozygous mutants possess decreased Sod1 activity, are sensitive to oxidative stress during development and possess altered neuromuscular junction morphology. Adult mutants develop a 50% reduction in large motor neurons and spend more time moving slower. These fish also spent 20% more time swimming on the bottom of the tank, suggesting an anxiety like phenotype.[182, 183]

In an over expression model developed by McGown and Ramesh *et al.*, a transgenic line over expressing human mutant *SOD1* was constructed adjacent to a Dsred element under the control of an *HSP70* promoter, independent of mutant *SOD1*. Consequently Dsred is only transcribed in the presence of heat shock or cellular stress. In the absence of heat shock, mutant *SOD1* over-expressing lines still exhibited Dsred expression,

specifically in their CNS, implying neuronal stress. Dsred expression was not detected in lines overexpressing WT *SOD1*. This mutant *SOD1* over expressing line model was found to have a decrease in glycinergic currents occurring in spinal motor neurons, changes in neuromuscular junctions and movement defects.[184] Riluzole, a compound utilised to treat motor neuron disease, decreased Dsred fluorescence in lines overexpressing mutant *SOD1*, implying it was decreasing neuronal stress, as a proof of principle. Both models are now being extensively utilised for small molecule chemical screens for motor neuron disease.[182, 184, 185]

1.4.4 Medaka as a model for Parkinson's disease

The Japanese fresh water fish, Medaka (*Oryzias latipes*) extensively utilised in the field of developmental biology, has also been utilised to model PD loss of function mutations. They additionally produce parkinsonian-like phenotypes in response to traditional PD chemical toxins, such as MPTP and MG132. In contrast to zebrafish, only stable mutations have been studied in Medaka in the context of PD. Loss of function alleles have been generated for *pink1*, *parkin* and *dj1*. *pink1 -/-* and *parkin -/-* Medaka have mild phenotypes similar to KO mice. Loss of function *pink1* and *parkin* Medaka develop normally; segregating in a Mendelian ratio, but have a decrease in mass compared to WT at 12 months of age. Both showed a decrease in spontaneous movement in the absence of neurodegeneration. Double mutants also developed normally, reaching adulthood, but showed a decrease in TH neurons of 30%, TH protein levels and a decrease in dopamine in their brains. Their brain tissue also had accompanying mitochondrial dysfunction, with a specific decrease in mitochondrial Complex I and II activity; the organelles were grossly enlarged with fragmented cristae. This data challenges the concept of *pink1* and *parkin* acting in a linear pathway in vertebrates. A *dj1* null Medaka has been generated, but has yet to be characterised.[186-190]

1.5 PINK1

1.5.1 PINK1 function

The initial focus of this thesis was to characterise and investigate gene-gene interactions in a stable loss of function zebrafish *pink1* mutant. Loss of function mutations in *PINK1* leads to early onset PD.[15] Clinically, *PINK1* linked PD manifests in

a similar manner to *PARK2* linked PD, both having an early onset of 18-50 years, a long disease duration (~20 years) and an excellent response to L-Dopa. Symptoms are indistinguishable from idiopathic PD.[191] Genetically, the disease segregates in an autosomal recessive manner, coupled with a large variety of extreme deleterious mutations (exon deletions, nonsense mutations), these mutations are considered to be pathogenic due to a loss of function effect. *PINK1* heterozygous mutations are over represented in sporadic PD cases compared to healthy controls, suggesting they may contribute to disease progression, although this is controversial. [192]

PINK1 linked PD, unlike *PARK2* linked PD, is not a common cause of EOPD, making up between 1-4% of early onset patients, depending on the population; however *PINK1* mutations are still more common than *DJ-1* mutations.[193, 194]

PINK1 is a serine/threonine kinase, additionally possessing a mitochondrial localisation signal, further linking mitochondrial dysfunction to PD pathogenesis.[15] PINK1 is expressed ubiquitously, with higher expression in organs with a large energy demand; namely the heart, muscle and the brain, within which expression is highest in the substantia nigra.[195] Functional studies have demonstrated its role in the mitophagy pathway, among others.[196, 197] PINK1 is believed to function in the same pathway as another PD related protein, the E3 ubiquitin ligase PARKIN, at least in D*rosophila*. However, whether this pathway is linear in vertebrates has been called into question.[190, 198] PINK1 deficiency results in mitochondrial dysfunction with a decrease in mitochondrial membrane potential, a decrease in ATP levels and a decrease in mitochondrial Complex I and IV activites.[199-201]

PINK1 protein is constantly expressed, trans-locating to the mitochondria where it is processed into two forms; firstly cleaved by a matrix processing peptidase to remove the mitochondrial targeting signal to form 60kDa □-MTS –PINK1. The 60kDa form is then cleaved again by PARL (presenilin associated rhomboid like protein) to a 52kDa form in the inner mitochondrial membrane, and finally is completely degraded by the proteosome.[202] Some of the 52kDa PINK1 isoform escapes to the cytoplasm, where it physically binds to, and inhibits PARKIN recruitment to the mitochondria.[203] Cleavage by PARL is believed to be dependant on the mitochondrial membrane potential. [204] When the membrane potential is substantially decreased, full length 60kDa PINK1 is not cleaved and accumulates on the outer mitochondrial membrane (OMM) where it recruits PARKIN. The PARKIN protein then ubiquitinates targets on the membrane,

marking the mitochondrion for recycling by mitophagy.[203, 205] Potential protein ubiquitination targets of PARKIN have been identified on the OMM, including p62, VDAC1, MFN1, MFN2.[206-209] Once ubiquitinated, the mitochondria migrate to the perinuclear area and are degraded by autophagy.[206]

TRAP1, a mitochondrial heat shock protein, has been shown to be a substrate of PINK1. TRAP1 exerts a neuroprotective effect by preventing cytochrome *c* release in the mitochondria. Overexpression of WT TRAP1 rescues *pink1 -/-* defects in D*rosophila* and in cell culture models.[210, 211]

PINK1 appears to have additional functions in maintenance of the mitochondrial network and its dynamics, although data is conflicting depending on the model. *pink1 -/-* D*rosophila* and PINK1 deficient rat DA neuronal cultures both have elongated mitochondria.[212, 213] Conversely, KD in other cell lines such as HELA and SH-SY5Y, produce fragmented mitochondria.[214, 215] Even with these discrepancies, and given its interactions both genetically and physically with many proteins involved in fission and fusion of the mitochondria, namely, DRP1, MFN1, MFN2 and OPA, PINK1 clearly influences mitochondrial dynamics [213, 216, 217].

To analyse the involvement of PINK1 and PARKIN in the mitophagy pathway at the cellular level, many studies rely on toxins such as CCCP that completely depolarise the mitochondrial membrane. This induces irreversible damage and the subsequent destruction of the whole organelle. If damage is only mild, such as in the case of oxidative stress, then the loss of the whole organelle is potentially costly to the cell.[206, 207] An alternative strategy is to remove only the damaged part of the organelle. The damaged section of organelle is identified by PINK1 and PARKIN, through currently unknown mechanisms, and a mitochondrial derived vesicle is generated around the damaged area. This vesicle then directly fuses with lysosomes without the addition of the classical autophagy proteins, see Figure 6.[218]

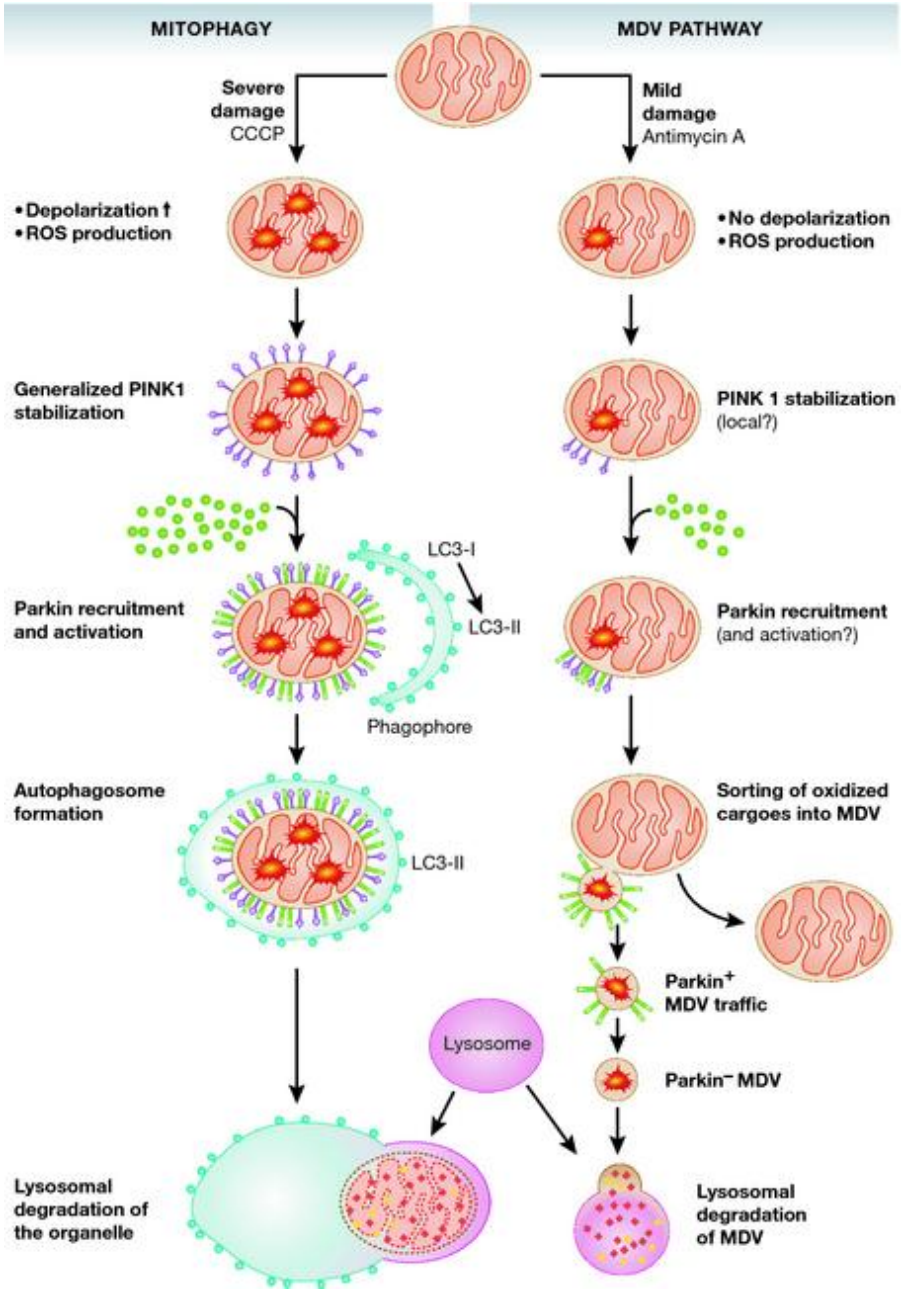

Figure 6. Models of the PINK1 and PARKIN mitophagy pathway. Flow diagram 1 (left) is the classic mitophagy model, severe mitochondrial damage, dissipates the mitochondrial membrane potential stabilising PINK1 on its surface and recruiting PARKIN. Post recruitment, PARKIN then ubiquitinates substrates for destruction, leading to phagophore formation around the damaged organelle (by LC3) and subsequent degradation by the lysosome. Flow diagram 2 (right), a model proposed by Mclelland *et al.*, demonstrates PINK1 PARKIN involvement in response to mild stress. Mild localised stress does not depolarise the mitochondrial membrane. PINK1 somehow localises around the damaged area only, recruiting and activating PARKIN. This somehow leads to the excision of the damaged material only in mitochondrial derived vesicles and subsequent degradation by the lysosomal. Figure reproduced with permission from Shlevkov 2014.[219]

New evidence suggests PINK1 has an active role in the heart and its development. PINK1 is highly expressed in the heart, as well as the brain, most likely due to its high energy requirements and large abundance of mitochondria.[195] In human patients with

end stage heart failure, cardiac tissue has been shown to have a large decrease in PINK1 protein levels (however not transcript levels). The decrease is so large that PINK1 protein was nearly undetectable in some heart failure patients, compared to healthy controls. With age, *Pink1* KO mice begin to develop cardiac hypertrophy, with an average increase in heart to body ratio of 18% by 8 months. Individual cardiomyocytes increased in size by 50%, compared to WT controls, with an absence of an increase in cell number.[220] Mitochondrial analyses in *Pink1* KO mice showed classical mitochondrial dysfunction, such as an increase susceptibility to oxidative stress, a decrease in ATP levels and a decrease in mitochondrial membrane potential. PINK1 function is clearly required for mitochondrial health in cardiac tissue, and not only purely for neuronal health.[220, 221]

1.5.2 Models of PINK1 deficiency

A variety of genetic models were constructed to gain a better understanding of PINK1 function through a reverse genetic approach. Loss-of-function *pink1* flies developed severe and robust phenotypes. These were most obvious in the morphology where mutants have the so-called downward turning wing phenotype and a degenerating thorax. The mutants can walk normally, however, have a decrease in flight ability and slower climbing speeds. Muscle fibres were disorganised and undergo degeneration. Analysis of mitochondria showed swollen organelles with a decrease in ATP levels. Sperm development was also found to be defective (again due to mitochondrial abnormalities) causing male sterility. Phenotypes become worse over time, leading to increase in susceptibility to oxidative stress and also a decrease in lifespan. A modest decrease in TH neurons was reported by two studies, implying neurodegeneration, however were found un-changed in another.[176, 222, 223]

These phenotypes were reminiscent of *parkin* KO *Drosophila* described by Greene *et al.* Overexpressing WT *parkin* on the *pink1* null background partially ameliorated thorax and wing morphological defects. Mitochondrial dysfunction in muscle was also restored with a complete reduction in muscle and TH cell degeneration. Conversely, overexpressing WT *pink1* on a *parkin* null background could not alter any phenotypes. Yang *et al.*, also overexpressed WT *dj1* on a *pink1* null background to also find it did not rescue any phenotypes. [176, 222, 223]

Flies carrying homozygous mutations for both *parkin* and *pink1* do not show a worsening of any phenotypes, with double mutants being indistinguishable from

single mutants. These genetic studies suggest not only *pink1* and *parkin* to be in the same linear pathway, but that also *parkin* acts downstream of *pink1*. In contrast, recent studies undertaken in vertebrates have challenged this concept.[176, 190, 222, 223]

Pink1 KO mice only develop very mild phenotypes compared to *pink1* KO D*rosophila*. Homozygous mutant mice generated by homologous recombination developed a 20% decrease in mass at 1 year. By 1.5 years they exhibited a decrease in spontaneous movement. Measurements of strength and anxiety remained unchanged compared to WT. Complex behaviours such as the acoustic startle-response was also identical between the mutant and WT.[199]

Although a significant decrease in dopamine was recorded in aged PINK1 deficient mice, there was a complete absence of TH cell loss. Although neuronal cell loss could not be detected, mitochondrial dysfunction was present, with decreases in ATP levels and reduced mitochondrial Complex activities.[129, 199, 224] Due to the lack of TH cell loss in single *Pink1, Parkin* and *Dj1* KO mice, a triple KO was made to explore any genetic interactions. Triple KO mice also displayed no gross deformity and exhibited no neurodegeration.[129] These data imply that PINK1 may confer a protective mechanism as opposed to it being required for maintenance of neuronal health, at least in mice.[129, 199]

pink1 deficient Medaka fish, containing a premature stop codon, have also been characterised. The stop codon results in a decrease in *pink1* transcript, most likely due to nonsense mediated decay, demonstrating loss of function. In keeping with mice, *pink1* KO Medaka develop normally, showing no gross morphological changes and exhibit a reduction in mass compared to WT at late stages (12/18 months). Unlike *Drosophila*, no defects in sperm, muscle or mitochondria could be identified. Similar to KO mice, *pink1* mutant Medaka show altered dopamine metabolism and a decrease in spontaneous movement, however in the absence of neurodegeneration. Medaka double mutants (KO for *pink1* and *parkin*) synergistically display a decrease in DA neurons, this conclusion arguing against *pink1* and *parkin* functioning in a linear pathway, at least in vertebrates. [188, 190]

1.5.3 p53-Inducible Regulator of Glycolysis and Apoptosis (TIGAR)

The initial focus of this study was the further characterisation of a loss of function *pink1* zebrafish model, including the investigation of gene-gene interactions. A gene of

interest for further study in the model was *tigarb*, an orthologue of the human gene *TIGAR* (p53-Inducible Regulator of Glycolysis and Apoptosis). *Tigarb* was identified through an unbiased genome wide expression study as it was shown to be significantly upregulated in *pink1 -/-* 5dpf larvae compared to their WT siblings.[201]

The p53 protein, a highly researched protein in cancerous mechanisms, possesses a broad range of functions that ultimately allow it to prevent tumour progression by reducing cellular stress.[225, 226] In a further study to understand p53 responsive genes, a microarray analysis following p53 induction identified several of these elements. One of these, uncharacterised at the time, was *TIGAR*.[227] The genomic structure of *TIGAR* is highly conserved across all vertebrates (mammals, birds, fish, amphibians etc), and is noticeably absent from invertebrates and other forms of complex life. The *TIGAR* sequence contains two separate p53 binding sites in humans, although only one is conserved in mammals, and codes for a protein of 30kDa. Its expression is rapidly induced, in a variety of difference cell lines following p53 induction by Adriamycin treatment. This p53 induction is believed to be only in response to mild repairable cellular damage, as chronic induction with high cellular stress leads to constant p53 upregulation. This will induced TIGAR upregulation. However after initial upregulation, *TIGAR* expression falls rapidly, whilst p53 induction remains constant. This implies TIGAR may be part of a molecular switch for p53 controlling its complex functions in response to different forms of stress.[228] *TIGAR* additionally possesses p53 independent induction, as cells lines not expressing p53, will still express *TIGAR* at basal levels.[228]

TIGAR function was elucidated due to its homology to the glycolytic enzyme 6-phosphofructo-2-kinase/fructose-2,6-bisphosphatase (PFK-2/FBPase-2).[228] PFK-2/FBPase-2 has the dual function of both kinase and bisphosphate activity, with the TIGAR protein only sharing homology to the bisphosphatase domain. Bensaad *et al.*, demonstrated that the function of TIGAR is to degrade fructose-2,6-bisphosphate to fructose-6-phosphate.[228] The former is a potent effector of 6-phosphfructo 1-kinase, a glycolytic stimulator. Fructose-2,6-bisphosphate additionally functions as an inhibitor of fructose-1,6-bisphosphatase, a gluconeogenic regulator.[229] By reducing levels of fructose-2,6-bisphosphate, degrading it to fructose-6-phosphate, TIGAR functions to inhibit glycolysis, see Figure 7.

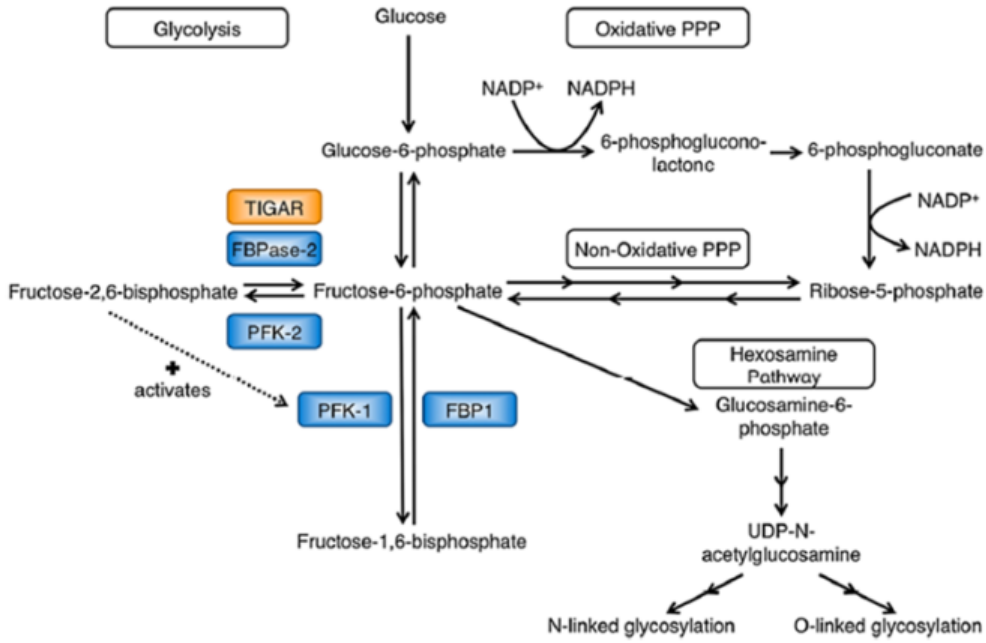

Figure 7. The metabolic pathways affected by enzymatic TIGAR function. Fructose-2.6-bisphosphate is converted to Fructose-6-phosphate, preventing allosteric activation of PFK-1.This in turn, diverting metabolism towards the pentose phosphate pathway and Hexosamine pathway. This not only lowers oxidative stress, but also provides materials for DNA repair. Reproduced with permission from Lee 2014.[230]

This inhibition leads to a diversion of metabolism towards the pentose phosphate pathway, causing not only a decrease in oxidative stress, but also a decrease in apoptosis.[228] Although TIGAR substrate specificity has recently been challenged by Gerin *et al.*, who demonstrated TIGAR has a far greater affinity for 2,3 bi-phosphoglycerate (23BPG), than for fructose-2,6-bisphosphate, the concept of TIGAR thus acting as a 23BPG phosphatase would actually increase glycolytic intermediates as opposed to inhibiting them. This new function of TIGAR calls into question its primary mode of action as a glycolytic inhibitor, or at least suggests its functions are more complex than first perceived. [228, 231]

Overexpressing TIGAR has been discovered to lower levels of ROS in response to chemical stress, metabolic, stress or starvation, as well as basal levels of ROS. The KD of TIGAR will increase levels of ROS under all previously described conditions. However, as basal levels of ROS represent important cellular signalling, processes such as autophagy can also be affected by TIGAR manipulation.[232, 233] Indeed, *TIGAR* KD was shown to robustly induce autophagy, not only in unstressed cells, but also those subjected to starvation or metabolic stress, whilst over expression of *TIGAR* was found

to reduce autophagy. Additionally, *TIGAR* KD stimulates autophagy even in p53 null cell lines, indicating p53 is not required for modulation of autophagy by TIGAR.[232]

DRAM, also a p53 responsive gene, functions in promoting autophagy. The increase in autophagy after *TIGAR* KD was found not to be effected by DRAM status, showing that both p53 responsive genes do not work in concert to manipulate autophagy pathway. TIGAR modulation of autophagy was demonstrated to be mTOR independent, as KD did not lead to a change in the down-stream targets of mTOR.[228]

The function of TIGAR to limit ROS has been demonstrated in cancer cell lines; when under hypoxic stress, a proportion of TIGAR relocates to the outer mitochondrial membrane. Stabilisation of Hypoxia-inducible factor 1-alpha (HIF1□) by small molecules such as DMOG also relocated TIGAR to the outer mitochondrial membrane. TIGAR's translocation was dependant on glucose and Hexokinase 2 (HK2), as depletion of both removed the re-localisation. TIGAR was found to bind exclusively to HK2 but not HK1, which can also bind to the OMM. TIGAR physically binding to HK2 enhances its activity (without altering TIGAR expression). The binding is retained by TIGAR, even in mutants without an FBPase-2 domain.[234] Mitochondrial localisation and HK2 binding is dependent only on 4 amino acids (human residues 258-261), and that co-localisation under hypoxia was shown to be HIF1□ dependant, as inhibition of HIF□ prevents relocation of TIGAR.[234] Furthermore, enhancing HK2 activity lowers ROS and cell death.[234] HK2 KD prevented TIGAR over expression to reduce ROS formation, mostly likely as it is required to maintain the mitochondrial membrane potential.[234, 235] This action appears to be cell type dependent as in cardiomyocytes; hypoxia causes a p53 dependant increase in *TIGAR* expression. Over expression of *TIGAR* increased apoptosis after hypoxia induction. Conversely KD of *TIGAR* was found to rescue the mitochondrial membrane potential and prevent apoptosis after hypoxic induction.[236]

Three KO mouse models have been constructed to understand the function of *Tigar in vivo*. In a similar manner to *p53* KO mice, *Tigar* KO mice develop normally and do not exhibit morphological defects. Homozygous mutants are viable, live to adulthood, with genotypes segregating in a Mendelian fashion.[237, 238]

As expected, *Tigar* KO shows an increased level of Fructose-2,6-bisphosphate in keeping with human cells. Expression *in vivo* showed *Tigar* to be highly expressed in the intestines of WT animals. Although crypt architecture was identical between both

genotypes, following toxin ablation, *Tigar* KO showed a decrease in size and number of regeneration within their crypts. Analysis of WT tissue showed a marked upregulation of *Tigar* 24-72 hours after toxin exposure, indicating that *Tigar* is required for proliferation of tissue during regeneration, likely due to its capacity to generate nucleotides and antioxidants required for growth.[237]

Conversely, *Tigar* deficient mice have been shown to be more protected in a model of ischemic injury. *Tigar* KO mice develop an increase in autophagy markers at sites of ischemic injury, phenocopying *p53* null mice. Both KO mice showed a reduction in build-up of defective mitochondria. Although, PARKIN was found to not translocate to the mitochondria during metabolic stress, in *P53/Tigar* KO animals there was a marked activation of BNIP3 that initiates autophagy as well as mitophagy during hypoxia. Consequently TIGAR may inhibit BNIP3 and indirectly inhibit mitophagy if over expressed.[232, 238]

1.5.4 Von Hippel-Lindau and hypoxia

The second phase of the *pink1* project involved the investigation of gene-gene interactions between *pink1* and *vhl* (Von Hippel-Lindau), loss of function mutations which lead to specific cancers.

As described above, *pink1 -/-* zebrafish exhibit an upregulation of *tigarb*, an inhibitor of glycolysis, implying a reduced glycolytic flux. In contrast, *vhl -/-* zebrafish exhibit an upregulation of glycolytic genes implying an enhanced glycolytic flux, common in many cancers. It was hypothesised that crossing these lines together, generating zebrafish homozygous for both *pink1* and *vhl* mutations, would normalise their glycolytic pathways and may lead to a rescue of phenotypes seen in *pink1* and *vhl* -/- larvae.

VHL disease is an autosomal dominant inherited disorder, caused by mutations in the *VHL* tumour suppressor gene. Patients carry heterozygous mutations and only develop tumours when the WT allele is mutated by exogenous mechanisms. Once both alleles have been mutated causing loss of function that leads to upregulation of many pathways involved in hypoxic signalling. The most commonly associated tumours with VHL disease are haemangioblastomas of the retinal and central nervous system, renal cell carcinomas and pancreatic islet tumours. Renal cysts can also develop, however are benign in nature and do not compromise organ function.[239]

The *VHL* gene codes for a 231 amino acid protein ($pVHL_{30}$) and a smaller $pVHL_{19}$ which is missing amino acids 1-53. A large variety of disease causing mutations have been described, however the majority (40%) consist of large deletions due to *alu* mediated recombination.[240] VHL is an E3 ubiquitin ligase and tumour suppresser with multiple complex functions; its main role appears to be in hypoxic signalling. Under normoxia, VHL constantly binds to the alpha subunits of HIF1a and HIF2a, marking them for degradation. Oxygen is required for the modification of HIF1 and HIF2 by PHD (prolyl hydroxylase) enzymes, which allows VHL to bind them. Under hypoxic conditions, as oxygen is unavailable for this reaction, HIF1 and HIF2 remain un-modified, and so VHL is unable to bind to them, allowing for their stabilisation. Once stabilised, they are able to act freely as transcription factors, leading to the transcription of a vast array of hypoxic responsive elements, promoting angiogenesis.[239, 241] In the absence of viable VHL, HIF1a is continually stabilised allowing for the transcription of its target genes, and hence dysregulation of hypoxic signalling occurs, making the cell act as if it is hypoxic even when it has the full requirement of oxygen.[241] See Figure 8.

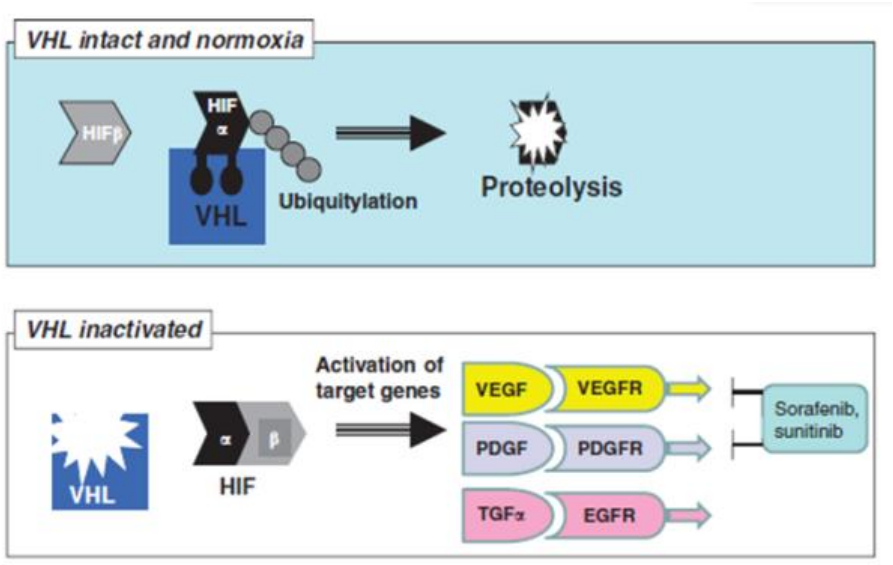

Figure 8. VHL and hypoxic signalling. The activity of VHL in response to oxygen levels within the cell. Under normoxia VHL continually binds to HIF1α marking it for degradation. During hypoxia, VHL is unable to bind to HIF1α HIF1α can then bind to HIF1β, and acts as a transcription factor for hypoxia responsive genes. Figure reproduced with permission from Maher 2010.[239]

Vhl homozygous mutations are embryonic lethal in mice. Consequently, as it develops *ex vivo*, the zebrafish has successfully been utilised to model VHL deficiency *in vivo*, through development. Microarray studies on the *vhl -/-* mutants demonstrate an upregulation of many genes involved in anaerobic metabolism (such as the glycolytic pathway), oxygen sensing, oxygen transport and angiogenesis, generating a robust

hypoxic response. Functionally, this leads to an increase in VEGF signalling leading to polycythaemia, increased blood flow and disorganised branched blood vessels in the vascular network. The vessels become leaky, which in the eye, where the vascular network is vastly increased, leads to retinal lesions and in some cases, retinal detachment from the neuronal layers. This is very suggestive of macular oedema which can also be observed in human patients with VHL disease. The *vhl* –/- zebrafish eventually begin to hyperventilate and although mature through the stages of development, die at 10dpf due to oedema.[242, 243]

1.6 Glucocerebrosidase 1

1.6.1 Gaucher's disease

The third part of this thesis concentrated on establishing loss of function models of zebrafish for Glucocerebrosidase (*gba1*) using KD/KO strategies and to assess if the zebrafish is a suitable model of *gba1* deficiency.

GBA1 is a lysosomal enzyme required for the conversion of Glucocerebroside (otherwise known as Glucosylceramide) to ceramide and glucose (see Figure 9), mutations in its gene present with Gaucher's disease (GD), a lysosomal storage disorder.

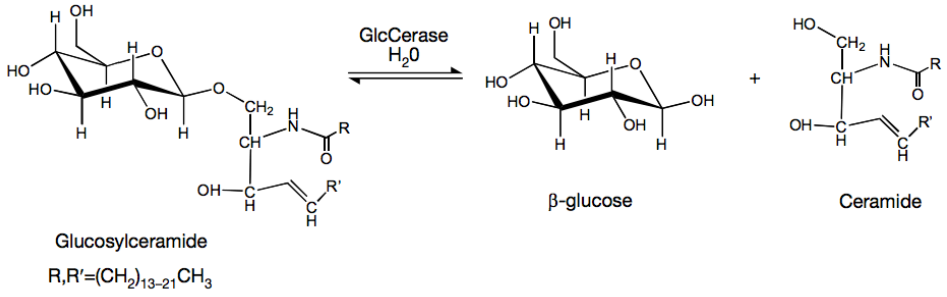

Figure 9. The GBA1 catalysed chemical reaction. GBA1 catalyses the conversion of Glucocerebroside (Glucosylceramide) to Ceramide and Glucose.

The *GBA1* gene is located in a highly gene-rich region within the human genome comprised of 7 genes and 2 pseudo genes within an 85 kb region located on human chromosome 1. Due to a duplication event, (present before the diversion of humans and primates) both *GBA1* and the nearby mitochondrial import gene *Metaxin* have very homologous pseudo-genes. The *GBA1* pseudogene possesses a 96% homology to

GBA1, but contains a 55bp deletion within exon 9, that can be utilised for diagnostic purposes.[244] The gene has two in frame ATG start sites producing polypeptides of different lengths which are both post-translationally processed to yield a 497 residue mature enzyme. *GBA1* is expressed ubiquitously in all tissues in a similar fashion to a housekeeper; however GBA1 enzyme activity rarely correlates with transcript levels.[244, 245]

So far, over 300 *GBA1* mutations have been reported, the majority being missense mutations (80%), but also nonsense mutations, splice site mutations and small indels producing frameshifts. The majority of *GBA1* mutations are found in exons 8 and 9, but they have also been observed in all other *GBA1* exons.[244] The presence of the pseudogene and its 55bp deletion, are also the cause of both reciprocal and non-reciprocal recombination events, termed complex alleles representing a distinct and significant portion of GD mutations. Despite the severity of certain mutations, there is a poor correlation between genotype and clinical presentation with the exception of the N370S and L444P mutations that more commonly give rise to types I and II GD respectively. The L444P and N370S mutations are the most prevalent, making up around 70% of cases either in a homozygous or compound heterozygous state.[244, 246]

Bi-allelic mutations in *GBA1* lead to GD, the most common lysosomal storage disorder with a prevalence of approximately 1/100,000.[247] The disorder presents with heterogeneous symptoms, giving rise to three subtypes, although this is increasingly viewed as a continuous spectrum.[92] Type 1 GD is based on the absence of neurological symptoms, making up 90% of all GD cases. It presents with highly variable symptoms, many patients can go undiagnosed for years as they appear almost asymptomatic. Common features in type I include anaemia, thrombocytopia, organomegaly and osteoporosis. Patients are also at a higher risk of certain cancers such as non-Hodgkin's lymphoma.[92, 93, 248, 249]

Type II GD, also known as neuropathic GD, leads to early death, approximately 9 months after birth due to neurological decline which is rapid and patients may also present with seizures and hypertonia. Progressive hepatosplenomegaly and other symptoms such as apnoea, cachexia and growth arrest also occur. A subset of patients (known as collodian babies), are born with congenital ichthyosis, with death occurring shortly after birth. Type III GD, also neuropathic in nature, is a chronic progressive form of the disease, presenting in childhood to adolescence. Symptoms range from

neurological decline with seizures, horizontal supranuclear palsy, and hydrocephalus to mild hepatosplenomegaly and cardiac valvular involvement.[92, 250-252]

Although type I GD has always been categorized as a non-neuropathic form of the disease, this has been brought into question with many type I patients presenting with PD in later life.[253]

Effective treatment is available. Enzyme replacement therapy (recombinant GBA1) is extremely effective at treating the majority of symptoms. However, enzyme replacement therapy is not a suitable treatment for type II or type III GD, as recombinant GBA1 does not cross the blood-brain barrier.[254, 255]

Glucocerebroside is a key component of sphingolipid metabolism in the salvage pathway which provides up to 80% of the cells ceramide requiements.[256] All *GBA1* mutations lead to partial if not complete loss of enzyme activity, leading to substrate accumulation of glucocerebroside and glucosylsphingosine within lysosomes. Due to the large lysosomal content of macrophages, the cells become engorged, the lysosomes pushing their nuclease to the side of the cell membrane. Within the cell the cytoplasm appears to possess many crinkles and striations. This has classically been described as a "wrinkled tissue paper" appearance. The swollen cells, known as "Gaucher cells" are highly activated macrophages, and congregate in particular organs leading to hepatosplenomegaly. Any cell of a mononuclear phagocyte lineage may be affected in this fashion, including kupffer cells (present in the liver), osteoclasts (present in bone) and microglial cells (present in the CNS). The latter microglial cells although don't directly cause disease; increase severity judging from conditional mouse models.[128, 257]

Gaucher cells secrete many chemokines, such as Interleukin-1β, that are elevated in the plasma of GD patients. Chitotriosidase, a human chitinase, a marker of activated macrophages, is markedly upregulated in its activity in GD patients' plasma. Indeed, it is utilised as a GD biomarker for evaluating efficacy of enzyme replacement therapy.[258, 259]

1.6.2 Models of *GBA1* deficiency

Drosophila possess two orthologues of *GBA1* too close to each other to create a chromosome with mutations in both genes with standard techniques. By simple molecular manipulation, animals with heterozygous mutations in both genes have been created (double hets). These mutant flies show a 30% decrease in Gba1 activity

and demonstrate activation of the unfolded protein response. Survival from larvae to adult is reduced by 50% compared to WT. Transgenic flies expressing either human WT *GBA1*, N370S or L444P mutations show further activation of unfolded protein response (UPR) compared to WT. Both mutant transgenic and double het flies show a decrease in flight capacity, with large reductions in climbing activity of up to 80% by 22dpf.[260]

The first *Gba1* KO mouse models constructed, possessed a neomycin resistance cassette inserted between exons 9 and 10. GBA1 activity in homozygous mutants was reduced to 4% of WT. All homozygous mutants were underweight, exhibited abnormal respiration and died within 24 hours of birth. Gaucher like cells were detected in the liver, spleen and brain, the phenotypes strikingly similar to type II GD collodian babies.[261]

As most human patients still retain some residual GBA1 activity, in order to more faithfully model the disease, mouse models were generated that possessed mutations seen in humans (L444P and RecNcil). The L444P mutation is one of the most common found in patients, whilst RecNcil is an example of a complex recombination allele genotyped using the *NciI* restriction enzyme. L444P mice retained 20% residual GBA1 activity, whilst RecNcil only had 4%. Both homozygous mutants all died 24-48 hours after birth. They would not feed and possessed very red dry skin. Glucocerebroside accumulation was detected in the skin of both mutants, however substrate accumulation in the brain could only be detected in the RecNcil mutant.[262]

Mice carrying *Gba1* point mutations seen in human patients have also been generated, including N370S, D409H, D409V and V394L. N370S homozygotes died during the neonatal period. All other mutants retained only 25% enzyme activity compared to WT, but did not model the disease, as all were viable and did not accumulate glycolipids in the brain. [263]

As KO mice develop such severe phenotypes that make study impractical, conditional KO were generated to analyse *Gba1* loss of function in particular organs. Enquist *et al.*, generated a conditional KO mouse that was a KO in all organs apart from the skin, the K14-lnl/lnl. K14 mice had a reduction in GBA1 activity by 95% and accumulated glucocerebroside in the brain, liver and spleen. Unlike complete KO mice, K14 mice are viable during the first week of life, however, after a symptom free period of ten days, they undergo rapid neurological decline. They develop abnormal gait and experience

motor dysfunction and seizures. K14 mice all had to be culled at 2 weeks of age due to excessive seizures leading to end stage paralysis.[128]

K14 brains contained a large reduction in neuronal cells as well as cellular density. Large neurons were surrounded by microglial like cells, many containing large vacuoles most likely due to substrate accumulation. K14 brains had increased caspase 3 and TUNEL staining, showing neuronal cell loss due to cell death, as well as microglial activation and astrogliosis. Conditional KO mice that retained GBA1 activity in skin and microglia (Nestin mice), develop phenotypes identical to the K14 mice, however, symptoms only start to appear a week after K14. Suggesting *Gba1* status in microglia effects disease duration as opposed to driving the primary pathology. From these mouse models it is clear that GBA1 activity is critical for neuronal survival.[128]

Other conditional mouse models have been constructed for other organs excluding neuronal tissue. Mistry *et al.,* constructed a conditional mouse KO that is *Gba1* null in all tissues of hematopoietic and mesenchymal lineages, reducing GBA1 activity in these tissues to 5% of WT activity. Although these mice were viable, they developed marked substrate accumulation of glycolipids in their liver and spleen (approximately 30 fold), similar to human disease. The *Gba1 -/-* mice display classic gibbus formation, hepatosplenomegaly and anaemia. Spleen size rising to 8 fold that of WT. Mutant mice go on to develop Gaucher cells, invading organs such as the bone leading to severe osteopenia.[264]

1.6.3 Glucocerebrosidase and Parkinson's disease

Interest in *GBA1* mutations has significantly increased in the biomedical field since the discovery that heterozygote *GBA1* mutations are a risk factor for PD and dementia with Lewy bodies. [8, 93, 265]

The association was first detected when it was noted that there was an over representation of PD in patients with type I GD, previously considered to be the non-neuropathic form of GD.[253] Type I GD is not 100% penetrant when assessing patients on traditional symptoms such as organomegaly. To assess for an association between GD type I and PD, sporadic PD patients were screened for *GBA1* mutations in Ashkenazi Jewish populations, as this population has unusually high incidence rates of both diseases. Of 99 patients screened, 30% carried a *GBA1* mutation, compared to only 5% of the controls. The vast majority of the mutation carriers were only heterozygous

for the common *GBA1* mutations implying that heterozygosity on its own may be a risk factor for PD.[266] Large scale screening studies have confirmed this association, making *GBA1* mutations the most common risk factor for PD. *GBA1* mutations have also be found to additionally be the most common risk factor for dementia with Lewy bodies.[102]

However, it has also been suggested that these mutations may in fact not be a risk factor, but actually a cause of autosomal dominant PD with lower penetrance.[267] The OR for gene mutations is approximate 5-15 depending on the population, meta-analysis have deduced OR of 3.51.[102] This OR is likely to be higher in reality as, due to practicalities, the majority of studies only screen for common *GBA1* mutations of N370S and L444P, which make up 70% of cases. This therefore will not identify the 30% of patients carrying one of the 300 recorded *GBA1* mutations.[93, 244]

Few functional studies have yet to be carried out on how *GBA1* mutations could lead to PD, reports mainly implicating SNCA interactions as a driver of pathology, however GBA1 deficiency may be even more key to PD than originally thought, due to the discovery that even PD patients without *GBA1* mutations display a decrease in GBA1 activity in brain tissue.[268]

1.6.4 GBA1 pathology due to loss of function mutations

The role of GBA1 in the development of synucleinopathies is poorly understood, with many questions remaining. Models have been put forward for both toxic gain of function, loss of function or a synergy of the two.[269]

Although a variety of *GBA1* mutations have been catalogued, thus far, no GD patients have been recorded that possess large deletions and exonic rearrangements, that are present in classic loss of function autosomal recessive inherited forms of disease such as *PINK1* and *PARK2* disease. The exceptions to these are patients containing complex alleles due to recombination with the pseudo gene. These have only been found in homozygous form in patients that are stillborn neonates. Complex alleles have been found in compound heterozygosity with other more common GD alleles, however, these also tend to present perinatal-lethal GD. As common *GBA1* mutations have been shown to cause a partial decrease in enzyme activity, this and KO mice would imply that complete loss of function of GBA1 in humans is incompatible with life. The

remaining disease genes could potentially be viewed as hypo-morphs or partial loss of function.[270, 271]

KO Mouse models of *Gba1* lead to rapid neurodegeneration, however, the effect of *Gba1* heterozygous mutations on neuronal health have yet to be investigated *in vivo*. In neuronal cell culture, complete loss of GBA1 activity by CBE (conduritol b epoxide , a specific GBA1 inhibitor) inhibition had no effect on cell viability, and did not affect basal levels of ATP, mitochondrial membrane potential or mitochondrial Complex activity; however GBA1 inhibition did lead to SNCA accumulation. This was complemented by inhibition of GBA1 by a KD.[272] A separate study by Manning-Bog *et al.*, also confirmed CBE inhibition of GBA1 to be sufficient to lead to SNCA accumulation in the absence of a change in SNCA transcript levels.[273]

The latter study assessed complete loss of function as seen in GD and not partial loss of function as seen in *GBA1* heterozygous mutations linked to PD. A study by Mazzulli utilised a KD approach to assess partial loss of GBA1 function on SNCA levels. GBA1 protein levels were reduced by 50%, leading to accumulation of glucocerebroside in the absence of neurotoxicity although lysosomal dysfunction was evident. Notably, this decrease in GBA1 protein led to an accumulation of SNCA in the absence of a change in transcript levels, suggesting protein aggregation. This data was confirmed using iPS neurons derived from GD patients fibroblasts, which also accumulated SNCA.[274]

The indirect consequences of GBA1 deficiency were also analysed with respect to SNCA accumulation. GBA1 substrates which accumulate upon GBA1 loss of function were found to increase SNCA aggregation *in vitro*. The same study also demonstrated that overexpression of WT SNCA prevented proper folding and transport of GBA1 in the endoplasmic reticulum. This reduced GBA1 protein levels and therefore GBA1 activity even further. Consequently, this suggests SNCA and GBA1 work in a bi directional feedback loop. Loss of GBA1 activity increasing SNCA levels *in vivo*, due to glucocerebroside induced aggregation. SNCA in turn preventing correct GBA1 folding and maturation in the lysosome, decreasing activity further. This demonstrates how loss of GBA1 activity may be a unifying pathogenic mechanism in PD. In patients without *GBA1* mutations there is SNCA accumulation in the form of Lewy body pathology. This could interfere with correct GBA1 processing leading to a decrease in GBA1 activity and subsequent increase in GBA1 substrates and further SNCA accumulation.[274]

This was demonstrated in a study by Gegg *et al.*, where brain tissue of patients with sporadic PD was analysed for GBA1 activity. Patients who did not possess *GBA1* mutations still had a decrease in GBA1 activity in different parts of their brain, especially the substantia nigra. This was accompanied by a decrease in GBA1 protein levels but not of the mRNA transcript levels, demonstrating that a decrease in GBA1 activity was a post transcriptional effect and not simply a downregulation of GBA1. [268]The study confirmed findings from Mazzulli *et al.*, that overexpression of SNCA reduces GBA1 protein levels but not transcript levels. [268]

Lowered mitochondrial Complex I activity is an important pathogenic mechanism observed in both sporadic PD and familial subtypes. Of note, decreased Complex I activity also reduces GBA1 activity. KD of *PINK1* produces mitochondrial dysfunction and oxidative stress in a neuronal cell culture system. Gegg *et al.*, also demonstrated it to decrease GBA1 protein levels and subsequent activity in these *PINK1* deficient cells.

SCNA accumulation following GBA1 deficiency has been recently challenged by Dermentzaki *et al*. Using CBE a at a range of concentrations, they could not detect SCNA aggregation and dysfunction of lysosomal or autophagy pathways.[275]

1.6.5 Toxic gain of function

Evidence for toxic gain of function has been highlighted through overexpression of different mutant *GBA1* constructs leading to accumulation of SNCA compared to WT in several different cell lines. Cullen *et al.*, analysed SNCA levels after overexpression of WT *GBA1*, GD associated *GBA1* mutations and loss of function *GBA1* mutations within neuronal cell culture systems. WT overexpression had no effect on the levels of SNCA, whilst overexpression of GD associated alleles N370S, D409V, L444P and D409H all increased the levels of SNCA. L444P and D409H, producing the most robust increase, with SNCA levels rising to 170% and 248% respectively to that of WT, notably without the activation of the unfolded protein response.[276]

Transgenic approaches using *Drosophila* overexpressed the human *GBA1* and the GD mutant allele RecNciI under the promoter of specific GAL 4 lines which expressed the transgenic protein in the eye cells of the *Drosophila*, including certain photoreceptor neurons and pigment cells. WT *GBA1* developed minor phenotypes, slightly affecting eye morphology. Overexpression of the mutant GD allele RecNciI led to severe rough eye phenotype, this occurred with large differences in sizes of the ocelli in transgenic

flies compared to controls. Mutant transgenic flies also show up regulation of markers indicative of ER stress.[277]

Analysis of mice heterozygous for either *Gba1* KO allele compared to point mutation mice, D409V demonstrated that *GBA1* mutations linked to PD may be toxic gain of function as at 6 months of age since *Gba1* -/+ D409V mice develop ubiquitinated SNCA deposits within their brains. Mice -/+ for *Gba1* null alleles do not develop any such pathology at the same time point, regardless of the fact that both alleles possess the same amount of residual GBA1 activity.[278]

In animal models, it has been demonstrated that overexpression of complex *GBA1* mutation alleles (RecNcil) in *Drosophila* lead to neurodevelopmental defects and endoplasmic reticulum stress (ER) compared to overexpression of WT *GBA1* alone.

1.6.6 GBA1 unfolded protein response and mitochondrial dysfunction

Secondary explanations of pathogenicity revolve around the unfolded protein response (UPR). To prevent misfolded proteins damaging cell homeostasis, they are recycled via endoplasmic reticulum associated degradation (ERAD). This occurs through ubiquitination, followed by degradation by the proteosome.[279] Under normal conditions GBA1 assembles in the ER and is then shuttled to the lysosome. Mutant GBA1 fails to fold properly and is ubiquitinated for degradation. Several E3 ubiquitin ligases have been identified that recognise mutant GBA1, namely PARKIN and ITCH, although the involvement of PARKIN has recently been questioned.[260, 280, 281] GBA1, being constitutively expressed, will cause mutant GBA1 to be constantly turned over activating the UPR, potentially overwhelming E3 ubiquitin ligases. This results in the neglect of their other substrates, leading to ER stress. Clearly UPR activation and ER stress would impact on SNCA turnover, likely leading to its cellular accumulation. Indeed, UPR activation has been detected in GD and GBA1 mutation carrying fibroblasts, as well as in fly models.[260, 280, 282] Conversely, UPR activation has not been seen in other models, such as brain tissue from neuropathic mouse models, and neuronal cultures treated with CBE.[128, 283] Clearly, the relationship between SNCA and UPR in the context of GD and Parkinson's related *GBA1* mutations requires further evaluation.

Mitochondrial dysfunction has also been suggested to explain how *GBA1* mutations may lead to PD. *GBA1* KD or inhibition via CBE, in fibroblasts leads to an increase in

ROS levels, a decrease in mitochondrial membrane potential, a decrease in ATP levels and fragmented mitochondrial network. The mitochondrial dysfunction observed in *GBA1* deficient fibroblasts is therefore very similar to those seen in *PARK2* mutant fibroblasts.[272, 284] Using primary neuronal cultures from the previously established neuropathic conditional *Gba1* KO mouse, Osellame *et al.* demonstrated defective autophagy and UPS breakdown, resulting in ubiquitinated aggregates and SNCA accumulation. Mitochondrial Complex 1 defects, increased ROS and fragmented mitochondria were also observed, similar to Cleeter *et al*. The dysfunction was revealed to be a defect in PARKIN recruitment to the OMM. [272, 285]

1.7 AIMS AND OBJECTIVES

Ultimately both projects were to establish whether the zebrafish could firstly model the human disease pathology and to identify benefits they would have over existing models of PD and GD. If the specific mutant suitably modelled the disease course in humans, the model in question could be used for further scientific analysis. Specifically genetic interactions and rescue experiments to identify new drug targets for both diseases and potential new protein functions.

Objectives for each project were as follows,

pink1

1. Further analyse mutant phenotypes in greater depth.

Identifying movement defects that are similar to PD motor symptoms exhibited by human patients. Evaluate the cause of the decrease in TH neurons in the *pink1 -/-* larvae.

2. Identify genetic interactions in *pink1 -/-* larvae.

To identify potential rescue mechanisms, up-regulated transcripts in *pink1 -/-* will be inhibited and *pink1 -/-* phenotype reassessed.

gba1

1. Generate *gba1* mutant zebrafish.

Loss of function models will be generated in a transient manner for pilot studies, following which, stable mutants will be generated. Loss of function will be assessed in both models of *gba1* deficiency.

2. Phenotype *gba1* mutant zebrafish.

Symptoms presented by GD patients in the clinic will be evaluated for similarity in the mutant *gba1* zebrafish. Phenotypes will be assessed biochemically, behaviourally and histologically. Once the model has been validated, pathology will be assessed in further detail to identify molecular defects in specific cellular pathways such as autophagy.

2 Materials and Methods

2.1 Chemicals and other reagents

All chemicals were purchased from Sigma Aldrich unless otherwise stated. All restriction enzymes and buffers were purchased from New England Biolabs.

2.2 Zebrafish husbandry

All adult and larval zebrafish were housed at the University of Sheffield; experimental procedures being in accordance with UK Home Office Animals (Scientific Procedures) Act 1986 (Project license PPL40/3402, held by Dr Oliver Bandmann, Personal license PIL 40/1009, held by Marcus Keatinge).

Fish were housed at a density of 40 per tank, whilst on a cycle of 14 hours of light, ten hours of dark. Adults and larvae were kept at constant temperature of 28°C.

2.3 Fin clipping

For genotyping, adult fish were anesthetised in a solution of tricaine (80ug/ml) and a small portion of the caudal fin was removed with sterile surgical scissors. The clipped fish was then moved to an individual tank, until the genotype was established.

2.4 DNA extraction

Genomic DNA, suitable for use in genotyping by polymerase chain reaction (PCR) was obtained using the REDExtract-N-Amp™ Tissue PCR Kit (Sigma).

A zebrafish fin clip, was placed in the well of a PCR tube, homogenised with a solution of 25 µl extraction solution and 6.25 µl tissue preparation solution. The sample was vortexed for ten seconds, incubated at room temperature for 15 minutes, vortexed again, then finally incubated for three minutes at 95 °C. Once the sample had cooled, 25 µl neutralisation solution B was added, and then the tube was vortexed for a final time.

2.5 Polymerase Chain Reaction

PCR was utilised to amplify both genomic and cDNA for analysis. Each PCR reaction was composed of 10 µl Biomix Red ™ (Bioline), 2 µl forward primer (10 µM), 2 µl reverse primer (10 µM), 4 µl H_2O and 2 µl of DNA. The reaction was heated to 95 °C for three minutes then went through the following cycle for a total of 34 cycles. Each cycle consisted of incubation at 95 °C for 30 seconds, 60 °C for 30 seconds, and 72 °C for 1 minute. This was followed by final 5 minutes incubation at 72 °C. The reaction was heated using a BIORAD DNA Engine gradient thermo cycler (BIORAD). Primers were designed using Primer3 software (v. 0.4.0) supplied by INTEGRATED DNA TECHNOLOGIES Ltd. For PCR, both the forward and reverse primers were used at 10 µM. For a list of all the primers used see Table 3 below. For qPCR reactions, primers were optimised for annealing temperature, concentration and efficiency. SYBR green master mix (Agilent) was utilised for the enzyme reaction, reaction incubated and analysed by Stratagene MxPro 3000p (Stratagene). *ef1 alpha* was used as a reference gene to which data was normalised too.

PRIMER	Sequence (5'-3')	Description
PINK1 Genotyping R	AGCTTCACCACCAGCTGAAC	PINK1 line genotyping
PINK1 Genotyping F	AAAGCAGATGTGTGGGCTGT	PINK1 line genotyping
GBA 178 G>A R	GGGAAAGTTCCCTCAAAAATG	GBA sanger line genotyping
GBA 178 G>A F	AGTACCGTTTCGTGAGAGTGC	GBA sanger line genotyping
MWO1 #4 R	ATGTCATGGGCGTAGTCCTC	GBA TALEN genotyping, all alleles
MWO1 #4 F	AAAGCAGCACGATATGTCCA	GBA TALEN genotyping, all alleles
M13 R	CAGGAAACAGCTATGAC	Colony PCR for TOPO Ta cloning
M13 F	GTAAAACGACGGCCAG	Colony PCR for TOPO Ta cloning
VHL Genotyping R	CGAGTTAAACGCGTAGATAG	VHL line genotyping
VHL Genotyping F	TAAGGGCTTAGCGCATGTTC	VHL line genotyping
PINK1 NMD R	CTGATGACGTTCAGCTGGTG	PINK1 qPCR
PINK1 NMD L	CCACAGACTGATGTGCAGGA	PINK1 qPCR
TigarB qPCR R	TCAGCATTTCTTTTATTGCATGA	TigarB qPCR
TigarB qPCR L	TGTGAGCTGGCTGAACGTAA	TigarB qPCR
Hdac9B qPCR R	CCTACAAGAGCTTTGAGAGTTGTG	Hdac9B qPCR
Hdac9B qPCR L	GAATTTAGCCGACAGAGTCTTTT	Hdac9B qPCR
Apex1 qPCR R	ACTTCCCATGGCAGTGTTTC	Apex1 qPCR
Apex1 qPCR L	TTTCGGGAGCTCTATCCAGA	Apex1 qPCR
TigarA qPCR R	TCAGGGATGGACAAACTTGG	TigarA qPCR
TigarA qPCR L	ATAGGACCAGCCCTTTCACC	TigarA qPCR
TigarB WISH R	TCAGCCAGCTCACAAAACTG	TigarB WISH probe
TIgarB WISH L	CTGCTGCAAGGTCAGGGTAT	TigarB WISH probe
TigarA WISH R	ATAGGACCAGCCCTTTCACC	TigarA WISH probe
TigarA WISH L	CATAGCTGAGGGAGGTCGAG	TIgarA WISH probe
EF1a qPCR R	TGACTCCAACGATCAGCTGT	qPCR House Keeper
EF1a qPCR L	TGGTACTTCTCAGGCTGACT	qPCR House Keeper
OTPa WISH R	ACTCTGCTGGCTGGAGGACTGGGTG	OTPa WISH PROBE
OTPa WISH L	GGAAAAGCATTTCGCCCTGGAGCG	OTPa WISH PROBE
TBMO2 RT PCR R	GACAGAGGTGTGTCAATACCCTGAC	TBMO2 efficacy detection
TBMO2 RT PCR L	TCAGTGACGTCATTTATCTGCAAC	TBMO2 efficacy detection
TBMO3 RT PCR R	TCTCAGCTGTCTGTATAGCTCTTTG	TBMO3 efficacy detection
TBMO3 RT PCR L	CTGCAAGGTCAGGGTATTGA	TBMO3 efficacy detection
PINK4 MO DEC R	TCTGCTAGACAGCAGCCAAA	PINK4 ie and ei efficacy detection
PINK4 MO DEC L	AACATTGGGGCTGGTTCAT	PINK4 ie and ei efficacy detection
PINK5 MO DEC R	TCAGGTGCCATTAGACAGGA	PINK5 MO efficacy detection
PINK5 MO DEC L	CTGACTTTGAACGGGCACTT	PINK5 MO efficacy detection
GBA MO 8 DEC R	TCCTCTTCAGACCTGTTTAGAATG	GBA MO 8 efficacy detection
GBA MO 8 DEC L	CAGGACCTGAATAATTATGTGACC	GBA MO 8 efficacy detection
GBA MO 9 DEC R	CCAGGACCTGAATAATTATGTGACC	GBA MO 9 efficacy detection
GBA MO 9 DEC L	TCCACAGTAGTGTGAGAATGGAG	GBA MO 9 efficacy detection

PRIMER	Sequence (5'-3')	Description
GBA MO 7 DEC R	GGTCCAGCCGGTCACATAAT	GBA MO 7 efficacy detection
GBA MO 7 DEC L	GATGACAACCGCCTTATGCT	GBA MO 7 efficacy detection
GBA NMD #3 R	GGGTGAAGTTCTGGAGATCG	GBA NMD qPCR
GBA NMD #3 L	AGTACCGTTTCGTGAGAGTGC	GBA NMD qPCR
GBA NMD #5 R	CACCGTTTGATCCCAGACTT	GBA NMD qPCR
GBA NMD #5 L	CACTTCAGCAAGTTCCTGTG	GBA NMD qPCR

Table 3. Primer list. A table listing all primers utilised in this study.

2.6 DNA gel electrophoresis

DNA gel electrophoresis was used to visualise PCR products. A 2% agarose gel was constructed from 2 grams of agarose powder heated in 100 ml of TAE buffer (40 mM Tris, 20 mM acetic acid, 1 mM EDTA) until fully dissolved. The solution was allowed to cool, and then poured into a gel tank with a comb to produce sample wells. Once the gel had set it was then moved to an electrophoresis tank and covered in fresh TAE(x1) buffer. Hyper ladder IV, 2 µl (Bioline) was pipetted into the first available well on every gel for sample size reference and concentration analysis. Samples were pipetted in the wells after this at 2 µl unless otherwise stated. Samples were electrophoresed at 150 volts for 15-30 minutes. DNA products were visualised under UV light in a GENi™ (SYNGENE).

2.7 Zebrafish Genotyping

Primers required for genotyping for each mutant line can be found in the primer list (Table 3). The primers were used to amplify the region containing the mutation using gDNA, and genotyped by direct sequencing at the University of Sheffield Core Genomics Facility using the Reverse primer. Sequencing data were analysed using FINCH TV, Version 1.4.0 (Geospiza Inc). All *pink1* sequences were reverse complemented and the lead up sequence, 5'GCGATCGCTTA was located.

5'GCGATCGCTTAT was WT

5'GCGATCGCTTAN was heterozygous for the *pink1* Y431* stop mutation

5'GCGATCGCTTAG was homozygous for the *pink1* Y431* stop mutation

The *gba1* sa1621 line was genotyped using the primer pair GBA 178 G>A. The primers were used to amplify the region containing the mutation, then genotyped by direct sequencing using the forward primer. The lead up sequence was 5'CACATGAAG located and used to genotype the allele.

5'CACATGAAGG was WT

5'CACATGAAGN was heterozygous for the sa1621 mutation

5'CACATGAAGA was homozygous for the sa1621 mutation

The *gba1* 23bp deletion was genotyped using the primer pair MWO1 #4. The primers were used to amplify the region containing the deletion, and then electrophoresed on 2% agarose gel for 25 minutes. Genotyping was performed directly from the photograph of the gel.

A product of size 203 was WT

A product of size 180 was a homozygous mutant for 23bp deletion.

2 products of both these sizes were heterozygous.

See Figure 10 for an example of *gba1* 23bp del genotyping

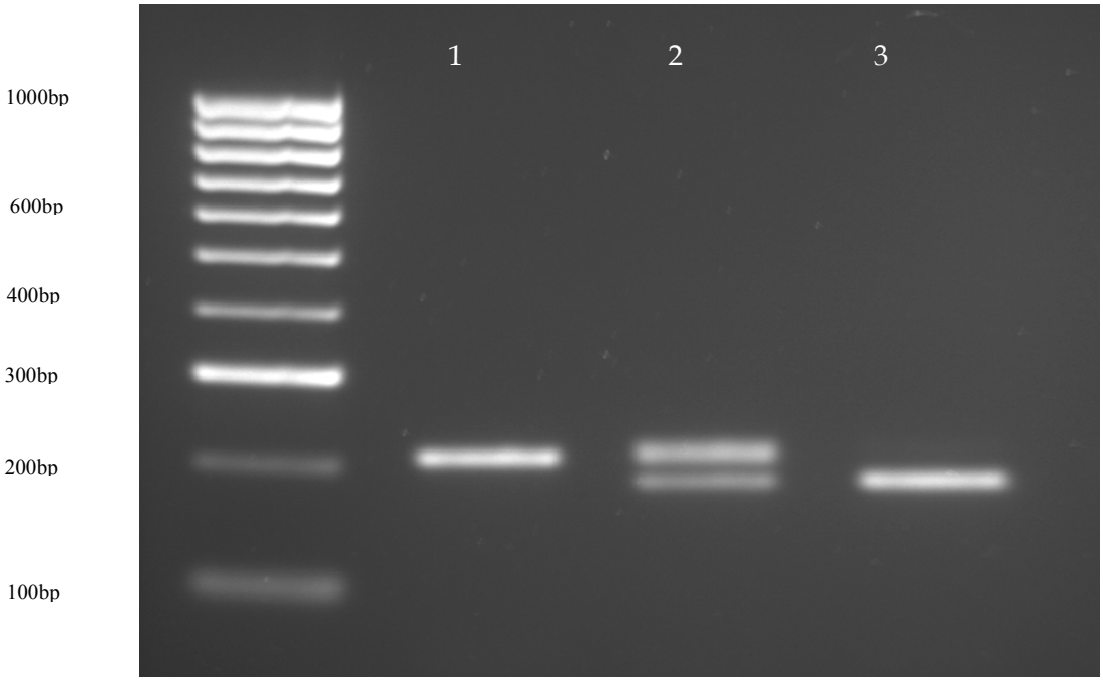

Figure 10. *gba1* 23bp del genotyping. Genomic PCR illustrating *gba1* 23bp del allele primers situated around the TALEN-targeted *MwoI* site of *gba1*. WT individuals produce a product of 203bp (Lane 1), 23bp del *gba1* -/- of 180bp (Lane 3) and 23bp del *gba1* -/+ individuals produce products of both sizes (Lane 2).

The 8bp and 7bp deletion TALEN lines were genotyped with MWO1 #4 primers and the PCR product digested with 1µl of *MwoI* restriction enzyme (NEB) and incubated at 60ºC for 4 hours. 2µl of digested PCR product was electrophoresed on a 2% gel for 30 minutes.

A single product at size 225 was a homozygous mutant

A single product at 110 was WT

A product at 225 and 110 was heterozygous.

The *vhl* line was genotyped using primer pair VHL genotyping. The primers were used to amplify the region containing the *vhl* mutation, and then electrophoresed on a 2% agarose gel for ten minutes to check PCR was successful, genotype was determined by digest. Briefly 5 µl of PCR product was digested in a mixture of 1.8 µl buffer 4 (NEB), 13 µl H2O and 0.2 µl *Bci IV* enzyme. The mixture was incubated for 4 hours at 37ºC then electrophoresed a 2% gel for 30 minutes.

A single product of size 200 was WT

A single product of size 400 was a homozygous mutant

A product at 200 and 400 was heterozygous

2.8 Basic Local Alignment Search Tool

To identify orthologues of human genes in zebrafish, the human protein sequence was located in ENSEMBL and pasted into the Basic Local Alignment Search Tool (BLAST) function of ENSEMBL. The species selected was '*Danio Rerio*' and the database selected was 'protein'. The sensitivity was selected at no optimisation. The sample was then run. The hit with the greatest homology was selected. This was repeated with the human cDNA and all settings remained the same, except that the database selected was DNA database (cDNA library specifically). Once the top hit was duplicated in these BLAST searches, the top cDNA and protein match (both these were coded for by the same gene) was compared to the orthologue assigned to Human gene by ENSEMBL itself to validate the match. Both genes had the basic genetic architecture compared (exon number for example) then genomic regions were compared. The area used for gene synteny comparison was 1.0 mega bases, by using the 'compare region' function in ENSEMBL.

2.9 RNA extraction

To extract RNA required for cDNA generation; 20 larvae / brain tissue (12 wpf), were placed in a microcentrifuge tube and all E3 media was removed. 250 µl of TRIzol® (Life Technologies) was added and the larvae homogenised with a 23 gauge needle, followed by incubation at room temperature for 5 minutes. 50 µl of Chloroform was then added; the tube was inverted 8 times, then left to incubate for a further 5 minutes at room temperature. The sample was then centrifuged in a microcentrifuge for 15 minutes at 13,000 rpm at 4 ̊C. 100 µl of the supernatant was removed and placed into a new sterile microcentrifuge tube. 100 µl of isopropanol was added, the tube was inverted to mix, then incubated at room temperature for ten minutes. The sample was then centrifuged again at the same settings. All supernatant was discarded and the RNA pellet washed with 70% ethanol and centrifuged for 5 minutes at 7,000 rpm, at 4°C. The supernatant was discarded again, and the RNA pellet RNA air dried for 3

minutes, followed by re-suspension in 20 µl DEPC treated H_2O. RNA extraction from brain tissue was identical, with two brains used per sample.

2.10 DNase Treatment

To remove DNA from purified RNA, the DNA-Free KIT ™ was utilised (Invitrogen™) 10 µl buffer and 1µl DNase 1 were added to the RNA, then incubated for 30 minutes at 37 °C. 2 µl DNAse inactivation solution was added, mixed and incubated at room temperature for 2 minutes. The contents were then centrifuged at 10,000g for 2 minutes. The RNA supernatant was then transferred to a fresh tube.

2.11 Reverse transcription

Purified RNA was firstly quantified by using a Nanodrop (Thermo scientific). 1000 ng RNA was made up to 10 µl with DEPC H_2O. The Verso cDNA synthesis kit (Thermo Scientific) was utilised for the reverse transcription reaction. 4µl 5X cDNA synthesis buffer, 2 µl dNTP MIX, 1 µl RNA primer and 1 µl Verso enzyme mix, was added to the 10 µl RNA. The mixture was incubated for 30 minutes at 42 °C then for 2 minutes at 95 °C.

2.12 PCR purification

PCR product was purified using QIAquick PCR purification KIT (Qiagen) as follows: 5 volumes of PB buffer was added to 1 volume of the PCR reaction and mixed. The mixture was placed in a QIAquick column and centrifuged for 60 seconds in a micro-centrifuge. The flow-through was discarded and 750 µl PE buffer added to the column and centrifuged again. The flow-through was again discarded and the column centrifuged for a further minute. The flow-through was again discarded and the column transferred to a fresh microcentrifuge tube. 30 µl EB was added to the centre of the column and incubated at room temperature for 1 minute. The column was then centrifuged for a final 60 seconds to elute the purified DNA.

2.13 Plasmid purification

The QIAprep mini-prep kit (Qiagen) was used to isolate plasmid DNA from bacterial cultures. Firstly 1-6ml of bacterial culture was centrifuged down with a micro-centrifuge and the supernatant discarded. The bacterial pellet was re-suspended with 250 µl Buffer P1 by vortexing. 250 µl of Buffer P2 was added and the microcentrifuge tube inverted 6 times to mix until the solution became clear. 350 µl of Buffer N3 was then added; the tube was then inverted 6 more times and afterwards centrifuged at 13,000 rpm for 10 minutes in a micro-centrifuge. The supernatant was then applied to a QIAprep spin column and centrifuged again for 1 minute. The flow-through was discarded and 750 µl Buffer PE added. The column was centrifuged for a further minute and the flow-through discarded. The column was centrifuged for a further minute to get rid of any residual buffer in the column. The spin column was then transferred to a fresh tube and 30 µl EB buffer added to the centre of the column. The column was incubated for 1 minute at room temperature then centrifuged for 1 minute to elute the plasmid DNA.

2.14 RNA purification

The RNeasy® Mini Kit (Qiagen) was used to purify RNA for TALEN injection. Firstly the sample volume was adjusted to 100 µl with RNase free water followed by the addition of 250 µl ethanol (100%). The sample was then transferred to an RNeasy Mini spin column placed in a 2ml collection tube and centrifuged for 15 seconds at 8000g. The flow-through was discarded and 500 µl Buffer RPE added to the RNeasy spin column and centrifuged again for 15 seconds. The flow-through was again discarded, and again 500 µl Buffer RPE was added to the column but then centrifuged for 2 minutes at 8000g. The column was then placed in a new tube and 30 µl RNase free water added to the centre. The tube was centrifuged for 1 minute to at 8000 g to elute the DNA.

2.15 Large scale Plasmid purification

The Nucleobond® Xtra Midi plasmid purification kit was used to purify plasmids at high concentrations from bacterial cell culture. Bacterial culture was firstly harvested by spinning at 6,000 g for 15 minutes at 4^{o}C. The supernatant was discarded and the

bacterial pellet re-suspended with 8ml re-suspension buffer RES. The cells were then lysed with 8 ml Lysis buffer LYS and the mixture inverted 5 times to mix. The mixture was then incubated at room temperature for 5 minutes. During the incubation, a Nucleobond® Xtra column with inserted filter was equilibrated with 12 ml Equilibration buffer EQU. Post incubation, the mixture was neutralised with 8 ml Neutralisation buffer NEU, then inverted 10 times to mix. Once a homogenous lysate was achieved, the mixture was poured into the Xtra column and allowed to flow through by gravity. The column was washed with 5 ml Equilibration buffer EQU and the filter was then discarded. The column was then directly washed with 8 ml buffer wash. The plasmid DNA was eluted and collected by applying 5 ml Elution buffer ELU to the column. The elute was then treated with 3.5 ml of room temperature isopropanol and centrifuged for 15 minutes at 5,000g to precipitate the plasmid DNA. The supernatant was discarded and the DNA pellet washed with 2 ml 70% ethanol by spinning again at 5,000g for 5 minutes. The supernatant was discarded and the pellet air dried for 5 minutes followed by dissolving it in 1 ml TE buffer.

2.16 Ligation independent Cloning and transformation

Molecular Cloning was achieved using the TOPO TA cloning® kit (Invitrogen, Life technologies). A PCR product was amplified and purified using a QIAquick PCR purification KIT (Qiagen). 4 µl of purified DNA, 1 µl TOPO vector, 1 µl salt solution (1:4 dilution with H_2O) were mixed together and incubated at room temperature for 30 minutes. Meanwhile chemically competent DH5β (NEB) cells were defrosted on ice for 30 minutes. The Cloning reaction was then added to the cells on ice and incubated for 30 minutes. The cells were then heat shocked at 42 °C for 30 seconds and returned to ice for a further 5 minutes. 900 µl of SOC media (Sigma) was added, and then incubated for 1 hour on a shaker at 37°C. During the incubation phase, agar plates containing ampicillin at a concentration of 0.1 mg/ml were also incubated at 37 °C to dry them. In close proximity to a Bunsen flame, 100 µl of the transformation was plated onto the agar plates and distributed evenly using a cell scraper. The plate was then incubated overnight at 37 °C. Insertion of the cassette was determined using colony PCR.

2.17 Colony PCR

To determine if TOPO TA cloning was successful, colony PCR was performed. After overnight incubation of the transformation plate, colonies were picked for analysis. A PCR master mix was made up as previously described, using M13 primers. For the DNA portion of the reaction, a single colony was picked using a sterile p10 pipette tip and dabbed into the PCR reaction. All reactions were amplified as standard and electrophoresed on a 2% agarose gel. Reactions positive for PCR cassette were sent for sequencing with M13 primers.

2.18 RIBO probe manufacture and design

To generate RNA probes, for whole mount in situ hybridisation (WISH), primer 3 (http://bioinfo.ut.ee/primer3-0.4.0/) was used to design primers that would amplify a region 700-1000 bp in length of cDNA. This sequence was searched against the cDNA database to determine the specificity of the probe. The PCR product was amplified and sub cloned into a TOPO TA, colonies positive for the cassette were sent off for sequencing and the orientation was determined. To generate the probe, the plasmid was cut at the opposite end of the cassette to transcription using a restriction enzyme. The cassette was also checked not to have a restriction site at the same site as the digesting enzyme by analysing the sequence with NEBcutter V2.0 (New England Biolabs) (http://tools.neb.com/NEBcutter2/). The restriction digest was constructed of 10 µg of plasmid DNA, 5 µl restriction enzyme and 10 µl appropriate buffer. The reaction was made up to 100 µl H_2O and incubated at the optimum temperature for the enzyme for 4 hours. 2 µl uncut plasmid and 5 µl of cut plasmid were electrophoresed on a 2% gel to determine if linearization was complete. The cut plasmid was purified using QIAquick PCR purification KIT (Qiagen). To generate the riboprobe , 1000ng cut plasmid, 2 µl transcription buffer, 2 µl DIG labelling mix, 2 µl of transcription enzyme (either T7, T3 or Sp6) and 1 µl RNAase were made up to 20 µl with H_2O, then incubated for 2 hours at 37 °C. All transcription reagents were purchased from Roche. Following incubation, 2 µl DNAse was added and the mixture incubated for a further 15 minutes. 2 µl of probe reaction was electrophoresed on a 2% gel to check for probe transcription and complete DNA digestion. 10 µl 7.5 M $NH_4C_2H_3O_2$ (Ammonium Acetate) and 60 µl Ethanol (both ice cold) was added to the transcription reaction and inverted to mix. The reaction was then centrifuged in a micro-centrifuge (13,000 rpm, 4

°C, and 15 minutes). The supernatant was discarded and the pellet washed with 100 µl ethanol (70%) and centrifuged again for 5 minutes. The supernatant was again discarded, the pellet air dried for 3 minutes and re-suspended in a 100 µl mixture of formamide and H_2O (70:30 respectively) then stored at -80 °C.

2.19 Embryo fixation

To preserve zebrafish larvae for whole mount in situ hybridisation (WISH), larvae were fixed. Zebrafish larvae were de-chorionated and put into 1.5 ml microcentrifuge tubes in groups of 20. All E3 media was removed and 500 µl 4% PFA (paraformaldehyde) solution (made up with sterile PBS) was added. The larvae were incubated on a rocker at room temperature for 2 hours. PFA was removed and replaced with 500µl 100% methanol, incubated at room temperature for 15 minutes and then stored at -20 °C.

2.20 Whole mount in-situ hybridisation

WISH was utilised to investigate the expression of specific mRNA transcripts. Fixed larvae were rehydrated in a series of 500 µl 5 minute washes of 75% methanol: 25% PBT, 50% methanol: 50% PBT, 25% methanol: 75% PBT, and finally 4 washes with 100% PBT. Larvae were then digested at room temperature with 500 µl 10 µg/ml proteinase K for the following time, depending on the age of larvae: 8 minutes for 24 hpf, 14 minutes for 48 hpf, 30 minutes for 72 hpf, 40 minutes for 96 hpf and 45 minutes for 120 hpf larvae. Proteinase K was then removed and replaced with 500 µl 4% PFA and incubated for 20 minutes at room temperature. Samples were then washed with 500 µl of PBT for 5 minutes, 5 times each. The PBT was removed and replaced with 500 µl Hyb A buffer (50% formamide, 5XSSC solution, 0.5 mg/ml tRNA, 0.1% tween 20, 50 ug/ml Heparin, pH was adjusted to 6.0 with 1M citric acid) and incubated at 70 °C for 5 hours. Hyb A solution was then replaced with a solution of Hyb A 2% riboprobe and incubated overnight at 70 °C. Each tube then had a brief wash with 70 °C 100% Hyb B solution (Hyb A without tRNA and Heparin) then sequential 500 µl washes at 70 °C for 15 minutes each with 75% HybB: 25% 2xSSC, 50% HybB: 50% 2xSSC, 25%Hyb B: 75% 2XSSC then 100% 2XSSC. Each sample was then washed twice with 0.2XSSC for 30 minutes at 70°C. Each sample then went through sequential washes of decreasing concentrations of 0.2xSSC at room temperature. Starting with 75% 0.2XSSC: 25% PBT

for ten minutes, then 50% 0.2XSSC: 50% PBT for ten minutes, then 25% 0.2XSSC: 75% PBT for ten minutes followed by a final 10 minutes PBT wash. Each sample was then incubated in 500 µl blocking buffer (2mg/ml Bovine serum albumin (BSA), 2% sheep serum, all dissolved in PBT) for 3 hours. Each sample was them incubated in 500 µl Blocking buffer with a 1:5000 dilution of anti-dig antibody (Roche) and protected from light at 4°C overnight.

The following morning each sample went through 6 washes of PBT for 15 minutes each. This was followed by 3, 5 minutes washes with 500 µl NTMT buffer (0.1M TrisHCl pH 9.5, 50 mM $MgCl_2$, 0.1M NaCl, 0.1% Tween 20). The Buffer was then exchanged with 500 µl staining solution (3.5 µl and 4.5 µl, BCIP and NBT respectively, per ml of NTMT). Samples were inspected every 15 minutes for stain development (appearance of purple stain). When the stain had developed satisfactorily, the samples were washed 3 times with PBT.

To remove any background, each sample was washed with 500 µl 50% methanol then incubated in 100% methanol, until all background had been cleared. Each sample was then washed again with 50% methanol, then twice with PBT. 4% PFA was then used to re-fix larvae for 20 minutes at room temperature. Each sample was washed 3 times with PBT, then placed into 75% glycerol and stored at 4°C.

2.21 Tyrosine Hydroxylase Neuron Counting

When assessing the number of DA neurons, 3 dpf larvae were always used, unless otherwise stated. The neurons were stained by WISH for Tyrosine Hydroxylase (TH) as a marker of DA neurons, unless otherwise stated. Zebrafish larva heads were mounted in glycerol for correct orientation and TH positive neurons counted by eye using axioplan 2 (Zeiss) compound microscope at X20 magnification. TH neuron count was assessed by counting DA subgroups 1, 2, 4 and 5 in the diencephalon. Groups were defined according to the descriptions of Rink and Wulliman.[165] For Each embryo TH neuron count, each experiment contained n of ten individuals (unless otherwise stated) in all groups. Each experiment was performed in triplicate (unless otherwise stated). The mean count of control groups in each experiment was set as 100%, and all counts expressed as a percentage of the control mean.

2.22 Tyrosine Hydroxylase Neuron staining and counting in 12 wpf zebrafish

In order to quantify TH neurons in 12 wpf zebrafish, IHC was employed to stain the neurons. This experiment was jointly undertaken between the author and Dr Yu-Chia Chen. Brain dissection and fixing was performed by the author. TH neuron staining and count was performed by Dr Yu-Chia Chen.

12 wpf were culled and brains removed then fixed as previously described in PFA, and dehydrated in 100% methanol. To stain, whole brains were rehydrated in a series of PBST/methanol, for 60 minutes each, at concentrations of 25%, 50%, 75% and 100%. Samples were then digested with proteinase K (10 µg/ml) in PBST at room temperature for 3 minutes. Samples were then refixed in 4%PFA at room temperature for 30 minutes. Each sample was then incubated in PBST twice for a single hour at room temperature. All samples were incubated in blocking buffer composed of 4% normal goat serum +1 % DMSO in PBST at 4°C for 24 hours.

For the next four following days, each sample was incubated with a anti Tyrosine Hydroxylase antibody diluted in blocking buffer (Mouse monoclonal anti-TH, DiaSorin Inc), at 4°C. Following incubation, each sample was washed twice with PBST for one hour at room temperature, then incubated overnight at 4°C in PBST.

Each sample was then incubated with an Alexa Fluor® 488 goat anti-mouse IgG diluted in blocking buffer as a concentration of 1/1000, for 24 hours at 4°C. Following incubation, each sample was washed twice with PBST for one hour at room temperature, and then incubated overnight at 4°C in PBST.

Each sample was incubated in a 50% glycerol/PBS solution, overnight at 4°C. Samples were then incubated in an 80% glycerol/PBS solution for 2 days at 4°C. Each sample was then mounted and imaged. TH neurons were counted according to Sallinens dfinition.[120]

2.23 Morpholino design and optimisation

The preferred exons junctions targeted for binding had their exon-intron boundary sequences sent to Gene-Tools for Morpholino design (http://www.gene-tools.com/). The Morpholino binding regions were then confirmed by direct sequencing. Possible

SNPs in the sequence would lead to rejection of the designed Morpholino. Morpholinos were ordered from Gene-Tools and re-suspended at 2 mM with H_2O and stored at room temperature with protection from light. A list of all Morpholino used in the experiments are listed in the Morpholino Table 4.

Morpholino	Sequence 5'-3'	Optimised concentration
TigarB i5e6	ACCTGGAGAGACAAAAGCAGGATCT	N/A -TOXIC
TigarB e2i2	TAGAGTGTTTATCTACCTTGCAGCA	0.9mM
TigarB i2e3	CCCTGACCTTCACATCAGATAAAAA	N/A low efficacy
GBA1 i8e9	TTGCTGTTAGTAAGGTACAAAGGCA	N/A low efficacy
GBA1 e8i8	GTGCTTTGAACGAGTCTGACCTGAA	0.9mM
GBA1 i6e7	GTCACTTAGAACCTATAGCCGAAAA	N/A toxic
VHL e1i1	GCATAATTTCACGAACCCACAAAAG	0.2mM
PINK1 e5i5	AGAGTCTCTGAGCTCTTACTGTTGT	0.9mM
PINK1 e4i4	GTGTTTTCATGTTTCCTCACTTCTT	N/A TOXIC
PINK1 i3e4	AGTGCCTGCAAAAATAGCAAAGCCA	N/A low efficacy

Table 4. Morpholino list

To inject zebrafish embryos, working concentration (0.9 mM, 0.5 mM or 0.25 mM) Morpholino was loaded into a glass needle (borosilicate glass capillary, by WPI) pulled using a Model P97 micro-pipette puller, by Shutter Instruments. The full needle was hooked to a Pv 820 Pneumatic Pico-pump (WPI) for injections. Injection speed was calibrated by injecting the Morpholino solution into a drop of mineral oil placed on top of a 100x0.1=10mm graticule (Pyser-SGI), in order to correctly set the speed and pressure to inject 0.5nl with each burst. To optimise Morpholinos, WT 1 cell stage zebrafish embryos were injected with 0.9 mM, 0.5 mM and 0.25 mM Morpholino. Phenol red (0.00011mg/ml) was used to colour the Morpholino solution, to ensure correct injection. Embryos were injected with 1 nl each and inspected on days 1, 2 and 3 post fertilisation, for mortality and deformity. Morpholino efficacy was determined by RT-PCR on days 1 and 3 post fertilisation compared to un-injected controls. Morpholinos were rejected if they lacked efficacy or were deemed toxic, definitions by Robu *et al*. [156]

2.24 TALEN design and construction

A TALEN pairs to make targeted germ line mutations in ZF embryos were designed and manufactured as follows. The cDNA sequence for *gba1* (ENSDART00000113093) was inputted into the TALEN TARGETTER https://boglab.plp.iastate.edu/node/add/talen. The targeter was set to allow spacers of 16bp as a minimum and 21bp as a maximum. Minimum repeat array was set at 15 and maximum at 21. A pair of TALENs, including a region with a wide large restriction enzyme site was chosen. In the case of the TALENs targeting, *gba1*, a position in exon 7 was chosen with an *MwoI* restriction enzyme present that could be used to assay TALEN efficacy. A pair of TALENs binding 5'TCTGTACCCTGATTACTT (RIGHT TAL) and 5'ATGCGCTGGGTGGAGTCCA (LEFT TAL) were chosen by the TALEN Targeter with plasmid codes of HD NG NN NG NI HD HD HD NG NN NI NG NG NI HD NG NG and NN NN NI HD NG HD HD NI HD HD HD NI NN HD NN HD NI NG respectively.

Self-ligating plasmids were purchased from Addgene (http://www.addgene.org/TALeffector/goldengate/voytas/Plate1/). Each TALEN was made in two parts and joined at the end. Part A was assembled into the F5 plasmid (pFusA) with the initial ten RVDS. The latter RVD plasmids would be assembled into pFUSBN, N=TOTAL RVD-11. For the initial assembly, 2 tubes were made up as follows:

For each A part – 1 µl of each RVA plasmid (100ng/µl), 1 µl pFusA (100ng/µl) 4 µl H_2O, 2µl T4 ligase buffer (NEB), 2 µl T4 ligase (NEB) and 1µl BSA1 (NEB). For each part B – 1 µl each RVD plasmid (150ng/µl), 1 µl pFusB (150ng/µl), 2 µl T4 DNA ligase buffer (NEB), 2 µl T4 DNA ligase (NEB), 1 µl Bsa1 (NEB), with the reaction made up to 20 µl with H_2O. Each reaction was then incubated in the following cycle for ten cycles: 37 °C for 5 minutes then 16 °C for ten minutes. This was followed by a 5 minute incubation at 50 °C, then at 80 °C. 0.3 µl 25mM rATP and 1µl plasmid safe nuclease were added to each reaction then incubated for 1 hour at 37 °C.

Each reaction was then transformed (as previously described) into DH10Beta cells (NEB) which were then spread onto LB agar plates (50 ug/ml Spectinomycin, 0.1 mM IPTG and XGal 40 µg/ml) and incubated overnight at 37 °C. The following day, 3 white colonies from each reaction were picked and used to inoculate 6 ml LB (50

ug/ml Spectinomycin) and shaken overnight at 37 °C. The following morning, all samples were centrifuged down and plasmids isolated with a Qiagen mini-prep kit.

The second assembly stage took place to combine parts A and B of each TALEN as follows: 5 µl H2O, 4 µl mini-prep A, 4 µl mini-prep B, 1 µl 150ng/µl plasmid E4, 1 µl 75 ng/µl pCAGT7TALEN, 2 µl T4 DNA ligase buffer (NEB), 2 µl T4 DNA ligase (NEB) and 1 µl Esp4I. The reaction was then incubated as follows for ten cycles: 37 °C for 5 minutes then 16 °C for ten minutes. Followed by a 5 minute incubation at 50 °C, then at 80 °C.

Each reaction was then again transformed into DH10Beta cells (NEB), and streaked onto LB agar plates with carbenecillin selection (50 ug/mL carbenecillin and 0.1 mM IPTG and XGal 40 µg/ml) and incubated over night at 37 °C. The following morning, 1 colony was picked from each subunit and used to inoculate 100 ml LB (50 ug/mL carbenecillin) in a baffled flask, and shaken overnight at 37 °C. The following morning each culture was purified using a Nucleo-bond midi-prep as previously described and the plasmid pellet re-suspended in 30 µl H_2O.

To generate TALEN mRNA, the final plasmids were linearized with a *NotI* digest as follows: - 6 µg DNA of each of the right and left constructs, 30 µl NEB3 buffer, 3µl 10 mg/ml BSA and 10 µl NotI, then H_2O up to 300 µl in a PCR tube. The reaction was incubated at 37°C for 1 hour. RNA was synthesised using an Epicentre T7 MessageMax ARCA kit (CAMBIO) as follows. 3 µl DNA (400 ng/µl), 4 µl NTP CAP mix, 1µl buffer, 1 µl 100 mM DTT and 1 µl enzyme mix was incubated for 30 minutes at 37°C, then 1µl DNAse was added, followed by a further incubation for 15 minutes. RNA was purified using Qiagen MinElute system™. RNA was stored at -80°C. To mutagenize zebrafish embryos, 1 nl of RNA solution (3.5 µl RNA and 0.5 µl Phenol RED) was injected into 1 cell stage WT embryos and grown up to adulthood to create mosaic F0.

2.25 Movement analysis of adult zebrafish

Adult locomotion was quantified using Viewpoint analysis software version 3, 22, 3, 9 and filmed on a CCTV LENS 2.8-12mm F1.4 camera (both Viewpoint). For filming 3 year old PINK1 line, fish were filmed individually for a period of 4 hours (1 hour acclimation and 3 hours analysed) between the hours of 3pm and 7pm. For the *gba1* line, fish were filmed individually for ten minutes after ten minutes acclimation time.

Low speed movements were defined as less than <5 cm/s. Medium speed movements were defined as 5<X<7cm/s. High speed movements were defined as movements over 7cm/s.

2.26 Bicinchoninic acid assay (BCA) protein assay

The BCA assay was utilised to determine protein concentration of zebrafish brain homogenates.

Adult zebrafish brains were homogenised as a 5% solution with a 100 µl glass on glass homogeniser (Decon instruments). Samples were kept on ice for the protein concentration to be measured. Two dilutions of 2.5 µl and 5 µl brain homogenates were made up to 50 µl with distilled H_2O. Each volume for each sample was measured in duplicate. 1 ml bicinchoninic acid was added to each sample and mixed, then incubated at 37^{o}C for ten minutes. 20 µl of 4% copper sulphate solution was then added to each sample, mixed, then incubated for 20 minutes at 37^{o}C. The absorbance was read at 562nm and protein concentration calculated from a standard curve established from a set of dilutions of bovine serum albumin.

2.27 Gba activity assay

Gba1 and 2 activities were determined as follows: Whole zebrafish brain was homogenised (in distilled water) and diluted to 2 mg/ml. For total Gba activity (TOTAL) of the homogenate, 10 µl homogenate was mixed with 90 µl H_2O. For basal Gba1 activity (Gba1), 10 µl homogenate was mixed with 80 µl H_2O and 10 µl NBDNJ (50 µM, N-Butyldeoxynojirimycin, a specific GBA2 inhibitor). For activated Gba1, 10 µl homogenate was mixed with 50 µl H_2O and 40 µl NAT (sodium taurocholate, GBA1 activator/GBA2 inhibitor) (40mg/ml). Each mixture was incubated on ice for 1 hour. 100µl substrate solution was added to each mixture (1.69mg/ml of 4-methylumbelliferyl-beta-D-glucopyranoside dissolved in McIlvaine citrate phosphate pH 5.4), and incubated for 1 hour at 28^{o}C. The reaction was stopped with the addition of 1 ml of 1 M glycine NaOH buffer pH 10.4 and vortexed. Samples were read alongside a 1 nm 4-methylumbelliferone standard, with excitation 365 nm, emission 450 nm. A blank was set up for all inhibitor conditions containing all reagents except for the brain lysate.

Gba1 activity was also measured using CBE as an inhibitor as part of a collaboration between the author and Dr Matthew Gegg. Dr Matthew Gegg performed the assay and analysis, the author performed the genotyping, brain removal and processing. The assay was conducted as follows.

Brains were homogenised in 75 µl RIPA buffer (150 mM NaCl, 1.0% (v/v) NP-40, 1% (w/v) sodium deoxycholate, 0.1% (w/v) SDS, 50 mM Tris, pH 7.4). Gba activity determined in samples (10 µg protein) by hydrolysis of 5 mM 4-methylumbelliferyl-β-D-glucopyransoside in McIlvaine citrate phosphate buffer (pH 5.4) in the presence of 22 mM sodium taurocholate at 37 °C for 1 hour. For CBE sensitive rate, duplicate samples were incubated in the presence of 5 mM CBE (15 minute pretreatment at 37 °C, plus present during assay). The reaction was stopped by addition of 0.25M glycine (pH 10.4) and 4-methylumbelliferone fluorescence measured at excitation 360 nm, emission 460 nm.

2.28 Total β Hexosaminidase activity assay

Total zebrafish brain was homogenised as previously described, and diluted to 1 mg/ml. 5 µl of this solution was diluted with 495 µl of McIlvaine citrate–phosphate buffer pH 4.5. 100µl of this further dilution was placed into a new 1.5 ml tube and warmed for 2 minutes at 37ºC. 100 µl of substrate solution (1.1 mg/ml of 4-methylumbelliferyl-2-acetamido-2-deoxy-beta-d-gluco-pyranoside in McIlvaine citrate–phosphate buffer pH 4.5) was then added to each sample, mixed and incubated for ten minutes at 37ºC. The reaction was stopped with 1 ml of 1 M glycine NaOH buffer pH 10.4 and vortexed. Samples were read along with a 1nm 4-methylumbelliferone standard, with excitation 365 nm, emission 450 nm. A blank was set up for containing all reagents except for the brain lysate.

2.29 Chitotriosidase activity assay

Zebrafish brains were homogenised as described and diluted to 2 mg/ml. To measure Chitotriosidase level 10 µl of brain homogenate was combined with 100 µl substrate solution (1.73mg/ml of 4-methylumberiferyl-beta-d-N, N', N'', -triacetychitotriose in McIlvaine citrate–phosphate buffer pH 5.2) mixed and incubated for 1 hour at 28ºC.

The reaction was stopped with 1 ml 1 M glycine NaOH buffer pH 10.4 and vortexed. Samples were read along with a 1nm 4-methylumbelliferone standard, with excitation 365 nm, emission 450 nm. A blank was set up for all conditions containing all reagents except for the brain lysate.

2.30 β Galactosidase activity assay

Zebrafish brains were homogenised as described and diluted to 2 mg/ml. To measure β-Galactosidase activity, 10µl brain homogenate was mixed with 40 µl of McIlvaine citrate–phosphate buffer pH 4.1. This was combined with 150 µl substrate solution (1mM 4-methylumbelliferyl-D-galactopyranoside dissolved in 4.1 buffer). The reaction was incubated for 15 minutes at 28 ^{o}C. The reaction was stopped with 1ml 1 M glycine NaOH buffer pH 10.4 and vortexed. Samples were read along with a 1nm 4-methylumbelliferone standard, with excitation 365 nm, emission 450 nm. A blank was set up for all conditions containing all reagents except for the brain lysate.

2.31 Haematoxylin and Eosin (H&E)/ Periodic acid–Schiff (PAS) staining

For histological analysis of 12 wpf zebrafish, sections were stained with either H&E or PAS. This experiment was jointly undertaken between the author and Dr Aswin Menke. Genotyping and fixation of samples was performed by the author, sectioning, staining and analysis was performed by Dr Aswin Menke.

Adult zebrafish were genotyped and fixed in Bouins fixative. Each sample was embedded in paraffin and subsequently cut into, 4 µm transversal or saggital sections were made and stained with haematoxylin and eosin. The slides were analysed on a Axioskop 2 plus microscope by a board-certified pathologist.

2.32 Microglial/Macrophage analysis

For analysis of the macrophages and microglial in *gba* genotypes, a GFP reporter and confocal imaging was utilised. This experiment was jointly undertaken, between the author and Dr Felix Ellett. Imaging and analysis performed by Dr Felix Ellett, genotyping and crossing performed by the author.

gba1 23bp del -/+ were crossed to Tg(mpeg1:EGFP-CAAX) described by Ellett *et al*.[286] Embryos were selected for GFP fluorescence, genotyped at 3 months. All subsequent embryo work was generated from an incross of *gba1* 23bp del -/+; Tg(mpeg1:EGFP-CAAX) and imaged at 4 dpf using UltraVIEWVoX spinning-disk confocal microscope (PerkinElmer Life and Analytical Sciences). 2µm optical sections were taken for three fields of view for each embryo, principally: the caudal haematopoietic tissue; trunk, and head region anterior to the yolk. Volocity 5 (Improvision; PerkinElmer Life and Analytical Sciences) was used for imaging analysis of GFP positive cell shape and volume, with cell boundaries defined using fluorescence intensity. All analysis was performed blinded to embryo genotype.

2.33 Mitochondrial Complex assays

Mitochondrial Complex assays were utilised to measure the activity of each mitochondrial Complex in the electron transport chain. These experiments were jointly undertaken between the author, Dr Marc DaCosta and Dr Heather Mortiboys. The author performed Morpholino injections, genotyped and extracted brains then processed all samples. Dr Marc Da Costa performed the Complex assays on brain material; Dr Heather Mortiboys performed the Complex assays on larvae. Assays were performed as previously decribed.[168]

2.34 Mass Spectrometry

Mass spectrometry methods where conducted as previously described.[287] Mass spectrometry experiments were jointly undertaken between the author and Dr Hai Bui. 12 wpf brains were extracted and flash frozen by the author. Mass spectrometry analysis of the samples was conducted by Dr Hai Bui.

2.35 Nomenclature

All human genes and proteins are referred to in uppercase, with genes and transcripts italicised. All mouse proteins are referred to in uppercase with genes in lowercase with the exception of the first letter. All mouse genes are in italics. All zebrafish genes and transcripts are represented in lower case italics whilst proteins are represented in lower

case with the exception the first letter that is written in uppercase. See below for examples. The only exception to this stated nomenclature is tyrosine hydroxylase that is referred to as TH through the entire thesis.

species / gene / protein

zebrafish /*pink1*/ Pink1

human / *PINK1* / PINK1

mouse / *Pink1* / PINK1

2.36 Statistical tests and analysis

All statistical tests were performed using Graphpad prism V.5 software (Graphpad). N numbers for all experiments donated by the prefix n and all errors bars shown denote the mean ± Standard error of the mean. All experiments performed in triplicate unless different n number stated or the data described as pilot data. All data analysed with either T test, one way ANOVA or two-way ANOVA unless otherwise stated.

Significance values denoted as follows.

Non-significant (ns): $p>0.05$

*: $p<0.05$

**: $p<0.01$

***: $p<0.001$

****:$p<0.0001$

3 The zebrafish as a model for *pink1* deficiency

3.1 Characterisation of the *pink1* Y431* zebrafish

3.1.1 *pink1* introduction

Prior to commencement of this study, no previous vertebrate model of PINK1 deficiency faithfully modelled the disease seen in humans, with no model demonstrating spontaneous DA cell loss.[129, 188] It was hypothesised that zebrafish would be a more suitable model for *pink1* deficiency, with the wider aim of using *pink1* mutant zebrafish for phenotypic drug discovery. Consequently a *pink1* mutant zebrafish allele was generated from an ENU mutagenesis screen conducted by Dr Sandrine Bretaud that identified a *pink1* allele with a nonsense mutation Y431*. The mutation leads to a premature stop codon appearing within the kinase domain of Pink1. The mutation was confirmed to be loss of function in kinase assays, and led to mitochondrial dysfunction in larvae and adult *pink1* -/- (Experiments conducted by Ms Helen Woodroof and Dr Heather Mortiboys). The mitochondria appeared swollen and less electron dense, with *pink1* -/- exhibiting a decrease in mitochondrial Complex activity, specifically in Complex I and III. This defect was present in 5dpf larvae and in adult fish in a manner that was not progressive in nature. Unlike *Pink1* KO mice and Medaka, *pink1* -/- loss of function zebrafish exhibited a loss of TH neurons in development by 5dpf of approximately 20% (experiments conducted by Dr Laura Flinn). This decrease increased to 50% at the age of 18 months. This was the first vertebrate model of *pink1* deficiency that demonstrated a loss of DA neurons. Not only does the loss appear very early in development, it also persisted through to adulthood.[200] As part of this thesis, further validation, and functional studies of this zebrafish model of *pink1* deficiency were carried out. The aim was to assess, firstly, whether zebrafish is a useful model species for studying *pink1* deficiency, and secondly whether there are any genetic interactions that can modify the phenotypes, identifying possible new drug targets for PD.

3.1.2 Zebrafish possess a single *PINK1* orthologue (ENSDARG00000001929)

Many studies have identified Zebrafish to have single orthologue of human *PINK1*, which possesses approximately 60% protein and DNA identity to the human gene, see Figure 11.

```
ENSP00000314508/1-536    MEFSSPSREECPKPLSRVSIMAGSLTGLLLLQAVSWASGARPCIPKSFGYSSVVCVCNAT
ENSDARP00000098103/1-518 ---------------MRETALFILLAGIITTARAD---SKDGCLALNFGHGSVVCVCNAT
                                          * : :   *:*::    ..   .   *:. .**:.*********

ENSP00000314508/1-536    YCDSFDPPTFPALGTFSRYESTRSGRRMELSMGPIQANHTGTGLLLTLQPEQKFQKVKGF
ENSDARP00000098103/1-518 YCDSLGRTVLPDAGQFLSYVSNKAGSRLMESQGQFQKNSTGAALRITLNPSQKFQHIKGF
                         ****:. ..:*  * *  * *.::* *:  * * :* * **:.* :**:*.****::***

ENSP00000314508/1-536    GGAMTDAAALNILALSPPAQNLLLKSYFSEEGIGYNIIRVPMASCDFSIRTYTYADTPDD
ENSDARP00000098103/1-518 GGAMTDAAAINILSLSSGAQDQLLRQYFSTDGIEYRFVRVPVASCDFSTRLYTYADTPED
                         *********:***:**. **: **:.*** :** *.::***:****** * *******:*

ENSP00000314508/1-536    FQLHNFSLPEEDTKLKIPLIHRALQLAQRPVSLLASPWTSPTWLKTNGAVNGKGSLKGQP
ENSDARP00000098103/1-518 YDLQNFTLAKEDVHMKIPLLQRAQALSAQPLYLFASAWSAPAWLKTNGALIGKGSLKGKP
                         ::*:**:*.:**.::****::**  *: :*: *:**.*::*:*******: *******:*

ENSP00000314508/1-536    GDIYHQTWARYFVKFLDAYAEHKLQFWAVTAENEPSAGLLSGYPFQCLGFTPEHQRDFIA
ENSDARP00000098103/1-518 GGKEHKTWAQYYIRFLEEYRKYNLSFWGLTSGNEPTAGEMTNYSFQALGFTPETQRDWIA
                         *.  *:***:*:::**: * :::*.**.:*: ***:** ::.*.**.****** ***:**

ENSP00000314508/1-536    RDLGPTLANSTHHNVRLLMLDDQRLLLPHWAKVVLTDPEAAKYVHGIAVHWYLDFLAPAK
ENSDARP00000098103/1-518 LDLGPALHSSSFSKTQLMILDDNRLMLPHWAKVVLSDIKAARYVHGIGVHWYFDRLVPPD
                          ****:* .*:. :.:*::***:**:*********:* :**:*****.****:* *.*..

ENSP00000314508/1-536    ATLGETHRLFPNTMLFASEACVGSKFWEQSVRLGSWDRGMQYSHSIITNLLYHVVGWTDW
ENSDARP00000098103/1-518 VTLTSTHHLYPDYFLFATEACAGWSPVDRGVRLGSWDRAEDYAHDIIQDLNNYVTGWTDW
                         .** .**:*:*: :***:***.* .  ::.********. :*:*.** :*  :*.*****

ENSP00000314508/1-536    NLALNPEGGPNWVRNFVDSPIIVDITKDTFYKQPMFYHLGHFSKFIPEGSQRVGLVASQK
ENSDARP00000098103/1-518 NLALNQDGGPNWVKNFVDSPIIVDPSKDIFYKQPTFYSMAHFSKFLWEESQRVGVSFSQQ
                         ***** :******:********** :** ***** ** :.*****: * *****:  **:

ENSP00000314508/1-536    NDLDAVALMHPDGSAVVVVLNRSSKDVPLTIKDPAVGFLETISPGYSIHTYLWRRQ
ENSDARP00000098103/1-518 TSLEMSAFIRPDASAVLIILNRSEEEVPFEVWDQTVGFLPGSAPPHSILTLLWNRQ
                         ..*:  *:::**.***:::****.::**: : * :****   :* :** * **.**
```

Figure 11. Clustal alignment of human GBA1 and Zebrafish Gba1. The human protein sequence (ENSP00000314508) aligned via clustal to its zebrafish orthologue (ENSDARP0000098103). Both sequences have considerable homology of approximately 60% over 100% coverage.

However, conserved synteny in the genomic loci of human and Zebrafish genes has yet to be illustrated, a further marker of true conservation between orthologues.

A 500kb stretch of genomic locus of each gene was compared in both species, revealing there was indeed a conserved gene synteny between them both. Upstream of the *PINK1* gene, four genes present in the human locus were also found, not only in same zebrafish locus, they also appear in the same sequential order. Specifically, these were *CAMK2N1*, *MUL1*, *FAM43b* and *CDA* at the human locus, their zebrafish orthologues being *camk2n1b*, *mul1b*, *fam43b* and *cda* respectively. All of which were found within 200kb of the *PINK1* locus. Synteny downstream of PINK1 did not appear to be

conserved, with no genes located in both species within 200kb. See Figure 12 for a graphical representation outlining the similarities and differences of both loci.

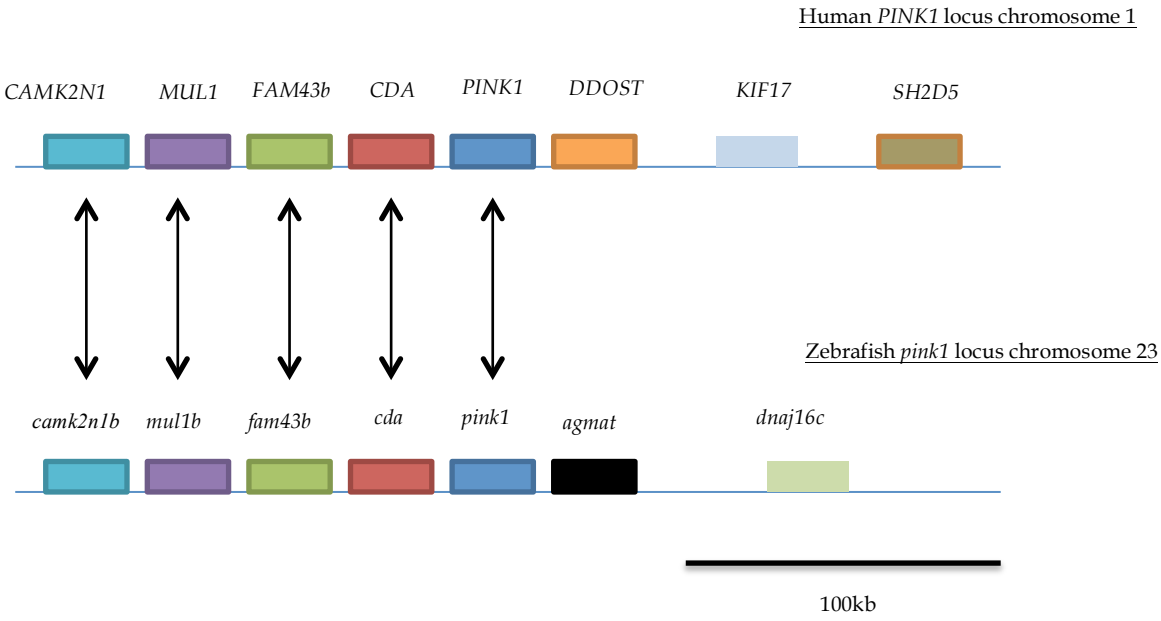

Figure 12. The genomic loci of the *PINK1* in human and zebrafish. Both zebrafish and humans share conserved gene synteny surrounding the *PINK1* gene, with four different genes (*CAMK2N1, MUL1, FAM43B* and *CDA* all upstream of the *PINK1* sequence), in the same order in both species. Demonstrating that *pink1* zebrafish is a true orthologue of human *PINK1*. Synteny down- stream of the *PINK1* does not appear to be conserved, with no genes in common in either species within the 300kb radius.

3.1.3 *pink1* Y431* transcript undergoes nonsense mediated decay

The Y431* allele, a nonsense mutation, codes for a premature stop codon within the kinase domain of *pink1*. Although this prevents the last 30% of the WT mRNA species from being translated into protein and one could hypothesise that the protein would not be able to fold properly or alternatively be kinase dead, further evidence was required to demonstrate loss of function. In parallel to the kinase assays that demonstrated the allele to be enzymatically non-functional, the experiment investigated possible activation of nonsense mediated decay (NMD) on the *pink1* transcript itself in *pink1* -/-. Subsequently, to further investigate whether the Y431* mutation results in decreased *pink1* mRNA levels, *pink1* qPCR was carried out in *pink1* -/- and WT. *pink1* -/-had an approximately 65% reduction in *pink1* transcript compared to WT controls ($P<0.0001$), see Figure 13. This suggests that NMD is occurring in the

pink1 -/- fish and further supports the assumption that the Y431* mutation results in Pink1 loss of function.[201, 288]

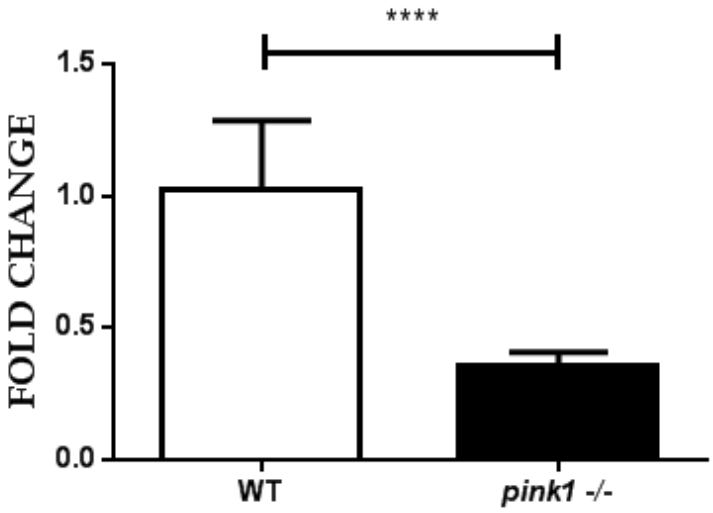

Figure 13. The *pink1* transcript expression in *pink1 - /-* compared to WT. The *pink1 -/- larvae* have a marked reduction in *pink1* transcript levels (approximately 65%) compared to the WT (P<0.001 Unpaired T test). *ef1a* was use as a reference gene.

3.1.4 Aged *pink1 -/-* zebrafish display a parkinsonian-like movement defect

To evaluate for parkinsonian like movement defects in aged fish, 3 year old fish were filmed and their total displacement analysed. Each fish (n of ten per genotype) was filmed for a total of 4 hours. Habituation time of 1 hour was deemed appropriate for each genotype and total displacement calculated over the next 3 hour period. 3 year old *pink1 -/-* zebrafish covered 30% less distance over time than WT controls (P <0.05, unpaired T test) (see Figure 14). This demonstrated that *pink1 -/-* may move less often, at slower speeds or both. Behaviour such as this is indicative of bradykinesia and freezing, key motor symptoms seen in PD.

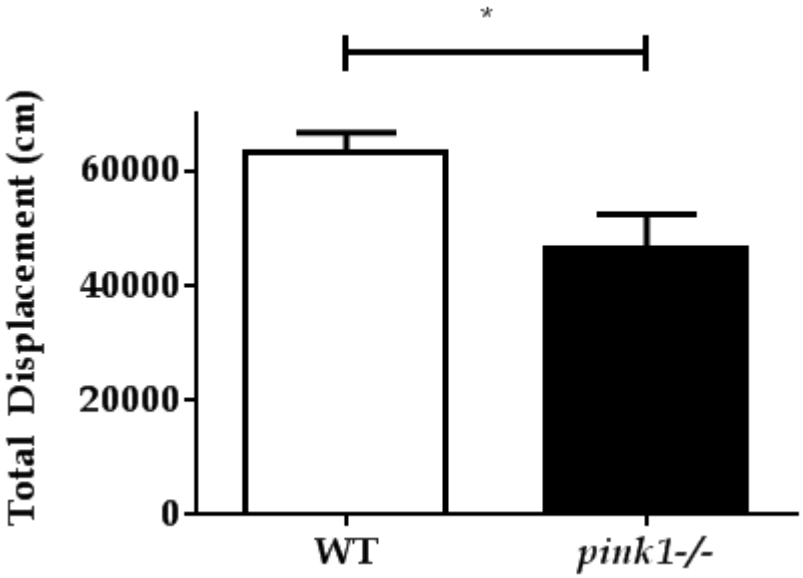

Figure 14. Total displacement of 3 year old *pink1 -/-* and WT controls. The *pink1 -/-* fish exhibited a decrease in total displacement (approximately 30% P<0.05 unpaired T Test, n=10 for both groups) over time, indicating slower and less frequent movements as seen in PD patients.

3.1.5 *pink1 -/-* larvae do not exhibit defects in neuronal development

Dr Laura Flinn *had previously* established that *pink1 -/-* larvae have a 25% reduction of TH neurons at 5dpf. This had been confirmed using DAT as a secondary marker, which also demonstrated a 25% reduction. [201] The nature of this reduction could either be due to cell death of the TH positive neurons, or a developmental phenotype. As zebrafish develop *ex vivo*, they present the perfect model to examine any possible neuro-developmental defects that may lead to the recorded TH neuron reduction. To investigate this, a series of neurodevelopmental markers were analysed in *pink1 -/-* and their WT controls. The markers stained by WISH included *shh*, *emx1*, *otpa*, *otpb*, *krox20*, and *pax2.1*. This experiment was jointly undertaken between the author and Ms Elena de Felice. Markers for *shh*, *emx1*, *otpb*, *krox20*, and *pax2.1,* were stained and analysed by Ms Elena de Felice. The marker *otpa* was stained and analysed by the author. Both genotypes were analysed throughout development at 1-5 days post fertilisation. No differences in change of expression of any gene were seen in either genotype qualitatively or quantitatively (see Figure 15), suggesting that Th neuron reduction in *pink1 -/-* larvae is not due to a developmental defect after 24hpf. This does not rule out developmental defects effecting TH neuron development pre 24dpf.

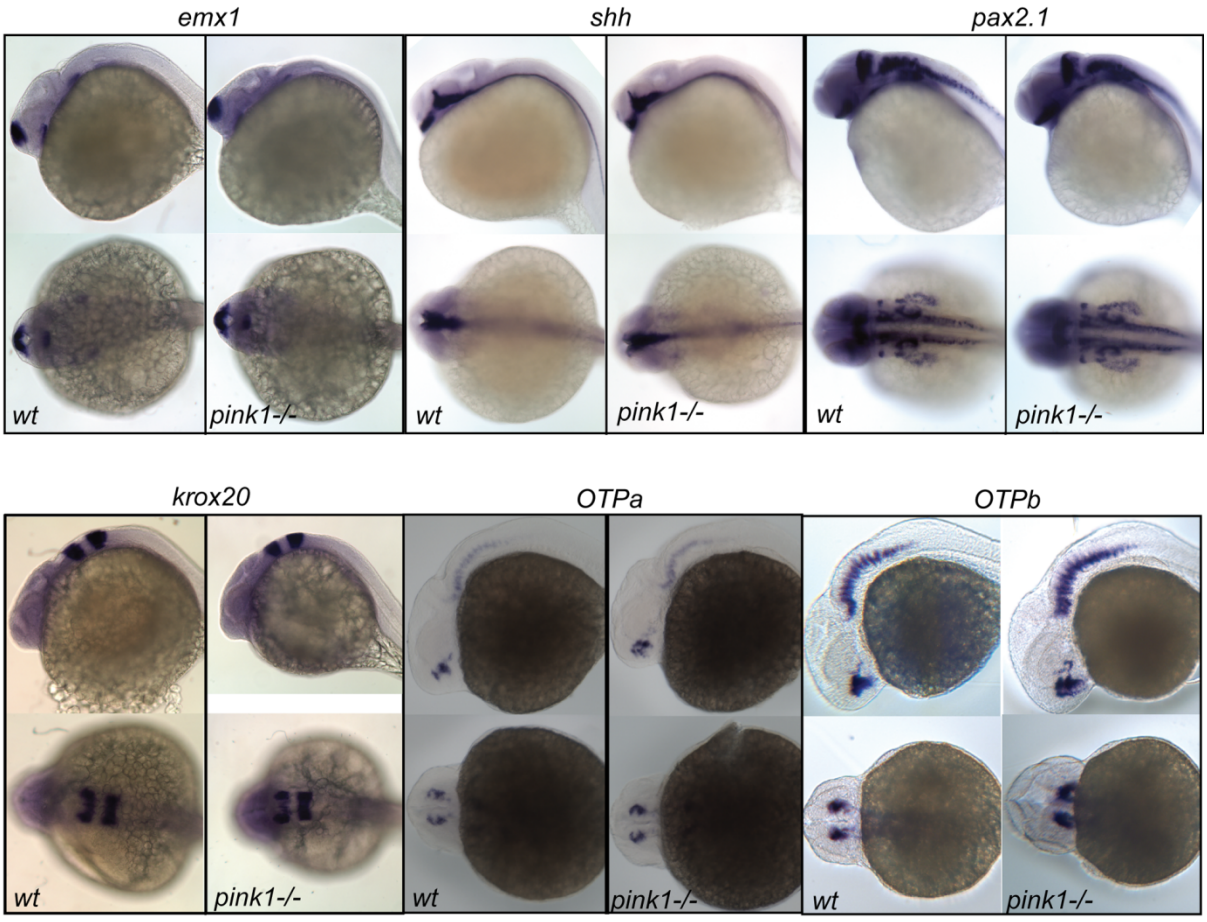

Figure 15. Developmental markers in *pink1 -/-* larvae. A series of neuronal developmental markers were analysed in *pink1 -/-* and WT from 1-5dpf (only 1dpf shown). These were emx1, shh, pax2.1, krox20, otpa and otpb. only 1dpf shown. No difference was observed in WISH staining in either group at any marker arguing against Th neuron reduction being due to a development defect at 24hpf and after.

3.1.6 *pink1 -/-* microarray re-annotation

Previous to the commencement of this thesis, microarray-based gene expression analysis had been conducted between *pink1 -/-* and WT controls at 5dpf to identify gene expression changes that may be leading to the reported Th neuron reduction. The original microarray had been annotated using ENSEMBL data of the Zebrafish genome during its 5th version. The zebrafish genome is now in its 9th assembly and considerably more detailed and annotated. Approximately 80% of the probe changes in the original microarray were to unannotated zebrafish genes. To re-annotate the microarray using the 9th version of the zebrafish genome, each probe was searched for via BLAST in the zebrafish cDNA database with multiple stringencies. When the zebrafish transcript was identified, the zebrafish transcript was search for using BLAST in the human genome to identity a suitable orthologue if ENSEMBL had not

automatically identified it as an orthologue of a human gene,. All probe hits that required re-annotation are highlighted in blue. See Table 5 for a re-annotated list of upregulated transcripts in the *pink1 -/-* 5dpf larvae and Table 6 for the down regulated transcripts.

FCAbsolute	GeneSymbol	GeneName
16.423103	hdac9b	histone deacetylase 9b
14.817871	tigarb	tp53-induced glycolysis and apoptosis regulator b
10.187797	cfh	Complement factor H
9.761307	CU463157.1	Similar to Complement factor H
9.706486	N/A	BLAST SEARCH GAVE NO HITS
7.7182097	N/A	Multiple HITS
7.0322556	ALPP	alkaline phosphatase, placental
5.9192815	rpl13a	ribosomal protein L13a
5.836889	myl6	myosin, light chain 6, alkali
5.437794	ccbl1	cysteine conjugate-beta lyase; cytoplasmic
5.365619	N/A	BLAST SEARCH GAVE NO HITS
5.274791	N/A	BLAST SEARCH GAVE NO HITS
5.229535	tom1l2	target of myb1-like 2 (chicken)
5.0453973	xkr9	XK, Kell blood group complex subunit-related family
4.987913	fbxo16	F-box protein 16
4.905778	apex1	APEX nuclease 1
4.9030137	si:dkey-238c7.13	A non -protein coding transcript
4.847179	uvrag	UV radiation resistance associated gene
4.8395343	zgc:101572	Protein kinase-like protein SgK196
4.778119	ccbl1	cysteine conjugate-beta lyase; cytoplasmic
4.6681256	crebl2	cAMP responsive element binding protein-like 2
4.5243216	N/A	BLAST SEARCH GAVE NO HITS
4.2470703	N/A	BLAST SEARCH GAVE NO HITS
4.1389275	CCDC137	coiled-coil domain containing 137
3.9723723	N/A	Multiple HITS
3.878004	capn8	calpain 8
3.8745248	N/A	BLAST SEARCH GAVE NO HITS
3.7615082	capn8	calpain 8
3.6562207	N/A	Multiple HITS
3.5966234	N/A	processed transcript si:ch73-44m9.2-001
3.59213	ptgs2b	prostaglandin-endoperoxide synthase 2b
3.549981	IMPG2	interphotoreceptor matrix proteoglycan
3.5278482	zgc:162239	acyl-CoA synthetase long-chain family member 1
3.5260308	FETUB	fetuin B
3.5236447	zgc:122979	DnaJ (Hsp40) homolog, subfamily B, member 5
3.3546922	FUT9 (3 of 16)	fucosyltransferase 9
3.3368623	N/A	Multiple HITS
3.291373	N/A	BLAST SEARCH GAVE NO HITS
3.2243793	N/A	BLAST SEARCH GAVE NO HITS
3.197398	pogza	pogo transposable element with ZNF domain
3.0550892	GJA4	gap junction protein, alpha 4
3.0521128	MATE 1	Multidrug and toxin extrusion protein 1
3.0221562	nudix	nucleoside diphosphate linked moiety X
2.999063	bhlhb3l	basic helix-loop-helix domain

FCAbsolute	GeneSymbol	GeneName
2.909844	N/A	BLAST SEARCH GAVE NO HITS
2.8619947	cdadc1	cytidine and dCMP deaminase domain containing 1
2.8518662	cyp8b1	cytochrome P450, family 8
2.8446841	SMU1	smu-1 suppressor of mec-8 and unc-52 homolog
2.8259096	N/A	BLAST SEARCH GAVE NO HITS
2.8096638	N/A	BLAST SEARCH GAVE NO HITS
2.7729554	yipf5	Yip1 domain family, member 5
2.7522666	ubtd1	ubiquitin domain containing 1
2.720866	ACY1	Aminoacylase-1 61% homology to human gene
2.7193558	N/A	Probe not specific
2.7091837	rgs2	regulator of G-protein signaling 2
2.686784	pex14	peroxisomal biogenesis factor 14
2.6860514	HSP3	Hermansky-Pudlak syndrome 3
2.6850827	taar65	trace amine associated receptor 65
2.6711266	N/A	Multiple HITS
2.64639	N/A	Multiple HITS
2.583023	N/A	BLAST SEARCH GAVE NO HITS
2.5543456	rh50	Rh50-like protein
2.5355914	NUDT16	nucleoside diphosphate linked moiety X
2.5262425	ENPP7	ectonucleotide pyrophosphatase/phosphodiesterase 7
2.4969575	N/A	BLAST SEARCH GAVE NO HITS
2.4912636	SH3BGRL3	SH3 domain binding glutamic acid-rich protein like 3
2.471074	N/A	BLAST SEARCH GAVE NO HITS
2.465009	N/A	BLAST SEARCH GAVE NO HITS
2.4475963	SH3BGRL3	SH3 domain binding glutamic acid-rich protein like 3
2.4423368	ACE	angiotensin I converting enzyme
2.4230134	ATPBD4	ATP binding domain 4
2.4093752	ubr3	ubiquitin protein ligase E3 component n-recognin 3
2.4026387	bokb	BCL2-related ovarian killer b
2.3753383	zmat2	zinc finger, matrin type 2
2.3702154	rh50	Rh50-like protein
2.3591704	N/A	BLAST SEARCH GAVE NO HITS
2.3576367	polr1b	polymerase (RNA) I polypeptide B
2.3572855	rhcg	Rhesus blood group, C glycoprotein
2.3397517	RAB35	RAB35, member RAS oncogene family
2.3275254	SLC16A8	similar to monocarboxylate transporter 3
2.3168197	st14b	suppression of tumorigenicity 14 (colon carcinoma) b
2.2862763	vti1a	vesicle transport through interaction with t-SNAREs
2.2692866	mylipb	myosin regulatory light chain interacting protein b
2.258262	N/A	BLAST SEARCH GAVE NO HITS
2.2536519	CAMKK1(2 of 2)	calcium/calmodulin-dependent protein kinase kinase 1
2.243251	slco2b1	solute carrier organic anion transporter family
2.240908	ntf3	neurotrophin 3
2.2320147	bhlhb3l	basic helix-loop-helix domain containing, class B
2.2305305	N/A	BLAST SEARCH GAVE NO HITS
2.2201831	nt5c3	5'-nucleotidase, cytosolic III
2.2149444	ZNF362	zinc finger protein 362
2.2083664	dapp1	dual adaptor of phosphotyrosine and 3-phosphoinositides
2.2026093	rgs2	regulator of G-protein signalling 2
2.1944575	SUSD3 (3 of 3)	sushi domain containing 3
2.1529658	gltpd2	similar to glycolipid transfer protein domain containing 1

FCAbsolute	GeneSymbol	GeneName
2.143542	zgc:66298	polymerase (RNA) I polypeptide B
2.1408815	TTF1 (6 of 6)	transcription termination factor, RNA polymerase I
2.1399355	N/A	BLAST SEARCH GAVE NO HITS
2.136245	cdk5	cyclin-dependent protein kinase 5
2.1317372	dcps	mRNA de-capping enzyme
2.1275663	guca1c	guanylate cyclase activator 1C
2.1216083	ubtd1	ubiquitin domain containing 1
2.115108	fam151a	family with sequence similarity 151, member A
2.0885773	rbm28	RNA binding motif protein 28
2.0721066	slc23a1	solute carrier family 23 (nucleobase transporters)
2.0627465	N/A	3 hits but all in the wrong direction
2.062203	N/A	BLAST SEARCH GAVE NO HITS
2.054885	si:ch211-9d9.1	Novel protein si:ch211-9d9.
2.04587	fbxl22	F-box and leucine-rich repeat protein 22
2.0447233	cx28.9	connexin 28.9
2.0266476	LOC796252	chemokine CXL-C24a
2.022967	LOC100001286	similar to C6orf106
2.0225506	bcl2l	bcl2-like 50% homology to human gene
2.0224402	rnf207	ring finger protein 207
2.0055213	otud7b	OTU domain containing 7B

Table 5.Up-regulated transcripts in *pink1 -/-* microarray. All genes highlighted in green were altered during re annotation.

FCAbsolute	GeneSymbol	Description
337.62494	A2LD1	AIG2-like domain 1
294.653	si:dkeyp-73d8.6	Homology to ATP-binding cassette, sub-family A
208.23721	N/A	BLAST SEARCH GAVE NO HITS
156.19023	lmbr1l	Danio rerio limb region 1 like
48.701042	im:7148382	IMAP family member 4 and GTPase
32.852505	BLOC1S2	biogenesis of lysosomal organelles complex-1, s2
31.081526	gltpd1-	glycolipid transfer protein domain containing 1
26.637669	polr2b	polymerase (RNA) II (DNA directed) polypeptide B
26.173359	BLOC1S2	biogenesis of lysosomal organelles complex-1, s2
25.223787	N/A	BLAST SEARCH GAVE NO HITS
24.581673	SLC17A3	solute carrier family 17 (sodium phosphate)
23.082857	A2LD1	AIG2-like domain 1
21.294308	N/A	BLAST SEARCH GAVE NO HITS
21.037832	N/A	Multiple HITS
20.258842	dhrs11a	dehydrogenase/reductase (SDR family) member 11a
20.244846	N/A	BLAST SEARCH GAVE NO HITS
20.155668	kmo	kynurenine 3-monooxygenas
16.645021	N/A	BLAST SEARCH GAVE NO HITS
14.625197	gpib	glucose phosphate isomerase b
14.02044	A2LD1	AIG2-like domain 1
14.008943	TSEN15	tRNA splicing endonuclease 15 homolog
12.349935	wnt9a	Danio rerio wingless-type MMTV integration site
11.57964	RAP1GAP	RAP1 GTPase activating protein
11.193585	N/A	BLAST SEARCH GAVE NO HITS
10.937099	FABP6	fatty acid binding protein 6, ileal

FCAbsolute	GeneSymbol	Description
10.151755	gpib	glucose phosphate isomerase b
10.0883045	A2LD1	AIG2-like domain 1
9.349176	N/A	BLAST SEARCH GAVE NO HITS
8.381044	psmg1	proteasome assembly chaperone
7.8119206	N/A	BLAST SEARCH GAVE NO HITS
7.7133327	TSG101	tumor susceptibility gene 101
7.341222	dnmt4	DNA (cytosine-5-)-methyltransferase 4
6.614778	si:ch211	si:ch211-260o22.1 no human orthologue
6.3371925	N/A	BLAST SEARCH GAVE NO HITS
6.1110654	N/A	BLAST SEARCH GAVE NO HITS
5.987409	N/A	BLAST SEARCH GAVE NO HITS
5.91139	N/A	BLAST SEARCH GAVE NO HITS
5.4998446	N/A	BLAST SEARCH GAVE NO HITS
5.3801837	olfml3a	olfactomedin-like 3a
5.192232	RAP1GAP	RAP1 GTPase activating protein
4.8446903	STARD8	StAR-related lipid transfer domain containing 8
4.7878747	N/A	BLAST SEARCH GAVE NO HITS
4.76362	hsf1	heat shock transcription factor 1
4.749809	UNC13C	unc-13 homolog C
4.7147145	N/A	BLAST SEARCH GAVE NO HITS
4.6948247	si:dkey-217f16.3	Processed transcript
4.5762057	UNC13C	unc-13 homolog C
4.4179616	N/A	BLAST SEARCH GAVE NO HITS
4.415685	N/A	BLAST SEARCH GAVE NO HITS
4.3336716	N/A	BLAST SEARCH GAVE NO HITS
4.331479	parp6a	poly (ADP-ribose) polymerase family, member 6a
4.285228	cyp24a1l	cytochrome P450, family 24, subfamily A, p1
4.225144	N/A	Multiple HITS
4.015451	N/A	BLAST SEARCH GAVE NO HITS
3.994224	N/A	BLAST SEARCH GAVE NO HITS
3.9867797	dnmt8	DNA (cytosine-5-)-methyltransferase 8
3.908932	N/A	BLAST SEARCH GAVE NO HITS
3.8250778	N/A	BLAST SEARCH GAVE NO HITS
3.822486	N/A	BLAST SEARCH GAVE NO HITS
3.801205	nedd1	neural cell expressed, down-regulated 1
3.798918	N/A	BLAST SEARCH GAVE NO HITS
3.7675848	pnrc2	proline-rich nuclear receptor co-activator 2
3.7333267	slc35c2	solute carrier family 35, member C2
3.7078235	N/A	BLAST SEARCH GAVE NO HITS
3.6977255	cyp24a1l	cytochrome P450, family 24, subfamily A
3.6936898	adh8a	Danio rerio alcohol dehydrogenase 8a
3.691377	N/A	BLAST SEARCH GAVE NO HITS
3.656716	N/A	BLAST SEARCH GAVE NO HITS
3.4622538	or115-15	odorant receptor, family F, subfamily 115, member 15
3.4027152	zgc:77778	Novel gene zgc:77778
3.3788104	N/A	BLAST SEARCH GAVE NO HITS
3.3629289	PAK6	p21 protein (Cdc42/Rac)-activated kinase 6
3.2621887	myt1	myelin transcription factor 1
3.238024	N/A	BLAST SEARCH GAVE NO HITS
3.1932921	N/A	BLAST SEARCH GAVE NO HITS
3.1537905	N/A	BLAST SEARCH GAVE NO HITS

FCAbsolute	GeneSymbol	Description
3.1504362	N/A	Multiple HITS
3.1422331	minal	MYC induced nuclear antigen-like
3.1365201	N/A	BLAST SEARCH GAVE NO HITS
3.11931	A2LD1	AIG2-like domain 1
3.1175594	N/A	BLAST SEARCH GAVE NO HITS
3.108831	minal	MYC induced nuclear antigen-like
3.105338	nek8	NIMA (never in mitosis gene a)-related kinase 8
3.0960152	GST?	Possible orthologue of glutathione S-transferase t2
3.0869365	tcf21	transcription factor 21
3.0493743	N/A	BLAST SEARCH GAVE NO HITS
3.0321693	znf511	zinc finger protein 511
3.0255601	ITLN1	Orthologue of Human Interlectin 1 and 2
3.0156412	N/A	BLAST SEARCH GAVE NO HITS
2.9421065	usp19	ubiquitin specific peptidase 19
2.8969617	N/A	BLAST SEARCH GAVE NO HITS
2.8825202	zgc:162431	coiled-coil domain containing 50
2.8793223	N/A	BLAST SEARCH GAVE NO HITS
2.7616208	ndrg1l	N-myc downstream regulated gene 1
2.7057443	ALPP	alkaline phosphatase, placental
2.7017643	rxfp2	relaxin/insulin-like family peptide receptor 2
2.6924372	PDRG1	p53 and DNA-damage regulated 1
2.6574495	sema3bl	sema domain, immunoglobulin domain
2.6233196	trpc4apb	transient receptor potential cation channel
2.6145089	GPR22 (2 of 2)	G protein-coupled receptor 22
2.612301	ttyh2	tweety homolog 2 (Drosophila)
2.603541	N/A	BLAST SEARCH GAVE NO HITS
2.594108	atp6v1e1	ATPase, H+ transporting, lysosomal
2.592997	trpc4apb	transient receptor potential cation channel
2.563882	CASP7	caspase 7, apoptosis-related cysteine peptidase
2.4672425	N/A	BLAST SEARCH GAVE NO HITS
2.4536474	N/A	BLAST SEARCH GAVE NO HITS
2.4451828	pdlim5	PDZ and LIM domain 5
2.4280818	h3f3d	H3 histone, family 3D
2.4169915	N/A	BLAST SEARCH GAVE NO HITS
2.4159079	zgc:162431	coiled-coil domain containing 50
2.406655	N/A	Multiple HITS
2.4065533	ormdl2	ORM1-like 2
2.4046388	ifnphi3	interferon phi 3
2.40159	irgf1	immunity-related GTPase family, f1
2.3965645	COX19	COX19 cytochrome c oxidase assembly
2.393588	N/A	BLAST SEARCH GAVE NO HITS
2.3926997	N/A	BLAST SEARCH GAVE NO HITS
2.325134	FIG4 (2 of 2)	SAC1 lipid phosphatase domain containing
2.324486	scinlb	scinderin like b
2.31802	sfswap	splicing factor, suppressor of white-apricot homolog
2.313321	or106-8	odorant receptor, family G, subfamily 106, member 8
2.3082094	zgc:77778	Novel gene zgc:77778
2.3035688	plp1a	proteolipid protein 1a
2.2929733	d2hgdh	D-2-hydroxyglutarate dehydrogenase
2.282499	ugt5g1	UDP glucuronosyltransferase 5 family
2.2780974	N/A	BLAST SEARCH GAVE NO HITS

FCAbsolute	GeneSymbol	Description
2.2714615	mapk1	mitogen-activated protein kinase 1
2.264065	h1fx	H1 histone family, member X
2.2367263	h1fx	H1 histone family, member X
2.196375	zbtb8os	zinc finger and BTB domain 8 opposite strand
2.1856678	N/A	BLAST SEARCH GAVE NO HITS
2.1851153	N/A	BLAST SEARCH GAVE NO HITS
2.1839597	aggf1	angiogenic factor with G patch and FHA domains 1
2.1829376	c1galt1a	glycoprotein-N-acetylgalactosamine,3-beta
2.1532488	N/A	BLAST SEARCH GAVE NO HITS
2.1515162	CCDC50	coiled-coil domain containing 50
2.1179307	pcmt	l-isoaspartyl protein carboxyl methyltransferase
2.1156254	cry2a	cryptochrome 2a
2.1147645	ncam1b	neural cell adhesion molecule 1b
2.1113217	zgc:165603	Possible orthologue of CUGBP, Elav-like
2.100326	N/A	BLAST SEARCH GAVE NO HITS
2.100112	LOC100000522	caspase 7, apoptosis-related cysteine peptidase
2.090073	si:ch1073	similar to nicotinamide nucleotide transhydrogenase
2.0878496	N/A	BLAST SEARCH GAVE NO HITS
2.0687912	zp3	zona pellucida glycoprotein 3
2.0626397	cyp26a1	cytochrome P450, subfamily XXVIA, polypeptide 1
2.0602734	CAMKV	similar to CaM kinase-like vesicle-associated protein
2.0586677	arrdc3	arrestin domain containing 3
2.0586	tmx3	thioredoxin-related transmembrane protein 3
2.0477684	sqstm1	sequestosome 1
2.0187578	arhgap4a	Rho GTPase activating protein 4a
2.0176172	N/A	BLAST SEARCH GAVE NO HITS
2.0170264	rxfp2	relaxin/insulin-like family peptide receptor 2
2.0129385	cyp26a1	cytochrome P450, subfamily XXVIA, polypeptide 1
2.0070715	N/A	BLAST SEARCH GAVE NO HITS
2.0065784	FBXL17	F-box and leucine-rich repeat protein 17

Table 6. The down-regulated transcripts in *pink1 -/-* microarray. All genes highlighted in green were altered during re annotation.

Of the 276 probes that had different expression between *pink1 -/-* and WT, 211 probes (76%) required re annotation. 73 probes (26%) did not match homology to any known zebrafish cDNA or cross reacted to a variety of transcripts equally. Of specific interest, the reference gene *rpl13a* appeared as upregulated in the *pink1 -/-*, a gene previously utilised for normalisation in qPCR studies. The majority of gene expression changes that were up regulated did not appear to be related and there were only three mitochondrial genes. The gene ontogeny terms of the remaining changed probes were diverse and included autophagy, mRNA processing, calcium binding, onco-proteins and endocytosis. In the down regulated probes, many could not be matched to a specific cDNA in the zebrafish genome. Of note, 5 down-regulated probes matched to one cDNA, of the AIG like-2 domain protein, an enzyme that catalyses the breakdown

of isodipeptide L-gamma-glutamyl-L-epsilon-lysine to 5-oxo-L-proline and free alkylamine.[289]

3.2 *pink1 -/-* Th neuron reduction is rescued by *tigarb* knockdown

3.2.1 *pink1 -/-* gene expression changes at 5dpf

From the microarray, several upregulated genes of interest were chosen for further investigation. These transcripts were coded for by the following genes, *tigarb*, a glycolytic inhibitor (up 14 fold), *hdac9b* a histone deacetylase (up 16 fold) and *apex1* a DNA repair enzyme (up 5 fold). In order to carry out functional studies with gene-gene interactions, these changes required confirmation. Each transcript was analysed by qPCR to investigate the specific gene expression changes. However, no changes in gene expression were found between *pink1 -/-* and WT controls at 5dpf, for either *hdac9b* or *apex1* (Figure 16). Of note, *tigarb* expression in *pink1 -/-* was found to be increased nearly 3 fold compared to WT controls ($P<0.001$ unpaired T test), and hence confirming the upregulation recorded in the microarray (Figure 16).

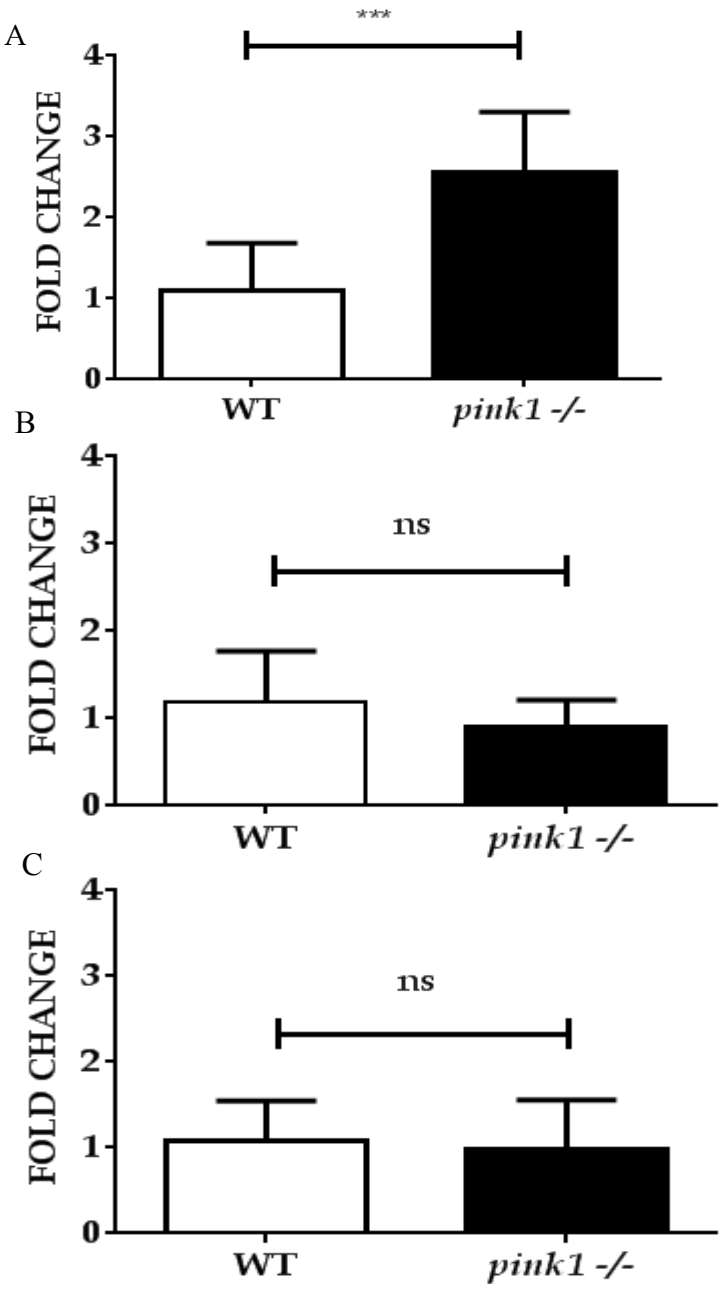

Figure 16. Gene expression analysis between *pink1 -/-* and WT. To confirm the upregulation of particular gene transcripts suggested in the *pink1 -/ -*microarray experiments, qPCR was undertaken to confirm or refute changes in the expression of *tigarb* (A), *hdac9b* (B) and *apex1* (C) in *pink1 -/-* 5dpf and compared to their WT. The only expression changes from the microarray that could be confirmed were for *tigarb* with *pink1 -/-* larvae having nearly a 3 fold increase ($P<0.001$ unpaired T test) in *tigarb* expression compared to WT at 5dpf. Specific mRNA expression levels were normalised to the reference gene *ef1alpha*.

3.2.2 *tigarb* is chronically upregulated during development in *pink1 -/-* larvae

tigarb expression in WT embryos was detected as early as 4hpf by RT-PCR (Figure 17) and ubiquitously expressed throughout development. To establish whether *tigarb* upregulation may be mediating Th neuron reduction during embryogenesis in *pink1 -/-*, expression had to be confirmed in the brain. An *in situ* hybridisation probe was constructed specifically for *tigarb* and utilised to stain for expression in *pink1 -/-* and their WT controls from 1-5 days post fertilisation. Expression was present through all age groups and was not spatially restricted. WISH confirmed *tigarb* upregulation in *pink1 -/-,* development, including increased expression in the *pink1 -/-* brains (Figure 18).

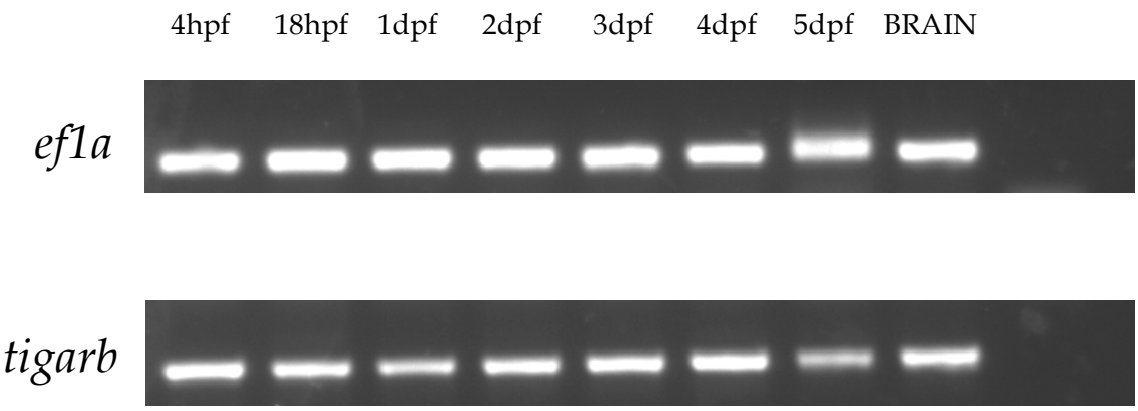

Figure 17. *tigarb* expression through development. *tigarb* transcript levels were measured throughout development from 4-120hpf by RT-PCR. *tigarb* expression was also confirmed in adult brain material. *ef1a* was utilised as a loading control.

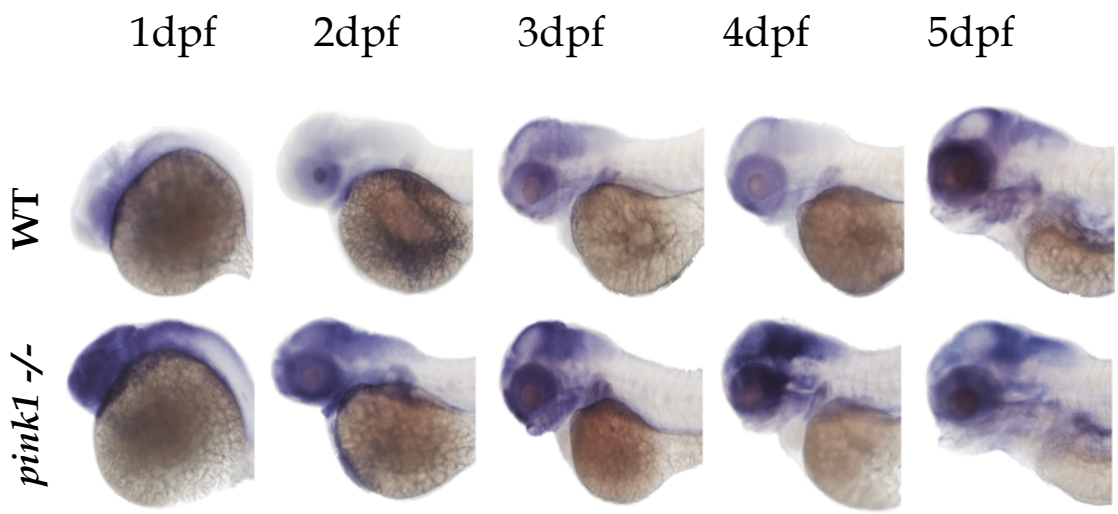

Figure 18. *tigarb* WISH through development in *pink1* -/-. Widespread *tigarb* expression was evident in all organs, with marked expression in the head and chronically increased in the *pink1* -/- throughout development.

3.2.3 *tigarb* Morpholino optimisation

Upregulation of *tigarb* could either be due to it being an activated survival mechanism or reflect involvement of *tigarb* in the mechanisms leading to the observed DA cell loss. To further investigate this, splice Morpholinos were designed to specifically KD *tigarb* in zebrafish embryos. Exons 2, 3 and 6 were chosen for targeting as their coding region was of functional importance for enzyme activity. For example, exons 2 and 3 code for the second and third residues that form the catalytic triad required for the bisphosphatase activity (Figure 19).[228]

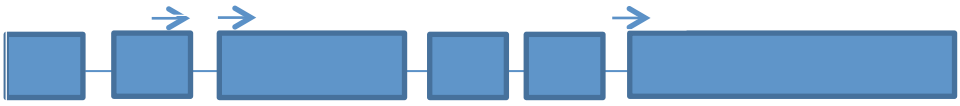

Figure 19. Schematic demonstrating Morpholino targets against *tigarb* exons. Morpholinos denoted by an arrow, were designed against the splicing boundaries of e2i2, i2e3 and i5e6.

Initial toxicity tests were performed by inspection of embryos at 1, 2, and 3 days post fertilisation, following injection of 0.25mM, 0.5mM and 0.9mM Morpholino at the 1 cell stage. Toxicity tests found *tigarb* Morpholinos directed at exons 2 and 3 to be non-

toxic, with only slight deformity seen in approximately 10% of subjects by 3dpf. In contrast, the Morpholino against exon 6 was found to be very toxic, the exon 6 Morpholino induced severe developmental delay of approximately 6 hours at the 24 hpf time point, and gross deformity, even at the lowest concentration. This Morpholino was therefore not used due to clear off target effects. As the effects of morpholinos generally wear off by 3dpf, to measure efficacy, RNA was extracted from morphants injected with all concentrations at 3dpf, reverse transcribed to generate cDNA and then amplified by PCR. Each sample was electrophoresed on a 2% agarose gel and compared to WT to investigate Morpholino effects on splicing.

For the Morpholino targeting exon 2 of *tigarb* (referred to as TBMO2), more than 90% aberrant splicing was achieved at 0.9mM (Figure 20). Exon 2 partly codes for the catalytic triad region of *tigarb*, and TBMO2 caused a complete skip of exon 2, confirmed by direct sequencing) that partly codes for t*igarb*'s catalytic triad. The exon deletion also resulted in a frame shift. Lower concentrations lead to lower levels of exon skipping.

Using a Morpholino targeting exon 3 of *tigarb* (TBMO3), did not have an effect on splicing even at 0.9mM and was therefore not chosen for further experiments either which only concentrated on the use of TBMO2.

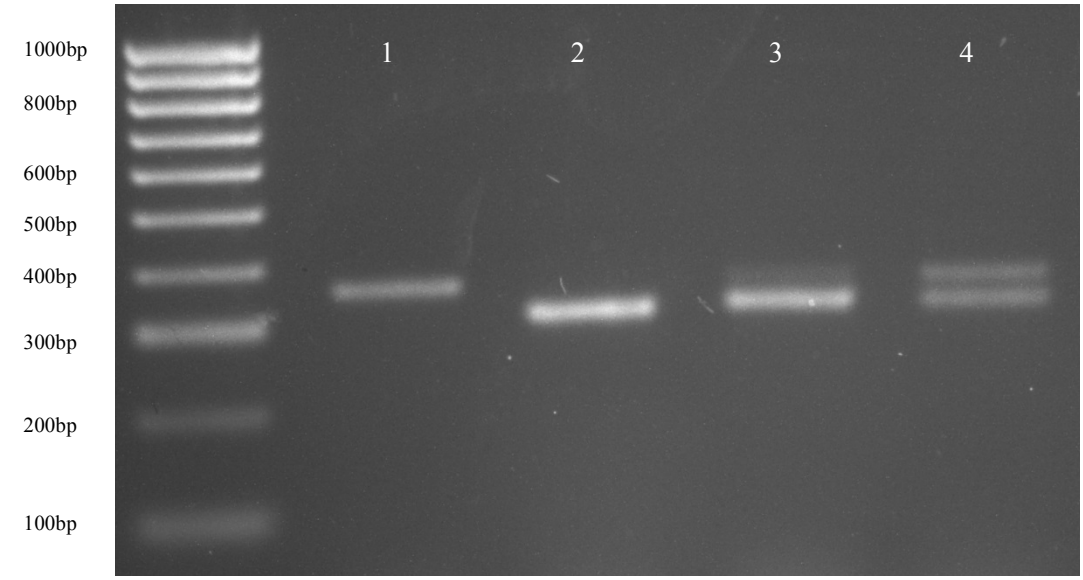

Figure 20. *tigarb* Morpholino 2 optimisation. A Morpholino designed to target exon 2 (e2i2) of *tigarb* was injected at several concentrations to ascertain toxicity and efficacy. Efficacy was measure by RT-PCR at 3dpf. Lane 1, uninjected controls, lane 2, 0.9mM, lane 3 0.5mM and lane 5, 0.25mM. The Morpholino was non- toxic at any concentration. With increasing concentration of the Morpholino, greater exon skip of exon 2 (confirmed by direct sequencing) was achieved, giving 90-100% KD at 0.9mM.

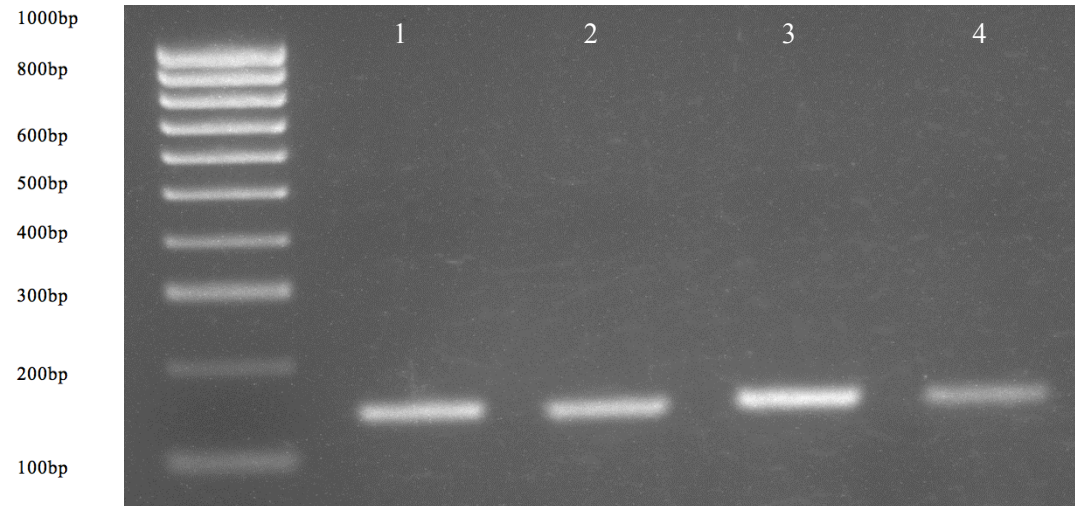

Figure 21. TBMO3 optimisation. A Morpholino designed to target exon 3 (i2e3) of *tigarb* was injected at several concentrations to ascertain toxicity and efficacy. Efficacy was measure by RT-PCR at 3dpf. Lane 1, uninjected controls, lane 2, 0.9mM, lane 3 0.5mM and lane 5, 0.25mM. The Morpholino was non- toxic at any concentration. However the Morpholino did not lead to any obvious splicing defects at any concentration.

3.2.4 *tigara* expression in *pink1 -/-* larvae

The zebrafish genome contains many orthologues of human genes, however, due to a duplication event, many of these have two copies in zebrafish. *Tigar* is no exception, with the zebrafish genome containing two orthologues with approximately 50% protein homology, *tigarb* and *tigara*. Only *tigarb* was demonstrated to be upregulated in the *pink1 -/-* microarray. As both orthologues may be functionally redundant, gene expression analysis of *tigara* was investigated by qPCR and WISH, in the *pink1 -/-* larvae and their WT controls. qPCR demonstrated approximately a twofold upregulation of *tigara* in the *pink1 -/-*; a similar trend to that of *tigarb*. However, this upregulation was very variable and not statistically significant (P=0.178 unpaired T test) (Figure 22). As these results were inconclusive, an *in situ* probe was constructed to stain *tigara* expression. Consequently WISH experiments using this probe were undertaken throughout development between WT controls and *pink1 -/-* larvae. *tigara* expression was similar to *tigarb*, ubiquitous and not spatially restricted. No staining was detected with the sense probe (Figure 23). Although *tigara* expression was demonstrated to be upregulated at certain time points, this was not found to be a robust phenotype on subsequent replicates or at all-time points. Consequently, increased *tigara* expression in *pink1 -/-* larvae was deemed inconclusive.

Considering *tigara* may be functionally redundant to *tigarb*, it is plausible that *tigarb* KD may result in an increase in *tigara* expression levels to compensate. However, gene expression analysis of *tigara* by qPCR in TBMO2 morphants demonstrated that *tigarb* KD did not change *tigara* expression levels (Figure 22).

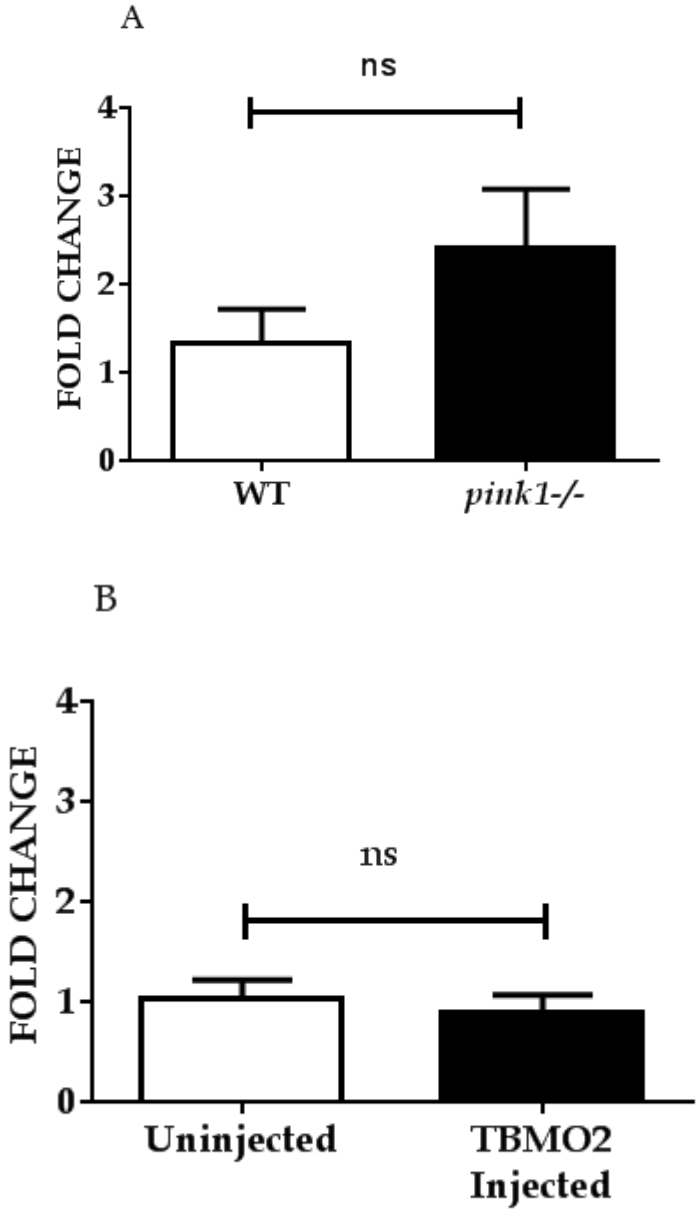

Figure 22. *tigara* expression levels quantified by qPCR. Figure 22A comparing *tigara* expression between *pink1 -/-* 5dpf larvae and their WT. *pink1 -/-*showing a trend for increased *tigara* expression compared to WT, however this was not statistically significant. Figure 22B comparing *tigara* expression levels in uninjected WT controls at 3dpf and WT TBMO2 injected larvae. No change in *tigara* expression levels between the two groups was detected; implying *tigarb* KD does not increase *tigara* expression due to functional redundancy. *ef1 alpha* was used as a reference gene for normalisation.

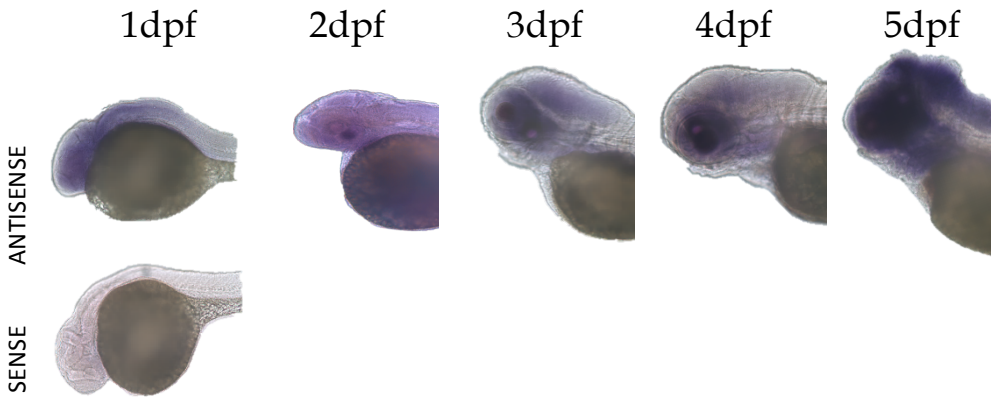

Figure 23. WISH of *tigara* in WT larvae during early development. Staining was ubiquitous and not spatially restricted in a similar manner to *tigarb* expression. No staining was detected with the sense probe, demonstrating antisense staining to be specific for *tigara*.

3.2.5 Knockdown of *tigarb* rescues Th neuron reduction in *pink1 -/-* larvae

With the Morpholino optimised, TBMO2 was utilised to inactivate *tigarb* in *pink1 -/-* and their WT controls, and investigate whether this would lead to either a rescue or a worsening of their phenotype in general and the effect on the number of DA neurons in particular. Morphants were morphologically normal in both genotypes and full KD was achieved in spite of *tigarb* upregulation in *pink1 -/-* larvae (Figure 24)

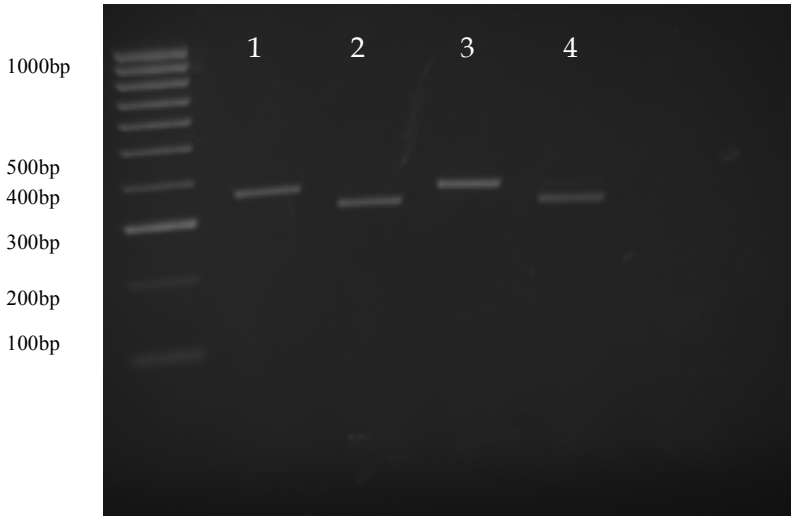

Figure 24. ***tigarb KD* in *pink1 -/-* and WT larvae.** *tigarb* KD in *pink1 -/-* larvae and their WT controls resulted in >90% KD determined by RT-PCR at 3dpf. Lane 1 WT uninjected, lane 2 WT TBMO2, lane 3 *pink1 -/-* uninjected and lane 4 *pink1 -/-* TBMO2. Morphants were morphologically normal regardless of genotype.

Analysis of TH-positive neurons at 3dpf demonstrated a 20% reduction in *pink1 -/-* uninjected larvae ($P<0.05$) compared to WT uninjected larvae, similar to that seen at 5dpf. KD of *tigarb* in WT controls led to a small increase in TH neurons of 5% although this was not statistically significant. KD of *tigarb* in *pink1 -/-* larvae resulted in a complete normalisation of the TH positive neuron level to that of WT controls (Figure 25). This suggests that *tigarb* upregulation in the *pink1 -/-* is responsible for the Th neuron reduction.

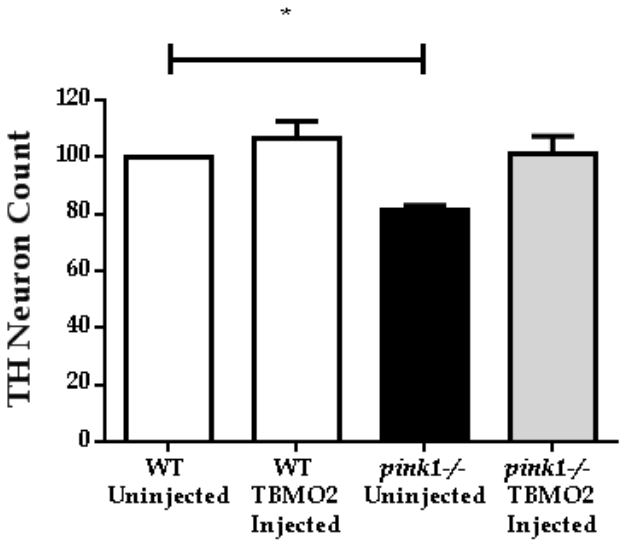

Figure 25. Knockdown of *tigarb* rescues Th neuron reduction in *pink1-/-* larvae. KD of *tigarb* in WT larvae had a small effect on TH level, raising it by 5% although this did not reach significance. The *pink1-/-* un-injected larvae at 3dpf exhibited a 20% decrease in TH neuron count compared to WT as seen at 5dpf ($P<0.05$, two way anova). KD of *tigarb* in *pink1-/-* led to a complete normalisation of the TH neuron count, with an average TH neuron count of approximately 100% compared to the uninjected WT. WT uninjected TH neuron counts normalised to 100%, experimental groups expressed as a percentage of this. See materials and methods for more detail.

3.2.6 *pink1* Morpholino design and optimisation

To further confirm the functional relevance of *tigarb* KD as a rescue mechanism in *pink1* deficiency, the author tested its effect in a different model of *pink1* deficiency with MO mediated *pink1* KD. *tigarb* KD, leading to a rescue of *pink1 -/-* phenotypes, needed to be confirmed in a second model of *pink1* deficiency. However, as all published Morpholinos did not phenocopy the stable Y421* mutant, a new *pink1* Morpholino had to be designed and optimised.

Morpholino sites in *pink1* were chosen by analysing each exon and evaluating it for ease of assay, and whether exon skip/intron inclusion would lead to a subsequent frame shift. See Figure 26 for a schematic, illustrating choice of exon/intron boundaries chosen for further analysis.

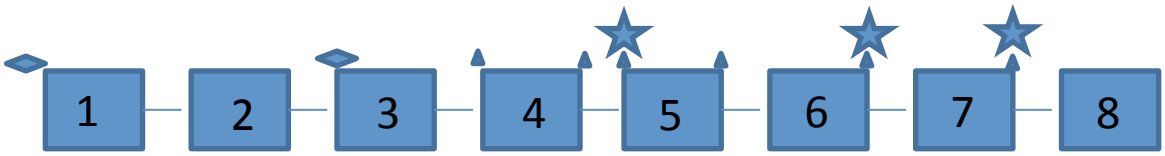

Figure 26. A schematic outlining *pink1* Morpholino design. *pink1* exons were labelled to denote locations of published *pink1* Morpholinos (diamond shape), novel designed gene tools Morpholino sites (triangle shape) and SNP sites (star shape). Consequently, exons were manufactured targeting exon 4 (i3e4 and e4i4) and exon 5 (e5i5).

The company Gene Tools were able to design morpholinos to the intron-exon boundaries and exon-intron boundaries of exons 4 and 5, as well as the exon-intron boundaries of exons 6 and 7. Each Morpholino binding site was sequenced beforehand, to confirm that the genomic sequences on ENSEMBL that would be utilised for Morpholino design were correct. Any putative Morpholino target sites which contained SNPs were rejected, as these would prevent Morpholino binding. This left morpholinos targeting two sites in exon 4 and the exon-intron site of exon 5. All 3 morpholinos were ordered and toxicity and efficacy established in a manner similar to that of TBMO2 optimisation.

Morpholino i3e4 was found to be non-toxic at all concentration levels injected, however lacked efficacy, causing as little as 30% aberrant splicing at 24hpf and 72hpf. This particular Morpholino appeared to cause an exon skip of exon 4 and activation of cryptic splices sites simultaneously (Figure 27).

Morpholino e4i4 was found to be toxic at the 0.9mM injection, with morphants exhibiting a large delay in development and gross deformity. Injections at 0.5mM and 0.25mM had morphants with deformities responding in a dose dependant manner, consequently the Morpholino was deemed too toxic for further use. The action of the Morpholino appeared to be that of an intron inclusion that was not possible to assay, due to its large size >1000bp with the polymerases commonly utilised for this type of RT-PCR (Figure 28).

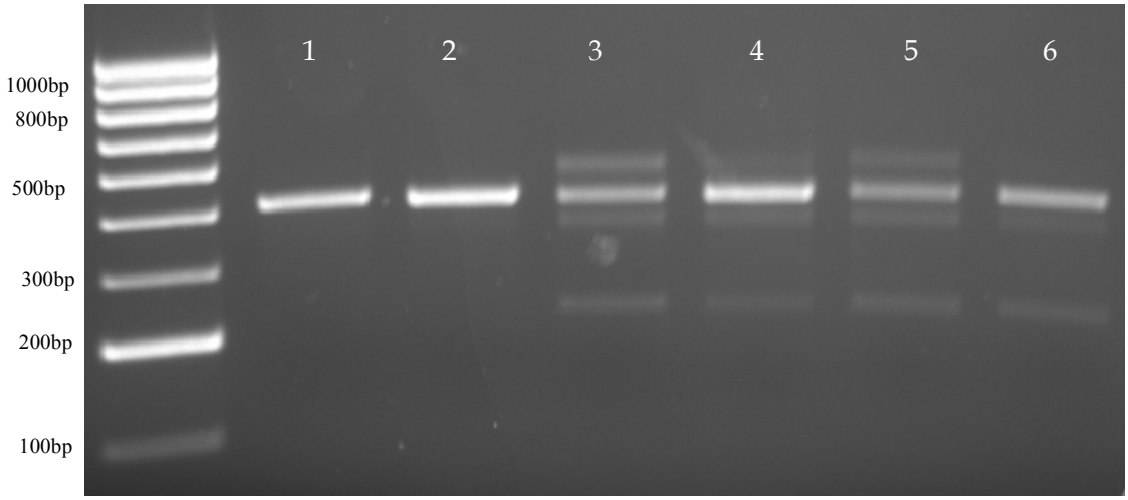

Figure 27. *pink1* Morpholino PINK4 (i3e4) optimisation. RT- PCR evaluating PINK4 (i3e4) efficacy. Lane 1 and 2, uninjected controls at 1 and 3 dpf respectively. Lanes 3 and 4, 0.9mM injected at 1 and 3 dpf. Lanes 5 and 6, 0.5mM injected at 1 and 3 dpf. The Morpholino was non toxic even at the highest dose. PINK4 (i3e4) causes likely activation of cryptic splice sites and an exon skip of exon 4. Even at highest dose and at the earliest time point, KD efficacy is still very low, with approximately 30% of the transcript being abnormally spliced.

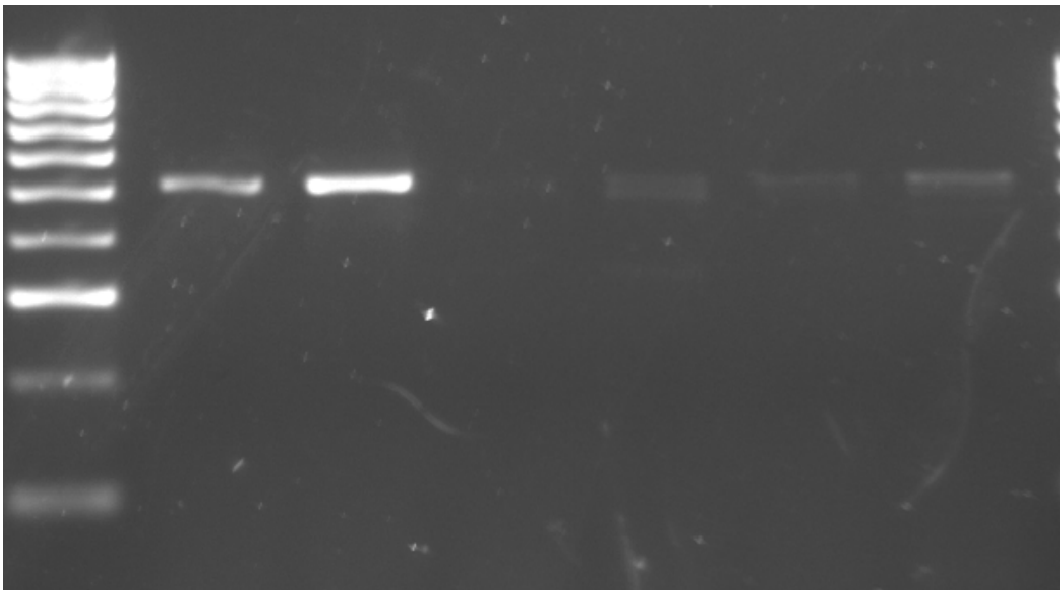

Figure 28. *pink1* Morpholino e4i4 optimisation. RT-PCR demonstrating efficacy of *pink1* Morpholino e4i4. Lanes 1 and 2, uninjected control at 1 and 3 dpf. Injections of 0.9mM of *pink1* morpholino e4i4 was toxic leading to excessive deformity and delays in development. Lanes 3 and 4 are injections of 0.5 mM at 1 and 3 dpf. Lanes 5 and 6 are injections of 0.25mM at 1 and 3 dpf. *pink1* Morpholino e4i4 appears to cause an intron inclusion which is not possible to assay with the current polymerases, due to its large size (2000bp). *pink1* Morpholino e4i4 is efficient, with over 90% abnormal splicing at 0.5mM.

Both Morpholinos were also co-injected to investigate synergistic splicing effects. The concentrations utilised for Morpholino e4i4, although toxic on their own, showed decreased toxicity when co-injected with Morpholino i3e4 for unknown reasons. More than 90% KD was achieved with the co-injection leading to an exon skip of exon 4 of

pink1 (Figure 29). Unfortunately co-injection of both of the *pink1* Morpholinos with TBMO2 was very toxic due to the large quantities of Morpholino injected (3 times what the author considers to be the potential highest dose).

The *pink1* Morpholino targeting the exon intron boundary of exon 5 (PINK5) was found to be non-toxic at all doses and led to more than >90% aberrant splicing at the highest dose. PINK5 led to an intron inclusion of intron 5 (77bp, confirmed by direct sequencing) and a small quantity (approximately 5%) of exon skip of exon 5 (Figure 30). A dose of 0.9mM PINK5 was chosen for co injection experiments. Co-injection of PINK5 and TBMO2 resulted in the expected KD efficacies (Figure 31).

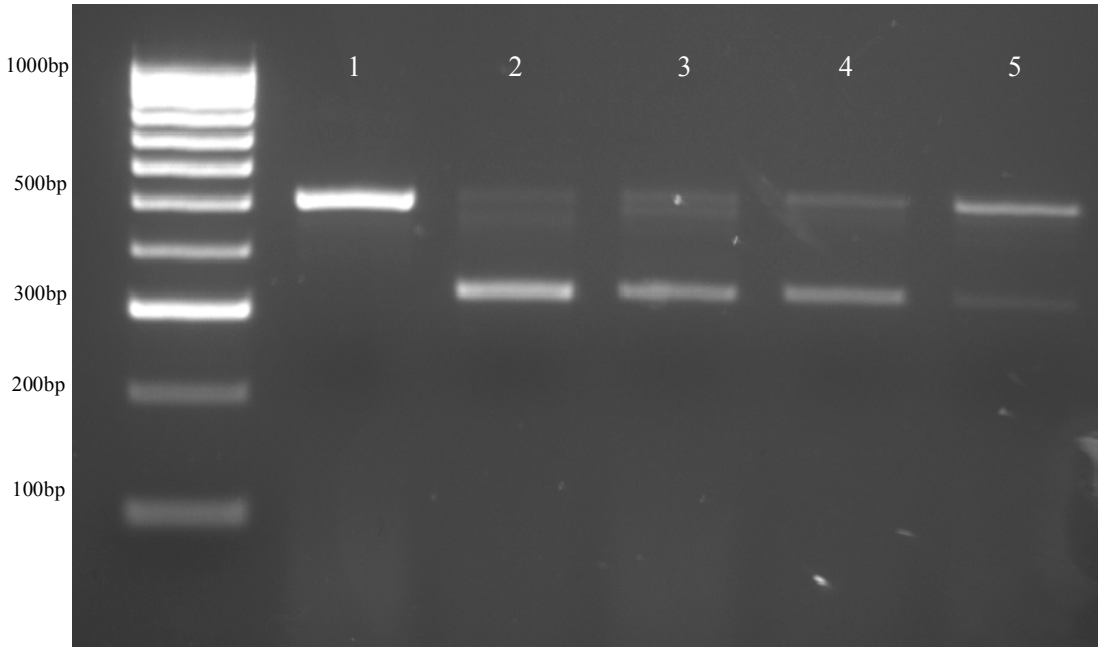

Figure 29. *pink1* MO4 co-knockdown optimisation. RT-PCR demonstrating efficacy of co-injection of both PINK4 Morpholino's. Lane 1, uninjected control at 3dpf. Lane 2 and 3 is co-injection of 0.45mM *pink1* i3e4+ *pink1* e4i4 at 1 and 3 dpf. Lanes 4 and 5 is 0.25mM at 1 and 3 dpf. Co-injection of both Morpholinos targeting exons 4 results in a 90% exon skip of exon 4 at highest dose, the effects not wearing off even at 3dpf. Injections of 0.25mM result in a similar KD efficacy although it had worn off by 3dpf.

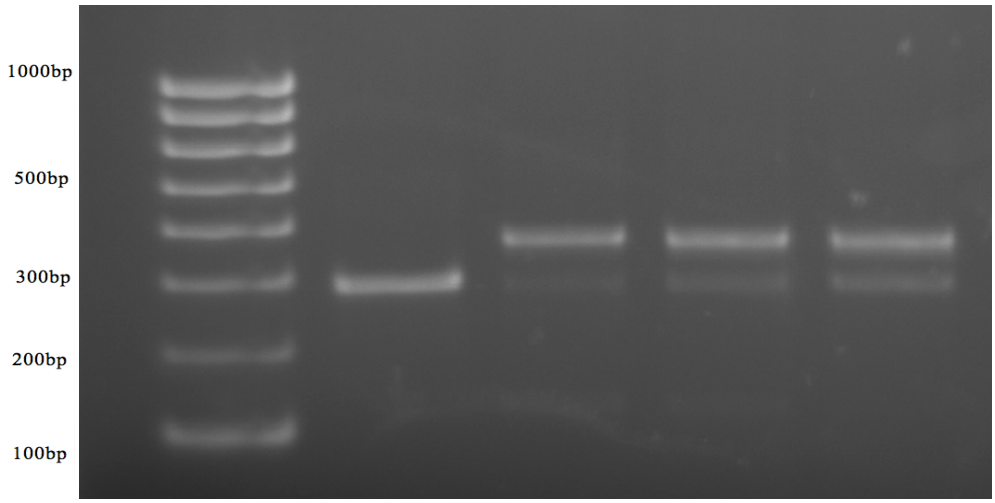

Figure 30. *pink1* MO5 optimisation. RT-PCR demonstrating efficacy of *pink1* Morpholino e5i5 (PINK5). Lane 1 uninjected control, lanes 2,3 and 4 representing injections of 0.9mM, 0.5 mM and 0.25mM respectively. All at 3dpf. PINK5 led to an intron inclusion of intron 5, confirmed by direct sequencing, and gave approximately 90% abnormal splicing and was non toxic at 0.9mM.

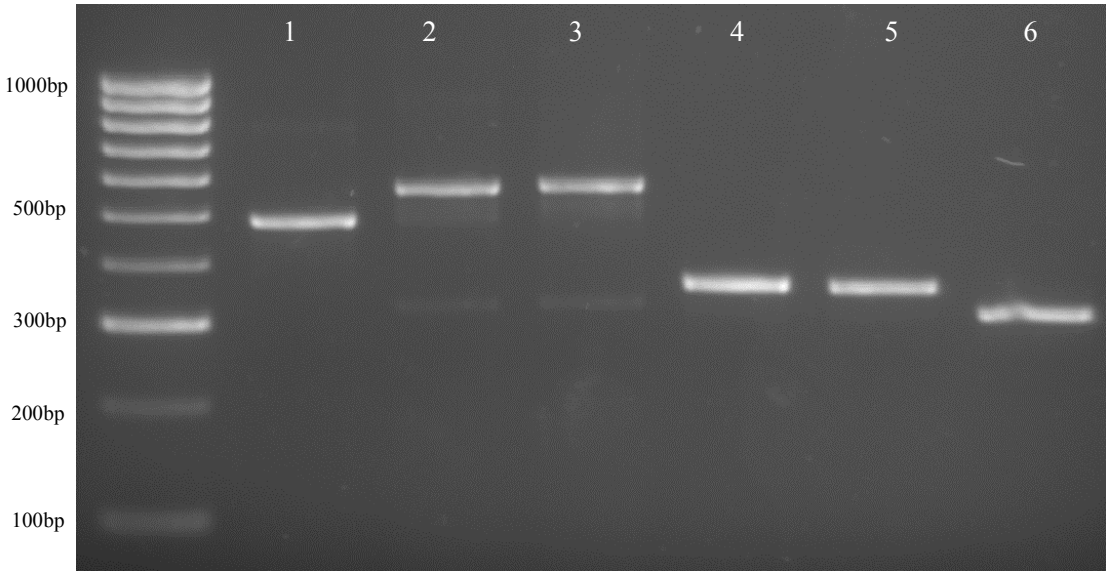

Figure 31. RT-PCR demonstrating PINK5 KD in co-injection experiments. Lanes 1-3 RT-PCR with PINK5 primers. Lanes 4-6 RT-PCR using TBMO2 primers. Lane 1 and 4 using uninjected control, lanes 2 and 5 PINK5 KD, lanes 3 and 6 CO injection with PINK5 and TBMO2. 90% KD was achieved in PINK5 injected larvae, and 100% KD in TBMO2 injected larvae. Co-injected larvae had more deformity than PINK5 injected, however heads appeared to be intact.

KD of *pink1* with PINK5 alone caused a 20% decrease in TH neurons at 3dpf seen in previous experiments in the stable mutant line ($P<0.05$) compared to uninjected and control Morpholino injected. Co-injection of PINK5 and TBMO2 led to the complete normalisation of the TH neuron count compared to uninjected and control Morpholino injected (Figure 32).

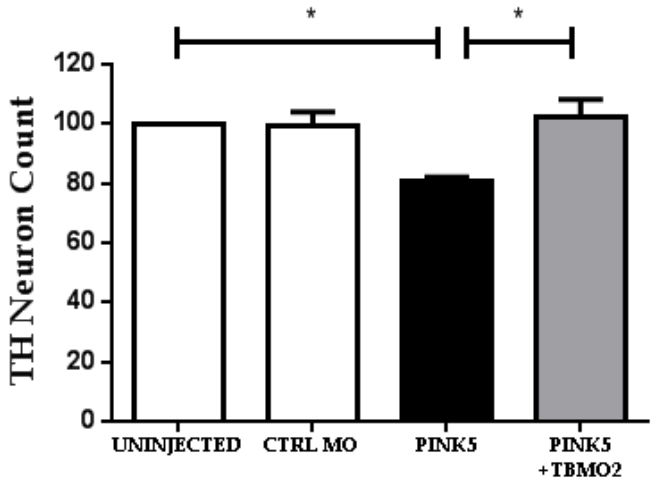

Figure 32. Co-knockdown of *pink1* and *tigarb* rescues Th neuron reduction. A *pink1* Morpholino (PINK5) was utilised to confirm *tigarb* KD rescues Th neuron reduction in a second model of *pink1* deficiency. *pink1* KD in Zebrafish leads to a 20% decrease in TH neurons at 3dpf ($P<0.05$). Co-injection with *tigarb* Morpholino prevents this neural cell loss.

3.2.7 Knockdown of *tigarb* rescues mitochondrial dysfunction

Once it had been confirmed that *tigarb* KD rescues Th neuron reduction in *pink1* -/- larvae, its method of action had to be addressed. *tigarb* expression was again rescued by Morpholino KD in the *pink1* -/- larvae and WT controls to investigate whether TH rescue was due to normalisation of mitochondrial dysfunction. At 3dpf uninjected larvae were found to have a decrease in mitochondrial Complex activities of Complexes I and III in a manner similar to *pink1* -/- at 5dpf. In contrast, KD of *tigarb* in *pink1* -/- larvae completely rescued the activity of Complex I and Complex III (Figure 33). The mitochondrial Complex assay experiments were jointly undertaken between the author and Dr Heather Mortiboys. Morpholino injections were performed by the author, Mitochondrial Complex assays performed by Dr Heather Mortiboys.

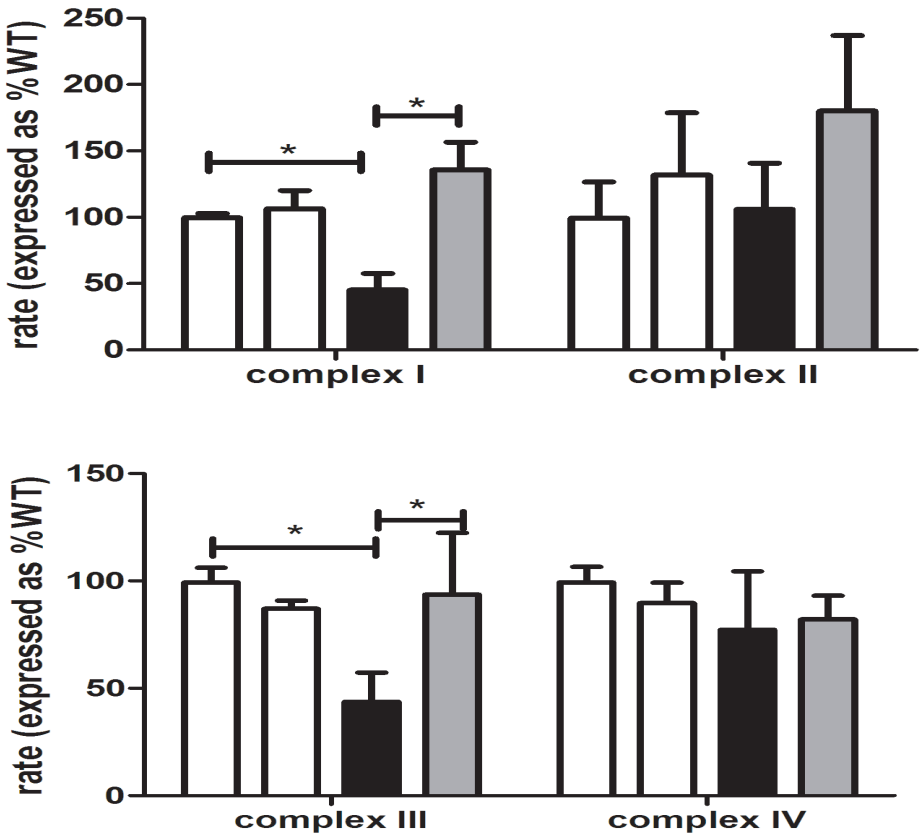

Figure 33. Mitochondrial Complex activities in *tigarb* morphants. To ascertain the rescue effect of *tigarb* KD in *pink1 -/-*, Mitochondrial Complex activity was measured in response to the KD of *tigarb* with TBMO2 at 3dpf. At this time point *pink1 -/-* larvae have a large reduction in Complex I and III which is completely rescued by the KD of *tigarb*. In each graph, first white bar represents WT uninjected, second white bar represents WT TBMO2 inject, the black bar represents *pink1 -/-* uninjected and the grey bar represents *pink1 -/-* TBMO2 injected.

3.2.8 *tigarb* KD does not rescue MPP+ mediated Th neuron reduction

As KD of *tigarb* rescues the Th neuron reduction seen in a genetic model that also exhibits Complex I inhibition (*pink1 -/-*), it was hypothesised that *tigarb* KD may also rescue Th neuron reduction induced by a chemical form of Complex I inhibition; in this case the classical PD toxin, MPP+.

Wildtype zebrafish larvae injected with TBMO2 and uninjected controls were treated at 48hpf with either 3mM MPP+ or standard E3 media for 24 hours. TBMO2 injection and MPP+ exposure did not affect morphology. When analysing the TH neuron counts of MPP+ treated larvae, uninjected control larvae had a 25% decrease in TH neuron count compared to E3 treated uninjected larvae ($P<0.05$ Two way anova). TBMO2 injected

larvae treated with E3 had an increase of 15% TH neurons compared to WT although this was not statistically significant. However *tigarb* KD in MPP+ treated larvae did not lead to normalisation of Th neuron reduction, with larvae having a 25% decrease compared to E3 uninjected larvae ($P<0.05$) (Figure 33).

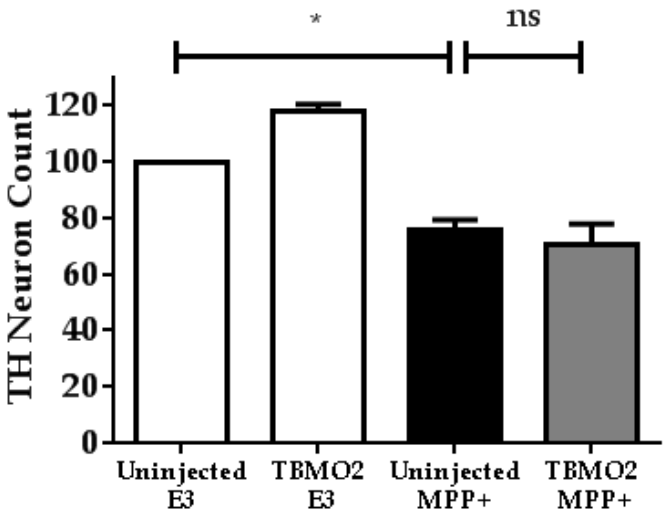

Figure 34. TB KD does not rescues TH loss in response to MPP+. KD of *tigarb* in E3 media treated larvae resulted in a 15% increase in TH neurons compared to E3 uninjected however this was not statistically significant. Treated larvae with 3mM MPP+ uninjected and TBMO2 injected resulted in a 25% reduction in TH neurons ($P<0.05$). This demonstrates *tigarb* KD does not rescue TH neurons after MPP+ treatment.

3.2.9 Knockdown of *vhl* rescues Th neuron reduction in *pink1 -/-* larvae

Mutations in *VHL* lead to activation of HIF1a and the hypoxic response, causing certain cancers in humans. *vhl* -/- zebrafish larvae have been shown to have an increased glycolytic flux.[242] Consequently *vhl* was chosen as a subject for gene-gene interaction studies in the *pink1* -/- larvae. It was hypothesised homozygocity for both *pink1* and *vhl* may lead to a normalisation of glycolysis and therefore a possible rescue of phenotype seen in either mutant. Initially *vhl* Morpholinos were utilised to KD *vhl* in *pink1* -/- larvae. Efficacy was determined by using *phd3* GFP reporter zebrafish as the control group. These transgenic fish possess *GFP* fused to the *phd3* promoter; consequently expression of *phd3* will also cause expression of GFP. *vhl* -/- show a very large upregulation of *phd3*, and so as a result of *vhl* deficiency in these reporter larvae, they fluoresce green. Zebrafish have such low basal expression of *phd3*, that uninjected WT larvae have very low to undetectable *phd3* and consequently GFP expression.

KD of *vhl* in *phd3* reporter zebrafish led to a large green fluorescence signal, indicating *vhl* deficiency, and no reduction of TH neurons was seen compared to *phd3* uninjected. Uninjected *pink1 -/-* larvae had the standard 25% decrease in TH neurons ($P<0.05$) compared to *phd3* uninjected controls. *vhl* KD in *pink1 -/-* larvae did not cause any morphological changes, and led to a complete rescue of Th neuron reduction (Figure 35).

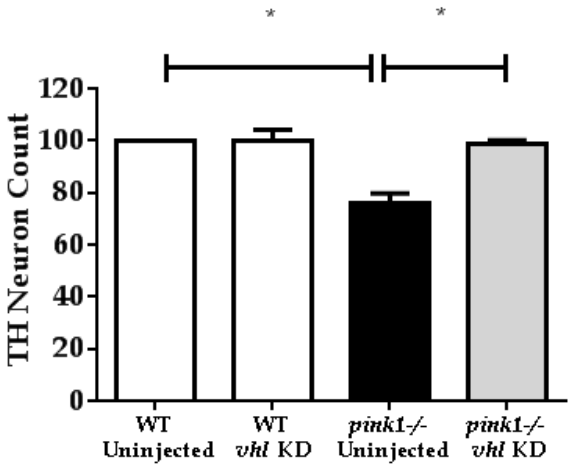

Figure 35. *vhl* KD rescues *pink1 -/-* Th neuron reduction. *pink1 -/-* larvae have an upregulation of *tigarb*, implying a state of inhibited glycolysis. *vhl -/-* larvae are in a chronic state of increased glycolytic flux. KD of *vhl* in WT had no effect on the TH neuron count. The *pink1 -/-* uninjected larvae had a 25% decrease compared to WT. KD of *vhl* in *pink1 -/-* larvae led to complete normalisation of TH neuron levels.

vhl deficiency activates hypoxic signalling, that also leads to a robust upregulation of TH expression.[290] The author subsequently wanted to confirm the rescue effect of *vhl* deficiency on TH neurons in *pink1 -/-* larvae by crossing the *pink1 -/+* with a stable *vhl* deficient line (*vhl -/+*). In addition, the author wanted to confirm with the apparent rescue of DA neurons with a second marker of DA neurons other than TH. This is due to the nature of *vhl* deficiency, as it leads to activation of Hif1a and its downstream targets. Tyrosine hydroxylase is known to be a direct target of Hif1□. Consequently, in case the rescue seen in *vhl* KD was actually an increase of TH expression (caused by Hif1□ activation) as opposed to an increase in DA neurons, DAT was chosen as a confirmatory marker. DAT had previously been utilised by Dr Laura Flinn to confirm Th neuron reduction in the *pink1 -/-* at 5dpf with a loss of approximately 25%, similar to TH.[201] Consequently the *pink1* Y431* line was crossed to a previously characterised *vhl* loss of function line previously characterised, to generate *pink1 -/+; vhl -/+*. As *vhl -/-* are not viable, with larvae dying at around 10dpf, the *pink1 -/+; vhl -/+* were

incrossed to generate *pink1 -/-; vhl -/+* adults from which all embryo work was to be conducted. Consequently, for each experiment, all larvae would have to be genotyped for *vhl* status. This cross to generate *pink1 -/-; vhl -/+* also demonstrated that *pink1 -/-* cannot rescue the lethality seen in *vhl -/-*, as no *pink1 -/-; vhl -/-* were found in the adult genotyping.

From incrossed experiments, *pink 1 -/-; vhl -/-* larvae were deemed to be indistinguishable from *pink1 +/+; vhl -/-* larvae, demonstrating that the presence of the *pink1 -/-* could not rescue the morphological phenotypes exhibited by *vhl -/-* during development. When the DAT neurons were analysed at 5dpf, *pink1 -/-; vhl +/+* showed a 20% decrease ($P<0.05$ two way anova) in DAT neurons compared to WT, in a similar manner documented by Flinn *et al 2013*. Upon analysis, *pink1 +/+; vhl -/-* demonstrated an even greater decrease in DAT neurons of approximately 30% ($P<0.01$ two way anova). This decrease was not rescued by *pink1 -/-; vhl -/-*, and in fact they showed a similar decrease in DAT neurons (Figure 36).

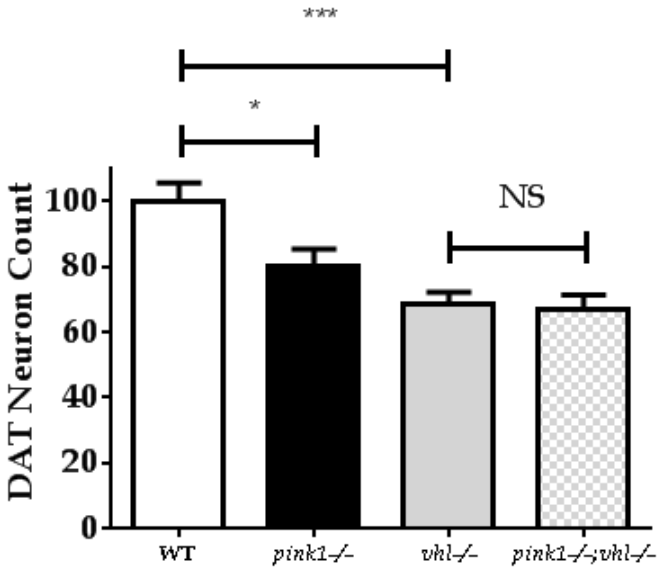

Figure 36. *vhl -/-* has a large decrease in DAT neurons at 5dpf compared to WT. *pink1 -/-* at 5dpf has a 20% decrease in DAT neurons at 5dpf similar to TH ($P<0.05$). *vhl -/-* have an even greater decrease in DAT neurons at 5dpf of 30% ($P<0.001$), unaffected by *pink1* genotype, seen in *pink1 -/-; vhl -/-* also have a large decrease in DAT neurons of 30%. Pilot data n=1

3.3 *pink1* results summary

The presented work contributed to the first characterisation of a stable mutant PD zebrafish line (part of the publication by Flinn *et al 2013.*, see appendix). This zebrafish model also highlights that DA neuronal cell reduction can start very early in *pink1*

deficiency, as *pink1 -/-* have a reduction of TH neurons by 3dpf. Gene expression analysis by WISH for neuronal developmental markers has suggested the neuronal loss being due to a developmental defect is unlikely after 24hpf, although may be causative before 24hpf. Gene expression studies also identified the upregulation of *tigarb* in *pink1 -/-* larvae which was further confirmed by WISH and qPCR. KD of *tigarb* was found to completely rescue Th neuron reduction and mitochondrial dysfunction in *pink1-/-* larvae. However *tigarb* KD could not rescue Th neuron reduction in MPP+ treated larvae. *vhl* was also found to be a modifier of *pink1* deficiency as KD of *vhl* in *pink1 -/-* larvae also rescued Th neuron reduction. The latter finding still requires further validation.

Overall, the study revealed that zebrafish are indeed a valid model for *pink1* deficiency and has revealed a potential new drug target, opening the potential for the *pink1* Y431* zebrafish as a platform for phenotypic drug discovery.

4 The zebrafish as a model for Glucocerebrosidase1 deficiency

4.1 Introduction and *gba1* expression profile

4.1.1 Introduction

Homozygous mutations in *GBA1* present as GD, whilst *GBA1* mutations remain the most common genetic risk factor for development of PD.[93] At the commencement of this study the only vertebrate models of GBA1 deficiency were mouse KO/conditional KO's, which either died shortly after birth, or did not faithfully model GD or PD. The zebrafish has been shown to be a useful model for studying neurodegeneration, so it was hypothesised that zebrafish could be a useful model for GD and *GBA1*-linked PD. At the time of study only KD approaches were available, so these were utilised to initially generate a loss of function zebrafish model. However, as stable mutant alleles had become available, due to the SANGER-led zebrafish mutation project, and with the advent of TALEN technology, a stable loss of function mutant was also generated and both mutant lines were characterised. The specific objectives of this part of the thesis were to validate a zebrafish model of *gba1* deficiency in its homozygous and heterozygous state, and to identify suitable phenotypes, amenable to high throughput zebrafish drug screens.

4.1.2 Zebrafish *gba1* orthologue identification and expression.

To identify a zebrafish orthologue of *GBA1*, the human protein sequence (ENSP00000314508) was aligned against the zebrafish proteome using the BLAST online tool, identifying a single hit, of approximately 50% homology to the human protein, ENSDARP00000098103 annotated as *gba1* in the zebrafish genome. To validate the hit, the putative protein orthologue sequence was then searched for in the human proteome, the top hit identified as ENSP00000314508, the human GBA1 protein. To confirm these BLAST results the human *GBA1* cDNA, ENST00000368373, was searched for against the zebrafish genome, identifying ENSDART00000113093, the annotated zebrafish *gba1* transcript, as the top hit, with 50% homology to the human cDNA. Both genes have a similar genetic structure, with similar numbers of exons (human 11, zebrafish 10), transcript length and protein size. From ENSEMBL, the zebrafish *gba1* codes for a single major isoform, 518 amino acids in length, zebrafish Gba1 sharing 57% identity to human GBA1. The human gene can be alternatively spliced into 5 different protein coding combinations, ranging in size from 423 to 536 amino acids in length. The main human GBA1 protein isoform being 497 amino acids in length. To

confirm that the identified orthologue was indeed the zebrafish orthologue of *GBA1*, the human and zebrafish genomic loci were compared to determine whether gene synteny was also conserved. No genes could be located up to 500kb upstream of *GBA1/gba1* that are present in both organisms. Up to 500kb downstream of *GBA1/gba1*, 3 genes were identified that were present in both organisms, namely *DAP3/dap3*, *RUSC1/rusc1* and *FDPS/fdps*, demonstrating partial conserved gene synteny between the loci of human *GBA1* and zebrafish *gba1*. See

Figure **37**.

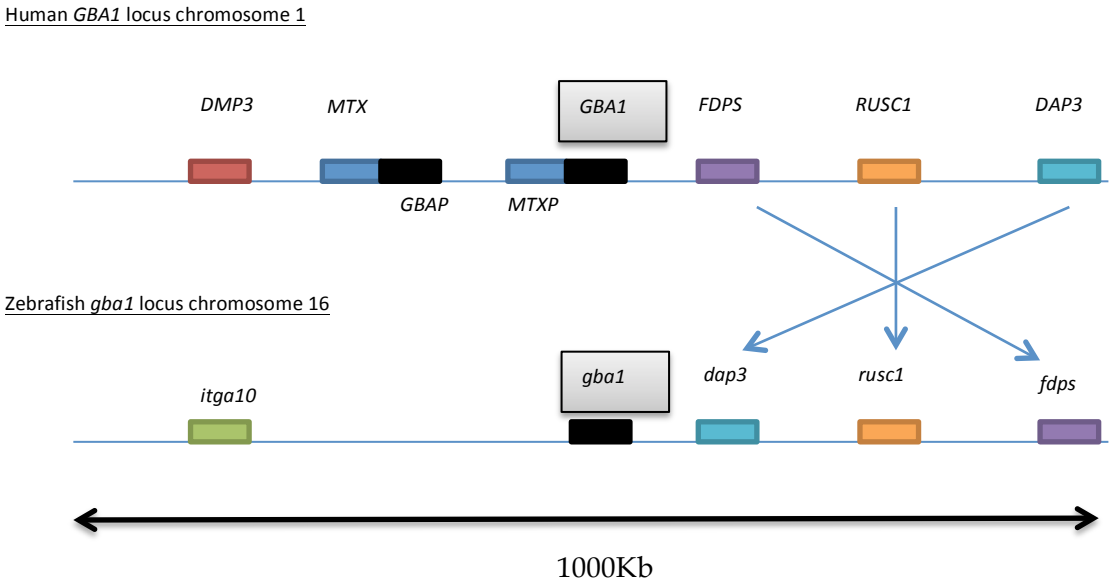

Figure 37. The Genomic loci of human and zebrafish *GBA1/gba1*. Cartoon comparing loci of *GBA1/gba1* orthologues.

To assess whether *gba1* is expressed during development, PCR was utilised to amplify a region of *gba1* cDNA from 1 to 5 days post fertilisation (dpf) and a selection of adult tissues. Expression was detected at a constant, and low level from days 1-5 of embryogenesis, with similar expression in fin, liver and brain from adult organs (38). To assess if expression was spatially restricted during development, a WISH probe was constructed to specifically stain for *gba1* expression. WISH at days 1, 2, 3 dpf revealed *gba1* expression was widespread with marked expression in the head. No staining was detected with the control sense probe (Figure 39).

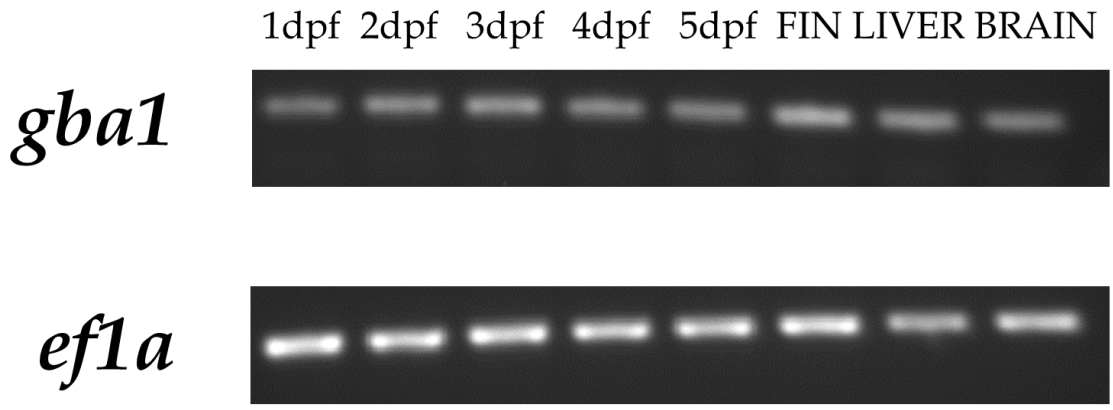

Figure 38. *gba1* expression in early development and adult tissues. *gba1* expression was monitored through early development and in a selection of key tissues by RT-PCR. Expression was low and constant at all-time points and tissues. *gba1* expression was additionally confirmed in the fin, liver and brain. *Ef1a* was utilised as a loading control.

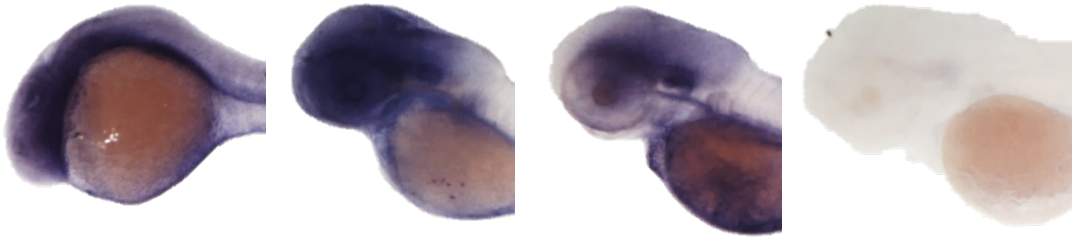

Figure 39. *gba1* expression through early development by WISH. *gba1* expression was monitored spatially by WISH. g*ba1* Expression at days 1, 2, 3 of development in Figure 39 A, B and C demonstrated gba1 expression to be ubiquitous and not spatially restricted. No staining could be detected with the control sense probe at 3dpf, Figure 39 D.

4.2 *gba1* Morpholino optimisation and knockdown

4.2.1 *gba1* Morpholino optimisation

To prevent *gba1* expression, a Morpholino strategy was employed to KD the transcript during zebrafish embryonic development. Of the 300 mutations characterised in the 11 exons of the *GBA1* human gene, 100 occur in exons 8 and 9. This also includes the most common mutations (N370S and L444P) that are found in 70% of patients. Exon 9 is also

the site of many complex alleles, due to recombination events with GBA1 and *GBA1* pseudogene, the latter containing a 55bp deletion in its 9th exon. Consequently, these sites were originally chosen for Morpholino KD. Exon junctions were sequenced for both genes to confirm the genomic sequence in ENSEMBL. Using the confirmed sequences, Gene tools were able to design Morpholinos binding to the i6e7 (MO7), e8i8 (MO8) and i8e9 (MO9) junctions. See

Figure 40 for a graphical representation of Morpholino binding sites.

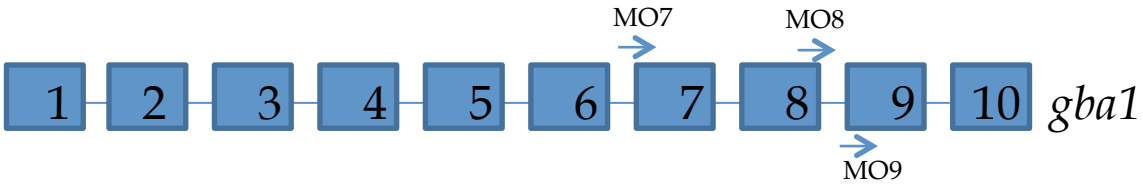

Figure 40. *gba1* Morpholino binding sites. A schematic illustrating Morpholino binding sites to *gba1*. Morpholinos were designed against i6e7 (MO7), e8i8 (MO8) and i8e9 (MO9).

Morpholinos were tested for efficacy and toxicity by injecting 1nl of 0.25mM, 0.5mM and 0.9mM into 1 cell stage WT embryos. MO7 was toxic at the highest doses (0.9mM and 0.5mM) and displayed low efficacy, see Figure 41. MO8 injected embryos showed no deformity or increased death compared to uninjected controls, at any dose and RT-PCR demonstrated the largest KD of the WT mRNA, leading to a simultaneous exon skip and intron inclusion (Figure 42). MO9 was toxic at 0.9mM and had low efficacy (Figure 42).

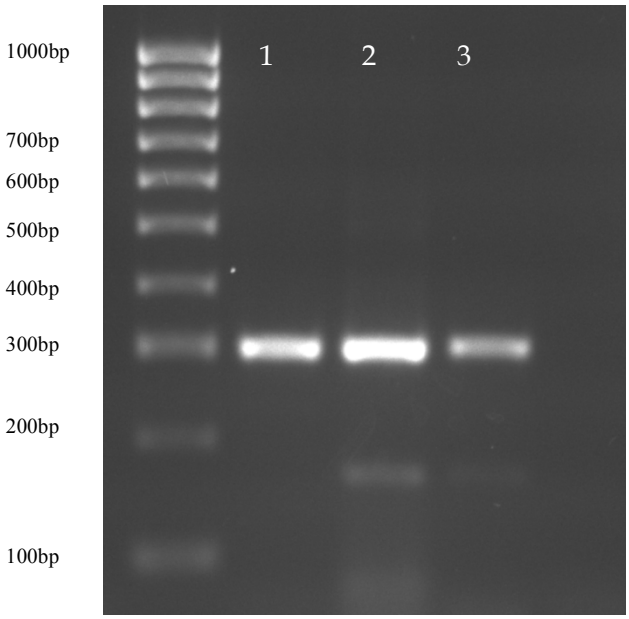

Figure 41. *gba1* MO7 optimisation. *gba1* MO7 was injected at a variety of concentrations to assess toxicity and efficacy. *gba1* MO7 was toxic at the highest doses (0.9mM and 0.5mM) and had low efficacy. Lane 1, uninjected, lane 2, 0.9mM injected, lane 3, 0.5mM injected. At the highest dose of 0.9mM, *gba1* MO7 caused less than 10% exon skip. No obvious effect on splicing could be detected.

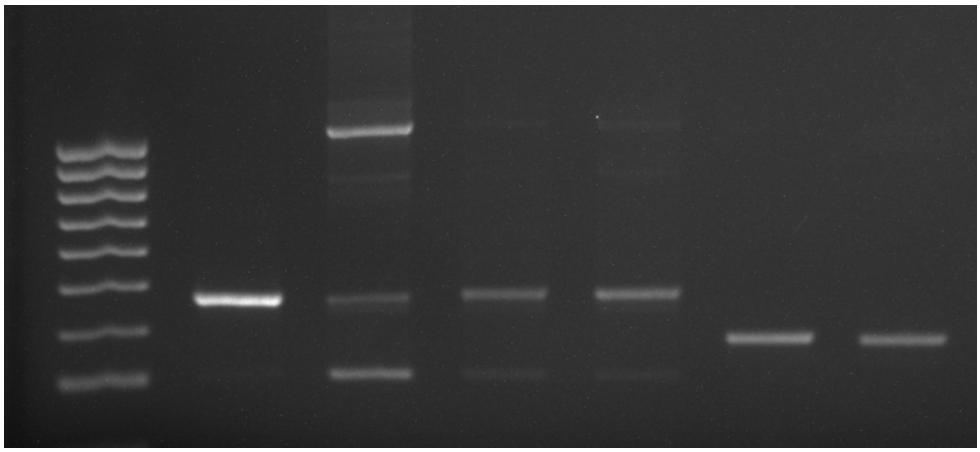

Figure 42. *gba1* MO8 and MO9 optimisation. RT-PCR demonstrating *gba1* MO8/MO9 optimisation. *gba1* MO8 was injected at a range of different concentrations to determine toxicity and efficacy. Lane 1 uninjected, lane 2, 0.9mM injected, lane 3, 0.5mM injected, lane 4, 0.25mM injected. *gba1* MO8 was non-toxic at all concentrations and achieved greatest KD at 0.9mM. *gba1* MO9 had low efficacy even when injected at the highest dose (0.9mM, lane 6), compared to uninjected, lane 5.

Due to its efficacy (~90% KD) and low toxicity, MO8 was selected as the optimal Morpholino for further *gba1* KD experiments in WT zebrafish embryos. To confirm abnormal splicing of the WT *gba1* transcript, the mis-spliced products produced by

MO8 were sub-cloned into a Topo-ta vector and sequenced to confirm the effects of the Morpholino. The sequenced products were identified to be intron inclusions of intron 8 (581 base pairs) and a complete exon skip of exon 8 (164 base pairs).

4.2.2 TH neuron count of Complex I inhibited *gba1* knockdown larvae

Initially, TH neurons were counted in WT uninjected and *gba1* MO8-injected zebrafish. Despite reliable KD of *gba1* with MO8, no decrease of TH neurons was observed (data not shown). Consequently, it was investigated whether *gba1* KD may sensitise WT zebrafish larvae to mitochondrial Complex I inhibition. WT uninjected and *gba1* MO8-injected zebrafish were then exposed to 3mM MPP+ (a robust Complex I inhibitor) for 24 hours. *gba1* KD with MO8-treated with control E3 media led no decrease of TH neurons compared to uninjected WT zebrafish, that was statistically significant, reproducing the results previously seen in unexposed zebrafish. Uninjected WT larvae treated with 3mM MPP+ had a 50% reduction of TH neurons compared to those uninjected WT controls treated with control E3 media. *gba1* MO8-injected larvae also treated with MPP+ had a 60% reduction of TH neurons compared to WT uninjected controls treated with E3 media, however this loss was not statistically significant to the MPP+ treatment alone, see

Figure **43**. To confirm this lack of a synergistic effect of *gba1* KD, in conjunction with Complex I inhibition, *gba1* MO8 was utilised to KD *gba1* in *pink1 -/-* larvae that exhibit a reduction in Complex I activity and a 20% reduction in TH neurons at 3dpf. The *gba1* MO8-injected WT zebrafish showed a no reduction of TH neurons that was statistically significant, consistent with previous findings. *pink1 -/-* uninjected larvae had a 20% reduction of TH neurons ($P<0.05$, two way ANOVA) compared to uninjected WT zebrafish. *gba1* KD in *pink1 -/-* larvae did not exacerbate loss of TH neurons beyond the initial 20% reduction (observed in the *pink1 -/-* uninjected zebrafish. This confirms *gba1* KD in WT larvae does not sensitise TH neurons to mitochondrial Complex I inhibition during development. See **Figure 44**.

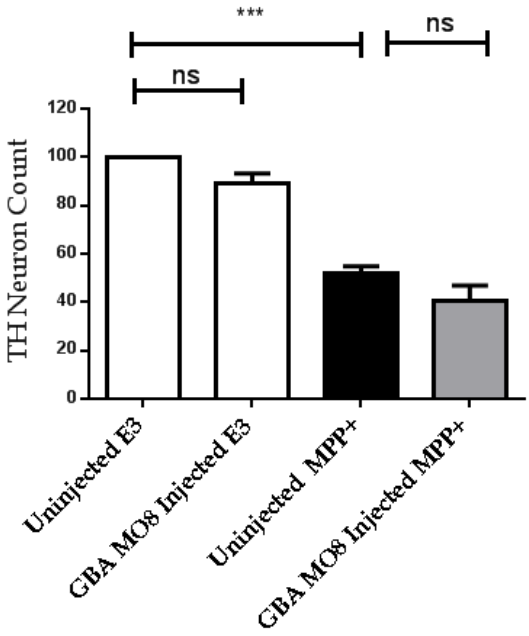

Figure 43. TH neuron count after *gba1* knockdown at 3dpf and with 3mM MPP+. *gba1* KD treated with control E3 media developed a no decrease in TH neurons compared to uninjected (P>0.05). Uninjected controls treated with 3mM MPP+ had a TH neuron decrease of 50% compared to uninjected E3 treated control (P<0.001 two way ANOVA). TH neuron count in *gba1* KD MPP+ treated larvae decreased by 60% compared to uninjected E3 treated control (P<0.001 two way ANOVA), although not statically significant decrease compared to uninjected larvae treated with 3mM MPP+ (P>0.05 two way ANOVA).

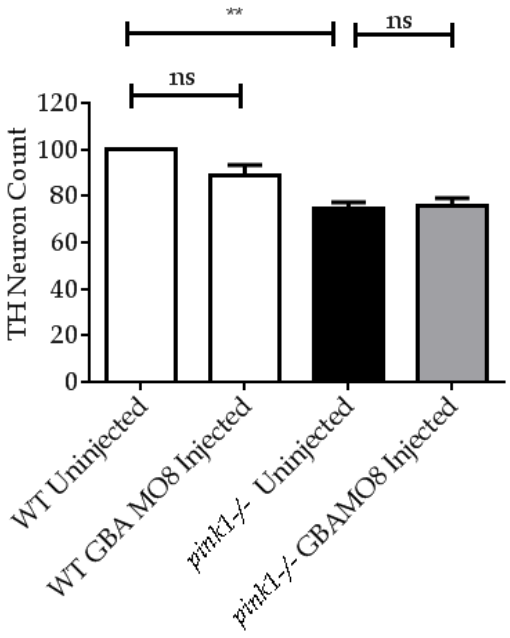

Figure 44. *gba1* knockdown in *pink1 -/-* larvae at 3dpf. *gba1* KD in WT larvae led to no decrease in TH cells, compared to WT uninjected controls. *pink1 -/-* uninjected larvae exhibited the standard 20-25% decrease in TH neurons compared to WT uninjected (P<0.01, two way ANOVA). KD of *gba1* in *pink1 -/-* did not increase the Th neuron reduction in *pink1 -/-* uninjected, demonstrating *gba1* deficiency does not increase Th neuron reduction due to Complex I inhibition at 3dpf.

4.3 *gba1* sa1621, zebrafish mutation project line

4.3.1 *gba1* sa1621characterisation

KD strategies, although somewhat effective, are transient in nature, with KD lasting only up to 3-5 days in WT zebrafish larvae. Studies examining cell death in Morpholino KD based studies are also difficult to interpret as un-validated Morpholinos may be producing nonspecific phenotypes due to off target p53-mediated effects. Consequently, stable mutant lines are preferable for reverse genetic studies, as they avoid these variables and additionally allow for the analysis of loss of function phenotypes from development to adulthood. Previously, stable mutant lines were generated from large scale ENU mutagenesis screens that are costly and time-consuming. A novel technique for targeted genome editing using TALENs has been developed for zebrafish embryos, as a robust method for producing insertions and deletions (indels) in a targeted fashion. Additionally, the zebrafish mutation project, a very large-scale ENU mutagenesis screen is being undertaken by the WELLCOME TRUST SANGER centre with the aim of identifying loss of function mutations in all zebrafish genes (http://www.sanger.ac.uk/resources/zebrafish/zmp/).

The zebrafish mutation project had already identified a point mutation (sa1621) affecting an essential splice site in exon 4 of the *gba1* transcript. The base affected was a G>A at the exon 4 intron 4 junction. A complete intron inclusion of intron 4 (2,718bp) would lead to a premature stop codon appearing at c.573, producing a truncated protein of 191 amino acids , as opposed to the WT 518 amino acids in length. See Figure 45.

Intron 3 gagagcaacagagattgagcaagtggaaatgaaaatggcctcggctttc
tcagttccgaatggtgtacatcgctctgtttcacagGTATAGAGTACCG
Exon 4 TTTCGTGAGAGTGCCGGTGGCCAGCTGTGATTTTTCAACTCGACTCTAC
ACGTATGCTGACACTCCAGAAGACTACGATCTCCAGAACTTCACCCTGG
Intron 4 CCAAAGAGGATGTTCACATGAAGgtagcatacacaaacaaaaacacacc
ttactacaaatagcggtctgcagtagtactcgcttgagggtaaatattg
cgtaaatagtgatttgattttcatttttgagggaactttccctttaagt

Figure 45 The Genomic sequence illustrating the sa1621 allele point mutation. *gba1* introns 3 and 4 are lower case and light and dark blue script respectively, exon 4 in upper case and purple script. The altered position in the sa1621 allele, generated from the zebrafish mutation project, is a G<A mutation of an essential splice site, at the exon 4 intron 4 boundary, highlighted in yellow.

Pilot data from a *gba1* $^{sa1621/+}$ incross at 5dpf demonstrated no TH neuronal cell loss at 5 dpf, suggesting the small decrease of the TH neuronal count seen in *gba1* KD larvae is likely to be an off target effect of the Morpholino , see Figure 46. When the sa1621 *gba1* -/+ incross was grown to adulthood and reached 12 wpf, it was noted that a significant proportion of the individuals were emaciated, exhibited movement difficulties and were lying on the bottom of the tank. Many had to be culled immediately in line with animal welfare protocol. The culled and live fish were all genotyped. All culled fish were all *gba1* $^{sa1621/ sa1621}$, the remaining *gba1* $^{sa1621/ sa1621}$were moved to a separate tank and behaviour analysed by visual inspection. The adults moved abnormally and would spontaneously exhibit violent, corkscrew-like, motions. See Video 1 in the supplementary data for an example of 12 wpf WT zebrafish locomotion and Video 2 for an example of *gba1* $^{sa1621/ sa1621}$ motion. The remaining fish also were then culled. Each fish was measured and weighed at the point of culling. The *gba1* $^{sa1621/ sa1621}$ had a 50% decrease in mass compared to WT (P<0.01), and a decrease in length of 10% (P<0.01), see

Figure **47**. Although all *gba1* $^{sa1621/ sa1621}$ had to be culled at 12 wpf, homozygosity did not appear to significantly affect viability before this time point, with the alleles segregating in a Mendelian fashion at genotyping with 21 WT (24.4%), 45 *gba1* $^{sa1621/ +}$ (52.3%) and 20 *gba1* $^{sa1621/ sa1621}$ (23.3%). Attempts were made to investigate fertility in the *gba1* $^{sa1621/ sa1621}$adults, however all successive breeding attempts failed to produce offspring, possibly due to defects in co-ordination as opposed to specific infertility.

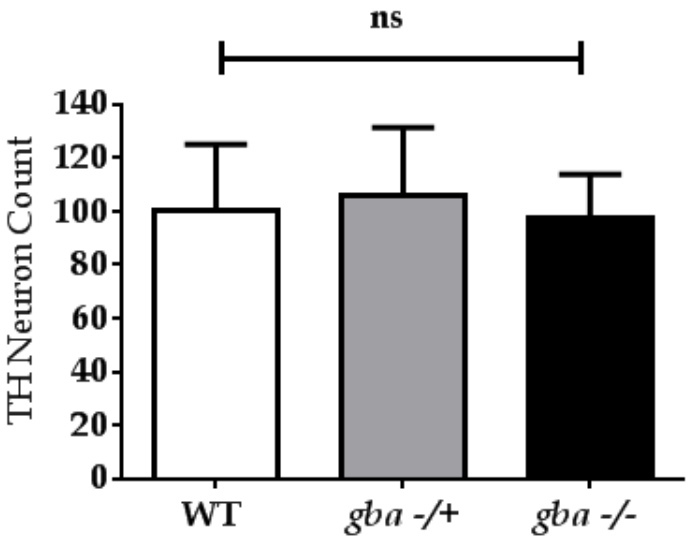

Figure 46. TH neuron count of 5dpf larvae in all sa1621 *gba1* genotypes . 5dpf larvae from a *gba1* $^{sa1621/+}$ incross were stained for TH by WISH, neurons were counted and then larvae were genotyped. There was no significant difference in TH neuron count between all *gba1* genotypes, WT:12, *gba1* $^{sa1621/+}$:18 and *gba1* $^{sa1621/sa1621}$:7. Pilot data, n=1.

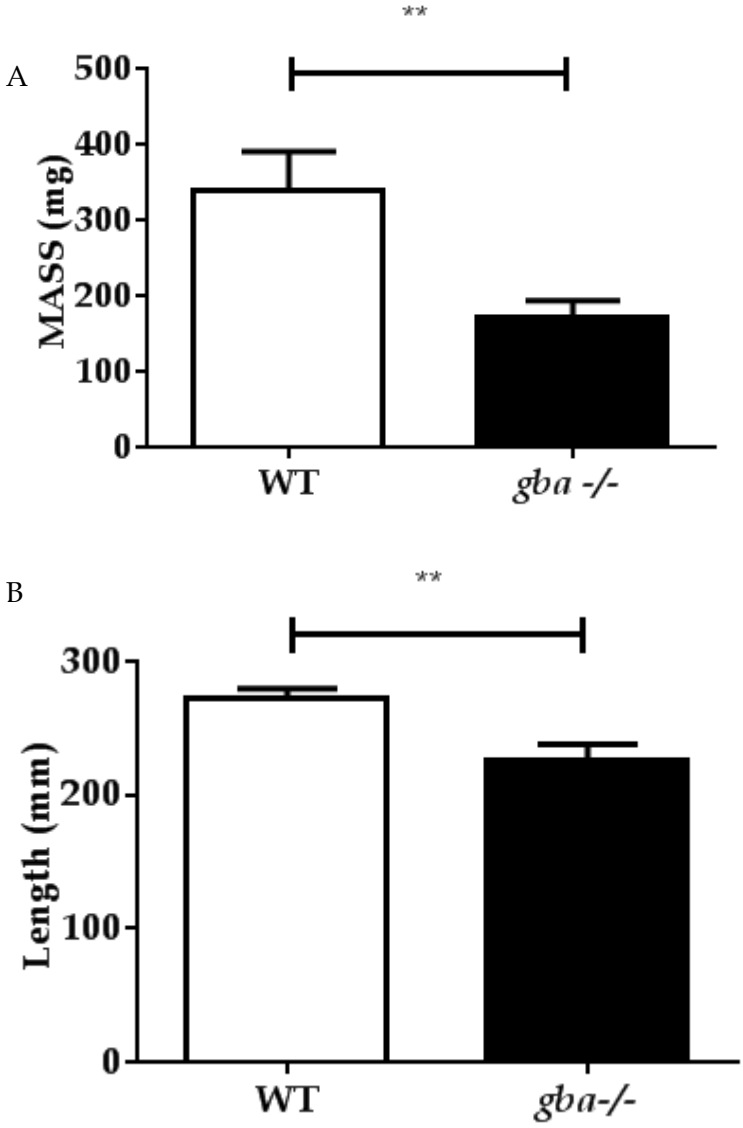

Figure 47. The length and mass of sa1621 *gba1 -/-* and WT controls at 12 wpf. A, sa1621 gba1 -/- have a 50% decrease in mass compared to WT controls at 12 wpf (P<0.05, unpaired T test). B, sa1621 gba1 -/- show a small, statistically significant decrease in length of 20% compared to WT (P<0.05, unpaired T test). N =10 for both measurements.

4.4 *gba1* TALEN mutagenesis

4.4.1 *gba1* TALEN construction

In parallel to the sa1621 characterisation, a second loss of function *gba1*-mutant was constructed using the TALEN system of gene editing. TALEN mutagenesis requires pairs of TALENs to be constructed with a spacer region of approximately 20bp. By targeting a region containing a large restriction enzyme site within the spacer region,

TALEN efficacy can be determined, as any small indels created will mutate the restriction site and prevent digestion. Exon 7 was chosen for targeting due to the presence of suitable TALEN sites flanking a *Mwo*I restriction site. See Figure 48 for the position of TALENs within the *gba1* gene.

Figure 48. TALEN binding site. The Genomic sequence of the *gba1* TALEN binding site showing introns 6 and 7 are in lower case and light blue script. Exon 7 of *gba1* is highlighted in red and uppercase. TALEN binding sites are highlighted in yellow. The *Mwo*I site in the spacer region is underlined and in black.

TALEN mRNA was injected into 1 cell stage WT embryos and genomic DNA (gDNA) extracted for restriction digest at 24 hpf. Exon 7 was amplified and digested with *Mwo*I. PCR products from uninjected single embryos gDNA extraction were completely digested by *Mwo*I. Digested PCR products from TALEN injected samples showed incomplete digestion with the presence of uncut products showing the TALEN possessed high efficacy. See Figure 49 for the restriction digest agarose gel image.

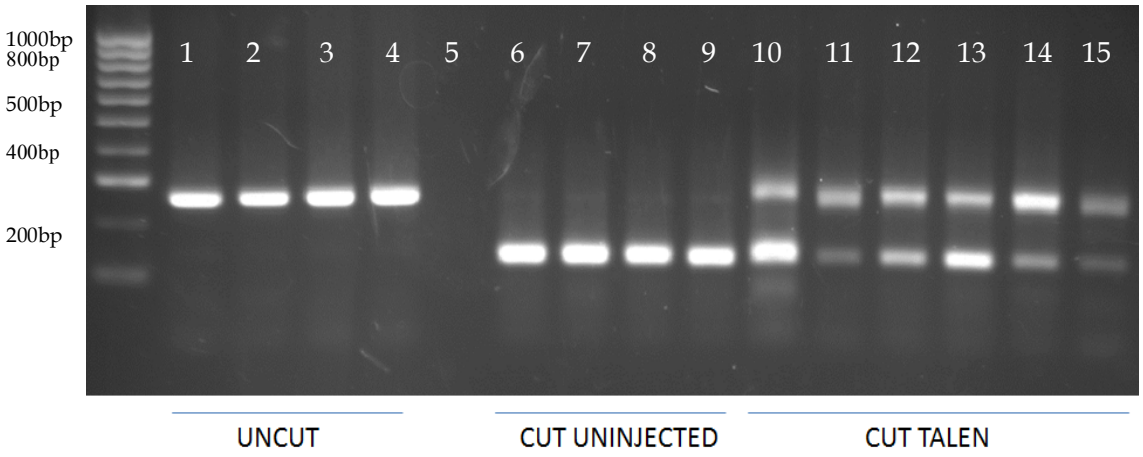

Figure 49. TALEN analytical restrictions digest. To test efficacy of *gba1* TALEN, PCR products of the target site from gDNA from single embryos 24 hours post injection, were subjected to digestion by *Mwo*I. The uncut PCR product of approximately 250 base pairs is shown in lanes 1-4. Uninjected controls cut with *Mwo*I gave complete digestion, leaving two products of similar sizes at 125bp mark (Lanes 6-9). TALEN-injected embryos (Lanes 10-15) resulted in incomplete digestion in all embryos examined, implying *Mwo*I site had been mutated by the TALEN in a highly efficacious way.

To confirm TALEN efficacy, PCR products of the target site using gDNA, pooled from 8 TALEN injected embryos, were sub-cloned into a Topo-ta vector, transformed into competent cells and plated then incubated overnight. Seventy-three colonies were picked for colony PCR and sequenced. Out of 73 colonies, 64% were WT, 23% contained deletions, and 13% contained a combination of insertions and deletions. No clones could be identified that contained insertions exclusively. The TALENs had a mutation generation rate of 33% in the pooled F0 mosaic embryos. The *gba1* TALEN produced a wide variety of different mutations; the largest alteration being a 77bp deletion. For a summary of the different *gba1* mutations caused by the TALEN and their incidence see Table 7.

	TOTAL	%	Description
WT	47	64	N/A
DELETION	17	23	3,6,7,10,17,29,68,77bp del
INSERTION	0	0	N/A
DEL + INS	9	13	22bp del + 46bp ins, 22bp del + 4bp ins, 8bp del + 5bp ins, 5bp del + 8bp ins, 3bp del +31bp ins, 51bp del + 7bp ins, 39bp del+8bp ins, 5bp del + 8bp ins

Table 7. TALEN mutation type summary. The total incidence of each mutation type (WT, deletion, insertion, deletion & insertion) for all sequenced clones, and their percentage incidence.

4.4.2 *gba1* TALEN founder identification

Once TALEN efficacy had been established and confirmed, 50 TALEN injected embryos (F0) were raised to breeding age. In order to determine whether TALEN mutations were transmitted to the germ line, F0 mosaic adults were crossed with WT adult zebrafish and 8 embryos from each cross was analysed by restriction digest. Each digest was compared to an undigested product. See

Figure **50** for representative digests of founder identification.

Eleven initial F0 TALEN-injected adults were crossed with WT zebrafish. Restriction digest identified 9 founders, the transmission rate being 81%. Some of the digests showed the presence of multiple products, implying the founder transmitted an allele to the germ line containing a large deletion (see

Figure **50**). Although a deletion or insertion of 1bp is only required for a frameshift mutation that can produce a premature stop codon, a large deletion or insertion would allow the resulting allele to be genotyped by analysing of product sizes of the PCR product, without the need for restriction digests (that can be effected by SNPs in the restriction site) or direct sequencing. Being able to genotype by PCR would be considerably cost and time effective. Consequently, the founder strategy was altered, to simply amplify the TALEN region and identity F0 individuals whose outcrossed progeny produced 2 PCR products of different sizes (indicating a large insertion or deletion). A total of 26 F0 individuals were outcrossed and the embryos were analysed by PCR. Eleven were definite founders confirmed by digest, 3 were non-transmitting F0 individuals, and 12 were potential founders unconfirmed by digest. A further 9 individuals were outcrossed however did not produce offspring. Three founders were outcrossed to WT TL fish and were grown to adulthood, producing the F1 generation.

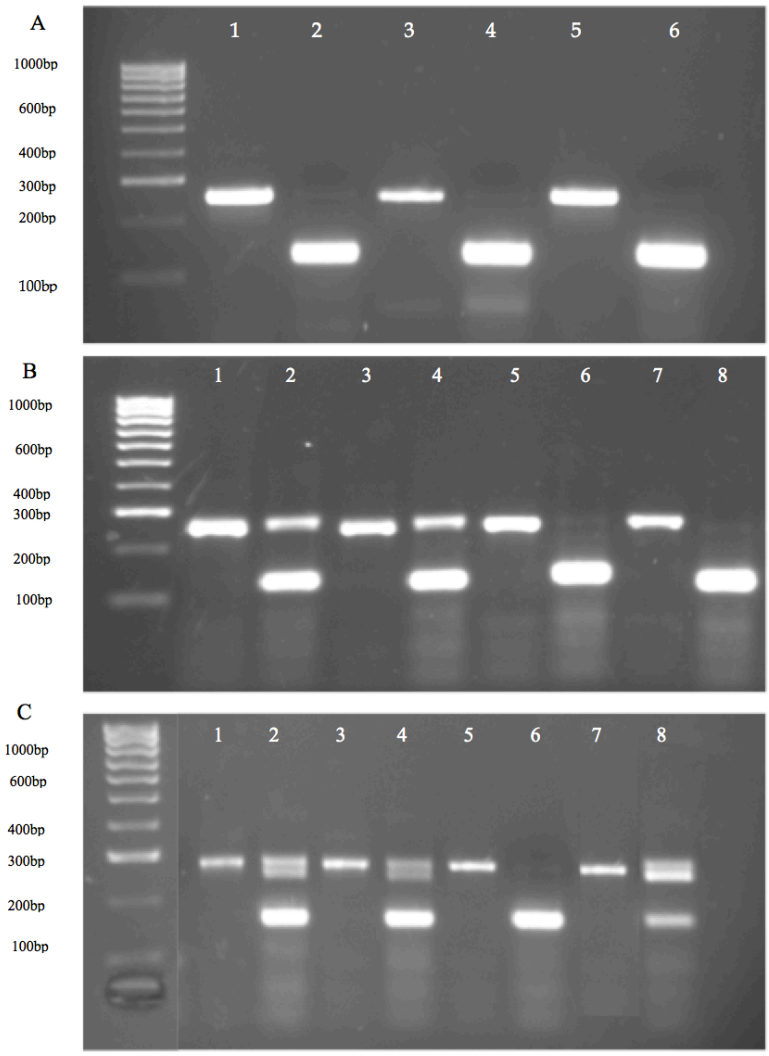

Figure 50. Founder identification restriction digests. Representation gels of founder identification using primers situated around the TALEN-targeted *MwoI* site of *gba1*. TALEN injected adult (F0) were outcrossed to WT individuals and the resultant progeny (F1) utilised for gDNA isolation and subsequent PCR of the TALEN region for restriction enzyme analysis. Gel A, An example of a PCR of F1 gDNA of 3 individual embryos from a non-transmitting F0 TALEN injected individual, alternating between undigested (Lane 1, 3 5) and *Mwo*I-digested PCR product (5µl) (Lane 2, 4, 6). WT PCR product gives complete digestion of the PCR product indicating no indels are present in the restriction site. Gel B, an example of a PCR of F1 gDNA from 7 individual embryos from a transmitting F0 TALEN-injected fish crossed with WT fish, alternating between undigested (Odd lanes, 1, 3, 5 etc.) and digested (even lanes, 2, 4, 6 etc.) with *Mwo*I. Note lanes 2 and 4 contains residual undigested PCR product indicating the presence of an indel within the restriction site, identifying the F0 injected fish as a mutation founder. Gel C, PCR of F1 embryos, F0 TALEN-injected fish crossed with WT fish, alternating between undigested (Odd lanes, 1, 3, 5 etc.) and digested (even lanes, 2, 4, 6 etc.) with *Mwo*I. Note lanes 2, 4 and 8 not only contains residual undigested PCR product (indicating the presence of an indel within the restriction site), identifying the F0 injected fish as a mutation founder. But also contains a second PCR product, indicating the allele is a large deletion that could be genotyped by PCR.

4.4.3 *gba1* TALEN allele selection

Three separate alleles were identified in the F1 generations; a 7, 8 and 23bp deletion (del), see Figure 51 for the sequence alterations. The 23bp del had the additional advantage of being so large that it could be genotyped by PCR without further downstream techniques such as restriction digest or direct sequencing. The 7bp del alleles were present in both sexes in the F1 outcross so were subsequently incrossed to generate homozygous mutants and to investigate if the allele phenocopied the sa1621 allele.

WT

GTTCTAAGTGACATTAAAGCAGCACGATATGTCCACGGCATTGGTGTTCACTGGTAT
TTTGATCGCCTTGTGCCGCCTGACGTCACCCTGACCTCCACACACCATCTGTACCCTG
ATTACTTCCTATTTGCAACTGAGGCATGCGCTGGGTGGAGTCCAGTGGATCGTGGTG
TGCGTCTGGGCAGCTGGGACAGGGCAGAGGACTACGCCCATGACATCATCCAG

7bp del

GTTCTAAGTGACATTAAAGCAGCACGATATGTCCACGGCATTGGTGTTCACTGGTAT
TTTGATCGCCTTGTGCCGCCTGACGTCACCCTGACCTCCACACACCATCTGTACCCTG
ATTACTTCCTATTTGCAACTGAGGCATGCGCTGGGTGGAGTCCAGTGGATCGTGGTG
TGCGTCTGGGCAGCTGGGACAGGGCAGAGGACTACGCCCATGACATCATCCAG

8bp del

GTTCTAAGTGACATTAAAGCAGCACGATATGTCCACGGCATTGGTGTTCACTGGTAT
TTTGATCGCCTTGTGCCGCCTGACGTCACCCTGACCTCCACACACCATCTGTACCCTG
ATTACTTCCTATTTGCAACTGAGGCATGCGCTGGGTGGAGTCCAGTGGATCGTGGTG
TGCGTCTGGGCAGCTGGGACAGGGCAGAGGACTACGCCCATGACATCATCCAG

23bp del

GTTCTAAGTGACATTAAAGCAGCACGATATGTCCACGGCATTGGTGTTCACTGGTAT
TTTGATCGCCTTGTGCCGCCTGACGTCACCCTGACCTCCACACACCATCTGTACCCTG
ATTACTTCCTATTTGCAACTGAGGCATGCGCTGGGTGGAGTCCAGTGGATCGTGGTG
TGCGTCTGGGCAGCTGGGACAGGGCAGAGGACTACGCCCATGACATCATCCAG

Embryos were monitored daily to check for potential deformity and mortality. All individuals in 7bp del incross developed normally. At 4 wpf, 20% of the incross looked comparatively small and underweight. A 7bp del outcross tank was used for a comparison. From the preliminary incross, a total of 32 individuals were raised to 8wpf and genotyped. 10 were WT (31%), 17 were 7bp del *gba1* -/+ (53%) and 5 were 7bp del *gba1* -/- (16%). All 7bp del *gba1* -/- were underweight and extremely small and

exhibited abnormal corkscrew like motions seen in the *sa1621 gba1 -/-*. Eventually all 7bp del *gba1 -/-* had to be culled at 12 wpf.

Due to an extremely skewed sex distribution, only females possessing the 23bp del allele could be identified in the F1 outcross, so a further outcross to F2 with WT had to be performed before a successive incross could be made. Only a single individual contained the 8bp del allele, so this was also outcrossed to generate the F2 generation.

Once the F2 23bp del *gba1 -/+* had grown to adulthood, they were incrossed to see if the 23bp del *gba1 -/-* produced a similar phenotype to the 7bp del *gba1 -/-* and sa1621 *gba1 -/-*. A total of 46 individuals were grown to 8 wpf and genotyped. Of these, 20% of the incross appeared underweight and smaller compared to a control outcross tank. Once genotyped, 14 were WT (31%), 21 were 23bp del *gba1 -/+* (45%) and 11 were 23bp del *gba1 -/-* (23%). All 23bp del *gba1 -/-* developed cork screw like motions that became uncontrollable so had to be culled, in an identical manner to 7bp del *gba1 -/-* and sa1621 *gba1 -/-* . The eldest 23bp del *gba1 -/-* was culled at 14wpf. See Videos 3 and 4 for examples of 23bp del *gba1 -/-* impaired mobility.

Both the 7bp del *gba1 -/-* and 23bp del *gba1 -/-* phenocopied the sa1621 *gba1 -/-* alleles. It was decided to use the 23bp del allele for subsequent studies, as genotyping could be performed by PCR alone without the need for restriction enzyme digestion, see Figure 10, and the phenotype matched the phenotype observed in the other gba1 mutant genotypes. To genotype the 7bp del and 8bp del required a MwoI digest and sa1621 genotyping required direct sequencing. Although all the different *gba1 -/-* mutant strains survive to adulthood, they all had to be culled at approximately 3 months of age and were seemingly unable to produce embryos. Consequently, all studies had to be performed from a 23bp del *gba1 -/+* incross, with each subsequent embryo requiring genotyping, as opposed to using 23bp del *gba1 -/-* adults to generate 23bp del *gba1 -/-* embryos. The 23bp allele was outcrossed to WT again to produce the F3 23bp del *gba1 -/+*. All subsequent experiments were performed on the F3 incross. No further experiment utilised the *gba1* sa1621 line, as all embryos that would be genotyped would require direct sequencing, which would not be cost effective.

WT

GTTCTAAGTGACATTAAAGCAGCACGATATGTCCACGGCATTGGTGTTCACTGGTAT
TTTGATCGCCTTGTGCCGCCTGACGTCACCCTGACCTCCACACACCATCTGTACCCTG
ATTACTTCCTATTTGCAACTGAGGCATGCGCTGGGTGGAGTCCAGTGGATCGTGGTG
TGCGTCTGGGCAGCTGGGACAGGGCAGAGGACTACGCCCATGACATCATCCAG

7bp del

GTTCTAAGTGACATTAAAGCAGCACGATATGTCCACGGCATTGGTGTTCACTGGTAT
TTTGATCGCCTTGTGCCGCCTGACGTCACCCTGACCTCCACACACCATCTGTACCCTG
ATTACTTCCTATTTGCAACTGAGGCATGCGCTGGGTGGAGTCCAGTGGATCGTGGTG
TGCGTCTGGGCAGCTGGGACAGGGCAGAGGACTACGCCCATGACATCATCCAG

8bp del

GTTCTAAGTGACATTAAAGCAGCACGATATGTCCACGGCATTGGTGTTCACTGGTAT
TTTGATCGCCTTGTGCCGCCTGACGTCACCCTGACCTCCACACACCATCTGTACCCTG
ATTACTTCCTATTTGCAACTGAGGCATGCGCTGGGTGGAGTCCAGTGGATCGTGGTG
TGCGTCTGGGCAGCTGGGACAGGGCAGAGGACTACGCCCATGACATCATCCAG

23bp del

GTTCTAAGTGACATTAAAGCAGCACGATATGTCCACGGCATTGGTGTTCACTGGTAT
TTTGATCGCCTTGTGCCGCCTGACGTCACCCTGACCTCCACACACCATCTGTACCCTG
ATTACTTCCTATTTGCAACTGAGGCATGCGCTGGGTGGAGTCCAGTGGATCGTGGTG
TGCGTCTGGGCAGCTGGGACAGGGCAGAGGACTACGCCCATGACATCATCCAG

Figure 51. F1 TALEN-induced *gba1* mutants. The genomic *gba1* exon 7 sequence illustrating TALEN deletions that transmitted to the F1 generation. Outcrossing F0 injected to WT in order to generate the F1 generation led to 3 different alleles being identified for further study, namely 8, 7 and 23bp deletion, all within exon 7. The *Mwo*I site is highlighted in green and deleted bases in red script.

4.5 *gba1* TALEN characterisation

4.5.1 *gba1* qPCR in *gba1 -/-* and WT brain tissue

The 23bp deletion leads to a frameshift and appearance of a premature stop codon 66bp downstream within exon 7 at c.1342, truncating the protein at position p.379 (WT is 518 amino acids in length). qPCR was utilised to demonstrate the stop codon led to nonsense mediated decay of the transcript. As it was unknown how the deletion may affect splicing, two pairs of primers were optimised. The first pair amplifying a region upstream of the deletion, the primers binding to exon 4, and the second pair binding to exons 8, 9 and 10, downstream of the deletion. RNA was extracted from 12 wpf brain tissue from WT and *gba1 -/-* zebrafish, 2 brains per replicate. qPCR using either primer

pair showed a decrease in *gba1* transcript levels of 50% (P<0.05) in the *gba1* -/- brain tissue compared to WT, indicating that the *gba1* mRNA transcript is unstable due to the appearance of a premature stop codon, suggestive of loss of function. See Figure 52.

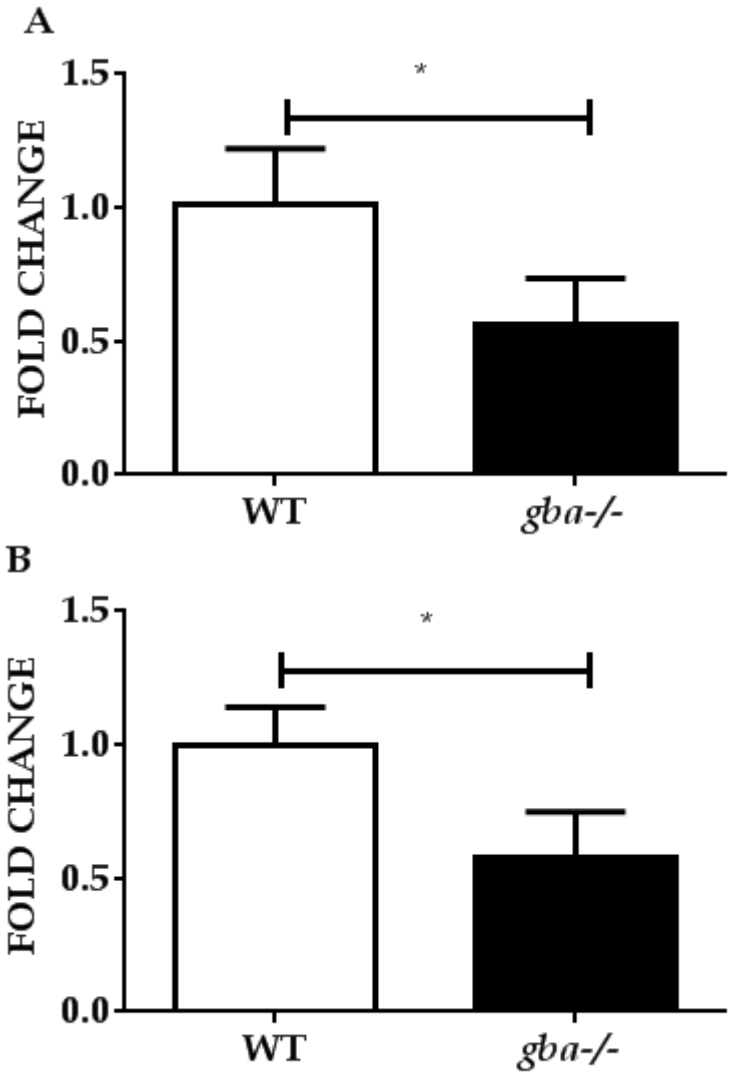

Figure 52. qPCR of *gba1* transcript in WT and *gba1* -/- brains. qPCR was utilised to investigate the 23bp del allele effect on stability of the *gba1* mRNA transcript. Primer pairs amplifying cDNA downstream of the deletion (Figure 52A) and upstream the deletion (Figure 52B) were utilised to quantify *gba1* transcript levels in WT and *gba1* -/- adult brains. Both primer pairs demonstrated a decrease of 50% (P<0.05 unpaired t test) of the *gba1* transcript in *gba1* -/- compared to WT, thus demonstrating that the mutation leads to mRNA instability and NMD, supporting the assumption that this 23 bp deletion results at least in partial loss of function. Data normalised to reference gene *ef1alpha*

4.5.2 Gba activity assay optimisation

Brain homogenates were utilised to assay Gba enzyme activity to quantify the loss of Gba1 activity due to the 23bp deletion, the assay itself had only previously been optimised for mammals; therefore, temperature and inhibitors required for the assay had to be re-evaluated for use in zebrafish. Traditionally, basal GBA1 activity is

determined by subtracting GBA2 inhibited activity from total GBA activity, using the specific GBA2 inhibiter N-Butyldeoxynojirimycin (DNJ). As this can be low, activated GBA1 activity is calculated by measuring total GBA activity in the presence of sodium taurocholate (NaT), an inhibitor that simultaneously inhibits GBA2 whilst activating GBA1. This can allow large improvements in signal to noise ratio.

Firstly, the assay temperature was assessed at 37°C (mammalian body temperature) and 28°C (zebrafish body temperature). Total Gba activity in zebrafish at 37°C was approximately 37 nmol/h/mg, whilst DNJ inhibited Gba activity was extremely low, even for basal Gba1 activity, at 5 nmol/h/mg. Upon inhibition with NaT, Gba1 activity was unchanged to basal Gba1 activity, when theoretically there should have been a marked Gba1 activity increase. Total Gba activity at 28°C was 55% lower than activity at 37°C, with similar decreases in activity in DNJ inhibited at 28°C compared to 37°C. Conversely, NaT activated Gba1 had 50% more activity at 28°C (10.25 nmol/h/mg) compared to NaT activated at 37°C. Although total Gba activity was lower at 28°C, this temperate was chosen for future experiments as it is more physiologically relevant to study activity in zebrafish, and NaT appeared to be more in zebrafish at 28°C, see Figure 53 .

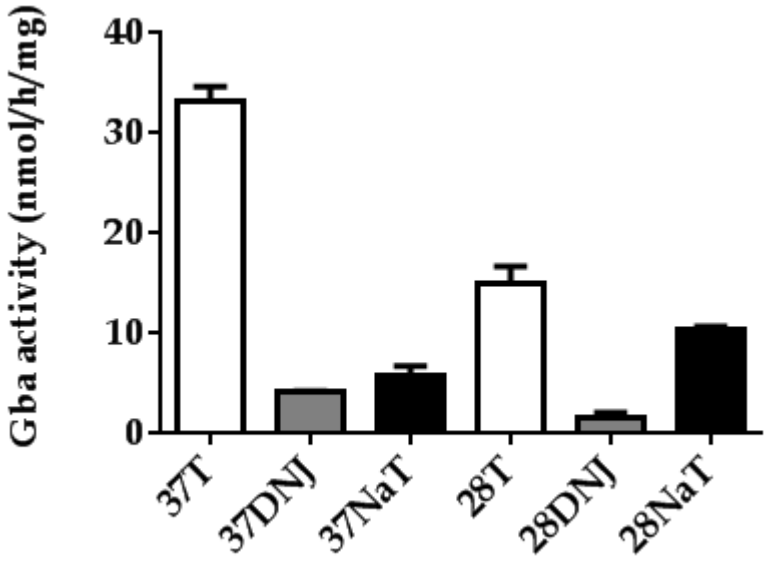

Figure 53.Gba activity assay temperature optimisation. Temperature optimisation for the GBA activity assay. Total (T) Gba activity at 37°C is much higher than at 28°C (the optimum zebrafish body temperature). Basal Gba1 activity (DNJ inhibited) is unexpectedly low compared to total Gba activity, only 10% of total Gba activity. NaT simultaneously inhibits GBA2 activity and activates GBA1 activity in mammals. Gba1 activated at 37°C does not raise Gba1 activity; conversely, the NaT treatment at 28 degrees raises it to 75% of total Gba activity.

The DNJ dose was revaluated over a range of increasing concentrations, to investigate whether there may be any residual Gba2 activity. The standard dose of 50uM was assayed, including increasing concentrations of 100, 150 and 200μM, see Figure 54.

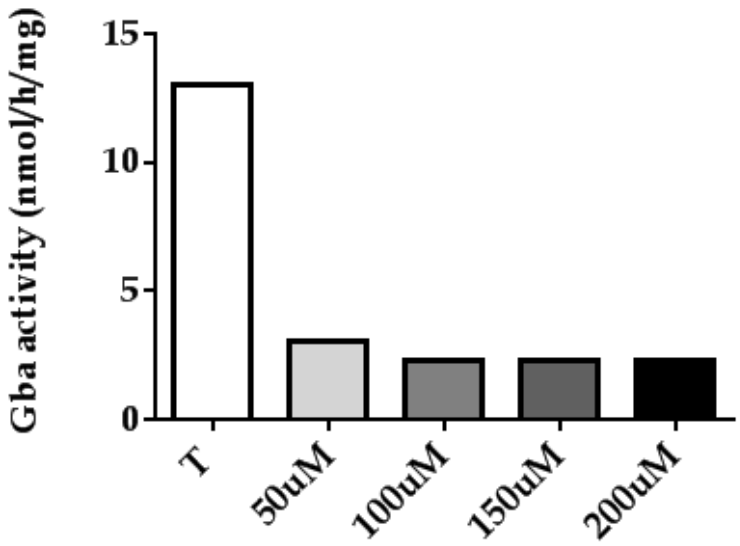

Figure 54. DNJ optimisation. The standard DNJ dose of 50μM is currently utilised in mammalian GBA assays. The dose was increased to investigate if further inhibition was required to prevent any residual Gba2 activity. 50μM DNJ reduced Gba activity to 33% of total uninhibited Gba activity. Increasing the concentration of the inhibitor to doses of 100, 150 and 200μM of DNJ had minimal further effects at decreasing Gba activity demonstrating 50uM is sufficient to inhibit all Gba2 activity.

Subsequent studies found NaT to be highly variable at modulating Gba activity, occasionally giving activity readings as low, or even lower than DNJ treatment groups (data not shown). To further optimise NaT-activated Gba1 activity, Triton X- 100 was tested. Triton X has been utilised in previous studies to further increase the action of NaT on Gba1 activity.[291] The addition of Triton X-100 to the NaT treatment led to a decrease of Gba activity compared to using NaT alone. Therefore, presence of Triton X-100 clearly does not give robust Gba1 activity enhancement when utilised in conjunction with NaT in zebrafish, see Figure 55.

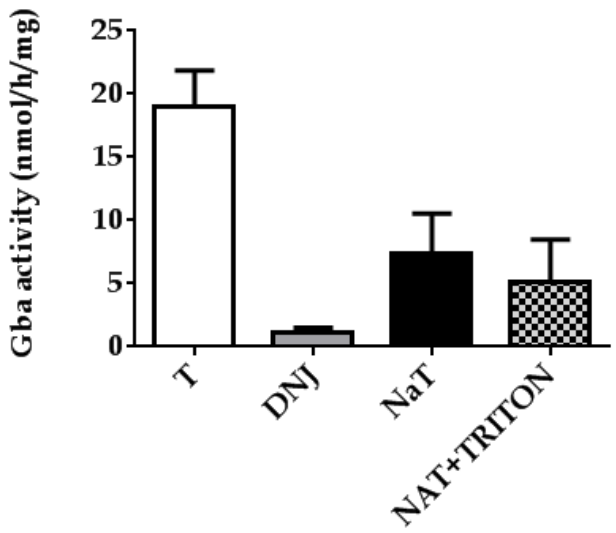

Figure 55. Triton X-100 effect on Gba1 activity. To further increase activated Gba1 activity, a combination of NaT and Triton X-100was applied to zebrafish brain homogenates. DNJ reduced Gba1 activity to 6% of the total, whilst NaT raised the activity to 38% of the total. In contrast, a combination of NAT and TRITON X only raised the activity to 26% of total activity. Triton X-100, therefore, does not enhance the ability of NaT to activate Gba in zebrafish.

The concentration of NaT was also re-evaluated, as more concentrated doses may be required to fully inhibit Gba2 and activate Gba1 in zebrafish. Increasing concentrations of NaT, up to 120mg/ml (from 40mg/ml) only decreased Gba activity to nearly background levels, in a similar manner to DNJ inhibited activity, see Figure 56.

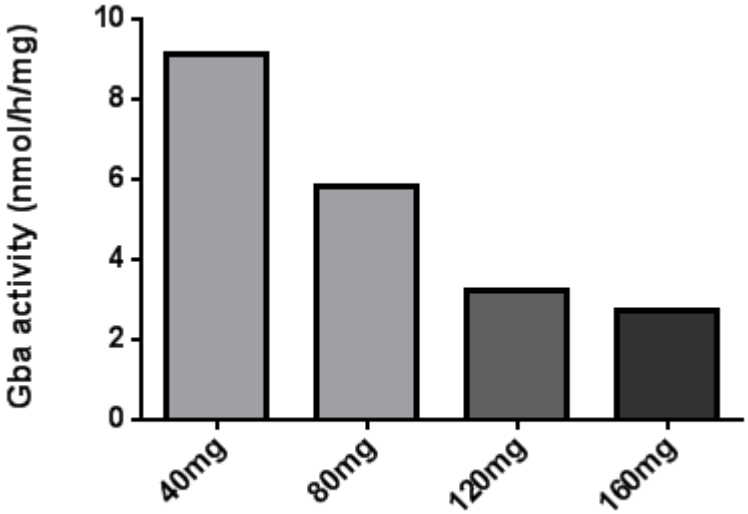

Figure 56. NaT re-optimisation. To further enhance Gba1 activity whilst inhibiting Gba2 in zebrafish, increasing concentrations of NaT were assayed with zebrafish brain homogenates. Increasing the concentration from 40mg/ml up to 160mg/ml meant that Gba activity decreased with increasing NaT concentrations, to levels barely above background, in a similar manner to DNJ inhibited activity.

As both inhibitors at standard concentrations showed Gba1 basal activity is very low, and increasing NaT is unable to increase basal Gba1 activity, inhibitors were utilised at

the standard concentrations for the Gba activity assays on mutant brain tissue. Total Gba activity was substantially reduced in DNJ and NaT treatment groups compared to uninhibited total Gba activity. Within treatment condition activity was unchanged between each genotype. These data imply the 23bp del does not lead to a loss of function of Gba1, in contrast to the qPCR data. However, the Gba activity assay may provide false negative data due to the assumption that both inhibitors function in a similar manner in zebrafish as they do in mammals. This has yet to be validated.

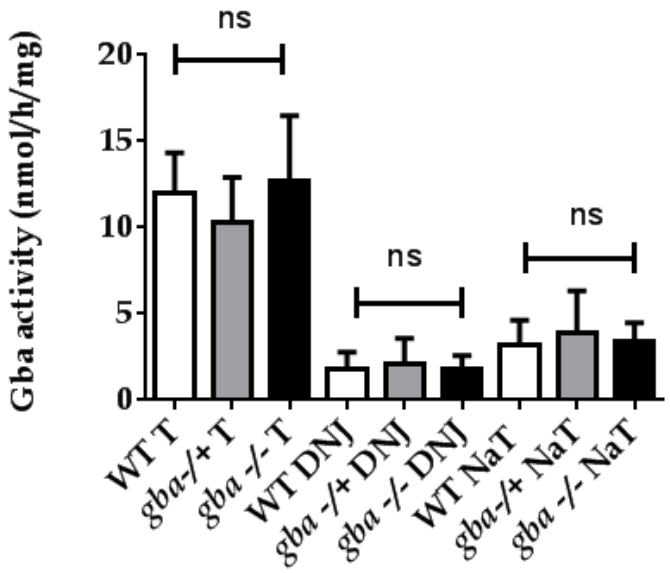

Figure 57. DNJ and NaT sensitive Gba activity in *gba* 23bp del genotypes. Using DNJ and Nat to inhibit Gba2 activity, no change in Gba1 activity could be detected in any of the *gba* 23bp del genotypes.

Consequently, the Gba1 activity assay was performed again, utilising different inhibitors that may behave in a similar manner in zebrafish as they do in mammals. CBE, an specific inhibitor of GBA1 in humans was employed to deduce the Gba1 sensitive fraction of each homogenised brain and thus deduce Gba1 activity. This experiment was jointly undertaken between the author and Dr Matthew Gegg. The author performed the brain extractions, genotyping and processing. Dr Matthew Gegg performed and analysed the assay. CBE sensitive Gba activity was reduced by 50% compared to WT in both 23bp del *gba* -/+ and 23bp del *gba* -/- ($P<0.05$ one way anova), demonstrating the *gba* 23bp del mutation does indeed lead to a loss of Gba1 activity.

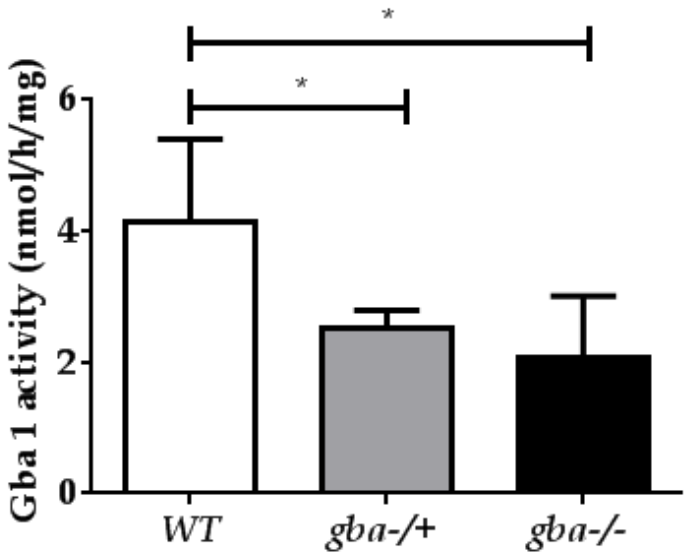

Figure 58. CBE sensitive, Gba activity in 23bp del *gba* genotypes. CBE sensitive Gba activity, representative of Gba1 activity in other species was reduced 50% in both 23bp del *gba* -/+ and 23bp del *gba* -/- ($P<0.05$ one way anova) compared to WT, demonstrating the deletion leads to a loss of function. Residual activity in *gba1* -/- may be due to lack of efficacy of GBA inhibitors in zebrafish.

4.5.3 *gba1* 23bp del *gba -/-* TH count at 5dpf

Incross of *gba1* 23bp del *gba1 -/+* (and all other TALEN alleles) develop normally through embryogenesis. No embryos showed signs of developmental delay or deformity. TH neuron count at 5dpf in *gba1* 23bp del *gba1 -/-* showed no decrease compared to WT or *gba1 -/+*. To confirm this data, *gba1* 8bp del genotypes also had their TH neurons analysed that also showed no decrease in *gba1 -/-*, compared to WT or *gba1 -/+*, see Figure 59.

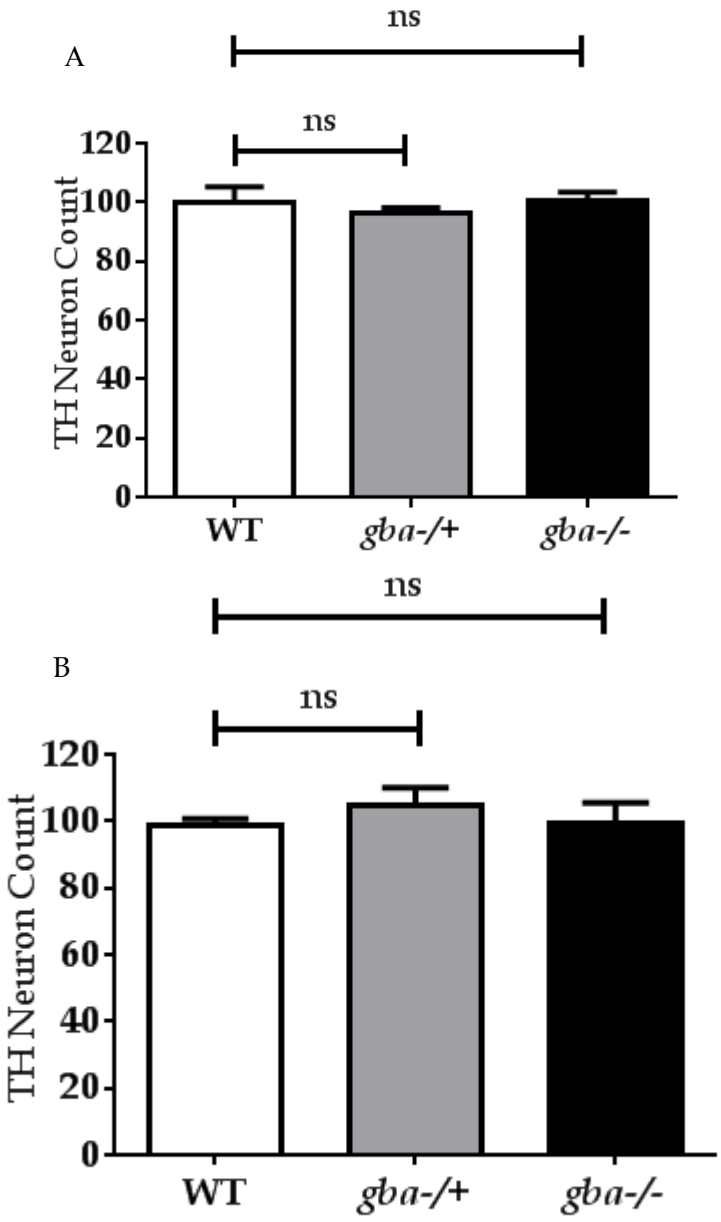

Figure 59. TH neuron counts in TALEN alleles at 5dpf. Figure 59A, 23bp del genotypes shows no decrease in TH neuron count in *gba1 -/-* and *gba1 -/+* compared to WT. Figure 59B, 8bp del genotypes showing no decrease in TH neuron count in *gba1 -/-* and *gba1 -/+* compared to WT.

4.5.4 TH neuron count at 12 wpf in *gba1* genotypes

In order to assess TH neuron count at older ages, TH-positive neuronal cells were stained by IHC and analysed by confocal microscopy at 12 wpf. TH positive neurons were counted by Sallinen's definition.[120] The experiment was jointly performed by the author and Dr Yu-Chia Chen. The author performed the genotyping, brain extraction and fixation. Dr Yu-Chia Chen performed the IHC. The caudal zone of the periventricular hypothalamus was also analysed for TH neuron count in WT (n=10), *gba1* -/+ (n=12) and *gba1* -/- (n=13). WT and *gba1* -/+ showed no difference in the number of TH positive cells counted in this region. g*ba1* -/- show a marked decrease in TH1-positive neurons compared to WT, with a decrease of 50% ($P<0.01$, one way ANOVA) (Figure 60A). TH1 positive neuronal cells were counted in the posterior tuberculum in all genotypes. *gba1* -/- showed a 25% decrease in TH neurons compared to WT ($p<0.01$, one way ANOVA, n= 12 and 10 respectively). *gba1* -/+ showed no statistically significant difference to WT. See Figure 60B.

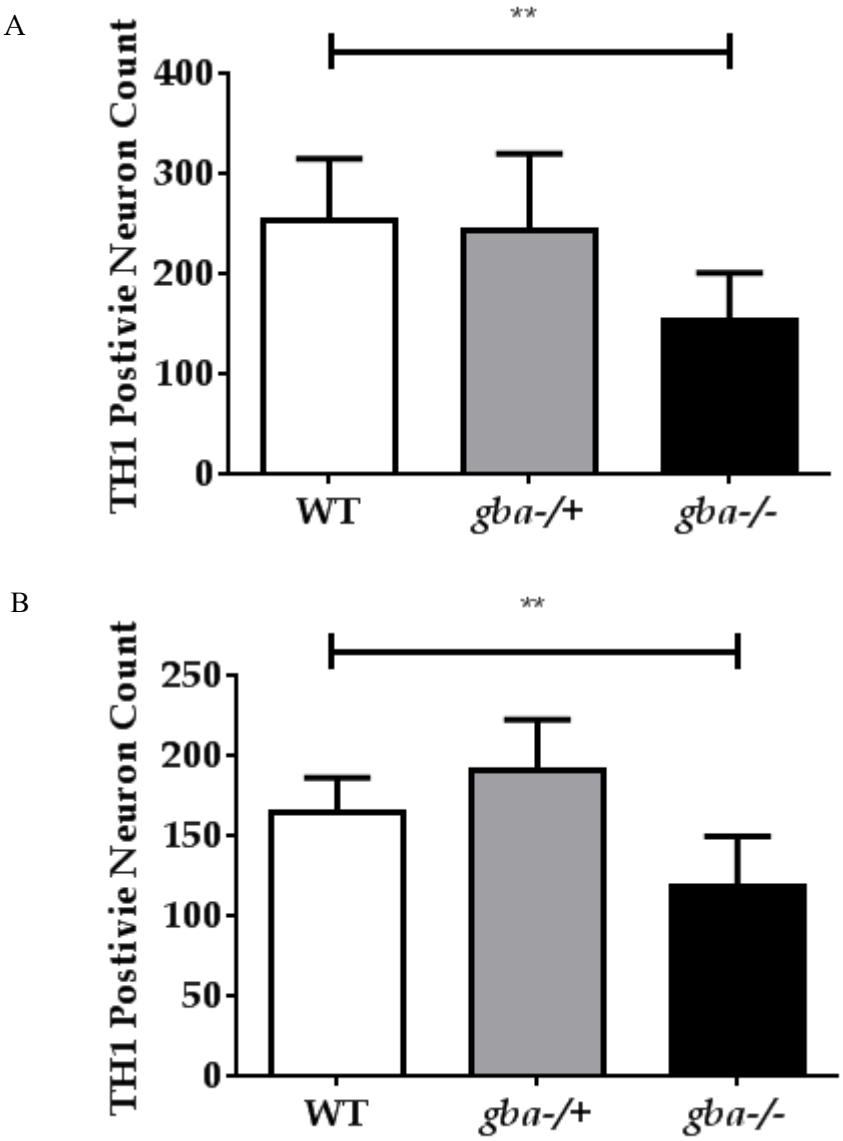

Figure 60. TH neuron counts in 12 wpf *gba1* genotypes. TH1 positive cells were counted in the brains of 12 wpf *gba1 -/-*,*gba1 -/+* and WT in the caudal hypothalamus (A) and the posterior tuberculum (B). In both regions *gba1 -/-* exhibited a decrease of 40-50% compared to WT ($P<0.01$), whilst *gba1 -/+* showed no decrease compared to WT in the caudal hypothalamus and a slight, non-significant increase of 10% in the posterior tuberculum. *gba1* genotype n numbers for caudal hypothalamus counts for WT, *gba1 -/+* and *gba1 -/-* were 9, 12 and 13 respectively. *gba1* genotype n numbers for posterior tuberculum counts for WT, *gba1 -/+* and *gba1 -/-* were 10, 13 and 12 respectively.

4.5.5 Microglial shape in *gba1 -/-* larvae

To assess if Gaucher like cells appear during embryological stages in *gba1 -/-* larvae, *gba1 -/+* were crossed with the Tg(mpeg1:EGFPcaax) transgenic reporter line that simultaneously labels microglia and macrophages with GFP. This experiment was jointly performed by the author and Dr Felix Ellett. Imaging and analysis was performed by Dr Felix Ellett. Genotyping was performed by the author. *gba1 -/+*;

Tg(mpeg1:EGFPcaax) were incrossed and microglial/macrophage morphology was assessed at 4dpf by confocal microscopy in all *gba1* genotypes. Three separate fields of view were analysed for each embryo, specifically the tail, the trunk and the head. Macrophages/microglia were analysed for a different morphological markers, including shape and volume. No differences were found between WT and *gba1 -/-* for cell shape or volume in either the tail or trunk. However, in the head, these GFP positive cells, most likely microglial, had normal volume in all *gba1* genotypes, however *gba1 -/+* and *gba1 -/-* both had a decrease in their spherical shape compared to WT ($P<0.05$ and $P<0.01$ respectively, one way ANOVA), see Figure 61.

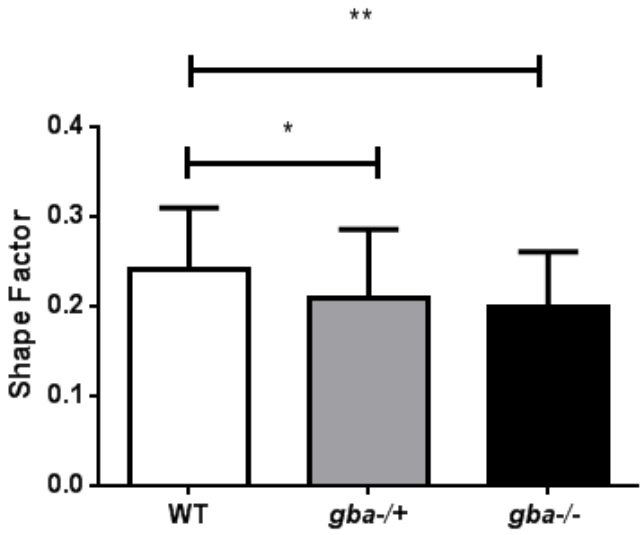

Figure 61. Shape factor of GFP positive cells in the head of each *gba1* genotype. *gba1 -/+* and *gba1 -/-* exhibited a decrease in shape factor compared to WT when analysed in the head of 4dpf larvae. WT microglia had an average shape factor of 0.2417 (47 GFP positive cells from 6 individuals), with *gba1 -/+* (140 GFP positive cells from 14 individuals) and *gba1 -/-* (91 GFP positive cells from 10 individuals) having a smaller shape factor of 0.2087 ($P<0.05$) and 0.1997 ($P<0.01$). This demonstrates that *gba1 -/+* and *gba1 -/-* GFP positive cells have a less spherical shape when compared to WT.

4.5.6 Mass measurements of 23bp del *gba1* genotypes

Pilot data from 7bp del and sa1621 incross showed the *gba1 -/-* developing a decrease in mass compared to WT. Mass measurement of the *gba1* 23bp del genotypes was undertaken at 9 and 12 wpf. The 23bp del *gba1 -/-* (from here on referred to as *gba1 -/-*) showed a decrease in mass at 9 wpf (30% decrease $P<0.05$) see

Figure 63. The incross was genotyped at 10wpf and all animals were segregated by genotype in separate tanks. The mass of the *gba1 -/-* was normalised to WT fish by 12 wpf, after segregation of genotypes into separate tanks. This demonstrates the decrease in mass seen at 9 wpf is not an inability of *gba1 -/-* to gain mass, but rather implies that

they were out competed for the limited food supply by their *gba1* -/+ and WT. Additionally, it was noted that food fed during the afternoon was not completely eaten by the next morning in the *gba1* -/- tank, whereas it was in the WT and *gba1* -/+ tank. By 12 wpf, all *gba1* -/- developed a curve in their spine, similar to the gibbus seen in conditional *Gba1* KO mice see Figure 62.[264]

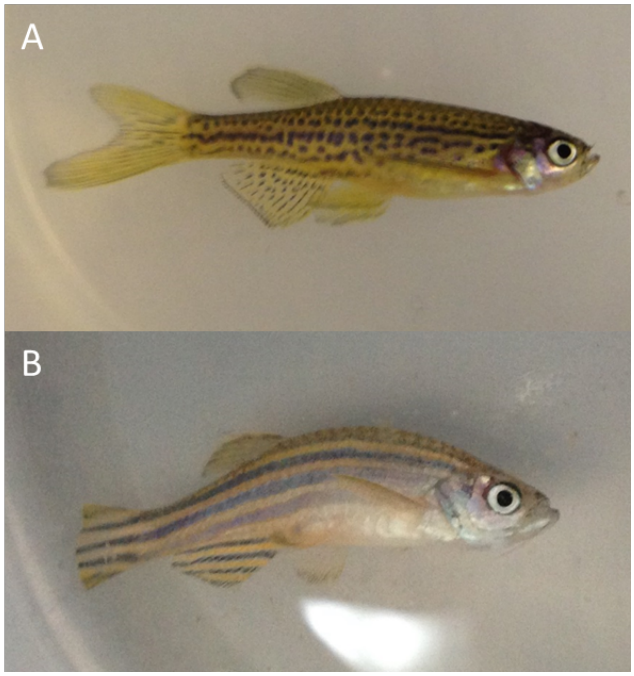

Figure 62. Photographs of 12 wpf WT and *gba1* -/-. WT individuals (Figure 62A) did not display any gross morphological deformities at 12 wpf. By 12 wpf many gba1 -/- exhibited a visible curve to their spine (Figure 62B), with a small minority even having an asymmetrical body axis. The spinal curvature is very similar to the gibbus exhibited by some conditional Gba1 mouse KO.

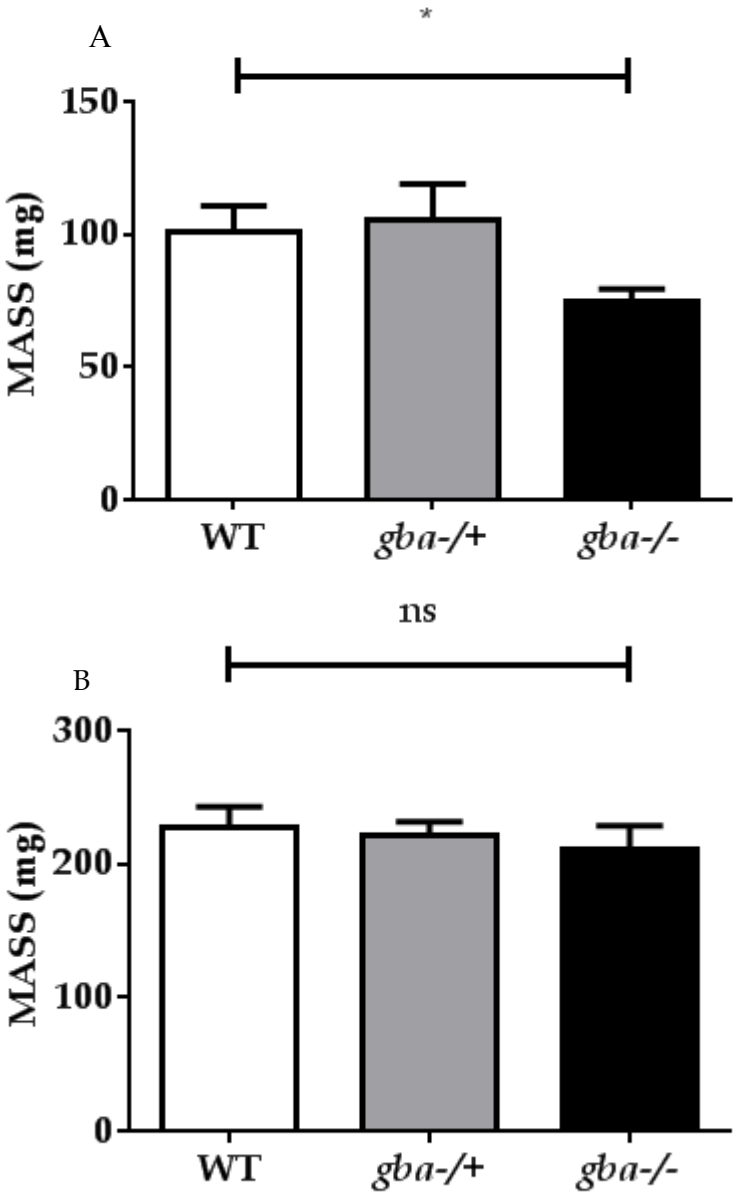

Figure 63. Mass of 23bp del *gba1* allele at 9 and 12 wpf. The mass of each genotype at 9 wpf (A) and 12 wpf (B). gba1 -/- show a significant decrease in mass compared to WT at 9 wpf (P<0.05, one way ANOVA, WT:16, gba1 -/+:10, gba1 -/-:26). The gba1 -/- mass normalises by 12 wpf, once they had been genotyped and put into genotype specific tanks. WT:27, *gba1* -/+:25, *gba1* -/-:24.

4.5.7 Movement analysis in *gba1* genotypes

Total displacement for each *gba1* genotype was assayed via video tracking software at 12 wpf. Each fish was filmed for ten minutes, with ten minutes tank habituation. *gba1* -/- showed a striking 60% decrease in total displacement compared to WT (P<0.0001). *gba1* -/+ fish demonstrated an intermediate phenotype with a small and non-significant decrease of 25% compared to WT (Figure 64A). Subsequently, activity phases were combined into large, small and inactive movements. WT fish spent a large proportion of their time performing larger movement compared to *gba1* -/- (P<0.0001), with the

opposite trend for inactive phases (P<0.0001), *gba1 -/+* fish had an intermediate phenotype in both movements compared to WT and *gba1 -/-*. All genotypes spent similar amounts of time making small movements (P>0.05). See Figure 64B.

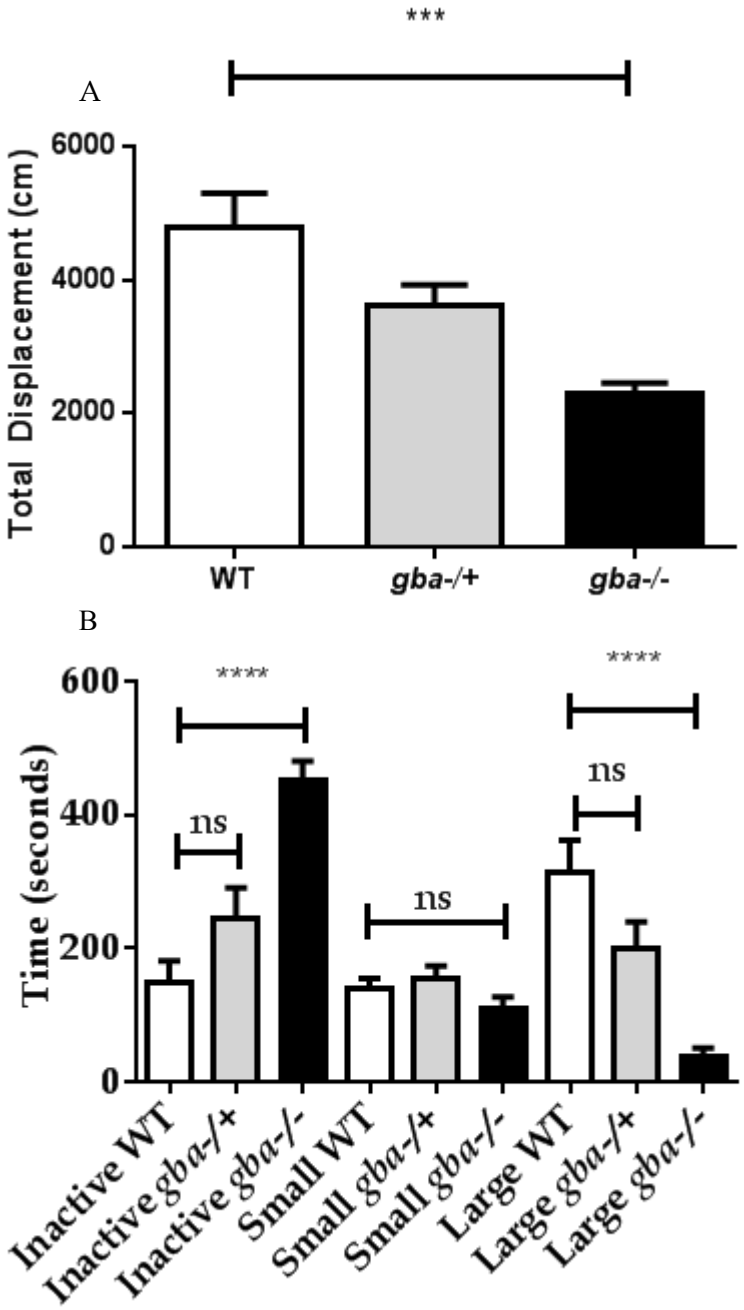

Figure 64. Total displacement of *gba1* genotypes. Total displacement and activity levels during spontaneous movement of *gba1* genotypes at 12 wpf. A, *gba1* -/- exhibit a large decrease of total displacement of approximately 60% compared to WT (P<0.0001, one-way ANOVA), *gba1* -/+ fish demonstrating a smaller, non-significant decrease of 25%. When average speeds where combined into 3 phases of activity (B), inactive, small and large movements, the large decrease in the *gba1* -/- total displacement was revealed to be due to more time in the inactive phase (P<0.0001) and fewer large movements (P<0.0001) compared to the WT.

4.5.8 Hematoxylin and Eosin (H&E) sections of *gba1* 23bp del genotypes

To further understand the severe phenotypes exhibited by the *gba1* -/-, H&E staining was conducted on sections taken from samples at 4, 9 and 12 wpf. No obvious pathology could be found when analysing H&E staining between WT and *gba1* -/-

4wpf individuals. This was jointly undertaken between the author and Dr Aswin Menke. The author genotyped and processed the fish, Dr Aswin Menke performed the staining and analysis.

By 9 wpf (when the abnormal motor phenotype with cork screw motions first became apparent) *gba1 -/-* develop aggregates of swollen cells with some resemblance of Gaucher's cells, the engorged macrophages seen in GD. These Gaucher-like cells form clusters in specific organs in the zebrafish body. This is most apparent in the brain, where these swollen cells accumulate specifically in the tectal ventricle (n=7). No Gaucher like cells could be detected in either *gba1 -/+* or WT individuals (n=5). Gaucher-like cells were also detected most notably in the thymus of *gba1 -/-* 9 wpf fish, with some individuals (although not all) exhibiting these accumulations in the liver, spleen, pancreas and gonads. No Gaucher-like cells could be detected in either *gba1 -/+* or WT 9 wpf fish (n=5). See Figure 65 for a representative example of Gaucher like cells in the tectal ventricle of *gba1 -/-* 9 wpf individuals.

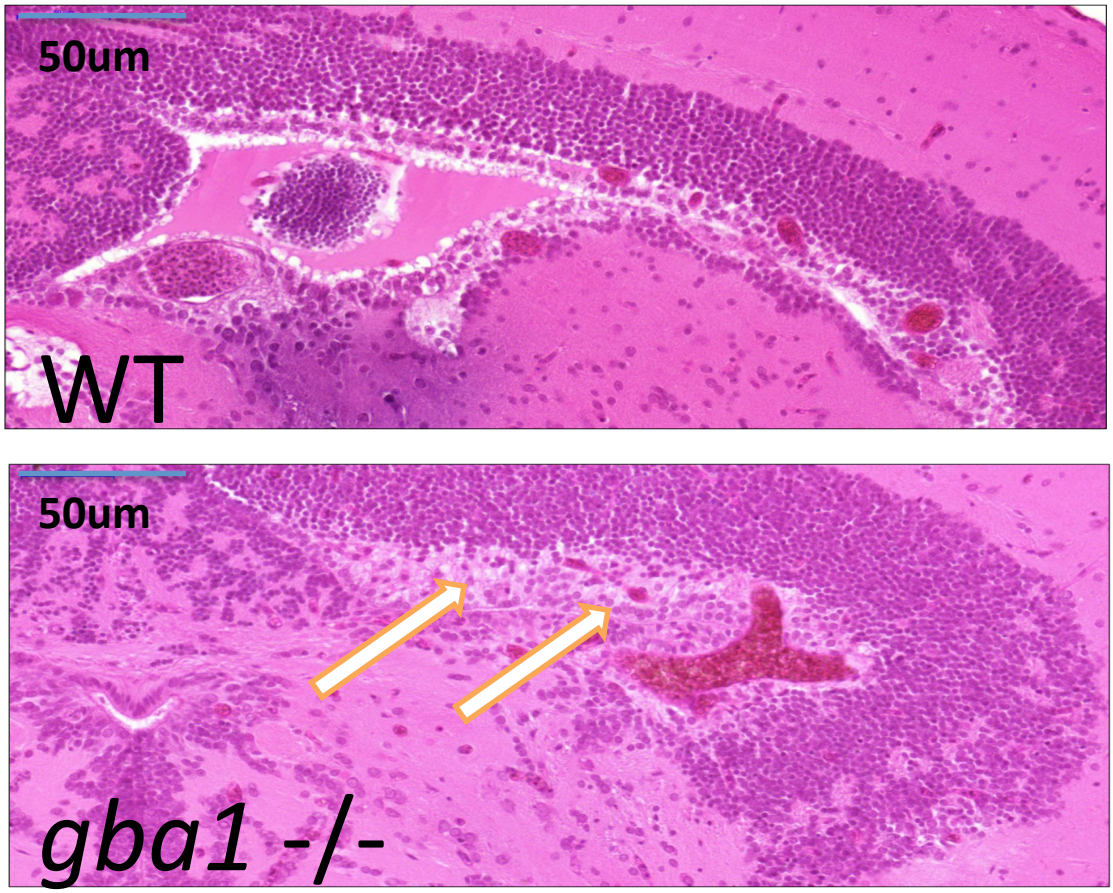

Figure 65. Gaucher like cells in 9 wpf *gba1 -/-* brain. H&E staining brain of 9 wpf *gba1 -/-* demonstrating the presence of Gaucher like cells (white arrows) in the tectal ventricle. Staining and analysis was performed by Dr Aswin Menke, genotyping and fixation by the author.

At 12 wpf, the pathology in the *gba1 -/-* individuals had worsened, with lesions appearing in the brain (see Figure 66). Gaucher-like cells were aggregated in the thymus and liver of all individuals (n=5), whilst more (although not all) individuals presented with aggregates in the spleen, pancreas and gonads, n=3, 4 and 4 respectively (see Figure 67). Periodic acid–Schiff (PAS) staining showed a build-up of glycolipids within the aggregated cells, presumably of the undigested glucocerebroside. At 12 wpf, the *gba1 -/+* fish showed minor cellular swelling in the tectal ventricle compared (n=5) to WT, with an absence of cellular swelling in any other organs.

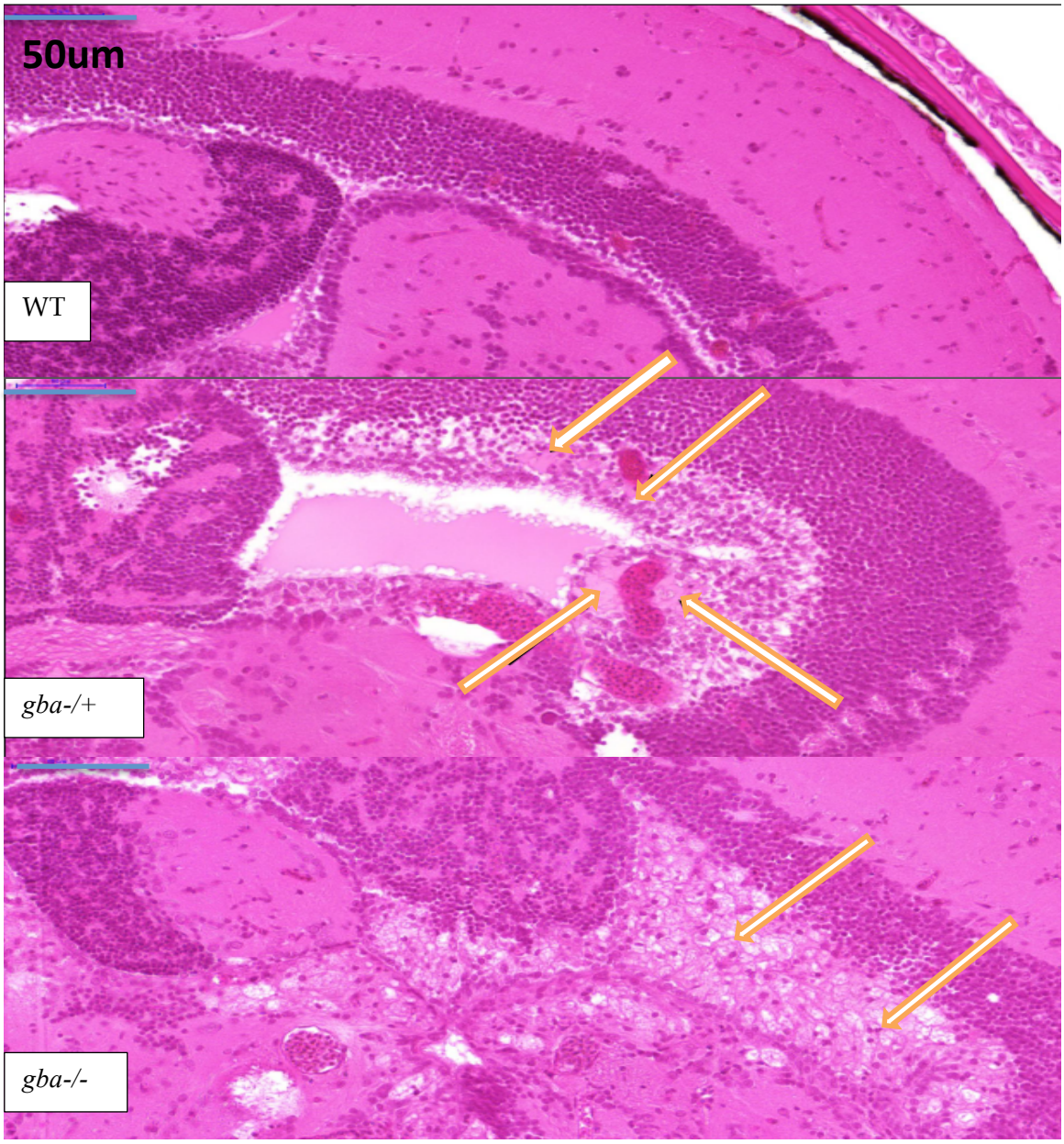

Figure 66. H&E sagittal brain sections of 12 wpf *gba1* -/+ genotypes. At 12 wpf, Gaucher-like cells and lesions accumulating in the tectal ventricle in *gba1* -/- (white arrows), *gba1* -/+.exhibit minor cellular swelling also within the tectal ventricle. No such cells could be identified in WT individuals. N= 5 for each group.

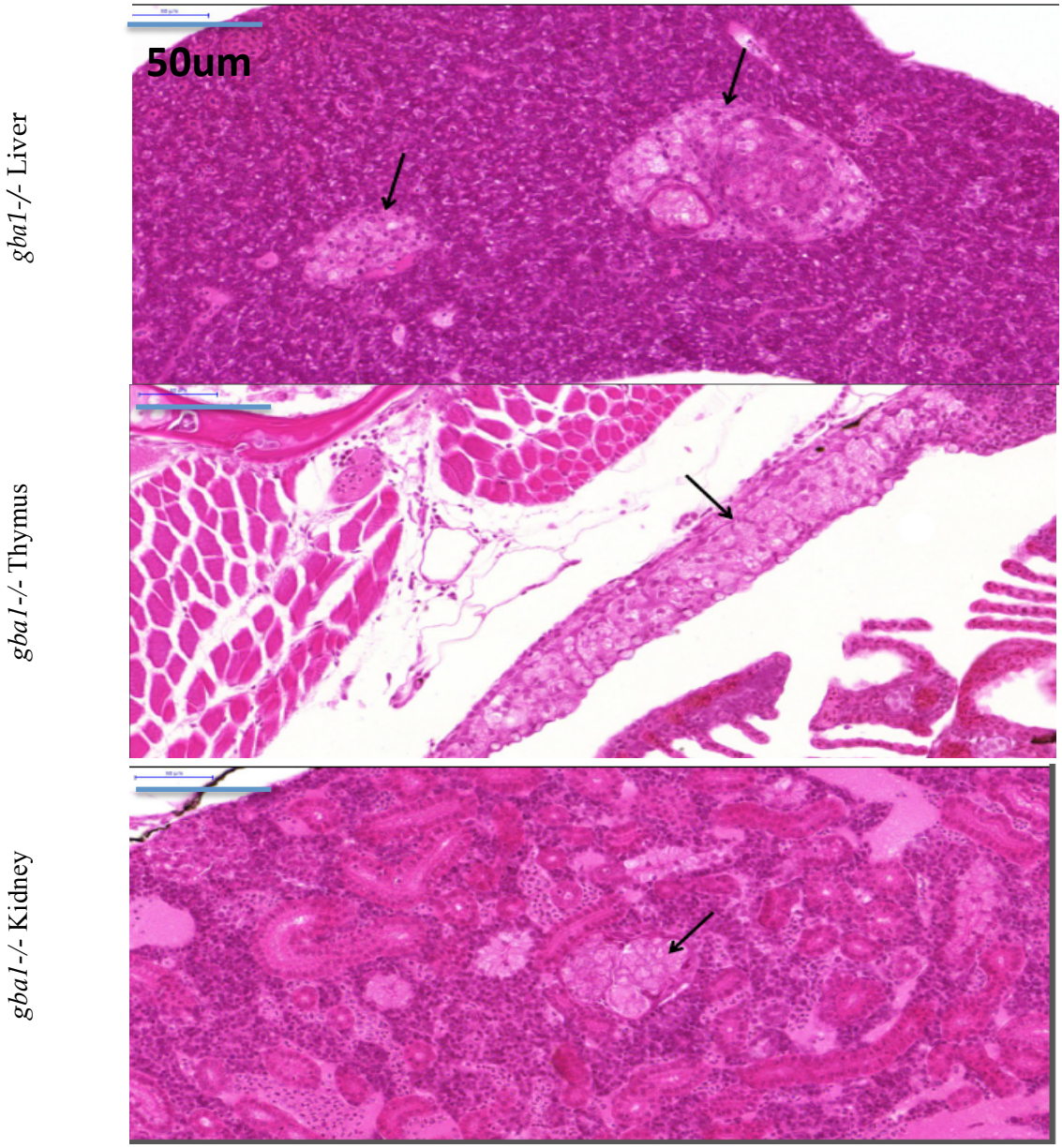

Figure 67. Gaucher like cells in 12 wpf *gba1* -/- visceral organs. H&E staining of liver, thymus and kidneys of 12 wpf *gba1* -/- demonstrating the presence of Gaucher like cells (black arrows). Staining and analysis was performed by Dr Aswin Menke, genotyping and fixation by the author.

4.6 Biochemical phenotypes of *gba1* 23bp del genotypes

4.6.1 Enzyme activities of classical GD biomarkers

In Gaucher's disease patients, chitotriosidase activity and total β-hexosaminidase activity are utilised as biomarkers to assess the effects of enzyme replacement therapy. Untreated Gaucher's disease patients show very large increases in the activity of both

these enzymes, with decreases throughout the course of treatment. The activities of both were analysed in the brain tissue of 12 wpf *gba1 -/-, gba1 -/+* and WT controls. Both classical GD biomarkers were markedly upregulated in the *gba1 -/-* brains, compared to WT, see

Figure **68**. Chitotriosidase had, on average, a ten-fold increase in activity in the *gba1 -/-* compared to WT and *gba1 -/+* ($P<0.00001$). Total β-hexosaminidase was also markedly elevated in the *gba1 -/-*, by 4 fold compared to WT ($p<0.00001$. β-galactosidase was additionally assayed in all *gba1* genotypes as a control enzyme, no significant increase or decrease in activity could be identified compared to WT (n=8 per genotype), see Figure 69.

Both biomarker assays for chitotriosidase and β-hexosaminidase are ideal read outs for high-throughput screening, due to their low cost, low technical difficulty and minimal material requirements. As the *gba1 -/-* exhibited such a marked increases in enzyme activity, it was hypothesised this may be the case in 5dpf larvae. This would be a fast simple and effective readout for zebrafish chemical screens, potentially able to identify new chemical treatments for treatment of GD. Single larvae from a *gba1 -/+* incross were assayed for total β-hexosaminidase activity at 5dpf, the homogenate was then utilised to genotype all individuals. In contrast to the 12 wpf, *gba1 -/-* brains, enzyme activity was unchanged in *gba1* 5dpf larvae of all genotypes. See Figure 70.

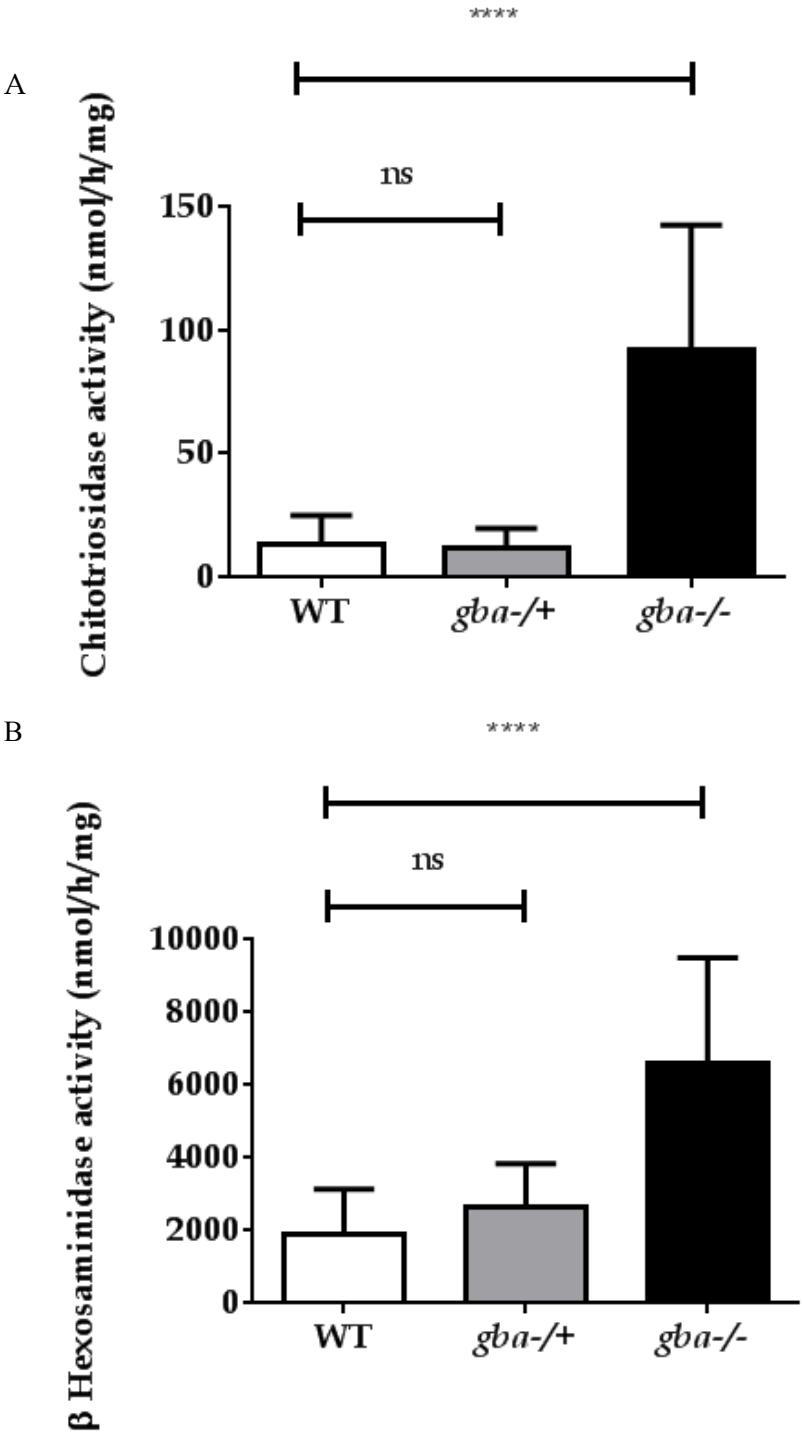

Figure 68. Total chitotriosidase and β-hexosaminidase activity in *gba1* genotypes. *gba1 -/-* brain tissues show marked elevation of traditional Gaucher's disease biomarkers at 12 wpf. A, total chitotriosidase activity is elevated by 10 fold compared to WT in gba1 -/- brains (P<0.00001) with no significant difference in activity between WT and gba1 -/+. B, total β-hexosaminidase activity is elevated 3.5 fold in gba1 -/- brains compared to WT (P<0.00001). β-hexosaminidase and chitotriosidase activity was assayed in all *gba1* genotypes (n=11).

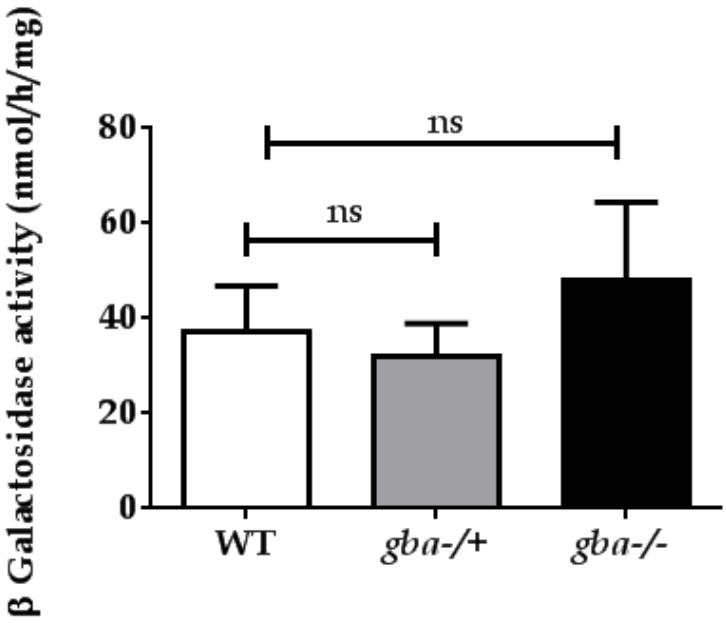

Figure 69. β-Galactosidase activity in *gba1* genotypes. β-Galactosidase activity was assayed in all *gba1* genotypes (n=8). Activity in *gba1 -/-* exhibited a small, non-significant increase of 20% in activity compared to WT. In contrast, activity in *gba1 -/+* exhibited a slight non-significant decrease in activity compared to WT of approximately 10%.

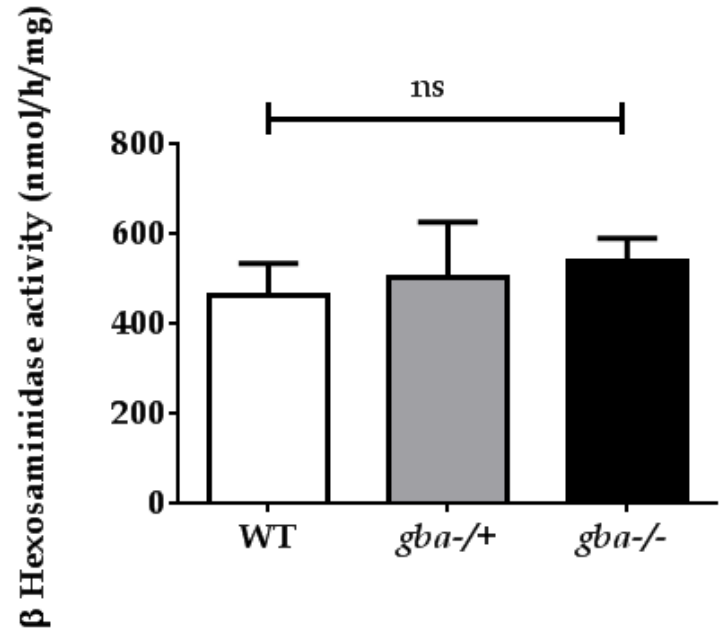

Figure 70. Total β-hexosaminidase activity in 5dpf larvae. β-hexosaminidase activity was measured in all *gba1* genotypes at 5dpf. No significant difference in activity was detected between WT, *gba1 -/+* and *gba1 -/-* , n= 7, 8 and 7 respectively.

4.6.2 Classical GD biomarkers are unchanged in *pink1 -/-*

Chitotriosidase activity is upregulated in activated macrophages and microglia. *pink1 -/-* have previously been demonstrated to have a 50% increase in microglia at 3dpf.

Chitotriosidase activity was measured in *pink1* -/- homogenates of 20 larvae at 5dpf compared to WT. *pink1* -/- homogenates had no significant changes in activity compared WT. See Figure 5. Clearly Chitotriosidase activity is not a suitable read of for phenotypic drug screens in *pink1* -/-.

Total β Hexosaminidase activity, another GD biomarker was assayed for in the *pink1* -/- 5dpf homogenates as a possible drug screen read out. Total β Hexosaminidase has previously been shown to decrease in cerebrospinal fluid in sporadic PD patients. 11 The assay is preferable as a drug screen read out due to its requirement for very small tissue samples (5µl homogenate of 2mg/ml protein) and the speed of assay (10 minutes). Total β Hexosaminidase activity was unchanged between *pink1* -/- and WT, see Figure 71.

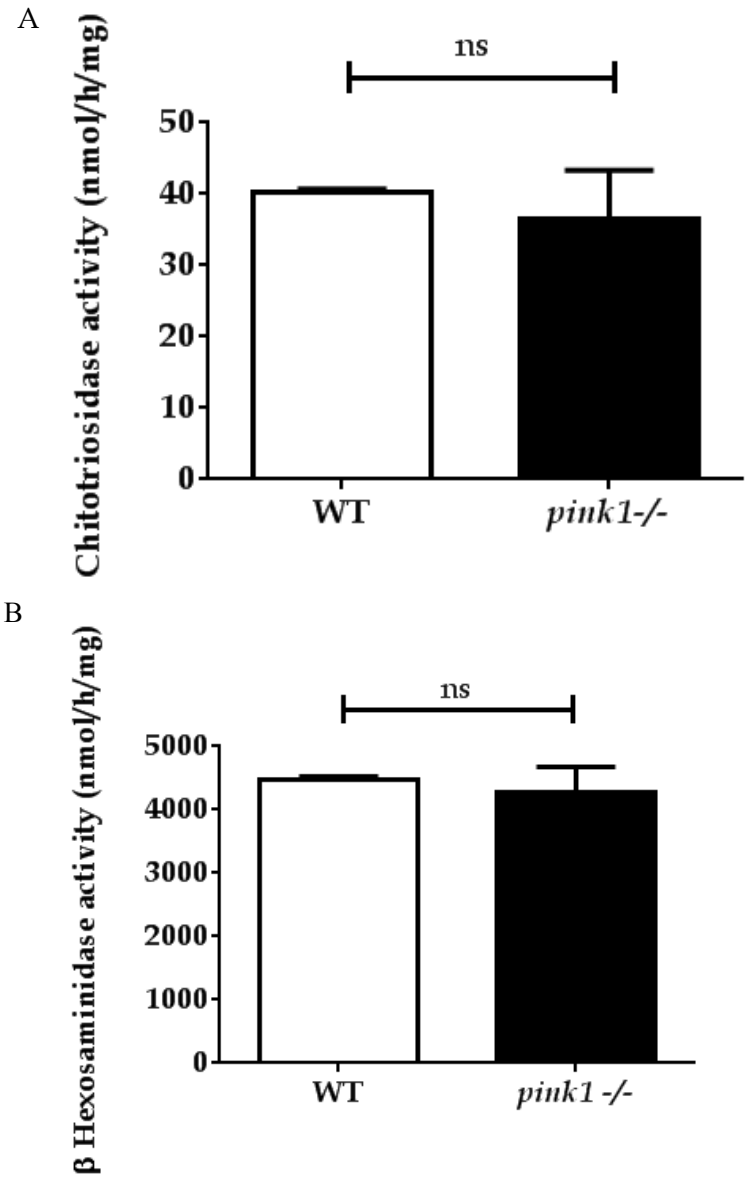

Figure 71. Chitotriosidase and beta hexosaminidase activities in *pink1 -/-* and WT. Figure 71A, *pink1 -/-* show no significant change in activity compared to WT. Figure 71B, total β-hexosaminidase activity is unchanged between *pink1 -/-* and WT.

4.6.3 Mass spectrometry analysis of sphingolipid metabolites in *gba1* alleles

Sphingolipid metabolites were analysed by mass spectrometry in 12 wpf *gba1 -/-*, *gba1 -/+* and WT brains to further elucidate the biochemical consequences of *gba1* deficiency. This was jointly undertaken between the author and Dr Hai Bui, the author genotyped extracted and processed the brain samples, Dr Hai Bui performed the mass spectrometry and subsequent analysis. *gba1 -/-* showed large dysregulation of most analysed metabolites compared to WT and *gba1 -/+ with* highly elevated levels of sphingosine, sphinganine, psychosine, glucosylceramides (all molecular weights),

lactosyceramide and gangliosides compared to WT ($P<0.00001$). Low molecular weight dihydroceramides (C14:0 to C18:0), ceramides (C14:0 to C20:0) and galactosylceramide (C16 and C18) also show a high accumulation in *gba1 -/-* brains compared to WT. However, high molecular weight dihydroceramides (C22:0 to C24:0), ceramides (C22:0 to C24:0) and galactosylceramide (C20 and C24), are all decreased in the *gba1 -/-*, showing a reduced levels compared to WT. All changes were statistically significant, with the exception of the decrease in in dihydroceramides (C22:0 to C24:0), ceramides C20 (increase), C23 and C24:1 (decrease). *gba1 -/+* brains showed few differences compared to WT, with the exception of galactosylceramide C20 and C22 that were statistically significant ($P<0.05$). See Table 8.

Metabolite	*gba1 -/-* % change	Significance	*gba1-/+* % change	Significance
Sph	101.8257993	****	7.616997247	ns
Sa	32.12020523	**	-4.598635528	ns
HexSph	2734.134563	***	0	ns
S1P	-12.79776202	*	6.388802447	ns
DHCer (C16:0)	78.44923164	**	-15.21157476	ns
DHCer (C18:0)	74.38079648	*	-20.52226775	ns
DHCer (C22:0)	-39.17801471	ns	30.96156414	ns
DHCer (C24:1)	-19.22123153	ns	9.932727669	ns
DHCer (C24:0)	-38.92186153	ns	-10.83898132	ns
Cer (C14:0)	135.044829	****	21.67382643	ns
Cer (C16:0)	102.6808401	****	-2.431257609	ns
Cer (C18:0)	41.85715181	****	-4.648751669	ns
Cer (C18:1)	115.8841224	****	16.62848969	ns
Cer (C20:0)	20.30314387	ns	-5.203168812	ns
Cer (C22:0)	-44.29546135	**	15.39658039	ns
Cer (C23:0)	-25.30982469	ns	8.456590168	ns
Cer (C24:1)	-4.024969258	ns	9.362985403	ns
Cer (C24:0)	-31.4830211	*	6.93120657	ns
HexCer (C14:0)	1382.157511	****	11.41672443	ns
HexCer (C16:0)	3466.013156	****	2.801254756	ns
HexCer (C18:0)	7957.318434	****	20.38332697	ns
HexCer (C20:0)	549.0958593	****	15.68309227	ns
HexCer (C22:0)	27.33122019	***	7.07047193	ns
HexCer (C23:0)	9.431597549	ns	10.71208532	ns
HexCer (C24:1)	42.95955413	****	9.658944035	ns
HexCer (C24:0)	-22.35357736	*	6.195719944	ns
GlucosylCer (C14:0)	210.373226	****	4.391630775	ns
GlucosylCer (C16:0)	9882.521703	****	21.61574145	ns
GlucosylCer (C18:0)	14514.04145	****	-7.169052539	ns
GlucosylCer (C20:0)	2885.8451	****	14.79933588	ns
GlucosylCer (C22:0)	529.5906243	****	15.11069321	ns
GlucosylCer (C23:0)	348.5546373	****	13.87395725	ns
GlucosylCer (C24:1)	421.7412698	****	18.88677559	ns
GlucosylCer (C24:0)	112.0538577	****	9.617032105	ns
GalactosylCer (C16:0)	46.97169221	*	5.671671856	ns
GalactosylCer (C18:0)	112.6041678	****	6.572369034	ns
GalactosylCer (C20:0)	-39.80263245	****	18.063784	*
GalactosylCer (C22:0)	-56.07424287	****	23.29432352	*

Metabolite	*gba1 -/-* % change	Significance	*gba1-/+* % change	Significance
GalactosylCer (C23:0)	-48.38752436	****	15.8204541	ns
GalactosylCer (C24:1)	-45.28273411	***	20.61044589	ns
GalactosylCer (C24:0)	-55.09351962	****	9.281332468	ns
LacCer (C16:0)	989.8202929	****	19.43392737	ns
LacCer (C18:0)	2092.221844	****	4.76117511	ns
LacCer (C20:0)	1481.346375	****	10.68494713	ns
LacCer (C22:0)	601.1440845	****	14.79503812	ns
LacCer (C23:0)	295.3751503	****	0.579652139	ns
LacCer (C24:1)	292.0227223	****	15.53764801	ns
LacCer (C24:0)	340.8251407	****	25.00821108	ns
GM3 (C16:0)	226.7453547	****	-8.165992634	ns
GM3 (C18:0)	230.2296156	****	9.119074479	ns
GM3 (C22:0)	458.1100752	****	-22.58397659	ns
GM3 (C24:1)	351.4096211	****	25.46355691	ns
GM3 (C24:0)	263.9855849	****	-6.904832976	ns

	KEY
>	100
>	80
>	60
>	40
>	20
	0
<	-20
<	-40
<	-60
<	-80

Table 8. Sphingolipid metabolite changes in *gba1 -/-* and *gba1 -/+* brains. Brains of 12 wpf *gba1 -/-*,*gba1 -/+* and WT were analysed by mass spectrometry for changes in sphingolipid metabolites (n=10 for all genotypes). The *gba1 -/-* brains showed marked dysregulation of metabolites, with a large accumulation of Gba1 substrate compared to WT. The *gba1 -/+* group showed a trend toward some changes compared to WT however these were not statistically significant. There were exceptions to this including a 80% decrease in GalactosylCer (C20:0) and GalactosylCer (C22:0) compared to WT, $P<0.05$. Abbreviatios, Sph: Sphingosine, Sa: Sphinganine, Hexsph: Phycosine, S1P, Sphingosine 1 Phosphate, DHcer: Dihydroceramide, Cer: Ceramide, HexCer: Heoxsylceramide, Glucosyl: Glucosylceramide, Galaccer: Galactosylceramide, LacCer: Lactosylceramide, GM3: GM3 gangliosides.

4.6.4 Mitochondrial Complex activities in *gba1* genotypes

Mitochondrial dysfunction has been demonstrated in familial forms of PD as well as GD mouse models.[284, 285] The activity of each Complex of the mitochondrial electron transport chain was analysed in each *gba1* 23bp deletion genotype. This was jointly undertaken between the author and Dr Marc DaCosta. The author genotyped, extracted and processed the samples, Dr Marc DaCosta performed the mitochondrial Complex assays and subsequent analysis. Activities of mitochondrial Complex I and II were unchanged between WT, *gba1 -/+* and *gba1 -/-* 12 wpf brains (Figure 72 A and B). In contrast, there was a specific decrease of 40% compared to WT of the activity in

mitochondrial Complexes III and IV (P<0.05). *gba1* -/+ brains showed no significant differences compared to WT. See Figure 72 C and D.

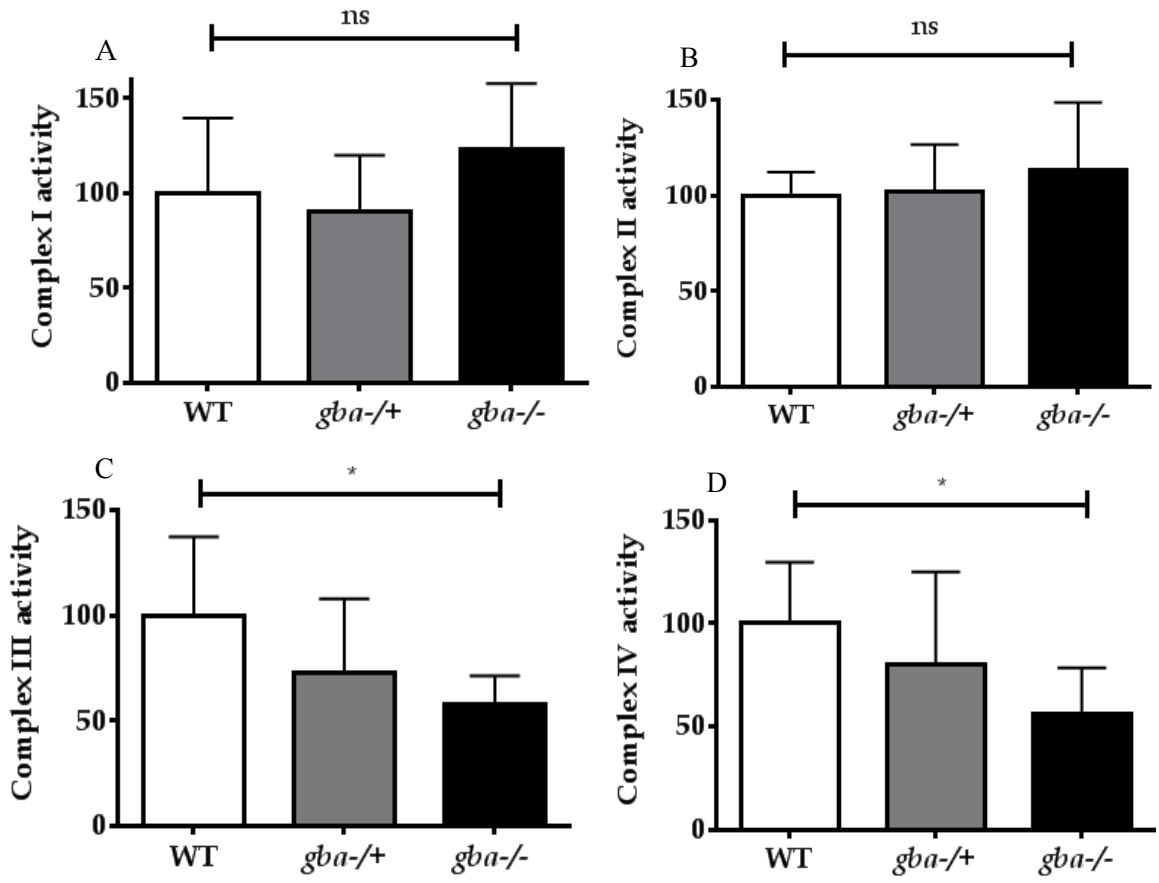

Figure 72. Mitochondrial Complex activities I-IV in *gba1* genotypes. Activity of mitochondrial Complex I, II, III and IV were analysed in 12 wpf *gba1* -/-, *gba1* -/+ and WT brains. No statistical differences were found between genotypes in Complex I and II activity (A and B). *gba1* -/- showed a large decrease of 50% in both Complex III and IV compared to WT (P<0.05 one way ANOVA) (C,D). *gba1* -/+ showed no significant decreased compared to WT.

4.7 *gba1* results summary

This study represents the first characterisation of a *gba1* loss of function model using teleost fish. All previous loss of function *in vivo* models had either utilised *Drosophila* or mice. Zebrafish were found to possess a single *gba1* orthologue, with conserved gene synteny, whose expression was low, but consistent and not spatially restricted, at least during early development. *gba*1 KD was found to not lead to substantial Th neuron reduction or synergistically increase Th neuron reduction seen in Complex I inhibited larvae. TALENs were employed to create a stable loss of function gba mutant. The

resultant allele produced juvenile fish with a marked movement phenotype and early lethality. H&E staining revealed many Gaucher like cells appearing in key GD organs as well as the brain. Mass spectrometry of sphingolipids showed accumulation of many metabolites in the sphingolipid pathway including *gba1* substrates within the brains of 12 wpf *gba1* -/-. This was accompanied by large increases in GD biomarkers. TH neuron count revealed a large decrease in the brain of *gba1* -/-, which may be a contributing factor to the decrease in spontaneous movements of *gba1* -/- at the same time point.

5 General Discussion

5.1 Overview

The aims of this research project were to establish the zebrafish as a new model for *pink1* and *gba1* deficiency; identify phenotypes of the resulting mutants; investigate potential new genetic interactions; and establish assays for phenotypic drug discovery. Both projects were successful in establishing loss of function models for the relevant gene, and mutants were characterised to investigate how useful they are as models of their respective neurological disorders. The *tigarb/vhl* interaction study, part of the *pink1* project, has produced potential novel drug targets to treat PD. The *gba1* project was successful in characterising the first teleost model of *gba1* deficiency, exhibiting phenotypes in a manner similar to the GD state of type 2 patients. Although new phenotypes were discovered in both mutant lines, none are currently suitable for phenotypic drug discovery.

5.2 *pink1 -/-* characterisation

The zebrafish *pink1 -/-* line was, until very recently, the only model of *pink1* deficiency which exhibited spontaneous and progressive DA neuron loss. Recent studies of rats exhibiting *PINK1* loss of function have now been reported, which progressively lose DA neurons and display motor dysfunction in a progressive manner. Gait dysfunction appears as early as 4 months of age, in the *PINK1 -/-* rats, while TH neuron counts showed a decrease of 25% at 6 months of age, increasing to 50% at 8 months of age, compared to WT. TH neuron count reduction was also found to occur in the absence of SNCA pathology.[292]

The demonstration of a late onset motor phenotype in aged (3 year old) *pink1 -/-* zebrafish may imply that a more marked decrease in TH neurons has occurred (compared to 18 months), which is in keeping with the progressive loss of TH neurons in PD patients. However, similar phenotypes have also been recorded in other vertebrate models of *pink1* deficiency which lack Th neuron reduction.[188, 199] Although Th neuron reduction increases between embryonic and adult (18 month old) time points from 20 to 50%, whether this decreases further during aging still needs to be addressed, by counting the TH neurons at the 3 year old time point. If Th neuron reduction was not large enough to cause PD like symptoms, the late onset defect in movement seen in *pink1* models that lack Th neuron reduction, could suggest a role of PINK1 in neurotransmitter homeostasis.[188, 224]

The *pink1 -/-* microarray that first identified *tigarb* upregulation in *pink1 -/-* during development was one of the first whole transcriptome studies comparing the effect of *pink1* loss of function to WT in an unbiased approach. Previously, a single *pink1* loss of function microarray had been published in zebrafish. Although, this relied on the use of a Morpholino strategy which can cause off target effects.[156] The study by Priyadarshini *et al.,* identified many gene expression changes in their *pink1* morphants involved in hypoxic signalling. This included a large decrease in *hifa* expression. Although this change would functionally agree with the *vhl* KD rescue described in this thesis, no single gene expression changes were similar between those described by Priyadarshini *et al.,* and those described by Flinn *et al.,* even after the re-annotation of the microarray in this thesis. These discrepancies may at least partially be due to the different time points utilised for each microarray study, 2 and 5dpf respectively, and the two different methods of model generation, Priyadarshini *et al*., utilised a transient KD approach, were as Flinn *et al*., utilised a kinase dead mutant. The latter may not even be producing Pink1 protein due to nonsense-mediated decay.[175, 192] The re-annotation of the microarray was successful in identifying many of the transcripts' human orthologues, but did not highlight any particular pathways previously implied in the pathogenesis of PD, such as dysregulation of mitophagy pathways or intracellular calcium homeostasis. This could be because gene expression changes leading to Th neuron reduction may be more specific to neuronal cells and the microarray was conducted with RNA extracted from whole larvae as opposed to cells of a DA neuron origin. Future gene expression studies in the *pink1 -/-* line, especially those which investigate the gene expression changes at different time points including adult *pink1* brains should focus purely on brain tissue. Isolating brain tissue from larvae is technically challenging, however one method to achieve this would be to use fluorescence activated cell sorting of labelled cells of interest.

To address whether the Th neuron reduction observed at 5dpf in the *pink1 -/-* was due to cell death or a developmental defect, the expression of key neuronal developmental genes was analysed in both genotypes. Spatial expression of all genes was identical in both genotypes suggesting Th neuron reduction was not developmental in origin, at least at the time points analysed. This is unsurprising as PD is a neurodegenerative disease and no evidence has shown it to be developmental in origin. This study highlights the advantages of using the zebrafish as a model due to its *ex vivo* development and transparency. Studies such as this would be impractical in other

vertebrate models such as mice. Furthermore, data from the microarray suggested that neuronal developmental defects were unlikely. This, in conjunction with developmental gene expression patterns examined by WISH, lead the author to conclude that the TH defects seen in *pink1* -/- were not caused by developmental dysregulation, but by neurodegeneration. But a developmental phenotype could still be causative for the reduction, as all time points analysed were 24hpf or later.

5.3 *tigarb* upregulation

The identification of up regulated *tigarb* in *pink1* -/- larvae through early developmental stages has not previously been reported in any *pink1* deficient model systems. The finding that *tigarb* KD ameliorates mitochondrial dysfunction and Th neuron reduction seen in the *pink1* -/- is also counter intuitive as all previous research implies *PINK1* linked Th neuron reduction to be due to oxidative stress. TIGAR is an oxidative stress response protein in humans; it's up-regulation reduces oxidative stress and apoptosis in other model systems including mice. Consequently an upregulation of *tigarb* in *pink1* -/- could be seen as a protective mechanism, as opposed to causing Th neuron reduction. KD of *tigarb* preventing cell loss in the *pink1* -/- larvae is in contrast to previous data where KD of TIGAR led to an increase in apoptosis.[228] This also contradicts models of stroke, where Tigar upregulation is neuroprotective.[293] Of note, *pink1* KO *Drosophila* develop a marked phenotype, (motor defects, TH neuron cell loss, male sterility) without possessing a *TIGAR* orthologue. This would suggest that Tigar over expression is not driving pathology in the *pink1* -/- zebrafish, rather, the metabolic changes induced by *tigarb* KD are neuroprotective.[130]

Initial characterisation of *tigarb* in WT and *pink1* -/- demonstrated expression is constant and not spatially restricted, although there was a more concentrated expression in the head. This is in keeping with previously described expression data described in numerous cancer cell lines and mouse tissue.[228, 231] At basal levels, TIGAR is constantly expressed under the control of an *sp1* promoter, in a p53 independent mechanism.[228, 294] *tigarb* is highly expressed in zebrafish brain, in keeping with expression data recorded for mice. This was to be expected due to the effects on *tigarb* levels on TH neurons.[293, 295] *tigara,* the *tigarb* paralogue, is also expressed in a ubiquitous fashion, however, its upregulation in *pink1* -/- larvae remains inconclusive due to conflicting WISH data. *tigara* upregulation would be unexpected as its

expression was unchanged in the *pink1* microarray. Western blotting could be utilised further evaluate the status of *tigara* expression in *pink1 -/-*, however this would require a functional antibody that is selective for *tigara* alone. No antibodies of this specificity are commercially available. A change in *tigara* expression may also be of no functional consequence as although *tigarb* has confirmed bisphosphatase activity, *tigara* does not. Of the catalytic triad required for the bisphosphatase activity, *tigarb* has 2 out of 3 residues conserved, whereas *tigara* only has 1 out of 3 conserved. However, this assumes Tigarb's catalytic activity is responsible for *pink1 -/-* Th neuron reduction.[296] Ultimately if the gene expression changes seen in the *pink1 -/-* larvae are different between the two *tigar* paralogues, this may be due to them evolving different functions.

5.4 *tigarb* Morpholino optimisation

Morpholino optimisation for *tigarB* was successful and led to the identification of a Morpholino capable of producing 100% KD without toxic off-target effects or deformity. The complete KD by TBMO2 also illustrates that *tigarb* is unlikely to be maternally expressed, or only maternally expressed at very low levels. The mechanism of TBMO2, an exon skip of exon 2 leads to a deletion of a part of the catalytic triad and also causes a frame shift. This suggests to total loss of function. To fully demonstrate the loss of function caused by TBMO2, bisphosphatase assays could be utilised. However, these are impractical, since they require the prior cloning, expression and purification of the truncated Tigarb protein resulting from the deletion of exon 2 and WT protein.

5.5 Inhibition of glycolysis as a pathogenic PD mechanism

Glycolysis is a complicated biochemical pathway which provides both energy in form of ATP and other metabolites such as NADH for the cell. Its flux is highly tissue and age specific, global inhibition of glycolysis may have far reaching consequences for many cell types. Its activity in the brain is poorly understood compared to other organs such as the liver. The majority of the brain's energy requirements is believed to be covered by oxidative phosphorylation. Although this is widely accepted, glycolytic flux still generates a sizable proportion of ATP for the brain of approximately 10% during wakefulness and 20% during sleep.[297] Any chronic alterations of this may have

negative effects on neuronal health. Glycolytic inhibition may be more relevant at the time point analysed in *pink1 -/-* model, as these were at early developmental stages since the brain of pre-term infants has been found to consume 90% of the body's glucose levels.[298] In the adult brain, glycolytic rates vary dramatically within different cell types and regions of the brain.[299] It is conceivable that, due to the brain's larger glucose requirement in development, glycolytic inhibition would lead to a decrease in ATP levels that could lead to Th neuron reduction during gestation. Consequently at birth, *PINK1* linked PD patients may have a reduced number of DA neurons compared to healthy individuals, so therefore are closer to the threshold required for developing motor symptoms, hence the early onset of *PINK1* linked PD.

A more plausible argument is that general glycolytic inhibition is pathogenic towards DA neurons regardless of developmental stage. Current literature is conflicting regarding the effect on glycolysis modulation on neuronal health, however this is likely to be dependent on which model is utilised. In contrast to other cell types, neurons preferentially metabolise glucose via the pentose phosphate pathway over glycolysis. Reducing the level of glycolysis even further might reduce levels of ATP to an extent neurons can no longer tolerate.[300] A study on sporadic patients' fibroblasts detected no change in glycolytic flux. Models of *pink1* deficiency have even shown an increase in glycolytic flux in *pink1 -/-* compared to WT, which is in direct contrast to the zebrafish data described in this study.[301-303] However, the former studies were all conducted in cell culture systems whose metabolic rates may be altered to that *in vivo*. More importantly, the *pink1* studies utilised *Pink1* KO mouse tissue that does not recapitulate early onset Parkinson's and most importantly does not exhibit TH cell loss. This may explain the discrepancies in glycolytic rates. [301-303]

Recent data in flies and worms has demonstrated a neuroprotective effect for Glucose Phosphate Isomerase (GPI), a glycolytic enzyme that converts glucose-6-phosphate into fructose 6-phosphate in a reversible fashion. Glucose-6-phosphate has the capacity to be fed into the glycolytic system if converted into fructose-6-phosphate, or can enter the pentose phosphate pathway. Data by Knight *et al*., has shown GPI inhibition to exacerbate phenotypes of DA neuron loss, exhibited by flies and worms both overexpressing SNCA. Overexpression of GPI was also found to be neuroprotective in both these *in vivo* models of PD, whilst its inhibition was found to exacerbate neurodegeneration.[304] Its mechanism of action was found to be producing glycolytic metabolites that were neuroprotective in nature, as small molecule inhibition of

glycolysis by 2-deoxyglucose led to neurodegeneration whilst addition of glucose ameliorated phenotypes exhibited by the fly PD models. Even though flies lack a *TIGAR* orthologue, glycolytic inhibition may still be key to their pathogenesis.[304]

The fly data discussed above is in keeping with the zebrafish *pink1* microarray data that revealed a downregulation the zebrafish orthologue of GPI, *glucose phosphate isomerase b (gpib)* whilst its paralogue, *glucose phosphate isomerase a (gpia)* remains unchanged. This is significant, as unlike GPI, Gpia and Gpib have preferences as to which direction metabolism proceeds. It has been demonstrated that Gpib preferentially catalyses glucose-6-phosphate to fructose-6-phosphate, whilst the reverse occurs in Gpia (Figure 73). Consequently, as upregulation of *tigarb* would results in a net accumulation of fructose-6-phosphate, the main metabolic product of Gpib. Downregulation of Gpib may be an attempt to normalise fructose-6-phosphate levels, further aiding the action of Tigarb. This further suggests inhibition of glycolysis in the *pink1 -/-* and a move of metabolism towards the PPP.[305]

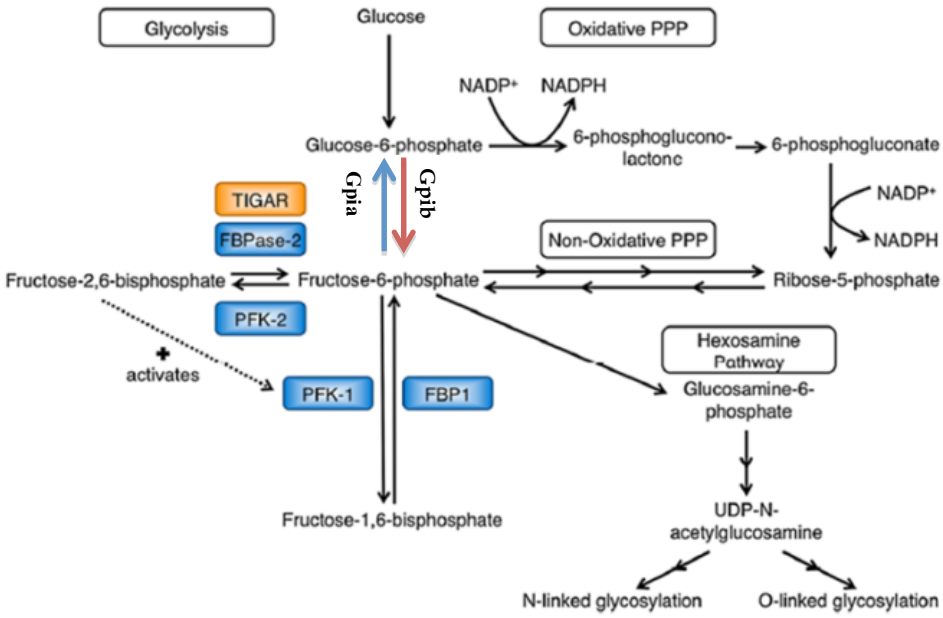

Figure 73. The zebrafish *gpi* paralogues in relation to the glycolytic pathway. Zebrafish paralogues and their preferred mechanism glycolytic flux are shown within the glycolytic pathway. The red arrow is showing preferred flux of Gpib, converting Glucose-6-phosphate to Fructose-6-phosphate, and the blue is arrow showing preferred flux of Gpia, which is opposite to its paralogue Gpib. Adapted with permission from Lee *et al*.[230]

The upregulation of *tigarb* and its inhibition of glycolysis may in fact be exerting its pathogenic effect through the inhibition of autophagy. PINK1 is required for the selective removal of damaged mitochondria via mitophagy, a pathway that is clearly

hindered in PINK1 KO models.[199, 205, 218] Upregulation of *tigarb* will in theory, lower oxidative stress, a key cellular signal for autophagy induction. TIGAR activity has been shown to modulate autophagy in a p53 independent manner.[232] TIGAR's modulation of autophagy can also modulate mitophagy independently of the PINK1/PARKIN pathway as TIGAR inhibition can activate mitophagy through the BNIP3 pathway.[238] Consequently, the upregulation of *tigarb* in the *pink1 -/-* zebrafish may be indirectly leading to inhibition of Pink1 independent mitophagy pathways in an effort to reduce oxidative stress. Consequently, KD of *tigarb* in the *pink1 -/-*, although it may result in an initial increase of oxidative stress, will increase the flux through mitophagy in a *pink1/parkin* independent manner, therefore indirectly decreasing oxidative stress by the removal of damaged mitochondria.

The lack of a rescue effect of *tigarb* KD when exposing larvae to MPP+ is inconsistent with the *pink1* data. However, this may be due to the dosing procedure. Although both *pink1* deficiency and MPP+ exposure both lead to mitochondrial Complex I inhibition and 20% reduction in TH neurons at 72hpf, the Complex I inhibition in *pink1 -/-*is chronic in nature. In contrast, the MPP+ exposure protocol is acute, with larvae receiving a single dose of the toxin at 48hpf until 72hpf. The administration of MPP+ in a single dose, and at a late time point, may overwhelm the neuroprotective power of *tigarb* KD. Consequently administering a less concentrated dose of MPP+ in a chronic fashion (such as administering daily and from fertilisation) may lead to a more chronic inhibition of Complex I inhibition and gradual decrease in TH neuron count, which could then possibly also be rescued by *tigarb* inactivation.

5.6 Future work for *pink1 -/-*

Although a developmental cause of TH neuronal cell loss in the *pink1 -/-* larvae has been largely excluded, the cause of cell loss (such as apoptosis) still requires explanation.

tigarb KD, as a rescue mechanisms in *pink1 -/-* still needs to be further explained. But, this has become more complicated as the role of Tigarb as a glycolytic inhibitor has recently been challenged. Its catalytic affinity for fructose-2,6-bisphosphate (originally described as Bensaad *et al.*) is several orders of magnitude lower than that for 23BPG, consequently, 23BPG may be the main physiological substrate of TIGAR *in vivo*, calling into question TIGAR's function as a glycolytic inhibitor. But this is difficult to

interpret, as cellular levels of 23BPG have never been recorded due to contamination from red blood cells which contain very high quantities of the metabolite. The function of 23BPG is still unknown (apart from in red blood cells where it has a role of regulating affinity of haemoglobin for oxygen). However, this still does not prevent TIGAR inhibiting glycolysis through its originally discovered function as it still has significant affinity for fructose-2,6-bisphosphate *in vivo*. The *pink1* microarray data also suggests pathogenic mechanisms may be due to the inhibition of glycolysis. This is not only due to *tigarb* upregulation but also due to downregulation of the *gpib* that has a high affinity towards Glucose-6-phosphate catabolism, a glycolytic intermediate.[305]

To fully understand *tigarb's* recue mechanism in *pink1 -/-,* confirmation of decreased glycolytic rate needs to be demonstrated biochemically, for example by measuring glycolytic metabolites. If there proves to be no dysregulation, it would add strength to the argument against *Tigar* being involved in inhibition of glycolysis, and would point to other novel functions, most likely involving its capacity to re-localise to the mitochondria and bind HK2 under cellular stress.[234] If *tigarb* rescue is due to increased mitophagic flux, specific markers of autophagy could be analysed for any potential changes.

To firmly establish TIGAR as a potential therapeutic target for *PINK1* disease/PD, stable *tigarb* mutants need to be generated to cross with the stable *pink1* mutant line to evaluate rescue effects in later life. This would allow evaluation of whether chronic loss of function of both proteins has negative consequences in aged fish. This is especially important, as the studies described in this thesis only examine a single time point (3dpf). *Tigar* inhibition studies should also be carried out in mammalian PINK1 loss of function models to demonstrate this rescue is not exclusively a teleost phenomenon. *Tigar* KD in other models of PD should also be investigated to ascertain potential therapeutic rescue in other forms of the disease, for example in *LRRK2* or *SNCA* linked PD.

To achieve this, TIGAR could be inhibited by KD in patient fibroblasts that have previously been characterised, and look for a rescue in phenotypes. For example, inhibiting TIGAR in LRRK2 patient fibroblasts and evaluating its effect on ATP levels and mitochondrial membrane potential. It would be prudent to investigate TIGAR levels in patient brain tissue also, to investigate whether PD, (both sporadic and PINK1

linked) is being driven by TIGAR upregulation. This could be achieved by analysing sporadic patient microarray data.

5.7 *vhl* knockdown rescues *pink1 -/-* Th neuron reduction

The rescue of Th neuron reduction by *vhl* KD is intriguing, but could not be confirmed using stable mutant lines and with a second marker of DA neurons. As the principle read out from the *vhl* KD experiments was TH positive cells stained by *in situ*, this may produce a false positive result as KD may only be increasing TH expression in the mutants as opposed to rescuing TH cell loss. This is especially important as TH is known to be a direct target of Hifa which accumulates in response to *vhl* deficiecny.[290] Consequently, staining for DAT would be a more suitable marker to confirm the TH cell rescue.

Increased expression of TH is unlikely to be a cause of the apparent TH cell rescue in the *pink1 -/-,* since there is no effect of *vhl* deficiency in WT control zebrafish, with an identical TH neuron count in WT with *vhl* KD and WT uninjected zebrafish larvae.

The confirmation of TH neuron rescue by *vhl* KD in a second model system is critical to be certain of its true significance and to be sure the TH cell rescue was not a non-specific consequence of the Morpholino injection (however unlikely it may be). Stable mutants were the most obvious choice and were available. Unfortunately, staining for DAT at 5dpf proved not to support the working hypothesis, as *vhl -/-* had an even larger cell loss (30%) than *pink1 -/-* (20%). This is likely due to developmental defects and general retardation as opposed to neurodegeneration itself. Complete loss of function of *vhl* is not compatible with life as both *vhl -/-* mice and zebrafish are not viable. *pink1 -/-* loss of function is mild in comparison as *pink1* status does not affect lifespan in zebrafish. Consequently, potential rescue of *pink1 -/-*, by *vhl* loss of function should analysed earlier in development where Th neuron reduction is present in *pink1* although not in *vhl,* such as 3dpf.

How *vhl* KD could rescue *pink1 -/-* phenotypes requires further investigation. The original hypothesis was a normalisation of glycolytic flux as both loss of function mutations have opposing rates of glycolysis. This is plausible, but as previously discussed TIGARs status as an glycolytic inhibitor has recently been questioned.[231] Another rescue explanation would be activation of Hifa in the *pink1 -/-* larvae due to

vhl KD. This has been shown to rescue defects seen in other PD models. Moreover, DJ1 has been found to be a direct negative regulator of *vhl/hif1a* interaction.[228]

5.8 *gba1* orthologue identification, expression and knockdown

This study was the first reverse genetic study of *gba1* in teleosts, and other than mouse models, represents the only other loss of function vertebrate model. Identification of a single orthologue of *GBA1* is in keeping with ENSEMBL data listing a single orthologue of *GBA1* in every other vertebrate with a sequenced genome. Although zebrafish possess many duplicated genes in their genome due to a genome duplication event, only a single *GBA1* orthologue could be identified in the zebrafish genome. Unlike humans, zebrafish lack a *GBA1* pseudo gene as this is only present in apes.[244]

Gene synteny was demonstrated to be partially conserved with high homology at not only at the DNA, but also at the protein level. Both the synteny and homology data clearly shows ENSDARG00000076058 to be the true zebrafish *gba1* and not *gba2*.

Expression analysis of WT tissue confirmed *gba1* expression occurs at consistent, although low levels throughout development, with earliest expression detected at 1dpf. Expression in adult zebrafish was confirmed in both liver and brain; key tissues for pathology seen in KO mouse studies and GD linked pathology. Expression was additionally monitored through development by WISH. The staining for expression was specific as no staining could be detected in the sense control probe. Expression was found to be in all organs and concentrated in the head. A similar study in murine developmental stages, also found *gba1* expression in all organs, through all development stages, in keeping with the observed expression pattern in zebrafish.[264, 306, 307]

Morpholino optimisation was successful in producing a Morpholino with high efficacy. Optimisation of the Morpholino targeting exon 8, led to high levels of abnormal splicing in the WT transcript, producing exon skips and intron inclusions. It was noted that 100% KD could not be achieved, even by injecting this Morpholino at toxic doses, suggesting that *gba1* may be maternally expressed.

KO mice die shortly after birth due to skin defects that lead to a loss of water. It was therefore unexpected that *gba1* KD did not grossly affect morphology or development, suggesting different roles of *gba1* in zebrafish skin formation. The modest reduction in

TH neurons seen in *gba1* KD (10-15%) was not statistically significant and likely to be due to a non-specific off target effect of the Morpholino as TH neuron count in 23bp del *gba1* -/- was unchanged compared to WT, and in all other stable mutants analysed in this thesis. The lack of phenotype may also be due to the residual WT transcript in the morphant group and the early time point analysed. If *gba1* deficiency phenotypes are indeed due to substrate accumulation, this may take time, especially if not all of the WT transcript has been mis-spliced as some mouse models have shown to have a large reduction in Gba1 activity with little or no phenotype. The latter is likely due to a higher activity level of Gba1 in the brains of some loss of function mouse models. It appears that if the residual GBA1 activity is more than 20% in the brain, neurological decline is prevented in mice.[263]

The apparent lack of synergistic decrease in TH neuron count in Complex I compromised larvae after MPP+ treatment, subjected to *gba1* KD is also unexpected, although it may be due to the early time point (3dpf). This is not the first study to investigate an interaction between GBA1 and Complex I deficiency. In a study by Gegg *et al.*, KD of *PINK1* in SH-SY5Y cell line already led to a 30% decrease in GBA1 activity and expression. It is therefore plausible that *pink1* -/- larvae already have a decrease in *gba1* activity, prior to *gba1* KD. Although this does not rule out a genetic interaction between the two, it is likely that it may take longer to modulate phenotypes, especially as stable mutants show minor phenotypes until 2 months of age, as opposed to 2-3 days. Gegg *et al.*, also utilised a similar approach of evaluating *gba1* activity in response to Complex I inhibition by using chemical insults, in this case rotenone. However, this showed no decrease in activity. Most likely to the long half-life of GBA1 *in vivo* (72 hours) and the short treatment period of the Complex I inhibitor (48 hours).[268]

5.9 *gba1* stable mutant line generation

The generation of a stable mutant *gba1* line using the TALEN system highlights its importance as a highly efficient genome editing technology. All previous targeted genome editing technology applicable for zebrafish were either not cost effective (Sigma Zinc Fingers) or limited by context dependence (Zinc fingers designed by the context dependant assembly method). For example, initial bioinformatics analysis of the *gba1* genomic sequence identified only 3 sites (2 overlapping) that could be utilised for zinc finger targeting by the context assembly method, whereas TALEN analysis

identified over 50. Further advantages of TALENs over zinc finger nucleases are that the construction is technically simple and very rapid. The resulting TALEN pair mutated *gba1* exon 7 in a targeted and highly efficient fashion. The initial screen on single embryos showed more than 50% mutation rate in some individuals. Sub cloning of undigested TALEN injected PCR products allowed direct sequencing of the mutations induced by the TALEN in the F0 mosaics individuals. Sequencing identified a mutation rate of 40%, producing deletions and indels of a similar magnitude as reported in the literature. The only exception was a complete lack of insertions.[308] As expected, the mutations were present in the germ line, with 80% of the F0 injected individuals identified as founders. Outcrossing two F0 founders to generate the F1 generation, and subsequent genotyping by digest identified the 7, 8 and 23bp del alleles. The 23bp del allele was preferred due to the capacity to genotype by PCR alone, which eventually proved to be extremely cost and time effective. The time taken from construction to having heterozygous adults that could be utilised for incross experiments was 6 months but would then obviously only represent F1 individuals. All F1 adults would require direct sequencing to ascertain their mutation, as F0 founders can still produce F1 individuals with different mutations if their germ line is a mosaic harbouring multiple mutations. Caution must also be taken when outcrossing each allele to remove background mutations. ENU screens for example, as they are not targeted, produce many mutations within a genome, and consequently, mutant alleles generated by this method have traditionally been outcrossed to WT individuals until the F5 generation is reached. At this point, any confounding mutations are deemed to have been removed from the line, and therefore the adults can be utilised for experiments. In contrast, TALENs produce targeted mutations, but may still induce off-target mutations. How often this occurs and how much they vary between TALEN pairs is still being evaluated, appropriate guidelines have not been developed yet.[309] The technical simplicity of TALEN construction, and the availability of loss of function mutations from the SANGER zebrafish mutation project, makes the zebrafish a highly amenable model organism for future reverse genetic work which allows the confirmation of mutant phenotypes in a further zebrafish stable mutant line in which the mutation has been generated using a different technique.

5.10 23bp del *gba1 -/-* loss of function

Mutants were generated to investigate loss of function of *gba1* in zebrafish, to determine whether zebrafish are a suitable model for GD or GBA1 linked PD. Analysing the mutations at a structural level, the *gba1* sa1621 mutant most likely leads to abnormal splicing due to the alteration of an essential splice site. If leading to complete insertion of the following intron, this would generate a premature stop codon downstream of the point mutation, and the deletion of the latter two thirds of the coding sequence at protein translation. All TALEN deletions in the F1 generation, lead to a similar scenario due to the creation of frame shifts. All alleles leading to a premature stop codon appear within exon 7, deleting the last third of the amino acid sequence at protein translation.

The 3D structure of zebrafish Gba1 has not been elucidated, but the 3D structure of human GBA1 is well characterized. The domains are not linear in their organisation, and the N and C terminal parts of the amino acid sequence bind to each other at several points within domains I and II. Disease causing mutations appear in all exons in the human gene, and it is plausible that any kind of deletion similar to those seen the stable mutant zebrafish would prevent proper folding of the enzyme, causing complete loss of function. See Figure 74 for a schematic of the structure of human GBA1.

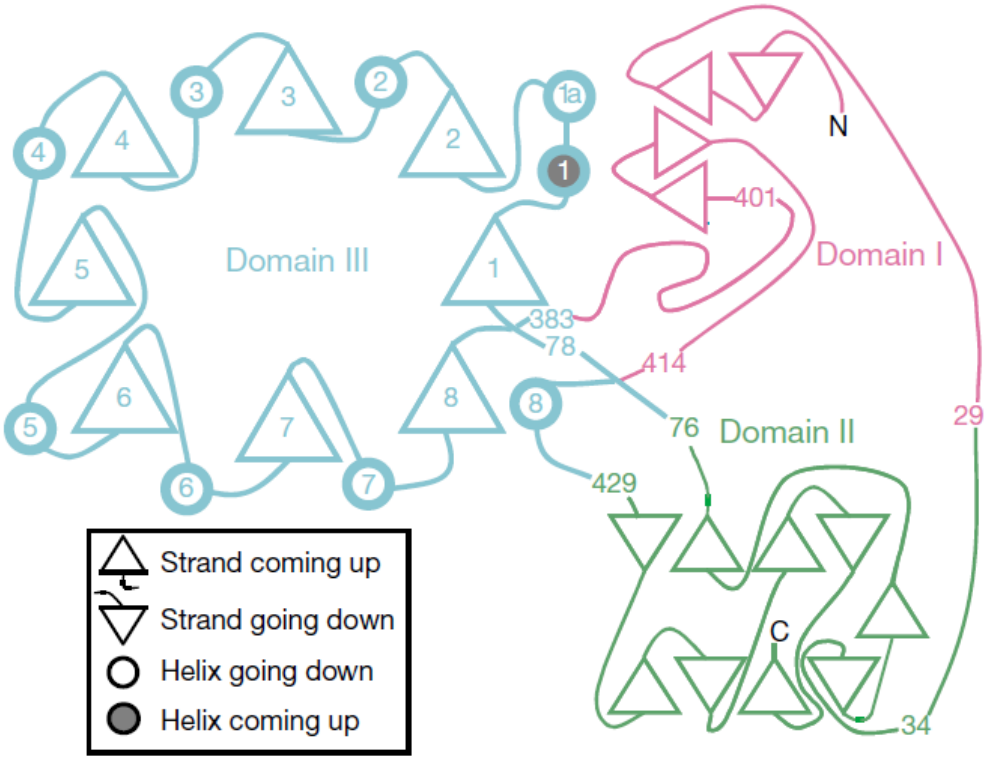

Figure 74. GBA1 cartoon structure. A cartoon illustrating the structure of GBA1. Triangles represent numbered β strands, whilst circles represent numbered α helices. Amino acids denoted in pink are associated with domain I, amino acids denoted in green are associated with domain II, whilst amino acids denoted in blue are associated with domain III. Certain amino acid residues are numbered in certain positions within the connecting groups for clarity. Note that the N and C terminals bind to each other at several locations to form domains II and III. Clearly a large deletion would lead to improper folding and loss of function. Reproduced from Dvir *et al*.[310]

To establish whether the 23bp del *gba1* -/- represented a true loss of function, qPCR was utilised to investigate potential activation of the nonsense mediated decay pathway. qPCR demonstrated a 50% reduction of the *gba1* transcript in the brains of *gba1* -/- to that of WT levels, implying the mutant transcript is unstable and being degraded by RNA surveillance pathways.[311] This suggests that the deletion does indeed lead to loss of function.

The GBA1 activity assay has previously been utilised as a robust tool for measuring the activity of GBA1 in homogenates of mammalian tissue, distinguishing it from GBA2 by the use of specific GBA2 inhibitors. To improve signal to noise ratios, NaT can be utilised, this simultaneously inhibits GBA2 whilst activating GBA1. The assay found no difference in activity between any Gba1 23bp del alleles suggesting the mutation has no effect on Gba1 function. This does not explain how several different mutations, that all produce premature termination codons, lead to such marked robust phenotypes (barrel roll movements, a decrease in mass and premature lethality). For the *gba1* 23bp

del allele, also includes organ invasion by Gaucher like cells seen in loss of function mouse models, and also activation of classical GD biomarkers such as Chitotriosidase and β hexosaminidase but also accumulation of GBA1 substrates within the brain, confirmed by mass spectrometry and PAS staining. Mass spectrometry revealed especially large increases in the level of Gba1 substrates in the 23bp del *gba1 -/-* compared to WT. These increases in the different glucocerebrosides ranged from a 5 fold increase compared to WT, to nearly a 100 fold increase, depending on the fatty acid side chain analysed. These results are similar to loss of function mouse models that accumulate similar levels of glucocerebroside in their brain, spleen and liver. Human patient tissue also exhibits similar changes to those seen in the zebrafish brain mass spectrometry data. Patient GD fibroblasts from Type I and II patients both exhibit large accumulations of ceramides and glucocerebrosides. GD patient plasma has also found to have large increases in levels of ceramides and glucocerebrosides. When analysing GD patients spleens, (an organ key in GD pathology), these changes were also present, but also contained a large accumulation of GM3.[312, 313] Studies of these small metabolites in patient brain tissue of type II and III GD also show large accumulations of in glucocerebrosides, ceramides, GM3 gangliosides. Of note these were found to be especially high in the cerebellum, a site of Gaucher like cell accumulation, within the *gba1 -/-* zebrafish brains. Human GD brains also have a large accumulation of the metabolite hexosyl-sphingosine (psychosine), which is never present in normal healthy brain tissue. Hexosyl-sphingosine was also undetected in the WT and *gba1 -/+* brains, but was detected in large quantities in the *gba1 -/-* zebrafish brains. These data combined suggest the zebrafish is a valid model for neuropathic GD.[128, 262, 314]

Although the Gba1 activity assay itself showed no difference in Gba1 activity between WT and *gba1 -/-* brain tissue this may be due to the specificity of the inhibitors utilised to differentiate Gba1 activity from Gba2 activity. DNJ inhibits Gba2, leaving residual Gba1 activity with basal readings at 5 nm/h/mg in zebrafish brain tissue. These readings are comparatively low compared to mammalian brain tissue, which gives much higher readings of approximately 12 nm/h/mg (both at 37°C). This may be a real physiological reflection of lower total Gba activities in zebrafish brain homogenates, with levels at 35 nm/h/mg compared to mouse brains with GBA1 enzymatic activity close to 100nm/h/mg (both at 37°C). Determining Gba1 activity merely from basal readings by inhibiting Gba2 are difficult to interpret due to their comparatively low

signals compared to total activity.[315] The majority of studies examining Gba1 activity use NaT that simultaneously inhibits Gba2 and activates Gba1. The optimisation experiments carried out by the author revealed that NaT, although inhibiting Gba2 quite successfully, did not lead to the activation of Gba1, even in the presence of Triton X-100. This suggests that either Gba1 activity is very low in zebrafish brain and is unchanged in mutant compared to WT, or NaT is inhibiting both Gba1 and Gba2. These inhibitors have never been tested before in zebrafish and had not been validated. A final possibility is that the Gba activity left in NaT and DNJ *gba1 -/-* groups is not in fact Gba1 but a different Glucocerebrosidase, such as the klotho protein.[315, 316] However, the morphological and behavioural phenotypes, the RNA instability, and the marked substrate accumulation in the brain of *gba1 -/-*, all reminiscent to patients and KO mouse models, suggest that the *gba1* 23bp del is indeed a loss of function allele. Based on the *gba1* structure, it is plausible to hypothesise that any of the alleles discussed in this thesis would lead to improper folding and subsequent null enzyme activity. When alternative inhibitors were used, specifically CBE, a specific irreversible inhibiter of Gba1 to assess the activity of the two enzymes, 23bp del *gba -/-* were found to have a 50% decrease in Gba activity in the CBE sensitive Gba activity. However, these experiments were again complicated by low Gba activity levels. Consequently, the Gba1 activity data generated by the NaT and DNJ inhibitors is likely to be false negative data, as the functional activity of these inhibitors has yet to be validated in zebrafish.

Alternatively, these stable mutants may confer a toxic gain of function. Indeed, arguments for toxic gain of function have been put forward to explain the link between partial GBA1 deficiency and PD.[269] However, this is unlikely for the 23bp del *gba1 -/-*, as toxic gain of function mutations tend to be due to microsatellite repeat expansions (for example the CAG expansion in Huntington's) or missense mutations (such as *LRRK2* linked PD) but only rarely as deletions or splice site alternations.[74, 91] In addition, the probability that three separate mutant alleles, essentially created at random (only exon 7 was defined as a target, not the nature and size of the actual mutation), in two separate regions of the gene, and different two different types of mutations, would all phenocopy each other due to toxic gain of function, is highly unlikely. Additionally, if the mutation were indeed loss of function, more of a phenotype would be expected in the heterozygous individuals.

5.11 *gba1 -/-* characterisation

The decrease in mass exhibited by the *gba1* 23bp del -/-, *gba1* 7bp del -/- and *gba1* sa1621 -/- would appear similar to that previously described in murine models of *Gba1* deficiency, however the reduction in mass of the mutant zebrafish is likely to be due to their inability to compete with their WT controls for limited food supplies due to their movement defect. This decreased mass was normalised back to WT levels upon re-housing in a genotype specific tank, suggesting that the decreased mass is not as a result of "failure to thrive".[261, 262]

As zebrafish develop *ex utero* and *gba1 -/-* survive until 12 wpf, they are far easier to study than *Gba1* KO mice, which die shortly after birth.[128, 261] The stereotyped "barrel rolling/corkscrew like motions" exhibited by the *gba1 -/-* zebrafish that generally occurred upon loss of balance are unlikely to be due to ear defects, as no detectable pathology could be found upon H&E staining in the ear. However, this does not exclude balance defects due to degeneration of the lateral line. The violent motions are reminiscent of seizures exhibited by the neuropathic conditional mouse KOs described by Enquist *et al.*, as the cork screw motions seen could be due to the combination of muscle spasms and the curvature of the body axis, however this requires further investigation.[128]

The gibbus formation and body axis defects seen at the 12 wpf in *gba1 -/-* is very similar to those exhibited by the conditional *Gba1* mouse KO that lack GBA1 activity in only in hematopoietic and mesenchymal stem cell lineages. These mice are viable and do not display neurological defects, however, show large substrate accumulation and organ invasion by Gaucher cells.[251, 264] These conditional KO mouse also develop severe bone complications including focal osteonecrosis and osteopenia, mimicking the bone phenotype typically seen in type I GD. Bone phenotypes were not evaluated in the adult stages of the 23bp del *gba1* -/- zebrafish, but should be investigated in the future Gaucher cell infiltration may be present in bone marrow of *gba1 -/-* at 12 wpf similar to the Gaucher cell infiltration observed in the bone marrow of conditional KO mice described by Mistry *et al*.[264]

5.12 23bp del *gba1 -/-* TH neuron loss

The TH neuron loss in *gba1 -/-* is progressive in nature, reaching a 50% decrease by 12 wpf. The lack of a decrease at 5dpf in the *gba1 -/-* is most likely due to the requirement for Gba1 substrate to build up in the brain tissue.[274] Although there appears to be a change in microglial morphology at 4dpf in the *gba1 -/+* and *gba1 -/-*, this requires further investigation to assess the functional consequences of these cells being less spherical. The lack of an upregulation of GD biomarkers at 5dpf in the *gba1 -/-* further implies that pathology in the embryological stages is limited or very subtle in nature, and takes time to manifest. The large TH neuron loss seen at 12 wpf, is in keeping with conditional KO mice described by Enquist *et al.* Although they did not quantify TH neuron count specifically, they noted conditional KO mice had smaller brains and a reduction of cellular density in the thalamus, cortex, cerebellum, pons and medulla. There was a large increase in apoptotic cells (measured by TUNEL and anti-caspase 3 staining). Additional markers of further neuronal populations should be investigated in the *gba1 -/-* 12 wpf zebrafish to determine whether TH neuron loss is specific or a consequence of global neurodegeneration.[128] No TH neuron loss could be detected in the *gba1 -/+* 12 wpf zebrafish compared to WT. This is likely due residual enzyme activity in the *gba1 -/+* individuals. As *GBA1* linked PD manifests as a late onset disease (at least when compared to *PINK1* linked PD) it could be expected that TH neuron loss is unlikely to be detected at this early time point of 12 wpf. This is especially true as although there was the appearance of minor cellular swelling within the tectal ventricle, there was no robust accumulation or deficiency of any metabolites in the sphingolipid pathway. It should also be noted that although *GBA1* mutations are the most common risk factor for PD, the vast majority of *GBA1* mutation carriers do not develop the disease.

5.13 23bp del *gba1 -/-* Gaucher cell invasion

H&E staining revealed the presence of Gaucher like cells invading organs in the 23bp del *gba1 -/-*which are also affected in GD and in GD mouse models. The Gaucher like cells were first detected at 9 wpf, with pathology worsening by 12 wpf, specifically in the thymus, liver, spleen, and pancreas; all these organs are affected in GD. However, unlike in mouse models of GBA1 deficiency, there was a distinct lack of Gaucher cell accumulation in the bones, which occurs in the conditional model described by Mistry

et al. These mice, although exhibiting hepatosplenomegaly, are viable and live to old age, bone invasion may therefore be a phenomenon that requires further time to appear in zebrafish. Unfortunately the 23bp del *gba1 -/-* do not survive long enough to investigate this possible phenomenon.[264] The accumulation of Gaucher like cells in the brains of the 23bp del *gba1 -/-*, has previously been documented in mouse models and human patients.[317, 318] The main accumulation site is within and adjacent to the tectal ventricle, a structure analogous to the cerebral aqueduct in humans. Over time this has evolved to be much smaller in the human brain than in zebrafish. In zebrafish, the tectal ventricle is located in the optic lobes, the ventral and lateral regions of the tectum opticum in zebrafish play an important role in the coordination of sensory signals and motoric integration. These regions are involved in a wide range of responses, including swimming. The brain lesions and Gaucher cells in this area are therefore a likely cause of the abnormal swimming behaviour seen in the 23bp del *gba1 -/-*. In addition, it also serves as the main visual area of the brain, functionally analogous to the visual areas of the cerebral cortex in mammals. The Corpus cerebellum, analogous to the cerebellum in humans, is the site of considerable sphingolipid metabolite accumulation in types II and III GD, the observed accumulation of Gaucher-like cells in the corpus cerebellum is therefore in keeping with the pathological changes observed in human GD patients.[314, 318]

PAS staining confirmed the Gaucher-like cells to be filled with glycolipids, however to confirm their status as genuine Gaucher cells, co-staining for microglial and macrophage markers should be carried out in the *gba1* 23bp del *gba1 -/-*, such as mac2 and puc.1. The appearance of minor cellular swelling the in the 23bp del *gba1 -/+* at 12 wpf, was unexpected and difficult to interpret, however it does suggest that heterozygous mutations for *gba1* is pathogenic, even at this comparatively early time point. Further investigation is required to ascertain whether this is neurodegenerative in nature. Most likely the *gba1 -/+* will have more marked phenotypes at older ages as TH cell loss could not be detected at this age. Major changes in sphingolipid composition were also not detected at this age.

5.14 23bp del *gba1 -/-* mitochondrial dysfunction

Mitochondrial dysfunction has been widely reported in models of PD, although only a small number of studies have been conducted in the context of GD, none in non-

mammalian models.[199, 201, 272, 284, 285] Mitochondrial dysfunction has been shown to decrease the activity of GBA1, however it is still uncertain whether GBA1 deficiency can lead to defects in the mitochondrial electron transport chain. In this thesis, 23bp del *gba1* -/- were found to have a specific decrease in mitochondrial Complex activities of Complexes III and IV compared to WT. No specific changes in activity were reported in any 23bp del *gba1* genotypes in Complexes I and II. The only prior study similar to this was by Osellame *et al.*, who found a specific decrease in Complex I and III, without a decrease in Complex IV activity, in cultured mouse *Gba1* KO neurons. No decrease in activity could be found in a chemically induced model of GBA deficiency by Cleeter *et al.*, who utilised CBE to inhibit GBA1 in cultured SH-SY5Y cell lines. The lack of an effect in the latter suggests that the acute nature of CBE treatment may only partially reflect any genetically determined GBA1 enzymatic deficiencies. The discrepancies between Complex I activity between this thesis and the report by Osellame *et al.*, could be due to the difference in species, and of the tissue used. This thesis utilised whole brain homogenates, whereas Osellame *et al.*, utilised cultured mouse neurons specifically from isolated midbrain neurons to investigate mitochondrial dysfunction. However, both confirm that Gba1 loss of function can result in mitochondrial dysfunction.[272, 285] In other mouse models of *Gba1* deficiency, Amyloid precursor protein has been found to co localise with COX IV. This in theory could be a represent a direct association between both proteins, which may help to explain the decrease in mitochondrial Complex IV seen in *gba* -/- brains.[319]

Models of other lysosomal storage disorders have also been recorded to exhibit mitochondrial dysfunction. Mouse models of GM1 glangliosidoses, have mutations in the gene coding for β-Galactosidase, and have a specific decrease in mitochondrial Complex IV activity, in a similar manner to *gba1* -/- zebrafish brains. They also exhibit a decrease in their mitochondrial membrane potential and defects in mitochondrial morphology.[320] Mouse models of Niemann pick disease, possess mutations in sphingomyelin phosphodiesterase, also show defects in mitochondrial Complex activity, specifically Complex V.[321] Clearly, mitochondrial dysfunction is a key feature of lysosomal storage disorders and not just specific to GD.

5.15 Future work for 23bp del *gba1 -/-*

The mutant zebrafish described in this thesis has proven to be a robust model of GD, with a marked reproducible phenotype in juvenile zebrafish. The GD phenotype displayed most reminiscent of type 2 GD, due to the marked neurological impairment. TH neuron loss at 12 wpf is especially novel as it is the first example of Gba1 deficiency leading to TH neuron loss in an SCNA independent fashion, as zebrafish do not possess an orthologue of *SCNA*. Whilst this does not rule out SNCA being a major factor in *GBA1* linked neurodegeneration it highlights SNCA independent neurodegenerative mechanisms. However, identifying these specific mechanisms requires further investigation.

As zebrafish do not possess a *SNCA* orthologue, they are an ideal model to analyse *SNCA* dependent and independent effects due to Gba1 deficiency. By crossing transgenic over-expressing *SNCA* lines to the *gba1* 23bp del line, further evaluation could be undertaken. Although it is difficult to predict how human SNCA would affect zebrafish nerve cells, it would be useful to assess the effect of possible SNCA aggregation in the context of gba1 deficiency.

Additionally, recent data has demonstrated SNCA can effect PD progression by moving between cells, a feature exacerbated by GBA1 deficiency. By expressing SNCA under specific promoters within the zebrafish larvae (such as within the olfactory bulb), potential transmission can be tracked through the brain by IHC in 23bp del *gba1* genotypes.[322]

Although not implicated in GD, *MAPT* has been linked to PD through GWAS. Hence over expressing *MAPT* may be useful to investigate interactions between these two genes in the context of PD, especially as a *MAPT* over expressing line has previously been characterised. [102, 323]

Gene- gene interactions could be further elucidated by over expressing and inhibiting other members of the sphingolipid pathway or other Glucocerebrosidases. Of these, sphingomyelinase and GBA2 are key examples. Sphingomyelinase (*SMPD1*) converts sphingomyelin to ceramide. Homozygous mutations lead to another lysosomal storage disorder, Niemann Pick disease, whilst heterozygous mutations (like *GBA1*) have been linked to PD, but this remains controversial.[324] By inhibiting

smpd1 in the 23bp del *gba1* -/+ or -/- by Morpholinos, may reveal phenotypes that would demonstrate an interaction between the mutations.

gba2 is another candidate gene for investigation in the 23bp del *gba1* genotypes as *Gba2* has recently been found to be a modifier of *Gba1* phenotypes in conditional mouse models of GD. The deletion of *Gba2* in a conditional *Gba1* KO mice described by Mistry *et al*., had a complete rescue of hepatosplenomegaly and bone defects exhibited by the conditional *Gba1* KO mouse previously described.[325] It should be noted that the conditional *Gba1* KO mice utilised by Mistry *et al*., retain GBA1 activity in the brain. *Gba2* deficient *Gba1* conditional KO mice, although they have a rescue of phenotypes, also undergo higher quantities of sphingolipid accumulation compared to either mutant alone. Consequently *Gba2* deletion in a full *Gba1* loss of function model may be even more destructive to neuronal tissue than *Gba1* loss of function on its own. But this requires further investigation.

limp2 is another obvious choice to inhibit in 23bp del *gba1* -/- zebrafish as it involved with trafficking Gba1 to the lysosome and has been implicated in PD in meta GWAS studies. But investigations in zebrafish would be impractical due to multiple *limp2* ortholgues.[102, 325]

As the majority of human *GBA1* -/+ carriers do not develop PD, it remains crucial to identify the factors that lead to disease development. One factor previously discussed is genetic interactions. The other is environmental factors. As Complex I inhibition has not be shown to synergistically increase TH neuron loss in *gba1* KD, it may be prudent to explore other toxins implicated in PD, or at least later time points. Suitable candidates would be investigating potential susceptibility to proteosome inhibitors such as MG132, as these have extensively been used to model PD.[170] Alternatively, as *gba1* mutations leads to lysosomal dysfunction, *gba1* -/- and -/+ may be more susceptible to inhibition of general lysosomal proteases, such as Cathepsin D with pepstatin A. Cathepsin D would be of particular interest as not only is it the main protease required for SNCA breakdown, but sole inhibition of the protease leads to neurodegeneration itself.[326, 327]

The Gaucher like cells described in this thesis, are likely to be true Gaucher cells judging from the areas they accumulate, although further confirmation is required. To achieve this, the 23bp del *gba1 -/+;Tg(mpeg1:EGFPcaax)* could be incrossed and grown to 12 wpf and a combined IHC for GFP and H&E could be conducted in order to investigate co-localisation as this transgenic reporter simultaneously labels microglia and macrophages with GFP.[286]

As thus far, the majority of phenotypes exhibited by 23bp del *gba1 -/-* such as the appearance at of Gaucher like cells within the brain are first recorded during juvenile stages. To further understand pathology, it would be useful to identify when phenotypes first begin. This could be achieved by analysing the phenotypes with the largest read out, specifically chitotriosidase activity in a time course fashion. Although brain tissue would be difficult to extract from whole embryos at early stages, whole embryos themselves could be used for the assay, until the individuals become large enough for brain extraction to become practical. If pathology is being driven by substrate accumulation as is currently thought, measuring levels of sphingolipid metabolites by mass spectrometry at earlier time points is also crucial. As in the case with chitotriosidase activity at early time points, brain removal is impractical, consequently whole larvae could be utilised for analysis, but would have to be genotyped before flash freezing.

Ultimately, using the 23bp del *gba1 -/-* larvae for drug based discovery for new therapeutics to treat GD and even PD would be desirable but currently two major difficulties remain. Firstly, suitable readout would need to be established since *gba1 -/-* larvae are phenotypically normal. The only abnormality detected so far were alterations to microglial shape, which is labour intensive to analyse and of uncertain functional significance. Using fluorescent read outs such as those for the lysosomal assays are ideal, however further lysosomal enzymes require testing for phenotypes in the 23bp del *gba1 -/-* larvae to identify potential new read outs. Alternatively, fluorescent dyes that label specific organelles such as lysotracker or mitotracker could be amenable to high throughput analysis.

5.16 Concluding remarks

This study highlights the zebrafish as a new model for PD and GD, proving to faithfully model at least some aspects of the disease where traditional models have

failed, or have proved to be impractical for study. Both models are prime candidates to identify readouts for phenotypic drug discovery to treat GD and PD, as well as models to further understand disease causing mechanisms.

6 Bibliography

1. Van Den Eeden SK, Tanner CM, Bernstein AL, et al. Incidence of Parkinson's disease: variation by age, gender, and race/ethnicity. Am J Epidemiol. 2003 Jun;157(11):1015-22.
2. Shulman JM, De Jager PL, Feany MB. Parkinson's disease: genetics and pathogenesis. Annu Rev Pathol. 2011;6:193-222.
3. Spillantini MG, Schmidt ML, Lee VM, Trojanowski JQ, Jakes R, Goedert M. Alpha-synuclein in Lewy bodies. Nature. 1997 Aug;388(6645):839-40.
4. Jankovic J. Parkinson's disease: clinical features and diagnosis. J Neurol Neurosurg Psychiatry. 2008 Apr;79(4):368-76.
5. Chaudhuri KR, Schapira AH. Non-motor symptoms of Parkinson's disease: dopaminergic pathophysiology and treatment. Lancet Neurol. 2009 May;8(5):464-74.
6. Calabresi P, Di Filippo M, Ghiglieri V, Tambasco N, Picconi B. Levodopa-induced dyskinesias in patients with Parkinson's disease: filling the bench-to-bedside gap. Lancet Neurol. 2010 Nov;9(11):1106-17.
7. Schapira AH, Jenner P. Etiology and pathogenesis of Parkinson's disease. Mov Disord. 2011 May;26(6):1049-55.
8. Lesage S, Brice A. Parkinson's disease: from monogenic forms to genetic susceptibility factors. Hum Mol Genet. 2009 Apr;18(R1):R48-59.
9. de Lau LM, Breteler MM. Epidemiology of Parkinson's disease. Lancet Neurol. 2006 Jun;5(6):525-35.
10. Kowal SL, Dall TM, Chakrabarti R, Storm MV, Jain A. The current and projected economic burden of Parkinson's disease in the United States. Mov Disord. 2013 Mar;28(3):311-8.
11. Schrag A, Schott JM. Epidemiological, clinical, and genetic characteristics of early-onset parkinsonism. Lancet Neurol. 2006 Apr;5(4):355-63.
12. Golbe LI. Young-onset Parkinson's disease: a clinical review. Neurology. 1991 Feb;41(2 (Pt 1)):168-73.
13. Schrag A, Ben-Shlomo Y, Quinn NP. Cross sectional prevalence survey of idiopathic Parkinson's disease and Parkinsonism in London. BMJ. 2000 Jul;321(7252):21-2.
14. Periquet M, Latouche M, Lohmann E, et al. Parkin mutations are frequent in patients with isolated early-onset parkinsonism. Brain. 2003 Jun;126(Pt 6):1271-8.
15. Valente EM, Salvi S, Ialongo T, et al. PINK1 mutations are associated with sporadic early-onset parkinsonism. Ann Neurol. 2004 Sep;56(3):336-41.
16. Miki Y, Swensen J, Shattuck-Eidens D, et al. A strong candidate for the breast and ovarian cancer susceptibility gene BRCA1. Science. 1994 Oct;266(5182):66-71.
17. Goate A, Chartier-Harlin MC, Mullan M, et al. Segregation of a missense mutation in the amyloid precursor protein gene with familial Alzheimer's disease. Nature. 1991 Feb;349(6311):704-6.
18. Lücking CB, Dürr A, Bonifati V, et al. Association between early-onset Parkinson's disease and mutations in the parkin gene. N Engl J Med. 2000 May;342(21):1560-7.
19. Ferreira JJ, Guedes LC, Rosa MM, et al. High prevalence of LRRK2 mutations in familial and sporadic Parkinson's disease in Portugal. Mov Disord. 2007 Jun;22(8):1194-201.
20. Klein C, Hedrich K, Wellenbrock C, et al. Frequency of parkin mutations in late-onset Parkinson's disease. Ann Neurol. 2003 Sep;54(3):415-6; author reply 6-7.
21. Thacker EL, Ascherio A. Familial aggregation of Parkinson's disease: a meta-analysis. Mov Disord. 2008 Jun;23(8):1174-83.
22. Wooten GF, Currie LJ, Bovbjerg VE, Lee JK, Patrie J. Are men at greater risk for Parkinson's disease than women? J Neurol Neurosurg Psychiatry. 2004 Apr;75(4):637-9.

23. Wirdefeldt K, Adami HO, Cole P, Trichopoulos D, Mandel J. Epidemiology and etiology of Parkinson's disease: a review of the evidence. Eur J Epidemiol. 2011 Jun;26 Suppl 1:S1-58.
24. Bach JP, Ziegler U, Deuschl G, Dodel R, Doblhammer-Reiter G. Projected numbers of people with movement disorders in the years 2030 and 2050. Mov Disord. 2011 Oct;26(12):2286-90.
25. Vossius C, Larsen JP, Janvin C, Aarsland D. The economic impact of cognitive impairment in Parkinson's disease. Mov Disord. 2011 Jul;26(8):1541-4.
26. Berg D, Lang AE, Postuma RB, et al. Changing the research criteria for the diagnosis of Parkinson's disease: obstacles and opportunities. Lancet Neurol. 2013 May;12(5):514-24.
27. Hughes AJ, Daniel SE, Kilford L, Lees AJ. Accuracy of clinical diagnosis of idiopathic Parkinson's disease: a clinico-pathological study of 100 cases. J Neurol Neurosurg Psychiatry. 1992 Mar;55(3):181-4.
28. Hughes AJ, Daniel SE, Ben-Shlomo Y, Lees AJ. The accuracy of diagnosis of parkinsonian syndromes in a specialist movement disorder service. Brain. 2002 Apr;125(Pt 4):861-70.
29. Cooper JA, Sagar HJ, Tidswell P, Jordan N. Slowed central processing in simple and go/no-go reaction time tasks in Parkinson's disease. Brain. 1994 Jun;117 (Pt 3):517-29.
30. Korosec M, Zidar I, Reits D, Evinger C, Vanderwerf F. Eyelid movements during blinking in patients with Parkinson's disease. Mov Disord. 2006 Aug;21(8):1248-51.
31. Ws Coriolano M, R Belo L, Carneiro D, et al. Swallowing in patients with Parkinson's disease: a surface electromyography study. Dysphagia. 2012 Dec;27(4):550-5.
32. Hallett M. Tremor: pathophysiology. Parkinsonism Relat Disord. 2014 Jan;20 Suppl 1:S118-22.
33. Sternberg EJ, Alcalay RN, Levy OA, Louis ED. Postural and Intention Tremors: A Detailed Clinical Study of Essential Tremor vs. Parkinson's Disease. Front Neurol. 2013;4:51.
34. Williams DR, Watt HC, Lees AJ. Predictors of falls and fractures in bradykinetic rigid syndromes: a retrospective study. J Neurol Neurosurg Psychiatry. 2006 Apr;77(4):468-73.
35. Giladi N, McDermott MP, Fahn S, et al. Freezing of gait in PD: prospective assessment in the DATATOP cohort. Neurology. 2001 Jun;56(12):1712-21.
36. Macht M, Kaussner Y, Möller JC, et al. Predictors of freezing in Parkinson's disease: a survey of 6,620 patients. Mov Disord. 2007 May;22(7):953-6.
37. Chaudhuri KR, Healy DG, Schapira AH, Excellence NIfC. Non-motor symptoms of Parkinson's disease: diagnosis and management. Lancet Neurol. 2006 Mar;5(3):235-45.
38. Abbott RD, Petrovitch H, White LR, et al. Frequency of bowel movements and the future risk of Parkinson's disease. Neurology. 2001 Aug;57(3):456-62.
39. Ross GW, Petrovitch H, Abbott RD, et al. Association of olfactory dysfunction with risk for future Parkinson's disease. Ann Neurol. 2008 Feb;63(2):167-73.
40. Schuurman AG, van den Akker M, Ensinck KT, et al. Increased risk of Parkinson's disease after depression: a retrospective cohort study. Neurology. 2002 May;58(10):1501-4.
41. Chaudhuri KR. Nocturnal symptom complex in PD and its management. Neurology. 2003 Sep;61(6 Suppl 3):S17-23.
42. Gagnon JF, Bédard MA, Fantini ML, et al. REM sleep behavior disorder and REM sleep without atonia in Parkinson's disease. Neurology. 2002 Aug;59(4):585-9.

43. Tracik F, Ebersbach G. Sudden daytime sleep onset in Parkinson's disease: polysomnographic recordings. Mov Disord. 2001 May;16(3):500-6.
44. Aarsland D, Larsen JP, Tandberg E, Laake K. Predictors of nursing home placement in Parkinson's disease: a population-based, prospective study. J Am Geriatr Soc. 2000 Aug;48(8):938-42.
45. Aarsland D, Påhlhagen S, Ballard CG, Ehrt U, Svenningsson P. Depression in Parkinson disease--epidemiology, mechanisms and management. Nat Rev Neurol. 2012 Jan;8(1):35-47.
46. Gallagher DA, Schrag A. Psychosis, apathy, depression and anxiety in Parkinson's disease. Neurobiol Dis. 2012 Jun;46(3):581-9.
47. Cummings JL. Intellectual impairment in Parkinson's disease: clinical, pathologic, and biochemical correlates. J Geriatr Psychiatry Neurol. 1988 Jan;1(1):24-36.
48. Emre M. Dementia associated with Parkinson's disease. Lancet Neurol. 2003 Apr;2(4):229-37.
49. Jain S. Multi-organ autonomic dysfunction in Parkinson disease. Parkinsonism Relat Disord. 2011 Feb;17(2):77-83.
50. Sakakibara R, Shinotoh H, Uchiyama T, et al. Questionnaire-based assessment of pelvic organ dysfunction in Parkinson's disease. Auton Neurosci. 2001 Sep;92(1-2):76-85.
51. Kaye J, Gage H, Kimber A, Storey L, Trend P. Excess burden of constipation in Parkinson's disease: a pilot study. Mov Disord. 2006 Aug;21(8):1270-3.
52. Goetz CG, Tanner CM, Levy M, Wilson RS, Garron DC. Pain in Parkinson's disease. Mov Disord. 1986;1(1):45-9.
53. Ford B. Pain in Parkinson's disease. Mov Disord. 2010;25 Suppl 1:S98-103.
54. Doty RL. Olfaction in Parkinson's disease and related disorders. Neurobiol Dis. 2012 Jun;46(3):527-52.
55. Bohnen NI, Studenski SA, Constantine GM, Moore RY. Diagnostic performance of clinical motor and non-motor tests of Parkinson disease: a matched case-control study. Eur J Neurol. 2008 Jul;15(7):685-91.
56. Tissingh G, Berendse HW, Bergmans P, et al. Loss of olfaction in de novo and treated Parkinson's disease: possible implications for early diagnosis. Mov Disord. 2001 Jan;16(1):41-6.
57. Tolosa E, Martí MJ, Valldeoriola F, Molinuevo JL. History of levodopa and dopamine agonists in Parkinson's disease treatment. Neurology. 1998 Jun;50(6 Suppl 6):S2-10; discussion S44-8.
58. Abbott A. Levodopa: the story so far. Nature. 2010 Aug;466(7310):S6-7.
59. Tomlinson CL, Stowe R, Patel S, Rick C, Gray R, Clarke CE. Systematic review of levodopa dose equivalency reporting in Parkinson's disease. Mov Disord. 2010 Nov;25(15):2649-53.
60. Nutt JG. Levodopa-induced dyskinesia: review, observations, and speculations. Neurology. 1990 Feb;40(2):340-5.
61. Ahlskog JE, Muenter MD. Frequency of levodopa-related dyskinesias and motor fluctuations as estimated from the cumulative literature. Mov Disord. 2001 May;16(3):448-58.
62. Group PS. Pramipexole vs levodopa as initial treatment for Parkinson disease: A randomized controlled trial. Parkinson Study Group. JAMA. 2000 Oct;284(15):1931-8.
63. Entacapone improves motor fluctuations in levodopa-treated Parkinson's disease patients. Parkinson Study Group. Ann Neurol. 1997 Nov;42(5):747-55.
64. Group D-BSfPsDS. Deep-brain stimulation of the subthalamic nucleus or the pars interna of the globus pallidus in Parkinson's disease. N Engl J Med. 2001 Sep;345(13):956-63.

65. Kleiner-Fisman G, Fisman DN, Sime E, Saint-Cyr JA, Lozano AM, Lang AE. Long-term follow up of bilateral deep brain stimulation of the subthalamic nucleus in patients with advanced Parkinson disease. J Neurosurg. 2003 Sep;99(3):489-95.
66. Weaver FM, Follett K, Stern M, et al. Bilateral deep brain stimulation vs best medical therapy for patients with advanced Parkinson disease: a randomized controlled trial. JAMA. 2009 Jan;301(1):63-73.
67. Rascol O, Payoux P, Ory F, Ferreira JJ, Brefel-Courbon C, Montastruc JL. Limitations of current Parkinson's disease therapy. Ann Neurol. 2003;53 Suppl 3:S3-12; discussion S-5.
68. Martin N, Boomsma D, Machin G. A twin-pronged attack on complex traits. Nat Genet. 1997 Dec;17(4):387-92.
69. Wirdefeldt K, Gatz M, Reynolds CA, Prescott CA, Pedersen NL. Heritability of Parkinson disease in Swedish twins: a longitudinal study. Neurobiol Aging. 2011 Oct;32(10):1923.e1-8.
70. Tanner CM, Ottman R, Goldman SM, et al. Parkinson disease in twins: an etiologic study. JAMA. 1999 Jan;281(4):341-6.
71. Marder K, Levy G, Louis ED, et al. Familial aggregation of early- and late-onset Parkinson's disease. Ann Neurol. 2003 Oct;54(4):507-13.
72. Peltonen L, Palotie A, Lange K. Use of population isolates for mapping complex traits. Nat Rev Genet. 2000 Dec;1(3):182-90.
73. Kerem B, Rommens JM, Buchanan JA, et al. Identification of the cystic fibrosis gene: genetic analysis. Science. 1989 Sep;245(4922):1073-80.
74. A novel gene containing a trinucleotide repeat that is expanded and unstable on Huntington's disease chromosomes. The Huntington's Disease Collaborative Research Group. Cell. 1993 Mar;72(6):971-83.
75. Polymeropoulos MH, Lavedan C, Leroy E, et al. Mutation in the alpha-synuclein gene identified in families with Parkinson's disease. Science. 1997 Jun;276(5321):2045-7.
76. Singleton AB, Farrer M, Johnson J, et al. alpha-Synuclein locus triplication causes Parkinson's disease. Science. 2003 Oct;302(5646):841.
77. Chartier-Harlin MC, Kachergus J, Roumier C, et al. Alpha-synuclein locus duplication as a cause of familial Parkinson's disease. Lancet. 2004 2004 Sep 25-Oct 1;364(9440):1167-9.
78. Johnson J, Hague SM, Hanson M, et al. SNCA multiplication is not a common cause of Parkinson disease or dementia with Lewy bodies. Neurology. 2004 Aug;63(3):554-6.
79. Burré J, Sharma M, Tsetsenis T, Buchman V, Etherton MR, Südhof TC. Alpha-synuclein promotes SNARE-complex assembly in vivo and in vitro. Science. 2010 Sep;329(5999):1663-7.
80. Kitada T, Asakawa S, Hattori N, et al. Mutations in the parkin gene cause autosomal recessive juvenile parkinsonism. Nature. 1998 Apr;392(6676):605-8.
81. Hague S, Rogaeva E, Hernandez D, et al. Early-onset Parkinson's disease caused by a compound heterozygous DJ-1 mutation. Ann Neurol. 2003 Aug;54(2):271-4.
82. Khan NL, Graham E, Critchley P, et al. Parkin disease: a phenotypic study of a large case series. Brain. 2003 Jun;126(Pt 6):1279-92.
83. Pramstaller PP, Schlossmacher MG, Jacques TS, et al. Lewy body Parkinson's disease in a large pedigree with 77 Parkin mutation carriers. Ann Neurol. 2005 Sep;58(3):411-22.
84. Hu CJ, Sung SM, Liu HC, Lee CC, Tsai CH, Chang JG. Polymorphisms of the parkin gene in sporadic Parkinson's disease among Chinese in Taiwan. Eur Neurol. 2000;44(2):90-3.

85. Hedrich K, Djarmati A, Schäfer N, et al. DJ-1 (PARK7) mutations are less frequent than Parkin (PARK2) mutations in early-onset Parkinson disease. Neurology. 2004 Feb;62(3):389-94.
86. Wilson MA. The role of cysteine oxidation in DJ-1 function and dysfunction. Antioxid Redox Signal. 2011 Jul;15(1):111-22.
87. Thomas KJ, McCoy MK, Blackinton J, et al. DJ-1 acts in parallel to the PINK1/parkin pathway to control mitochondrial function and autophagy. Hum Mol Genet. 2011 Jan;20(1):40-50.
88. Cilia R, Siri C, Rusconi D, et al. LRRK2 mutations in Parkinson's disease: Confirmation of a gender effect in the Italian population. Parkinsonism Relat Disord. 2014 Apr.
89. Gaig C, Ezquerra M, Marti MJ, Muñoz E, Valldeoriola F, Tolosa E. LRRK2 mutations in Spanish patients with Parkinson disease: frequency, clinical features, and incomplete penetrance. Arch Neurol. 2006 Mar;63(3):377-82.
90. Ishihara L, Gibson RA, Warren L, et al. Screening for Lrrk2 G2019S and clinical comparison of Tunisian and North American Caucasian Parkinson's disease families. Mov Disord. 2007 Jan;22(1):55-61.
91. Zimprich A, Biskup S, Leitner P, et al. Mutations in LRRK2 cause autosomal-dominant parkinsonism with pleomorphic pathology. Neuron. 2004 Nov;44(4):601-7.
92. Sidransky E. Gaucher disease: complexity in a "simple" disorder. Mol Genet Metab. 2004 2004 Sep-Oct;83(1-2):6-15.
93. Sidransky E, Nalls MA, Aasly JO, et al. Multicenter analysis of glucocerebrosidase mutations in Parkinson's disease. N Engl J Med. 2009 Oct;361(17):1651-61.
94. Neumann J, Bras J, Deas E, et al. Glucocerebrosidase mutations in clinical and pathologically proven Parkinson's disease. Brain. 2009 Jul;132(Pt 7):1783-94.
95. Zimprich A, Benet-Pagès A, Struhal W, et al. A mutation in VPS35, encoding a subunit of the retromer complex, causes late-onset Parkinson disease. Am J Hum Genet. 2011 Jul;89(1):168-75.
96. Sheerin UM, Charlesworth G, Bras J, et al. Screening for VPS35 mutations in Parkinson's disease. Neurobiol Aging. 2012 Apr;33(4):838.e1-5.
97. Braschi E, Goyon V, Zunino R, Mohanty A, Xu L, McBride HM. Vps35 mediates vesicle transport between the mitochondria and peroxisomes. Curr Biol. 2010 Jul;20(14):1310-5.
98. Leverenz JB, Umar I, Wang Q, et al. Proteomic identification of novel proteins in cortical lewy bodies. Brain Pathol. 2007 Apr;17(2):139-45.
99. Manolio TA. Genomewide association studies and assessment of the risk of disease. N Engl J Med. 2010 Jul;363(2):166-76.
100. Jonsson T, Stefansson H, Steinberg S, et al. Variant of TREM2 associated with the risk of Alzheimer's disease. N Engl J Med. 2013 Jan;368(2):107-16.
101. Nalls MA, Plagnol V, Hernandez DG, et al. Imputation of sequence variants for identification of genetic risks for Parkinson's disease: a meta-analysis of genome-wide association studies. Lancet. 2011 Feb;377(9766):641-9.
102. Lill CM, Roehr JT, McQueen MB, et al. Comprehensive research synopsis and systematic meta-analyses in Parkinson's disease genetics: The PDGene database. PLoS Genet. 2012;8(3):e1002548.
103. Alonso A, Zaidi T, Novak M, Grundke-Iqbal I, Iqbal K. Hyperphosphorylation induces self-assembly of tau into tangles of paired helical filaments/straight filaments. Proc Natl Acad Sci U S A. 2001 Jun;98(12):6923-8.
104. Ishizawa T, Mattila P, Davies P, Wang D, Dickson DW. Colocalization of tau and alpha-synuclein epitopes in Lewy bodies. J Neuropathol Exp Neurol. 2003 Apr;62(4):389-97.

105. Lubbe S, Morris HR. Recent advances in Parkinson's disease genetics. J Neurol. 2013 Jun.
106. Tanner CM, Kamel F, Ross GW, et al. Rotenone, paraquat, and Parkinson's disease. Environ Health Perspect. 2011 Jun;119(6):866-72.
107. Tanner CM, Ross GW, Jewell SA, et al. Occupation and risk of parkinsonism: a multicenter case-control study. Arch Neurol. 2009 Sep;66(9):1106-13.
108. Dick FD, De Palma G, Ahmadi A, et al. Environmental risk factors for Parkinson's disease and parkinsonism: the Geoparkinson study. Occup Environ Med. 2007 Oct;64(10):666-72.
109. Jiménez-Jiménez FJ, Mateo D, Giménez-Roldán S. Exposure to well water and pesticides in Parkinson's disease: a case-control study in the Madrid area. Mov Disord. 1992;7(2):149-52.
110. Firestone JA, Smith-Weller T, Franklin G, Swanson P, Longstreth WT, Checkoway H. Pesticides and risk of Parkinson disease: a population-based case-control study. Arch Neurol. 2005 Jan;62(1):91-5.
111. Betarbet R, Sherer TB, MacKenzie G, Garcia-Osuna M, Panov AV, Greenamyre JT. Chronic systemic pesticide exposure reproduces features of Parkinson's disease. Nat Neurosci. 2000 Dec;3(12):1301-6.
112. McCormack AL, Thiruchelvam M, Manning-Bog AB, et al. Environmental risk factors and Parkinson's disease: selective degeneration of nigral dopaminergic neurons caused by the herbicide paraquat. Neurobiol Dis. 2002 Jul;10(2):119-27.
113. Goldman SM, Tanner CM, Olanow CW, Watts RL, Field RD, Langston JW. Occupation and parkinsonism in three movement disorders clinics. Neurology. 2005 Nov;65(9):1430-5.
114. De Michele G, Filla A, Volpe G, et al. Environmental and genetic risk factors in Parkinson's disease: a case-control study in southern Italy. Mov Disord. 1996 Jan;11(1):17-23.
115. Hernán MA, Takkouche B, Caamaño-Isorna F, Gestal-Otero JJ. A meta-analysis of coffee drinking, cigarette smoking, and the risk of Parkinson's disease. Ann Neurol. 2002 Sep;52(3):276-84.
116. Langston JW, Ballard P, Tetrud JW, Irwin I. Chronic Parkinsonism in humans due to a product of meperidine-analog synthesis. Science. 1983 Feb;219(4587):979-80.
117. Javitch JA, D'Amato RJ, Strittmatter SM, Snyder SH. Parkinsonism-inducing neurotoxin, N-methyl-4-phenyl-1,2,3,6 -tetrahydropyridine: uptake of the metabolite N-methyl-4-phenylpyridine by dopamine neurons explains selective toxicity. Proc Natl Acad Sci U S A. 1985 Apr;82(7):2173-7.
118. Schapira AH, Cooper JM, Dexter D, Clark JB, Jenner P, Marsden CD. Mitochondrial complex I deficiency in Parkinson's disease. J Neurochem. 1990 Mar;54(3):823-7.
119. Mizuno Y, Sone N, Saitoh T. Effects of 1-methyl-4-phenyl-1,2,3,6-tetrahydropyridine and 1-methyl-4-phenylpyridinium ion on activities of the enzymes in the electron transport system in mouse brain. J Neurochem. 1987 Jun;48(6):1787-93.
120. Sallinen V, Torkko V, Sundvik M, et al. MPTP and MPP+ target specific aminergic cell populations in larval zebrafish. J Neurochem. 2009 Feb;108(3):719-31.
121. Doudet D, Gross C, Lebrun-Grandie P, Bioulac B. MPTP primate model of Parkinson's disease: a mechanographic and electromyographic study. Brain Res. 1985 May;335(1):194-9.
122. Willis GL, Donnan GA. Histochemical, biochemical and behavioural consequences of MPTP treatment in C-57 black mice. Brain Res. 1987 Feb;402(2):269-74.
123. Przedborski S, Levivier M, Jiang H, et al. Dose-dependent lesions of the dopaminergic nigrostriatal pathway induced by intrastriatal injection of 6-hydroxydopamine. Neuroscience. 1995 Aug;67(3):631-47.

124. Cleeter MW, Cooper JM, Schapira AH. Irreversible inhibition of mitochondrial complex I by 1-methyl-4-phenylpyridinium: evidence for free radical involvement. J Neurochem. 1992 Feb;58(2):786-9.
125. Beal MF. Experimental models of Parkinson's disease. Nat Rev Neurosci. 2001 May;2(5):325-34.
126. Jackson-Lewis V, Blesa J, Przedborski S. Animal models of Parkinson's disease. Parkinsonism Relat Disord. 2012 Jan;18 Suppl 1:S183-5.
127. Zu Y, Tong X, Wang Z, et al. TALEN-mediated precise genome modification by homologous recombination in zebrafish. Nat Methods. 2013 Apr;10(4):329-31.
128. Enquist IB, Lo Bianco C, Ooka A, et al. Murine models of acute neuronopathic Gaucher disease. Proc Natl Acad Sci U S A. 2007 Oct;104(44):17483-8.
129. Kitada T, Tong Y, Gautier CA, Shen J. Absence of nigral degeneration in aged parkin/DJ-1/PINK1 triple knockout mice. J Neurochem. 2009 Nov;111(3):696-702.
130. Greene JC, Whitworth AJ, Kuo I, Andrews LA, Feany MB, Pallanck LJ. Mitochondrial pathology and apoptotic muscle degeneration in Drosophila parkin mutants. Proc Natl Acad Sci U S A. 2003 Apr;100(7):4078-83.
131. Itier JM, Ibanez P, Mena MA, et al. Parkin gene inactivation alters behaviour and dopamine neurotransmission in the mouse. Hum Mol Genet. 2003 Sep;12(18):2277-91.
132. Palacino JJ, Sagi D, Goldberg MS, et al. Mitochondrial dysfunction and oxidative damage in parkin-deficient mice. J Biol Chem. 2004 Apr;279(18):18614-22.
133. Perez FA, Palmiter RD. Parkin-deficient mice are not a robust model of parkinsonism. Proc Natl Acad Sci U S A. 2005 Feb;102(6):2174-9.
134. Meulener M, Whitworth AJ, Armstrong-Gold CE, et al. Drosophila DJ-1 mutants are selectively sensitive to environmental toxins associated with Parkinson's disease. Curr Biol. 2005 Sep;15(17):1572-7.
135. Kim RH, Smith PD, Aleyasin H, et al. Hypersensitivity of DJ-1-deficient mice to 1-methyl-4-phenyl-1,2,3,6-tetrahydropyrindine (MPTP) and oxidative stress. Proc Natl Acad Sci U S A. 2005 Apr;102(14):5215-20.
136. Yamaguchi H, Shen J. Absence of dopaminergic neuronal degeneration and oxidative damage in aged DJ-1-deficient mice. Mol Neurodegener. 2007;2:10.
137. Lee SB, Kim W, Lee S, Chung J. Loss of LRRK2/PARK8 induces degeneration of dopaminergic neurons in Drosophila. Biochem Biophys Res Commun. 2007 Jun;358(2):534-9.
138. Wang D, Tang B, Zhao G, et al. Dispensable role of Drosophila ortholog of LRRK2 kinase activity in survival of dopaminergic neurons. Mol Neurodegener. 2008;3:3.
139. Tong Y, Yamaguchi H, Giaime E, et al. Loss of leucine-rich repeat kinase 2 causes impairment of protein degradation pathways, accumulation of alpha-synuclein, and apoptotic cell death in aged mice. Proc Natl Acad Sci U S A. 2010 May;107(21):9879-84.
140. Liu Z, Wang X, Yu Y, et al. A Drosophila model for LRRK2-linked parkinsonism. Proc Natl Acad Sci U S A. 2008 Feb;105(7):2693-8.
141. Ramonet D, Daher JP, Lin BM, et al. Dopaminergic neuronal loss, reduced neurite complexity and autophagic abnormalities in transgenic mice expressing G2019S mutant LRRK2. PLoS One. 2011;6(4):e18568.
142. Tong Y, Pisani A, Martella G, et al. R1441C mutation in LRRK2 impairs dopaminergic neurotransmission in mice. Proc Natl Acad Sci U S A. 2009 Aug;106(34):14622-7.
143. Howe K, Clark MD, Torroja CF, et al. The zebrafish reference genome sequence and its relationship to the human genome. Nature. 2013 Apr;496(7446):498-503.

144. Lieschke GJ, Currie PD. Animal models of human disease: zebrafish swim into view. Nat Rev Genet. 2007 May;8(5):353-67.
145. Barbazuk WB, Korf I, Kadavi C, et al. The syntenic relationship of the zebrafish and human genomes. Genome Res. 2000 Sep;10(9):1351-8.
146. Peterson RT, Link BA, Dowling JE, Schreiber SL. Small molecule developmental screens reveal the logic and timing of vertebrate development. Proc Natl Acad Sci U S A. 2000 Nov;97(24):12965-9.
147. Peterson RT, Shaw SY, Peterson TA, et al. Chemical suppression of a genetic mutation in a zebrafish model of aortic coarctation. Nat Biotechnol. 2004 May;22(5):595-9.
148. Yu PB, Deng DY, Lai CS, et al. BMP type I receptor inhibition reduces heterotopic [corrected] ossification. Nat Med. 2008 Dec;14(12):1363-9.
149. Yu PB, Hong CC, Sachidanandan C, et al. Dorsomorphin inhibits BMP signals required for embryogenesis and iron metabolism. Nat Chem Biol. 2008 Jan;4(1):33-41.
150. Bowman TV, Zon LI. Swimming into the future of drug discovery: in vivo chemical screens in zebrafish. ACS Chem Biol. 2010 Feb;5(2):159-61.
151. Haffter P, Granato M, Brand M, et al. The identification of genes with unique and essential functions in the development of the zebrafish, Danio rerio. Development. 1996 Dec;123:1-36.
152. Nasevicius A, Ekker SC. Effective targeted gene 'knockdown' in zebrafish. Nat Genet. 2000 Oct;26(2):216-20.
153. Kettleborough RN, Busch-Nentwich EM, Harvey SA, et al. A systematic genome-wide analysis of zebrafish protein-coding gene function. Nature. 2013 Apr;496(7446):494-7.
154. Bill BR, Petzold AM, Clark KJ, Schimmenti LA, Ekker SC. A primer for morpholino use in zebrafish. Zebrafish. 2009 Mar;6(1):69-77.
155. Draper BW, Morcos PA, Kimmel CB. Inhibition of zebrafish fgf8 pre-mRNA splicing with morpholino oligos: a quantifiable method for gene knockdown. Genesis. 2001 Jul;30(3):154-6.
156. Robu ME, Larson JD, Nasevicius A, et al. p53 activation by knockdown technologies. PLoS Genet. 2007 May;3(5):e78.
157. Meng X, Noyes MB, Zhu LJ, Lawson ND, Wolfe SA. Targeted gene inactivation in zebrafish using engineered zinc-finger nucleases. Nat Biotechnol. 2008 Jun;26(6):695-701.
158. Sander JD, Dahlborg EJ, Goodwin MJ, et al. Selection-free zinc-finger-nuclease engineering by context-dependent assembly (CoDA). Nat Methods. 2011 Jan;8(1):67-9.
159. Cermak T, Doyle EL, Christian M, et al. Efficient design and assembly of custom TALEN and other TAL effector-based constructs for DNA targeting. Nucleic Acids Res. 2011 Jul;39(12):e82.
160. Cho SW, Kim S, Kim JM, Kim JS. Targeted genome engineering in human cells with the Cas9 RNA-guided endonuclease. Nat Biotechnol. 2013 Mar;31(3):230-2.
161. Chang N, Sun C, Gao L, et al. Genome editing with RNA-guided Cas9 nuclease in zebrafish embryos. Cell Res. 2013 Apr;23(4):465-72.
162. Fu Y, Foden JA, Khayter C, et al. High-frequency off-target mutagenesis induced by CRISPR-Cas nucleases in human cells. Nat Biotechnol. 2013 Sep;31(9):822-6.
163. Ran FA, Hsu PD, Wright J, Agarwala V, Scott DA, Zhang F. Genome engineering using the CRISPR-Cas9 system. Nat Protoc. 2013 Nov;8(11):2281-308.
164. Rink E, Wullimann MF. Connections of the ventral telencephalon and tyrosine hydroxylase distribution in the zebrafish brain (Danio rerio) lead to identification of an ascending dopaminergic system in a teleost. Brain Res Bull. 2002 2002 Feb-Mar 1;57(3-4):385-7.

165. Rink E, Wullimann MF. Development of the catecholaminergic system in the early zebrafish brain: an immunohistochemical study. Brain Res Dev Brain Res. 2002 Jul;137(1):89-100.
166. Bretaud S, Lee S, Guo S. Sensitivity of zebrafish to environmental toxins implicated in Parkinson's disease. Neurotoxicol Teratol. 2004 2004 Nov-Dec;26(6):857-64.
167. Xi Y, Yu M, Godoy R, Hatch G, Poitras L, Ekker M. Transgenic zebrafish expressing green fluorescent protein in dopaminergic neurons of the ventral diencephalon. Dev Dyn. 2011 Nov;240(11):2539-47.
168. Flinn L, Mortiboys H, Volkmann K, Köster RW, Ingham PW, Bandmann O. Complex I deficiency and dopaminergic neuronal cell loss in parkin-deficient zebrafish (Danio rerio). Brain. 2009 Jun;132(Pt 6):1613-23.
169. Fett ME, Pilsl A, Paquet D, et al. Parkin is protective against proteotoxic stress in a transgenic zebrafish model. PLoS One. 2010;5(7):e11783.
170. Bretaud S, Allen C, Ingham PW, Bandmann O. p53-dependent neuronal cell death in a DJ-1-deficient zebrafish model of Parkinson's disease. J Neurochem. 2007 Mar;100(6):1626-35.
171. Sheng D, Qu D, Kwok KH, et al. Deletion of the WD40 domain of LRRK2 in Zebrafish causes Parkinsonism-like loss of neurons and locomotive defect. PLoS Genet. 2010 Apr;6(4):e1000914.
172. Ren G, Xin S, Li S, Zhong H, Lin S. Disruption of LRRK2 does not cause specific loss of dopaminergic neurons in zebrafish. PLoS One. 2011;6(6):e20630.
173. Anichtchik O, Diekmann H, Fleming A, Roach A, Goldsmith P, Rubinsztein DC. Loss of PINK1 function affects development and results in neurodegeneration in zebrafish. J Neurosci. 2008 Aug;28(33):8199-207.
174. Xi Y, Ryan J, Noble S, Yu M, Yilbas AE, Ekker M. Impaired dopaminergic neuron development and locomotor function in zebrafish with loss of pink1 function. Eur J Neurosci. 2010 Feb;31(4):623-33.
175. Sallinen V, Kolehmainen J, Priyadarshini M, Toleikyte G, Chen YC, Panula P. Dopaminergic cell damage and vulnerability to MPTP in Pink1 knockdown zebrafish. Neurobiol Dis. 2010 Oct;40(1):93-101.
176. Clark IE, Dodson MW, Jiang C, et al. Drosophila pink1 is required for mitochondrial function and interacts genetically with parkin. Nature. 2006 Jun;441(7097):1162-6.
177. Duyao MP, Auerbach AB, Ryan A, et al. Inactivation of the mouse Huntington's disease gene homolog Hdh. Science. 1995 Jul;269(5222):407-10.
178. Lumsden AL, Henshall TL, Dayan S, Lardelli MT, Richards RI. Huntingtin-deficient zebrafish exhibit defects in iron utilization and development. Hum Mol Genet. 2007 Aug;16(16):1905-20.
179. Zeitlin S, Liu JP, Chapman DL, Papaioannou VE, Efstratiadis A. Increased apoptosis and early embryonic lethality in mice nullizygous for the Huntington's disease gene homologue. Nat Genet. 1995 Oct;11(2):155-63.
180. Diekmann H, Anichtchik O, Fleming A, et al. Decreased BDNF levels are a major contributor to the embryonic phenotype of huntingtin knockdown zebrafish. J Neurosci. 2009 Feb;29(5):1343-9.
181. Schiffer NW, Broadley SA, Hirschberger T, et al. Identification of anti-prion compounds as efficient inhibitors of polyglutamine protein aggregation in a zebrafish model. J Biol Chem. 2007 Mar;282(12):9195-203.
182. Da Costa MM, Allen CE, Higginbottom A, Ramesh T, Shaw PJ, McDermott CJ. A new zebrafish model produced by TILLING of SOD1-related amyotrophic lateral sclerosis replicates key features of the disease and represents a tool for in vivo therapeutic screening. Dis Model Mech. 2014 Jan;7(1):73-81.

183. Cachat J, Stewart A, Grossman L, et al. Measuring behavioral and endocrine responses to novelty stress in adult zebrafish. Nat Protoc. 2010 Nov;5(11):1786-99.
184. McGown A, McDearmid JR, Panagiotaki N, et al. Early interneuron dysfunction in ALS: insights from a mutant sod1 zebrafish model. Ann Neurol. 2013 Feb;73(2):246-58.
185. Ramesh T, Lyon AN, Pineda RH, et al. A genetic model of amyotrophic lateral sclerosis in zebrafish displays phenotypic hallmarks of motoneuron disease. Dis Model Mech. 2010 2010 Sep-Oct;3(9-10):652-62.
186. Ansai S, Sakuma T, Yamamoto T, et al. Efficient targeted mutagenesis in medaka using custom-designed transcription activator-like effector nucleases. Genetics. 2013 Mar;193(3):739-49.
187. Matsui H, Taniguchi Y, Inoue H, Uemura K, Takeda S, Takahashi R. A chemical neurotoxin, MPTP induces Parkinson's disease like phenotype, movement disorders and persistent loss of dopamine neurons in medaka fish. Neurosci Res. 2009 Nov;65(3):263-71.
188. Matsui H, Taniguchi Y, Inoue H, et al. Loss of PINK1 in medaka fish (Oryzias latipes) causes late-onset decrease in spontaneous movement. Neurosci Res. 2010 Feb;66(2):151-61.
189. Matsui H, Ito H, Taniguchi Y, Inoue H, Takeda S, Takahashi R. Proteasome inhibition in medaka brain induces the features of Parkinson's disease. J Neurochem. 2010 Oct;115(1):178-87.
190. Matsui H, Gavinio R, Asano T, et al. PINK1 and Parkin complementarily protect dopaminergic neurons in vertebrates. Hum Mol Genet. 2013 Jun;22(12):2423-34.
191. Hatano Y, Li Y, Sato K, et al. Novel PINK1 mutations in early-onset parkinsonism. Ann Neurol. 2004 Sep;56(3):424-7.
192. Abou-Sleiman PM, Muqit MM, McDonald NQ, et al. A heterozygous effect for PINK1 mutations in Parkinson's disease? Ann Neurol. 2006 Oct;60(4):414-9.
193. Tan EK, Yew K, Chua E, et al. PINK1 mutations in sporadic early-onset Parkinson's disease. Mov Disord. 2006 Jun;21(6):789-93.
194. Brooks J, Ding J, Simon-Sanchez J, Paisan-Ruiz C, Singleton AB, Scholz SW. Parkin and PINK1 mutations in early-onset Parkinson's disease: comprehensive screening in publicly available cases and control. J Med Genet. 2009 Jun;46(6):375-81.
195. Blackinton JG, Anvret A, Beilina A, Olson L, Cookson MR, Galter D. Expression of PINK1 mRNA in human and rodent brain and in Parkinson's disease. Brain Res. 2007 Dec;1184:10-6.
196. Matsuda S, Kitagishi Y, Kobayashi M. Function and characteristics of PINK1 in mitochondria. Oxid Med Cell Longev. 2013;2013:601587.
197. Corti O, Brice A. Mitochondrial quality control turns out to be the principal suspect in parkin and PINK1-related autosomal recessive Parkinson's disease. Curr Opin Neurobiol. 2013 Feb;23(1):100-8.
198. Deng H, Dodson MW, Huang H, Guo M. The Parkinson's disease genes pink1 and parkin promote mitochondrial fission and/or inhibit fusion in Drosophila. Proc Natl Acad Sci U S A. 2008 Sep;105(38):14503-8.
199. Gispert S, Ricciardi F, Kurz A, et al. Parkinson phenotype in aged PINK1-deficient mice is accompanied by progressive mitochondrial dysfunction in absence of neurodegeneration. PLoS One. 2009;4(6):e5777.
200. Hoepken HH, Gispert S, Morales B, et al. Mitochondrial dysfunction, peroxidation damage and changes in glutathione metabolism in PARK6. Neurobiol Dis. 2007 Feb;25(2):401-11.
201. Flinn LJ, Keatinge M, Bretaud S, et al. TigarB causes mitochondrial dysfunction and neuronal loss in PINK1 deficiency. Ann Neurol. 2013 Dec;74(6):837-47.

202. Lin W, Kang UJ. Characterization of PINK1 processing, stability, and subcellular localization. J Neurochem. 2008 Jul;106(1):464-74.
203. Fedorowicz MA, de Vries-Schneider RL, Rüb C, et al. Cytosolic cleaved PINK1 represses Parkin translocation to mitochondria and mitophagy. EMBO Rep. 2014 Jan;15(1):86-93.
204. Deas E, Plun-Favreau H, Gandhi S, et al. PINK1 cleavage at position A103 by the mitochondrial protease PARL. Hum Mol Genet. 2011 Mar;20(5):867-79.
205. Narendra DP, Jin SM, Tanaka A, et al. PINK1 is selectively stabilized on impaired mitochondria to activate Parkin. PLoS Biol. 2010 Jan;8(1):e1000298.
206. Narendra D, Tanaka A, Suen DF, Youle RJ. Parkin is recruited selectively to impaired mitochondria and promotes their autophagy. J Cell Biol. 2008 Dec;183(5):795-803.
207. Narendra D, Kane LA, Hauser DN, Fearnley IM, Youle RJ. p62/SQSTM1 is required for Parkin-induced mitochondrial clustering but not mitophagy; VDAC1 is dispensable for both. Autophagy. 2010 Nov;6(8):1090-106.
208. Gegg ME, Cooper JM, Chau KY, Rojo M, Schapira AH, Taanman JW. Mitofusin 1 and mitofusin 2 are ubiquitinated in a PINK1/parkin-dependent manner upon induction of mitophagy. Hum Mol Genet. 2010 Dec;19(24):4861-70.
209. Lee JY, Nagano Y, Taylor JP, Lim KL, Yao TP. Disease-causing mutations in parkin impair mitochondrial ubiquitination, aggregation, and HDAC6-dependent mitophagy. J Cell Biol. 2010 May;189(4):671-9.
210. Pridgeon JW, Olzmann JA, Chin LS, Li L. PINK1 protects against oxidative stress by phosphorylating mitochondrial chaperone TRAP1. PLoS Biol. 2007 Jul;5(7):e172.
211. Zhang L, Karsten P, Hamm S, et al. TRAP1 rescues PINK1 loss-of-function phenotypes. Hum Mol Genet. 2013 Jul;22(14):2829-41.
212. Yu W, Sun Y, Guo S, Lu B. The PINK1/Parkin pathway regulates mitochondrial dynamics and function in mammalian hippocampal and dopaminergic neurons. Hum Mol Genet. 2011 Aug;20(16):3227-40.
213. Poole AC, Thomas RE, Andrews LA, McBride HM, Whitworth AJ, Pallanck LJ. The PINK1/Parkin pathway regulates mitochondrial morphology. Proc Natl Acad Sci U S A. 2008 Feb;105(5):1638-43.
214. Dagda RK, Cherra SJ, Kulich SM, Tandon A, Park D, Chu CT. Loss of PINK1 function promotes mitophagy through effects on oxidative stress and mitochondrial fission. J Biol Chem. 2009 May;284(20):13843-55.
215. Exner N, Treske B, Paquet D, et al. Loss-of-function of human PINK1 results in mitochondrial pathology and can be rescued by parkin. J Neurosci. 2007 Nov;27(45):12413-8.
216. Poole AC, Thomas RE, Yu S, Vincow ES, Pallanck L. The mitochondrial fusion-promoting factor mitofusin is a substrate of the PINK1/parkin pathway. PLoS One. 2010;5(4):e10054.
217. Mai S, Klinkenberg M, Auburger G, Bereiter-Hahn J, Jendrach M. Decreased expression of Drp1 and Fis1 mediates mitochondrial elongation in senescent cells and enhances resistance to oxidative stress through PINK1. J Cell Sci. 2010 Mar;123(Pt 6):917-26.
218. McLelland GL, Soubannier V, Chen CX, McBride HM, Fon EA. Parkin and PINK1 function in a vesicular trafficking pathway regulating mitochondrial quality control. EMBO J. 2014 Feb;33(4):282-95.
219. Shlevkov E, Schwarz TL. For Parkin, it's not all or nothing. EMBO J. 2014 Feb;33(4):277-9.

220. Billia F, Hauck L, Konecny F, Rao V, Shen J, Mak TW. PTEN-inducible kinase 1 (PINK1)/Park6 is indispensable for normal heart function. Proc Natl Acad Sci U S A. 2011 Jun;108(23):9572-7.
221. Siddall HK, Yellon DM, Ong SB, et al. Loss of PINK1 increases the heart's vulnerability to ischemia-reperfusion injury. PLoS One. 2013;8(4):e62400.
222. Park J, Lee SB, Lee S, et al. Mitochondrial dysfunction in Drosophila PINK1 mutants is complemented by parkin. Nature. 2006 Jun;441(7097):1157-61.
223. Yang Y, Gehrke S, Imai Y, et al. Mitochondrial pathology and muscle and dopaminergic neuron degeneration caused by inactivation of Drosophila Pink1 is rescued by Parkin. Proc Natl Acad Sci U S A. 2006 Jul;103(28):10793-8.
224. Kitada T, Pisani A, Porter DR, et al. Impaired dopamine release and synaptic plasticity in the striatum of PINK1-deficient mice. Proc Natl Acad Sci U S A. 2007 Jul;104(27):11441-6.
225. Vousden KH, Prives C. Blinded by the Light: The Growing Complexity of p53. Cell. 2009 May;137(3):413-31.
226. Muller PA, Vousden KH. p53 mutations in cancer. Nat Cell Biol. 2013 Jan;15(1):2-8.
227. Jen KY, Cheung VG. Identification of novel p53 target genes in ionizing radiation response. Cancer Res. 2005 Sep;65(17):7666-73.
228. Bensaad K, Tsuruta A, Selak MA, et al. TIGAR, a p53-inducible regulator of glycolysis and apoptosis. Cell. 2006 Jul;126(1):107-20.
229. Okar DA, Manzano A, Navarro-Sabatè A, Riera L, Bartrons R, Lange AJ. PFK-2/FBPase-2: maker and breaker of the essential biofactor fructose-2,6-bisphosphate. Trends Biochem Sci. 2001 Jan;26(1):30-5.
230. Lee P, Vousden KH, Cheung EC. TIGAR, TIGAR, burning bright. Cancer Metab. 2014;2(1):1.
231. Gerin I, Noël G, Bolsée J, Haumont O, Van Schaftingen E, Bommer GT. Identification of TP53-induced glycolysis and apoptosis regulator (TIGAR) as the phosphoglycolate-independent 2,3-bisphosphoglycerate phosphatase. Biochem J. 2014 Mar;458(3):439-48.
232. Bensaad K, Cheung EC, Vousden KH. Modulation of intracellular ROS levels by TIGAR controls autophagy. EMBO J. 2009 Oct;28(19):3015-26.
233. Scherz-Shouval R, Shvets E, Fass E, Shorer H, Gil L, Elazar Z. Reactive oxygen species are essential for autophagy and specifically regulate the activity of Atg4. EMBO J. 2007 Apr;26(7):1749-60.
234. Cheung EC, Ludwig RL, Vousden KH. Mitochondrial localization of TIGAR under hypoxia stimulates HK2 and lowers ROS and cell death. Proc Natl Acad Sci U S A. 2012 Dec;109(50):20491-6.
235. Sun L, Shukair S, Naik TJ, Moazed F, Ardehali H. Glucose phosphorylation and mitochondrial binding are required for the protective effects of hexokinases I and II. Mol Cell Biol. 2008 Feb;28(3):1007-17.
236. Kimata M, Matoba S, Iwai-Kanai E, et al. p53 and TIGAR regulate cardiac myocyte energy homeostasis under hypoxic stress. Am J Physiol Heart Circ Physiol. 2010 Dec;299(6):H1908-16.
237. Cheung EC, Athineos D, Lee P, et al. TIGAR is required for efficient intestinal regeneration and tumorigenesis. Dev Cell. 2013 Jun;25(5):463-77.
238. Hoshino A, Matoba S, Iwai-Kanai E, et al. p53-TIGAR axis attenuates mitophagy to exacerbate cardiac damage after ischemia. J Mol Cell Cardiol. 2012 Jan;52(1):175-84.
239. Maher ER, Neumann HP, Richard S. von Hippel-Lindau disease: a clinical and scientific review. Eur J Hum Genet. 2011 Jun;19(6):617-23.

240. Franke G, Bausch B, Hoffmann MM, et al. Alu-Alu recombination underlies the vast majority of large VHL germline deletions: Molecular characterization and genotype-phenotype correlations in VHL patients. Hum Mutat. 2009 May;30(5):776-86.
241. Maxwell PH, Wiesener MS, Chang GW, et al. The tumour suppressor protein VHL targets hypoxia-inducible factors for oxygen-dependent proteolysis. Nature. 1999 May;399(6733):271-5.
242. van Rooijen E, Voest EE, Logister I, et al. Zebrafish mutants in the von Hippel-Lindau tumor suppressor display a hypoxic response and recapitulate key aspects of Chuvash polycythemia. Blood. 2009 Jun;113(25):6449-60.
243. van Rooijen E, Voest EE, Logister I, et al. von Hippel-Lindau tumor suppressor mutants faithfully model pathological hypoxia-driven angiogenesis and vascular retinopathies in zebrafish. Dis Model Mech. 2010 2010 May-Jun;3(5-6):343-53.
244. Hruska KS, LaMarca ME, Scott CR, Sidransky E. Gaucher disease: mutation and polymorphism spectrum in the glucocerebrosidase gene (GBA). Hum Mutat. 2008 May;29(5):567-83.
245. Svobodová E, Mrázová L, Lukšan O, et al. Glucocerebrosidase gene has an alternative upstream promoter, which has features and expression characteristic of housekeeping genes. Blood Cells Mol Dis. 2011 Mar;46(3):239-45.
246. Tayebi N, Stubblefield BK, Park JK, et al. Reciprocal and nonreciprocal recombination at the glucocerebrosidase gene region: implications for complexity in Gaucher disease. Am J Hum Genet. 2003 Mar;72(3):519-34.
247. Mehta A. Epidemiology and natural history of Gaucher's disease. Eur J Intern Med. 2006 Nov;17 Suppl:S2-5.
248. Chérin P, Rose C, de Roux-Serratrice C, et al. The neurological manifestations of Gaucher disease type 1: the French Observatoire on Gaucher disease (FROG). J Inherit Metab Dis. 2010 Aug;33(4):331-8.
249. Landgren O, Turesson I, Gridley G, Caporaso NE. Risk of malignant disease among 1525 adult male US Veterans with Gaucher disease. Arch Intern Med. 2007 Jun;167(11):1189-94.
250. Mignot C, Doummar D, Maire I, De Villemeur TB, Group FTGDS. Type 2 Gaucher disease: 15 new cases and review of the literature. Brain Dev. 2006 Jan;28(1):39-48.
251. Grabowski GA. Phenotype, diagnosis, and treatment of Gaucher's disease. Lancet. 2008 Oct;372(9645):1263-71.
252. Goker-Alpan O, Schiffmann R, Park JK, Stubblefield BK, Tayebi N, Sidransky E. Phenotypic continuum in neuronopathic Gaucher disease: an intermediate phenotype between type 2 and type 3. J Pediatr. 2003 Aug;143(2):273-6.
253. Neudorfer O, Giladi N, Elstein D, et al. Occurrence of Parkinson's syndrome in type I Gaucher disease. QJM. 1996 Sep;89(9):691-4.
254. Erikson A. Remaining problems in the management of patients with Gaucher disease. J Inherit Metab Dis. 2001;24 Suppl 2:122-6; discussion 87-8.
255. Brady RO, Pentchev PG, Gal AE, Hibbert SR, Dekaban AS. Replacement therapy for inherited enzyme deficiency. Use of purified glucocerebrosidase in Gaucher's disease. N Engl J Med. 1974 Nov;291(19):989-93.
256. Kitatani K, Idkowiak-Baldys J, Hannun YA. The sphingolipid salvage pathway in ceramide metabolism and signaling. Cell Signal. 2008 Jun;20(6):1010-8.
257. Jmoudiak M, Futerman AH. Gaucher disease: pathological mechanisms and modern management. Br J Haematol. 2005 Apr;129(2):178-88.
258. Hollak CE, van Weely S, van Oers MH, Aerts JM. Marked elevation of plasma chitotriosidase activity. A novel hallmark of Gaucher disease. J Clin Invest. 1994 Mar;93(3):1288-92.

259. de Fost M, Hollak CE, Groener JE, et al. Superior effects of high-dose enzyme replacement therapy in type 1 Gaucher disease on bone marrow involvement and chitotriosidase levels: a 2-center retrospective analysis. Blood. 2006 Aug;108(3):830-5.
260. Maor G, Filocamo M, Horowitz M. ITCH regulates degradation of mutant glucocerebrosidase: implications to Gaucher disease. Hum Mol Genet. 2013 Apr;22(7):1316-27.
261. Tybulewicz VL, Tremblay ML, LaMarca ME, et al. Animal model of Gaucher's disease from targeted disruption of the mouse glucocerebrosidase gene. Nature. 1992 Jun;357(6377):407-10.
262. Liu Y, Suzuki K, Reed JD, et al. Mice with type 2 and 3 Gaucher disease point mutations generated by a single insertion mutagenesis procedure. Proc Natl Acad Sci U S A. 1998 Mar;95(5):2503-8.
263. Xu YH, Quinn B, Witte D, Grabowski GA. Viable mouse models of acid beta-glucosidase deficiency: the defect in Gaucher disease. Am J Pathol. 2003 Nov;163(5):2093-101.
264. Mistry PK, Liu J, Yang M, et al. Glucocerebrosidase gene-deficient mouse recapitulates Gaucher disease displaying cellular and molecular dysregulation beyond the macrophage. Proc Natl Acad Sci U S A. 2010 Nov;107(45):19473-8.
265. Nalls MA, Duran R, Lopez G, et al. A multicenter study of glucocerebrosidase mutations in dementia with Lewy bodies. JAMA Neurol. 2013 Jun;70(6):727-35.
266. Aharon-Peretz J, Rosenbaum H, Gershoni-Baruch R. Mutations in the glucocerebrosidase gene and Parkinson's disease in Ashkenazi Jews. N Engl J Med. 2004 Nov;351(19):1972-7.
267. Anheim M, Elbaz A, Lesage S, et al. Penetrance of Parkinson disease in glucocerebrosidase gene mutation carriers. Neurology. 2012 Feb;78(6):417-20.
268. Gegg ME, Burke D, Heales SJ, et al. Glucocerebrosidase deficiency in substantia nigra of parkinson disease brains. Ann Neurol. 2012 Sep;72(3):455-63.
269. Siebert M, Sidransky E, Westbroek W. Glucocerebrosidase is shaking up the synucleinopathies. Brain. 2014 Feb.
270. Mignot C, Gelot A, Bessières B, et al. Perinatal-lethal Gaucher disease. Am J Med Genet A. 2003 Jul;120A(3):338-44.
271. Strasberg PM, Skomorowski MA, Warren IB, Hilson WL, Callahan JW, Clarke JT. Homozygous presence of the crossover (fusion gene) mutation identified in a type II Gaucher disease fetus: is this analogous to the Gaucher knock-out mouse model? Biochem Med Metab Biol. 1994 Oct;53(1):16-21.
272. Cleeter MW, Chau KY, Gluck C, et al. Glucocerebrosidase inhibition causes mitochondrial dysfunction and free radical damage. Neurochem Int. 2013 Jan;62(1):1-7.
273. Manning-Boğ AB, Schüle B, Langston JW. Alpha-synuclein-glucocerebrosidase interactions in pharmacological Gaucher models: a biological link between Gaucher disease and parkinsonism. Neurotoxicology. 2009 Nov;30(6):1127-32.
274. Mazzulli JR, Xu YH, Sun Y, et al. Gaucher disease glucocerebrosidase and α-synuclein form a bidirectional pathogenic loop in synucleinopathies. Cell. 2011 Jul;146(1):37-52.
275. Dermentzaki G, Dimitriou E, Xilouri M, Michelakakis H, Stefanis L. Loss of β-glucocerebrosidase activity does not affect alpha-synuclein levels or lysosomal function in neuronal cells. PLoS One. 2013;8(4):e60674.
276. Cullen V, Sardi SP, Ng J, et al. Acid β-glucosidase mutants linked to Gaucher disease, Parkinson disease, and Lewy body dementia alter α-synuclein processing. Ann Neurol. 2011 Jun;69(6):940-53.
277. Suzuki T, Shimoda M, Ito K, et al. Expression of human Gaucher disease gene GBA generates neurodevelopmental defects and ER stress in Drosophila eye. PLoS One. 2013;8(8):e69147.

278. Sardi SP, Clarke J, Kinnecom C, et al. CNS expression of glucocerebrosidase corrects alpha-synuclein pathology and memory in a mouse model of Gaucher-related synucleinopathy. Proc Natl Acad Sci U S A. 2011 Jul;108(29):12101-6.
279. Kaufman RJ. Orchestrating the unfolded protein response in health and disease. J Clin Invest. 2002 Nov;110(10):1389-98.
280. Ron I, Rapaport D, Horowitz M. Interaction between parkin and mutant glucocerebrosidase variants: a possible link between Parkinson disease and Gaucher disease. Hum Mol Genet. 2010 Oct;19(19):3771-81.
281. McNeill A, Healy DG, Schapira AH, Taanman JW. Glucosylceramidase degradation in fibroblasts carrying bi-allelic Parkin mutations. Mol Genet Metab. 2013 Aug;109(4):402-3.
282. Lee YJ, Kim SJ, Heo TH. Protective effect of catechin in type I Gaucher disease cells by reducing endoplasmic reticulum stress. Biochem Biophys Res Commun. 2011 Sep;413(2):254-8.
283. Farfel-Becker T, Vitner E, Dekel H, et al. No evidence for activation of the unfolded protein response in neuronopathic models of Gaucher disease. Hum Mol Genet. 2009 Apr;18(8):1482-8.
284. Mortiboys H, Thomas KJ, Koopman WJ, et al. Mitochondrial function and morphology are impaired in parkin-mutant fibroblasts. Ann Neurol. 2008 Nov;64(5):555-65.
285. Osellame LD, Rahim AA, Hargreaves IP, et al. Mitochondria and quality control defects in a mouse model of Gaucher disease--links to Parkinson's disease. Cell Metab. 2013 Jun;17(6):941-53.
286. Svahn AJ, Graeber MB, Ellett F, et al. Development of ramified microglia from early macrophages in the zebrafish optic tectum. Dev Neurobiol. 2013 Jan;73(1):60-71.
287. Bui HH, Leohr JK, Kuo MS. Analysis of sphingolipids in extracted human plasma using liquid chromatography electrospray ionization tandem mass spectrometry. Anal Biochem. 2012 Apr;423(2):187-94.
288. Baker KE, Parker R. Nonsense-mediated mRNA decay: terminating erroneous gene expression. Curr Opin Cell Biol. 2004 Jun;16(3):293-9.
289. Oakley AJ, Coggan M, Board PG. Identification and characterization of gamma-glutamylamine cyclotransferase, an enzyme responsible for gamma-glutamyl-epsilon-lysine catabolism. J Biol Chem. 2010 Mar;285(13):9642-8.
290. Schnell PO, Ignacak ML, Bauer AL, Striet JB, Paulding WR, Czyzyk-Krzeska MF. Regulation of tyrosine hydroxylase promoter activity by the von Hippel-Lindau tumor suppressor protein and hypoxia-inducible transcription factors. J Neurochem. 2003 Apr;85(2):483-91.
291. Wenger DA, Clark C, Sattler M, Wharton C. Synthetic substrate beta-glucosidase activity in leukocytes: a reproducible method for the identification of patients and carriers of Gaucher's disease. Clin Genet. 1978 Feb;13(2):145-53.
292. Dave KD, De Silva S, Sheth NP, et al. Phenotypic characterization of recessive gene knockout rat models of Parkinson's disease. Neurobiol Dis. 2014 Jun.
293. Li M, Sun M, Cao L, et al. A TIGAR-regulated metabolic pathway is critical for protection of brain ischemia. J Neurosci. 2014 May;34(22):7458-71.
294. Zou S, Gu Z, Ni P, Liu X, Wang J, Fan Q. SP1 plays a pivotal role for basal activity of TIGAR promoter in liver cancer cell lines. Mol Cell Biochem. 2012 Jan;359(1-2):17-23.
295. Katsel P, Tan W, Fam P, Purohit DP, Haroutunian V. Cycle checkpoint abnormalities during dementia: a plausible association with the loss of protection against oxidative stress in Alzheimer's disease. PLoS One. 2013;8(7):e68361.
296. Li H, Jogl G. Structural and biochemical studies of TIGAR (TP53-induced glycolysis and apoptosis regulator). J Biol Chem. 2009 Jan;284(3):1748-54.

297. Boyle PJ, Scott JC, Krentz AJ, Nagy RJ, Comstock E, Hoffman C. Diminished brain glucose metabolism is a significant determinant for falling rates of systemic glucose utilization during sleep in normal humans. J Clin Invest. 1994 Feb;93(2):529-35.
298. Altman DI, Perlman JM, Volpe JJ, Powers WJ. Cerebral oxygen metabolism in newborns. Pediatrics. 1993 Jul;92(1):99-104.
299. Vaishnavi SN, Vlassenko AG, Rundle MM, Snyder AZ, Mintun MA, Raichle ME. Regional aerobic glycolysis in the human brain. Proc Natl Acad Sci U S A. 2010 Oct;107(41):17757-62.
300. Herrero-Mendez A, Almeida A, Fernández E, Maestre C, Moncada S, Bolaños JP. The bioenergetic and antioxidant status of neurons is controlled by continuous degradation of a key glycolytic enzyme by APC/C-Cdh1. Nat Cell Biol. 2009 Jun;11(6):747-52.
301. Ambrosi G, Ghezzi C, Sepe S, et al. Bioenergetic and proteolytic defects in fibroblasts from patients with sporadic Parkinson's disease. Biochim Biophys Acta. 2014 May;1842(9):1385-94.
302. Yao Z, Gandhi S, Burchell VS, Plun-Favreau H, Wood NW, Abramov AY. Cell metabolism affects selective vulnerability in PINK1-associated Parkinson's disease. J Cell Sci. 2011 Dec;124(Pt 24):4194-202.
303. Requejo-Aguilar R, Lopez-Fabuel I, Fernandez E, Martins LM, Almeida A, Bolaños JP. PINK1 deficiency sustains cell proliferation by reprogramming glucose metabolism through HIF1. Nat Commun. 2014;5:4514.
304. Knight AL, Yan X, Hamamichi S, et al. The glycolytic enzyme, GPI, is a functionally conserved modifier of dopaminergic neurodegeneration in Parkinson's models. Cell Metab. 2014 Jul;20(1):145-57.
305. Dando PR. Distribution of multiple glucosephosphate isomerases in teleostean fishes. Comp Biochem Physiol B. 1974 Mar;47(3):663-79.
306. Reiner O, Horowitz M. Differential expression of the human glucocerebrosidase-coding gene. Gene. 1988 Dec;73(2):469-78.
307. Ponce E, Witte DP, Hung A, Grabowski GA. Temporal and spatial expression of murine acid beta-glucosidase mRNA. Mol Genet Metab. 2001 Dec;74(4):426-34.
308. Cade L, Reyon D, Hwang WY, et al. Highly efficient generation of heritable zebrafish gene mutations using homo- and heterodimeric TALENs. Nucleic Acids Res. 2012 Sep;40(16):8001-10.
309. Grau J, Boch J, Posch S. TALENoffer: genome-wide TALEN off-target prediction. Bioinformatics. 2013 Nov;29(22):2931-2.
310. Dvir H, Harel M, McCarthy AA, et al. X-ray structure of human acid-beta-glucosidase, the defective enzyme in Gaucher disease. EMBO Rep. 2003 Jul;4(7):704-9.
311. Kervestin S, Jacobson A. NMD: a multifaceted response to premature translational termination. Nat Rev Mol Cell Biol. 2012 Nov;13(11):700-12.
312. Fuller M, Rozaklis T, Lovejoy M, Zarrinkalam K, Hopwood JJ, Meikle PJ. Glucosylceramide accumulation is not confined to the lysosome in fibroblasts from patients with Gaucher disease. Mol Genet Metab. 2008 Apr;93(4):437-43.
313. Ghauharali-van der Vlugt K, Langeveld M, Poppema A, et al. Prominent increase in plasma ganglioside GM3 is associated with clinical manifestations of type I Gaucher disease. Clin Chim Acta. 2008 Mar;389(1-2):109-13.
314. Nilsson O, Svennerholm L. Accumulation of glucosylceramide and glucosylsphingosine (psychosine) in cerebrum and cerebellum in infantile and juvenile Gaucher disease. J Neurochem. 1982 Sep;39(3):709-18.
315. Burke DG, Rahim AA, Waddington SN, et al. Increased glucocerebrosidase (GBA) 2 activity in GBA1 deficient mice brains and in Gaucher leucocytes. J Inherit Metab Dis. 2013 Sep;36(5):869-72.

316. Hayashi Y, Okino N, Kakuta Y, et al. Klotho-related protein is a novel cytosolic neutral beta-glycosylceramidase. J Biol Chem. 2007 Oct;282(42):30889-900.
317. Xu YH, Sun Y, Ran H, Quinn B, Witte D, Grabowski GA. Accumulation and distribution of α-synuclein and ubiquitin in the CNS of Gaucher disease mouse models. Mol Genet Metab. 2011 Apr;102(4):436-47.
318. Beaujot J, Joriot S, Dieux A, et al. Phenotypic variability of prenatally presenting Gaucher's disease. Prenat Diagn. 2013 Oct;33(10):1004-6.
319. Xu YH, Xu K, Sun Y, et al. Multiple pathogenic proteins implicated in neuronopathic Gaucher disease mice. Hum Mol Genet. 2014 Aug;23(15):3943-57.
320. Takamura A, Higaki K, Kajimaki K, et al. Enhanced autophagy and mitochondrial aberrations in murine G(M1)-gangliosidosis. Biochem Biophys Res Commun. 2008 Mar;367(3):616-22.
321. Yu W, Gong JS, Ko M, Garver WS, Yanagisawa K, Michikawa M. Altered cholesterol metabolism in Niemann-Pick type C1 mouse brains affects mitochondrial function. J Biol Chem. 2005 Mar;280(12):11731-9.
322. Bae EJ, Yang NY, Song M, et al. Glucocerebrosidase depletion enhances cell-to-cell transmission of α-synuclein. Nat Commun. 2014;5:4755.
323. Paquet D, Bhat R, Sydow A, et al. A zebrafish model of tauopathy allows in vivo imaging of neuronal cell death and drug evaluation. J Clin Invest. 2009 May;119(5):1382-95.
324. Gan-Or Z, Ozelius LJ, Bar-Shira A, et al. The p.L302P mutation in the lysosomal enzyme gene SMPD1 is a risk factor for Parkinson disease. Neurology. 2013 Apr;80(17):1606-10.
325. Mistry PK, Liu J, Sun L, et al. Glucocerebrosidase 2 gene deletion rescues type 1 Gaucher disease. Proc Natl Acad Sci U S A. 2014 Apr;111(13):4934-9.
326. Sevlever D, Jiang P, Yen SH. Cathepsin D is the main lysosomal enzyme involved in the degradation of alpha-synuclein and generation of its carboxy-terminally truncated species. Biochemistry. 2008 Sep;47(36):9678-87.
327. Tyynelä J, Sohar I, Sleat DE, et al. A mutation in the ovine cathepsin D gene causes a congenital lysosomal storage disease with profound neurodegeneration. EMBO J. 2000 Jun;19(12):2786-92.

7 Appendix